Bedload fill of abandoned channels

Léo Szewczyk

PSL UNIVERSITÉ PARIS

THÈSE DE DOCTORAT
DE L'UNIVERSITÉ PSL

Préparée à MINES ParisTech

Bedload fill of abandoned channels

Remplissage de chenaux abandonnés par la charge de fond

Soutenue par
Léo SZEWCZYK
Le 18 Décembre 2020

Ecole doctorale n° 398
Géosciences, Ressources Naturelles et Environnement

Spécialité
Géosciences et géo-ingénierie

Composition du jury :

Christian, GORINI Professeur, Sorbonne Université	*Président du jury*
Gilles, ARNAUD-FASSETTA Professeur, Université de Paris	*Rapporteur*
Frédéric, CHRISTOPHOUL Professeur, Université Paul Sabatier	*Rapporteur*
Philippe, CLAUDIN Directeur de Recherche, ESPCI Paris	*Examinateur*
François, METIVIER Professeur, IPGP	*Examinateur*
Michal, TAL Maitre de Conférences, CEREGE	*Examinateur*
Isabelle, COJAN Directeur de recherche, MINES ParisTech	*Directeur de thèse*
Jean-Louis, GRIMAUD Enseignant Chercheur, MINES ParisTech	*Co-encadrant*

MINES ParisTech | PSL

Abstract

This PhD is a contribution to the understanding of bedload sediment deposition in abandoned channels. Experimental and field investigations were combined to link hydrology and geomorphic evolution, and to propose an architectural model for bedload fills.

Experiments conducted using a fixed-bank and bed flume under constant sediment and water supply showed identical deposition processes under varied channel geometry, which occurred in two phases for channel plug formation. Sedimentation initiated downstream of the bifurcation in a flow separation zone whose size increased with the diversion angle. Channel plug then formed and thickened through the amalgamation of bars. In free flow conditions, i.e., without perturbation of the water surface slope, channel plug length and volume are controlled by the channel diversion angle. When the water-surface slope is modified in the disconnecting channel, channel plug geometry may be better predicted using the water surface slope –or length- ratio between the two channels.

Field surveys conducted in channels in both open- and closed-stages allowed comparisons with the experimental results. The morphologies of the channel plug deposits are similar in natural cases to the one observed in flume experiments, suggesting comparable deposition processes. Field observations in disconnecting channels allowed enriching the architectural model by integrating lateral accretion deposits occurring in early stages of abandonment, and characterizing fining-upwards and downstream trends of bedload deposits. Observations in channels abandoned for centuries showed that coarse-grained fill deposits architecture can be preserved through time provided that no reactivation of the channel occurred.

Finally, an experimental relationship linking the channels length ratio and plug length tested with field data appeared reliable to estimate a minimum channel plug length, and suggested that the remaining plug length consists of heterolithic deposits.

Résumé

Cette thèse contribue à la compréhension des processus de dépôts des sédiments grossiers dans les chenaux abandonnés. La combinaison d'études expérimentales et de terrain a permis de lier hydrologie et évolution géomorphologique des remplissages formés par la charge de fond, et de proposer un modèle de leur architecture.

Des expériences réalisées grâce à un modèle analogique au lit et bancs fixes auquel était fourni un apport constant d'eau et de sédiment ont montré que les sédiments sont déposés par des processus identiques indépendamment de la géométrie du chenal. Le bouchon de chenal se forme en deux phases. La sédimentation est initiée dans une zone de séparation du courant dont la largeur augmente avec l'angle de diversion. La formation et l'amalgamation de barres poursuit ensuite l'extension et l'épaississement du bouchon de chenal. En écoulement libre, c'est-à-dire sans perturbation de la surface libre de l'eau, la longueur et le volume du bouchon de chenal sont contrôlés par l'angle de diversion. Quand la surface libre est modifiée dans le chenal en cours de déconnexion, la géométrie du bouchon de chenal est contrôlée par le ratio entre les surfaces libres, ou les longueurs, des deux chenaux.

Des études de terrain effectuées dans des chenaux aux stages ouverts et fermés de la déconnexion ont permis de comparer observations naturelles et résultats expérimentaux. La morphologie du bouchon de chenal est similaire dans les deux cas, suggérant des processus de dépôts comparables. Les études de terrain réalisées dans des chenaux en cours de déconnexion ont permis d'enrichir le modèle architectural en intégrant des dépôts formés par accrétion latérale déposés lors de la phase initiale de déconnexion, et d'observer une tendance grano-décroissante normale et vers l'aval des dépôts de charge de fond. Des observations dans des chenaux abandonnés depuis plusieurs siècles ont montré que les dépôts de remplissage grossiers peuvent être préservés dans le temps, tant que le chenal n'est pas réactivé.

Finalement, une relation expérimentale liant le ratio de longueur entre les chenaux et la longueur du bouchon de chenal a été testée sur des données de terrain. Elle parait fiable pour estimer la longueur minimale du bouchon de chenal, et suggère que le reste de la longueur du bouchon est formée par des dépôts hétérolithiques.

Acknowledgments

First and foremost I would like to thanks my supervisors *Jean-Louis Grimaud* and *Isabelle Cojan* for their support, guidance and trust. I have learned a great deal thanks to you during these three years.

I would also like to thank the members of my jury, the rapporteurs *Gilles Arnaud-Fassetta* and *Frédéric Christophoul*, and the examiners *Philippe Claudin*, *Christian Gorini*, *François Métivier* and *Michal Tal*, for accepting to read and evaluate my work.

I am thankful to *Hervé Piégay* for his help in selecting study sites and his input both on the field and during the later reflexion I am indebted to *Aurélien Baudin*, *Cyril Leipp*, *Yasmina Habaoui*, *David Marquez* for their help in building the experimental flume used during this PhD, and to *Loïc Marlot* for his invaluable help during the field surveys. I am also grateful to *Armand Crouzet* and *Pierre Maria* for conducting some of the experiments used in this dissertation. Likewise, I am grateful to *Christine Franke* for her financial support that allowed us to buy the sediment feeder for the flume experiments and fund radiocarbon dating. I am also grateful to *Laurent de Windt* and *Alexandrine Gesret* for their help with the doctoral school covid situation. Finally, this journey would not have been possible without the discreet yet relentless and essential work of *Sylvie Boj* and *Véronique Lachasse*, who made sure that every administrative task went smoothly.

These years have also been a formidable human experience. I consider myself extremely lucky to have done my PhD at the Centre de Géosciences where I have met truly wonderful people. Alas, three years is far too short a time to live among such excellent and admirable persons. I am thinking first of the people that put up with my lame jokes at the morning tea far too often, *Caroline*, *Christine* and *Damien* and his map but also to those who left before the end (totally unrelated to my sense of humour): *Martin*, *Kiki*, *Thomas* and *Saro*. A few special thanks are in order. Thanks *Loïc* for being the delicate, refined and elegant creature that you are, and a totally, totally, trustworthy fellow werewolf. Also thanks for feeding me during my quarantine. *Alexandre* (and your boar), thank you for all the boar- and shoulder-related laughs, and for being an equally trustworthy adventurer that would never, ever, purposely anger a dragon I'm negotiating with. Be wary of saucisson. *Bob*, you are an amazing and patient story teller who let me be a lizard. It was lovely to share apartments in the mountains with you and to see you put on skis. *Nicolas*, thank you for feeding me cheese while I was at

my lowest, at my best, and generally speaking when I was hungry. Also thanks for your grace in accepting your national team humiliating and oh so painful and very public defeat and allowing me to gloat. *Laure*, if I ever need someone to accompany me in the forbidden crossing of a dangerous and dark tunnel, I'll choose you. *Manon*, thanks for the honey and medicines I somehow always need and you somehow always have. *Marine*, I can now confess that I sometimes enjoyed the vegetables you brought. *Aurélien*, I saw you sip that champagne glass. *Jean*, I wouldn't have wanted to put my finger in the DopaMines affair with anyone else, but maybe it is time to let go? *Léa*, I loved that you managed to be consistently disappointed by the subtlety of my jokes. *Audrey*, thanks for your family stories, they are always surprising. *Anaïs*, I will see Anès some day. *Anaïs*, it was a pleasure to endure your toothpick attacks.

More widely, I am grateful to the PhD students and postdocs (and even a few "non-precarious" persons) for the atmosphere and feeling of comradery that I felt, whether it was at lunch for the tarot breaks, during the board games nights or week end activities or on the ski slopes. I don't know half of you as well as I should like, and I like less than half of you half as well as you deserve.

The aforementioned persons fed my soul with the warmth of friendship, but alas the flesh is weak and also has needs. I would have failed long ago if not for the delicious and totally balanced diet I followed. I owe *Pablo* and *Alicia* at least five kilos, but it was worth it. Huge thanks to *Chiara* and *Lele* for the icy desserts (and sometimes afternoon and week end breaks).

A special thought for some special persons. *Morgane*, well, for being you and always supportive when I need to complain. *Maxime*, for being such a good gaming partner, even though we are terrible. *Margaux*, for the 8 years I have known you. It might have been different had we not have been partnered since year one. *Hadrien*, I still don't always understand you, but I love the red beard. *Eudes*, thanks for always letting me lean on you when necessary. These past years I could not see you bunch as much as I wanted to, despite the constant promises. I hope I will do better now.

Finally, I would not have succeeded without my family. I am grateful to my parents, *Christine* and *Kléber*, for always, always supporting me and gently pushing me to accomplish my best. You encouraged my curiosity since as long as I can remember, and always gave me the means to satiate it. *Martin*, big brother, as much as I hated to admit it at times, you have always been

a model for me. *Juliette* and *Salomé*, you made him better and the family is greater with you in it. Last but definitely not least, *Lisanne*, you fully supported me and endured my moods during this adventure. This would have been harder without you. *Ik heb nu iets om naar uit te kijken*. I love you all very much.

Reading back this rant, I realise once again how good these PhD years were and the sheer number of amazing people I know. Dear reader, if you do not know any of these persons, but are still reading, first I am impressed at your persistence, and second, worry not, this is the end and the actual stuff you came to read follows.

I bid you all a very fond farewell, and enjoy the read!

Contents

Abstract ..... *i*

Résumé ..... *iii*

Acknowledgments ..... *v*

Contents ..... *ix*

List of Figures ..... *xiii*

List of Tables ..... *xviii*

Introduction *1*

Chapter 1: Channel abandonment and infilling – Literature review *5*

1.1. Introduction **6**

1.2. Fluvial systems **6**

1.3. Floodplain dynamics and resulting sedimentary facies **10**
1.3.1. Channel migration deposits and associated facies 11
1.3.1. Overbank deposits and associated facies 13
1.3.3. Relation to abandoned channels 14

1.4. Channel abandonment processes **15**
1.4.1. Avulsions 15
1.4.1.1. Avulsion types 15
1.4.1.2. Avulsion initiation 16
1.4.1.3. Avulsion styles 17
1.4.2. Chute cutoffs 19

1.5. Current models for abandoned channels fill **25**
1.5.1. Channel fill nature and geometry 25
1.5.2. Current knowledge on processes controlling channel infilling 30
1.5.2.1. Regional controls on channel abandonment and fill 30
1.5.2.2. Bifurcation dynamics and its control on disconnection 33
1.5.2.3. Closed-stage channel filling processes 40

1.6. Conclusion **42**

Chapter 2: Bedload dynamics and deposition in abandoned channels using an experimental bifurcation setup *45*

2.1. Experimental evidences for bifurcation angles control on abandoned channel fill geometry **46**
2.1.1. Abstract 46
2.1.2. Introduction 46
2.1.3. Methods 48
2.1.3.1. Experimental design 48
2.1.3.2. Data acquisition 51
2.1.3.3. Sediment transport law 52
2.1.4. Results 53
2.1.4.1. Bifurcation geometries allowing channel disconnection 53
2.1.4.2. Sand plug formation dynamics and architecture 57
2.1.4.3. Controls on sand plug length and volume 58
2.1.5. Discussion 60
2.1.5.1. Bifurcation angle control on abandonment 60
2.1.5.2. Bifurcation angle control on sand plug extent 61
2.1.5.3. Mechanism for channel abandonment 62
2.4.5.4. Comparison with field cases and upscaling 63
2.1.5.5. Sand plug architecture integration to reservoir modelling 65
2.1.6 Conclusion 67

2.2. Influence of additional forcing parameters on plug geometry **68**

2.2.1. Erodible sand bed 68
2.2.2. Differential base level and associated backwater dynamics 71
2.2.2.1. Experimental design 71
2.2.2.2. Results 73
2.2.3. Interpretation 79

2.3. Conclusion 81

Chapter 3: Experimental abandonments in curved channels geometries: insights on the architecture of cutoff bedload fills 83

3.1. Introduction 84

3.2. Methodology 86
3.2.1. Experimental design 86
3.2.2. Data acquisition 90

3.3. Results 93
3.3.1. Bedload deposits in the case of local avulsions 93
3.3.2. Effects of cutoff channel width on bifurcation (un)stability 96
3.3.3. Bedload deposits in the case of cutoff incision 97
3.3.4. Controls on channel fill architecture 104

3.4. Discussion 107
3.4.1. Geometrical controls on channel equilibrium 107
3.4.2. Deposition process and architectural elements of abandoned channel fills 109
3.4.3. Controls on bedload fill deposits geometry and volume 111
3.1.4. Experimental predictive model for channel plug length and volume 114

3.5. Conclusion 118

Chapter 4: Gravel fill dynamics and depositional patterns in chute cutoffs channels of a bedload dominated river: the Ain River, France 121

4.1. Abstract 122

4.2. Introduction 122

4.3. Study area 125
4.3.1. Geomorphic setting 125
4.3.2. Studied channels 126

4.4. Methods 130
4.4.1. Channel fill sedimentary bodies mapping 130
4.4.1.1. DEM 130
4.4.1.2. Aerial pictures analysis 130
4.4.1.3. Observations and data collection on the field 131
4.4.2. Estimation of the bedload deposits in the abandoned channel 132

4.5. Results 135
4.5.1. Channel facies description and interpretation 135
4.5.2. Channel fill architecture in the studied channels 138
4.5.2.1. Open-stage channel: the CHA site 138
4.5.2.1. Closed-stage channels 144
4.5.3. Geometrical controls on planar geometry and volume of channel fills 147

4.6. Discussion 149
4.6.1. Depositional processes of the bedload fill 149
4.6.2. Grain-size changes associated with plug formation 152
4.6.3. Geometry, extent and volumes of channel plugs 153
4.6.4. Cutoffs initiation and bifurcations stability 156

4.7. Conclusion 157

Chapter 5: Long-term preservation of coarse-grained fill deposits: tests on field observations 159

5.1. Introduction 160

5.2. Reconstruction of a pluri-centenal abandoned channel fill architecture: the Vimpelles avulsion channel (Seine, France). 162
5.2.1. Geographical and geological contexts 162
5.2.2. Methods 165
5.2.3. Channel fill present architecture 167
5.2.4. Coarse-grained fill deposits long-term preservation 169
5.2.4.1. Evidences of several phases of activity 169
5.2.4.2. Recent moderate-energy reworking events 170

5.3. Coarse-grained fill deposits preservation in several systems 173
5.3.1. Studied abandoned channels 173
5.3.1.1. The Boire Torse channel 174
5.3.1.2. The Rijnstrangen channel 176
5.3.2. Results and discussion 178

5.4. Cutoff channel plug length prediction using aerial pictures 180
5.4.1. Study area 180
5.4.2. Channel selection and measurement method 180
5.4.2.1. Data source 180
5.4.2.2. Channel selection 182
5.4.2.3. Measurement method and uncertainties 183
5.4.3. Results and discussion 185

5.5. Conclusion 190

Chapter 6: Conclusion and perspectives 193

6.1. Main contributions of the PhD 193
6.1.1. Experimental results 193
6.1.2. Comparison with field examples 194

6.2. Future work and perspectives 195
6.2.1. Experimental setup improvement 195
6.2.2. Complexification of the flume experiments 196
6.2.3. Transitional phase and heterolithic deposits study 197
6.2.4. Channel fill under tidal influence 198

References 201

Appendix A: Supplementary material for Section 2.2 215

Appendix B: Supplementary material for Chapter 4 – Ain River channels aerial pictures 221

Appendix C: Supplementary material for Chapter 4 – Allier River channels aerial pictures 227

Appendix D: Location and log of the auger and corer holes made in tne Vimpelles channel 231

List of Figures

Figure 1.1: Satellite images of the four major types of fluvial systems. **(a)** Straight river (Gunnison River, USA). **(b)** Braided river (Rakaia River, South Island, New Zealand). **(c)** Anastomosed river (Columbia River, Canada). **(d)** Meandering river (Tchoulym River, Russia). Source: Google Earth Pro. 7

Figure 1.2: Diagram showing the variety of morphologies taken by rivers between the dominant types when the control factors vary. The main channel types are located at the appropriate positions within the diagram. Shading is intended to reflect sediment character. From Church (2006). 9

Figure 1.3: Representation of the typical planform and vertical geometry of the deposits formed by three major types of fluvial systems in aggrading setting. **(a)** Braided rivers. Low lateral mobility. **(b)** Anastomosed river. Lateral migration and avulsions. **(c)** Meandering river. Lateral migration. From Jerolmack & Mohrig (2007). 10

Figure 1.4: One example of floodplain cross section using a Flumy simulation (Lopez et al. 2008) that shows the spatial relationships between the abandoned channels and other lithofacies in a fluvial meandering reservoir. 11

Figure 1.5: Architecture, grainsize evolution and heterogeneities across a point bar. **(a)** Typical depositional sequence of meandering channel deposits (from Donselaar & Overeem 2008). **(b)** Internal architecture of a point bar displaying internal facies heterogeneities (from Deschamps et al. 2012). 13

Figure 1.6: Avulsion types. From Stouthamer (2000), Slingerland & Smith (2004) and Bernal et al. (2012). 16

Figure 1.7: Models for avulsions by incision **(a)** and progradation **(b)**. Both panels show partial reoccupation of either an old abandoned channel **(a)** or an active tributary **(b)**. From Mohrig et al. (2000). 18

Figure 1.8: Cutoff mechanisms and geometries. **(a)** Headward erosion. **(b)** Embayment incision. **(c)** Scroll slough. **(d)** Neck formation. **(e)** Mid-channel bar formation. Adapted from Grenfell (2012). Proportions were taken from Lewis & Lewin (1983) after a study of 145 cutoffs in gravel bed rivers of Wales. The missing 18 percents are multi-loop (13%) and artificial cutoffs (5%). 20

Figure 1.9: Satellite images showing chute cutoff initiation and evolution on the Ucayali River, Peru. Chute is initiated by incision of part of the point bar between two abandoned channels (1996) (1&2), leading to their widening (1997) (3). They become dominant by 2000 and the disconnected channel narrows quickly and a sand plug forms on its upstream part (4). 23

Figure 1.10: Cutoff formation processes. **(a)** Embayment formation on a meander bend of the Missouri River, USA. **(b)** Flooded swales in the Amazonian floodplain. Pictures from Constantine et al., 2010b. 22

Figure 1.11: Sketch and pictures of headward erosion processes (Powder River, Montana, USA). **(a)** Schematic representation of the meander bend in 1985. **(b)** Isometric drawing of the gully. **(c-d)** Pictures of the gully facing upstream (c) and downstream (d). Adapted from Gay et al., 1998. 21

Figure 1.12: Satellite images showing neck cutoff initiation and evolution on the Ucayali River, Peru. The upstream arm of the bend migrates northward (1985-2014) until it joins the downstream arm of the bend, disconnecting the apex of the meander bend (2015). 24

Figure 1.13: Conceptual sketch illustrating the abandoned channel shape after disconnection **(a)** and channel plug architecture immediately after disconnection **(b)** and after the active channel migration **(c)**. After Rowland et al., (2005) Not to scale. 26

Figure 1.14: Channel fill deposits model for cross-sections along a channel bend. Arrows show the relative orientations of the active channel and bars. Bridge et al. (1986). 27

Figure 1.15: Example of detailed architecture analysis in an abandoned channel fill in a Rhine River cutoff (Netherlands). a: laminated clays. b: clayey silts. c: silts. d: silty sands (Toonen et al., 2012). Based on their observations the authors proposed that the channel fill grainsize evolution translates a global decrease in energy in the abandoned channel, with some flood-related coarser deposits intertwined in the fill. 28

Figure 1.16: Conceptual sketches displaying the geometry and lithology of the channel fill depending on the disconnection type. **(a)** Avulsion. **(b)** Chute cutoff. **(c)** Neck cutoff. After Toonen et al. (2012) and Dieras (2013). 29

Figure 1.17: Illustrative sketch of backwater effects on channel water-surface elevation. x>L: Normal flow. 0<x<L: transitional region. x<0: offshore river plume. *hs*: water depth at the shoreline. *hn*: normal flow depth. Adapted from Lamb et al. (2012). 31

Figure 1.18: Diagram representing the scales, interactions and effects of the controls on bifurcation formation. 31

Figure 1.19: Sketch of a bifurcation highlighting the geometric and hydraulic factors controlling bifurcation stability. 34

Figure 1.20: Effect of the upstream slope advantage and curvature on flow (a) and sediment erosion or deposition (b). From Kleinhans et al., 2008 & 2013. 36

Figure 1.21: Sketch illustrating the relationship between length and slope ratios in cutoff cases that allows slope ratio measurement without having access to elevation data. 37

Figure 1.22: Effects of the diversion angle on the flow separation zone. Flow velocity modeling for a 60° bifurcation. μ: fraction of the total abandoned channel width occupied by the downstream flow cross-section. ε: flow separation zone **(a)**. Relationship between the diversion angle value and the flow separation zone width **(b)**. **(a-b)** from Constantine et al. (2010b). Relationship between the diversion angle value and the flow separation zone length and width at the upstream and downstream entrances of a water intake. *Lu*: length upstream. *Ld*: length downstream. *Wu*: width upstream. *Wd*: width downstream. From Keshavarzi & Habibi (2005) **(c)**. 39

Figure 1.23: Diagram representing the local and geometric factors controlling bifurcation stability and their interactions. 40

Figure 1.24: Channel fill deposits as described by Allen (1965) after the works of Fisk (1947) and Schumm (1960) **(a)** and representation of a channel fill cross-section filled by clays as commonly described, as pointed out by Donselaar & Overeem (2008) (**b**). Allen (1965) and Donselaar & Overeem (2008). 42

Figure 2.1: 3-D sketch showing the occurrences of deposits associated with abandoned channels in an alluvial plain. 47

Figure 2.2: Overhead view of the experimental setup together with the different angles considered and the levee breach setup. 49

Figure 2.3: Evolution of the experiments. **(a-c)** Overhead pictures of the setup for the symmetrical **(a)** and asymmetrical configurations without **(b)** and with levee breach **(c)**. **(d-f)** Evolution of water discharge measurement at the output of the distributary channels for symmetrical **(d-e)** and asymmetrical **(f-g)** configurations. **(g)** Asymmetrical 90° configurations with varying slope ratios *S2/S1*. 50

Figure 2.4: Planar growth of sand plug from overhead pictures. **(a)** Consecutive growth phases of the sand plug for $\beta 2$ = 30°. **(b)** Final states of the sand lug for different $\beta 2$ angles. Contours are drawn every 15 min. The mean sand plug length is represented with a black circle, together with uncertainties. 54

Figure 2.5: Final topography of Experiment 5 showing the active (1) and disconnected (2) channels. **(a)** Elevation DEM. **(b)** Shaded relief of the same DEM. Contour lines represent 1.5 mm elevation. 55

Figure 2.6: Mean longitudinal elevation profiles of the sand plugs for increasing $\beta 2$ angles without **(a)** and with levee breach **(b)**. Profiles were corrected for bottom slope to facilitate comparisons. The grey area corresponds to the active channel. Empty triangles correspond to the furthest location where the sand plug occupies the entire channel width, while full triangles indicate the subaqueous extremity of the sand plug. 56

Figure 2.7: Relationships between the sand plug length and volume, and the incidence angle $\beta 2$ **(a, b)** and slope ratio S2/S1 for $\beta 2$ = 90° **(c)**. The regression line for total sediment in panel **(b)** was not calculated since only three points were aligned. 59

Figure 2.8: Transport law. Volumetric flux per unit width, as a function of Shield parameter θ. The dashed line corresponds to Eq. (1) fitted to the data **(a)**. Regime relationship between dimensionless discharge Q^* and slope measured in the experiments. The solid blue line corresponds to the threshold theory (Eq. 2, $\theta t = 0.17$ and $Cf = 0.06$). The shaded area and dashed lines indicate uncertainty based on varying friction coefficient Cf value **(b)**. 64

Figure 2.9: Conceptual architecture of sand plug derived from experimental observations: overhead view **(a)**, longitudinal profile **(b)** and transverse sections **(c)**. 66

Figure 2.10: Final interpreted overhead pictures of the fixed-bed experiments **(a, b)** and of the sand bed experiments **(a', b')**. 69

Figure 2.11: Mean longitudinal elevation profiles of the sand deposits for the sand bed (Exp. 20, 21) and fixed-bed (Exp. 7, 9) experiments. The grey area corresponds to the active channel. Triangles indicate the length of the sand plug in asymmetrical experiments cases. 71

Figure 2.12: Plan view of final states of sand plugs for Exps. 9 **(a)** and 21 **(b)**. Growth stages are indicated by the colors. 71

Figure 2.13: Plan view of final states of sand plugs for different β2 angles with a base level of 0 cm **(a)** and with a base level rise of 0.5 cm **(b)**. Growth stages are indicated by the colours. 74

Figure 2.14: Mean longitudinal elevation profiles of the sand plugs for increasing β2 angles in no-forcing **(a)** a base level elevation of 0.5 cm **(b)** and a base level elevation of 1 cm **(c)** scenarios for low diversion angles (15 to 22.5°), symmetrical or slightly asymmetrical experiments. Profiles were corrected for bottom slope to facilitate comparison. The grey area corresponds to the active channel. 75

Figure 2.15: Comparison between mean longitudinal elevation profiles of the sand plugs for increasing β2 angles in no-forcing **(a)** and base level elevated by 0.5 cm **(b)** scenarios. Profiles were corrected for bottom slope to facilitate comparison. The grey area corresponds to the active channel. 76

Figure 2.16: Plots of sand plug length **(a)** and volume **(b)** and the incidence angle β2 for highly asymmetrical bifurcations. 77

Figure 2.17: Plot of sand plug length on free flow zone length. Dashed point indicates that backwater zone length was calculated as the mean of distributary 2 and the inlet channel slope as distributary 2 was flat. 78

Figure 2.18: Plot of disconnection time and base level elevation. 78

Figure 3.1: Overhead view of the experimental setup showing the open- **(a)** and closed- **(b)** meanders configurations as well as the walls that were removed to simulate incision. Each configuration was reversible. 87

Figure 3.2: Final deposits DEM of experiments S1 & S2 **(a)** and N1 & N2 **(b)** illustrating the swath method used to build the deposits longitudinal mean elevation profiles. Contour line are spaced by 2 mm. 91

Figure 3.3: Interpreted overhead photograph **(a)** and total sand deposits **(b)** and emerged sand deposits **(c)** mapped using color and saturation computer treatments of the picture. 92

Figure 3.4: Final occupation maps and temporal occupation of curved channels for the reoccupation experiments. Experiment AR-OM1 **(a)** Experiment AR-OM2 **(b)** Experiment AR-CM1 **(c)** Experiment AR-CM2 **(d)**. 95

Figure 3.5: Final occupation maps and temporal occupation curve of the curved channels for straight channel experiments with modified width E1 & E2 **(a-b)** up to the upstream channel width (AR-OM1) **(c)**. 97

Figure 3.6: Final occupation maps and temporal occupation curve of the curved channels for cutoff incision experiments. **(a)** Experiment S1. **(b)** Experiment S2. **(c)** Experiment N1. **(d)** Experiment N2. 98

Figure 3.7: Planar growth of the bedload deposits in the curved channels through time for avulsion with reconnection **(a-d)** and cutoff incision experiments **(e-h)**. Contour lines were drawn at regular intervals. The mean channel plug lengths are represented with a black circle together with uncertainties. 100

Figure 3.8: Equilibrium water surface elevation along the straight and curved (dashed line) channels for open **(a)** and closed-meander **(b)** experiments. 101

Figure 3.9: Longitudinal mean elevation profiles of the bedload deposits in the curved channels as measured using the method illustrated in Figure 2. **(a)** Open-meander geometries. **(b)** Closed-meander geometries. Grey boxes indicate the active channel. Full arrows indicate the extremities of the upstream channel plugs and dashed arrows the extremities of the downstream channel plugs. 103

Figure 3.10: Effects of the diversion angle on the channel plug deposits length **(a)** and volume **(b)** for the cutoff and avulsion (Section 2.2) experiments at different base level elevations.Total sediment volumes indicated for cutoff incision experiments are indicated only in view of the upstream diversion angle. Dashed lines represent relationships between the sandplugs length and volume and the diversion angle defined in Chapter 2. 105

Figure 3.11: Relationships between the slope ratio *S2/S1* and channel plug length **(a)** and volume **(b)**. 106

Figure 3.12: Relationships between the length ratio L_1/L_2 and upstream channel plug length. 112

Figure 3.13: Geometrical parameters used to measure the theoretical channel plug volume. 115

Figure 3.14: Relationships between the channels water-surface slope ratio or length ratio and the channel plug volume, compared with Chapter 3 experiments upstream channel plugs volume, assuming equivalence between both ratios (Eq. 1.4). 117

Figure 4.1: Location **(a)**, simplified geological map **(b)** of the study area and 2019 aerial photographs of the cutoffs (**c**, Martinaz; **d**, Mollon; **e**, Châtillon). Simplified 1/50000 geological map from Ambérieux-en-Bugey map, Kerrien et al. 1987. River course drawn on the geological map is that of 2017-2018, terrace contour has been modified accordingly to take into account river bank erosion and cutoffs. Red dots and boxes on the aerial photographs indicate the location of the pictures shown in Figs. 4.5 and 4.6. 123

Figure 4.2: Dates of cutoff formation and average daily discharge at the gauging station of Chazey-sur-Ain (from January 1st, 2000 to February 1st, 2020) **(a)** and aerial views of channel morphology evolution **(b)**. Cutoff dates from Grenfell et al. (2012) and Dieras (2013) for Martinaz and Mollon cutoffs. Thresholds for sediment transport data are from Rollet (2007) and 2- and 5-years flood discharge from the Chazey-sur-Ain gauging station. 126

Figure 4.3: Evolution of the geomorphic features of a cutoff in open-stage after a major winter flood, the Châtillon (CHA) cutoff in July 2018 **(a)** and June 2019 **(b)**. (See Fig. 4.1 for site location and Fig. 4.2 for the duration and amplitude of the winter flood). 127

Figure 4.4: Geomorphic features of cutoffs in closed-stage, the Mollon (MOL) **(a)** and Martinaz (MAR1 & MAR2) **(b)** cutoffs as of July 2018. 129

Figure 4.5: Channel fill elements. **(a)** Channel lag deposits in the thalweg on the upstream part of the channel plug (Mollon) (Fig. 4.1d). **(b**) Channel lag deposits in the downstream active part of the channel (Martinaz) (Fig. 4.1c). **(c)** Laterally accreting and **(d)** downstream migrating gravel bar deposits (Châtillon). The bar on (c) was vegetalized between 2018 and 2019, with the dashed line indicating the 2018 limit of vegetation extension. **(e)** Sandy flood deposits covering a gravel bar near the bifurcation of the Mollon channel (Fig. 4.1d). **(f)** Sandy to clayey fining upward deposits overlying gravels preserved in the topographic lows of the channel plug (Martinaz) (Fig. 4.1c). 137

Figure 4.6: Notable disconnection features of the Châtillon cut off. **(a)** Characteristic geometry of a prograding gravel bar during the early stage of the plug (facies F-II). The crest between the gently sloping toss face and the steep lee face creates an undulating topographic step across the channel reach reflecting migration process by lobes as the prograding bar (facies F-II) overlies the channel lag deposits of the former active channel (facies F-I) (Fig. 4.1e). **(b)** Finer grained gravel-bar (facies F-III) that migrated on the early plug deposits (facies F-II) during the high waterstage of winter 2018-2019 (Fig. 4.1e). **(c)** Toe of the prograding gravel bar (facies F-II) (medium grain size) below water level, toe contour is drawn based on the grain size contrast with the coarse channel lag deposits (facies I), it is considered as the downstream limit of the channel plug deposits (Fig. 4.1e). 140

Figure 4.7: Contrast in grain-size between active channel lag and the different generations of fill bars for the mature closed-stage MOL site and open-stage CHA site **(a)**. Examples of grainsize distribution of samples from channel lag, early and late stage fill bars **(b)**. Wolman counts designation refers to Table 1 and Fig. 3 and 4. Roman numerals refer to the facies of Table 2 sampled as shown in Fig. 6. MAR sites values are not displayed as the number of samples do not allow meaningful comparison. Reach D_{50} value comes from Rollet (2007). 142

Figure 4.8 Cross sections of the bed topography of the CHA cut-off. (see Fig. 3 for section location).Data come from dGPS and DEM and physical measurements data along segments that could not be surveyed. 143

Figure 4.9: Bedload fill volume estimation for CHA, MOL and MAR sites. Scheme illustrating the methods to evaluate the pre-abandonment cross-sectional area **(a)** and plot of the pre-abandonment cross-sectional area of the channel plotted against the cross-sectional area **(b)**. Dieras et al.'s (2013) d transect was subdivided in two smaller ones based on geomorphic assumptions for comparison with new transects. 146

Figure 4.10: Dimensionless channel plug length function of the channel diversion angle **(a)** and length ratio **(a')**, and dimensionless channel area **(b)** and volume **(c)** function of the channels length ratio. Data comes from this study (4 sites) and from Citterio & Piégay (2009) (5 sites). Data for the volume of bedload deposits in the MOL and MAR cutoffs are measured or extracted from Dieras et al. (2013). 148

Figure 4.11: Scheme of a channel fill planform **(a-d)** and cross-sectional architecture during a cutoff process **(a'-d')** in a bed load dominated river. Roman numerals refer to the facies of Table 4.2 and Fig. 4.7. 151

Figure 5.1: Schematic representation of the channel plug length and growth pattern based on bifurcation and channels geometry and downstream hydraulic effects. 161

Figure 5.2: The Bassée alluvial plain context. Simplified geological map of the Seine River basin **(a)**. Catchment area of the Bassée alluvial plain and current Seine course **(b)**. Geomorphologic map of the downstream part of the Bassée alluvial plain showing the Old Seine paleo channels reconstruction and the studied channel position **(c)**. Schematic cross-section of the Bassée alluvial plain **(d)**. Deleplancque et al. (2018) and Petit et al. (in press), adapted from Mégnien et al. (1965). 163

Figure 5.3: Current channel morphology. Aerial picture and boreholes position **(a)**. Lidar DEM and cross-sections positions **(b)**. 164

Figure 5.4: Interpreted cross-sections. A, B and E from Petit et al. (in press). 166

Figure 5.5: Interpreted coarse-grained deposits map. 167

Figure 5.6: Close-up on the Vimpelles channel plug deposits showing its topographic step and the downstream variations in coarse deposits fill volume. 168

Figure 5.7: Reconstruction of the temporal and morphologic evolution of the Vimpelles channel. 171

Figure 5.8: The Boire Torse channel localisation and the cross-sections position, after Arthuis et al. (2015) and Miéjac & Arthuis (2007). 174

Figure 5.9: Channel cross-sections in the Boire Torse and measurement method. Cross-sections from Miéjac & Arthuis (2007). 175

Figure 5.10: Location and geology of the studied area showing the Rijnstrangen disconnected channel **(a)** and laser altimetry view of the Rijnstrangen channel with the cross-sections positions **(b)**. From Toonen et al. (2012). 176

Figure 5.11: Interpreted cross-sections of the channel fill geometry in the Rijnstrangen channel. a: Bioturbated non-laminated clays. b: Calcareous, humic finely laminated (<1 cm) clayey silts showing flood pulses. c: Calcareous, humic laminated (1-3 cm) silts showing flood pulses. d: Calcareous, coarsely laminated (>3 cm) silty sands showing flood pulses and plant debris. e: Gravels and sands. From Toonen et al. (2012). 177

Figure 5.12: Percentage of coarse-grained fill deposits in cross-sections in function of the distance to the channel bifurcation point for 5 different river channels. 178

Figure 5.13: Lower Mississippi Valley position along the Mississippi River reach and situation of the Yazoo and Boeuf-Tensas basins in the Lower Mississippi Valley. 181

Figure 5.14: Examples of the typical geometries mapped in the Lower Mississippi Valley and illustrations of the criterions used for channel selection. Maps from Krinitzsky et al., 1965 Saucier, 1967. 183

Figure 5.15: Ain and Allier rivers and Lower Mississippi Valley (LMV) apparent channel plug length function of the channel length ratio. 186

Figure 5.16: Conceptual sketch representing channel fill deposits appearance at the end of the disconnection **(a)** and the sediments architecture at the end of the channel fill **(b)**. Differentiation and accurate mapping of the open-stage deposits can then only be made using coring **(c-d)**. Cores are from Jordan & Pryor (1992). 187

Figure 5.17: Mississippi River abandoned channel fill in Hickman County (Kentucky). Boreholes position in the channels **(a)**. Borehole data taking into account the surface topography and longitudinal distance in the channel and interpreted facies longitudinal evolution **(b-c)**. Data from Alexandrowicz (2015). 189

Figure A1: Final deposits of the 8 asymmetrical experiments, without and with levee breach. **(a-b)** $\beta 2 = 30°$. **(c-d)** $\beta 2 = 45°$. **(e-f)** $\beta 2 = 60°$. **(g-h)** $\beta 2 = 90°$. 217

Figure B1: Temporal evolution of the CHA site. 222

Figure B2: Temporal evolution of the MOL/MAR sites. 223

Figure B3: Aerial views of the closed stage of the five historical cutoffs (1954-1965) described in Table 4.1. 224

Figure C1: Aerial views of the closed stage of the five historical cutoffs (1946-1960) described in Table E2. 229

Figure D1: Location of each borehole in the Vimpelles channel. 232

Figure D2: Borehole sampling method. Coring using a hand auger **(a)**. Samples retrieved using a hand auger **(b)** and a Russian corer **(c)**. Hand auger sampling is less continuous but allow sampling of sands and thin layers of fine gravels while the Russian corer can only sample peat, clays and silts. 233

Figure D3: Log of each of the 38 boreholes. Designation corresponds to the number of the GPS waypoint made to locate the borehole. 234

List of Tables

Table 2.1: List of experiments and associated parameters. 49

Table 2.2: List of sand bed experiments and associated parameters. Sand bed volume is not accounted in sand plug volume. 68

Table 2.3: List of base level variation experiments and associated parameters. 72

Table 3.1: List of the experiments and resulting channel plug characteristics. 88

Table 4.1: Summary of the studied channels characteristics. 128

Table 4.2: Sedimentary facies. 135

Table 4.3: Wolman Pebble Counts sampling data. 141

Table 5.1: Mississippi and Arkansas River channel plugs measurements. 184

Table A1: List of experiments and detail of all associated parameters. 216

Table B1: Hydraulic parameters, cross-sectional area and filled area of the cross sections displayed in Figures 4.3, 4.4 & 4.8. 225

Table C1: Allier River channel plugs measurements. 229

Introduction

Channel abandonment is a ubiquitous process that allows the reorganization of fluvio-hydrological networks and sediment distribution in alluvial plain. Following the disconnection of parts of the river course, they form sinks for sediments while previously stored deposits are reworked by active channels. The nature, geometry and architecture of the abandoned channels sedimentary fill will impact the future evolution of the alluvial plain. For instance, fine-grained fills (clays or peat) are strongly cohesive that will reduce the lateral mobility of the active channel and narrow the meander belt. On the other hand, as the fraction of coarse-grained fill deposits increases in abandoned channels, hydraulic connectivity of floodplain sediment increases. Abandoned channels also have immediate economical value as fish nurseries, fluvial transportation hubs or touristic and leisure areas. Furthermore, abandoned channels have ecological values as they are diversity hotspots that can be used to bolster the population of endangered species or reintroduce them. Finally, the fine-grained part of abandoned channels usually preserves biogeochemical indicators and artefacts propitious to archaeological studies.

Channel abandonment initiate with the formation of a short plug of coarse deposits isolating the channel from the active one(s). This channel plug is described as a wedge-shaped sedimentary body formed by the bedload part of the sedimentary charge. After the channel disconnection and isolation from bedload sediment supply, finer-grained sediments brought by overbank events or autochtonous sedimentation such as plant detritus and peat deposits slowly heal the paleo-thread. Numerous studies have described coarse deposits in channels but limited studies focused on their extent in relation with geomorphic processes. Hence, numerical models devised to reconstruct the spatio-temporal evolution of channelized fluvial systems often assume a 100% clay infill of the abandoned channels in the sake of simplicity due to the lack of constraints on coarse-grained fill deposits architecture and extent.

While it has been established that the bifurcation geometry before channel disconnection affects the local hydraulic dynamics and induces deposition, controls on coarse-grained fill sediments deposition are not well known. It has been suggested that the channel and bifurcation geometry controls the channel plug extent, for instance through bifurcation angle value or difference in slope between the two channels. However, few studies have quantified bifurcation dynamics throughout the whole disconnection process. Thus much remains to be

done to link hydrology, geomorphology and sedimentary deposits architecture. Currently, important progresses in the understanding of channel abandonment have been made using either field or modelling studies but only a few attempts have been made to link the two approaches.

This dissertation aims at linking channel geometry, hydraulic processes and coarse-grained fill sediments deposition and architecture in abandoned channels. The approach was process-based with at first a series of flume experiments whose results were compared to observations made on the field in channels abandoned by both mixed- and bedload dominated rivers. The dissertation is composed of six chapters:

- Chapter 1 summarizes the current knowledge on channel abandonment and the resulting sedimentary fills with a focus on the coarse-grained bedload deposits.
- Chapter 2 presents experimental data on channel abandonment using a flume with a modular bifurcation. The effects of diversion angle and water-surface variations are discussed. An architectural model for bedload deposits in abandoned channel is proposed.
- Chapter 3 focuses on bedload deposition in curved experimental channels and discusses the influence of hydraulic effects on the sedimentation patterns in the abandoned channels.
- Chapter 4 focuses on the architecture and temporal evolution of bedload deposits in several modern curved channels disconnected by chute cutoffs in the Ain River to tentatively link hydrology, sedimentation processes and bedload fill architecture. The Ain river was selected as its bedload dominated nature enables easy comparison with the flume experiments.
- Chapter 5 discusses the long term preservation of bedload deposits in abandoned channels. The relationships that were experimentally determined between the channel plug architecture and forcing parameters are tested against field data acquired on well-documented mixed-load rivers such as the Seine and Mississippi rivers.
- Chapter 6 summarizes the conclusions of this work and discusses possible next steps for bedload channel fill study.

Chapter 1: Channel abandonment and infilling – Literature review

Ce chapitre présente une étude bibliographique sur les environnements dans lesquels se forment les chenaux abandonnés, leurs morphologies, processus de formation, ainsi que sur les facteurs contrôlant leur abandon et remplissage, et leurs interactions avec les autres objets géomorphologiques des plaines alluviales. Bien que cette étude bibliographique se décrive toutes les étapes du remplissage des chenaux abandonnés, elle se concentre sur les processus de dépôt et architectures des dépôts grossiers de charge de fond.

This chapter presents a literature review on abandoned channels environments, morphology and formation as well as on the nature and geometry of their fills, the controls on their abandonment and infilling and their relation with the other features of the floodplain. Although this literature review describes all stages of abandoned channel infilling, it focuses heavily on the deposition processes and architecture of the coarse-grained bedload deposits.

1.1. Introduction

Abandoned channels are widespread features in floodplains across the planet. They form as the result of avulsions or cutoffs associated with river migration and aggradation. As they form elongated topographic depressions, the abandoned channels are efficient sediments sinks (Aalto et al., 2008; Lauer & Parker, 2008; Dieras et al., 2013). Abandoned channels are studied for a broad range of applications. The lithology, architecture and geometry of abandoned channels infilling have a significant impact on the latter evolution and physical properties of the floodplain (Howard, 1992; Smith et al., 1998; Flipo et al., 2014; Schwendel et al., 2015), making it an economical (agriculture, fluvial transportation, nautical sport areas) and societal (flood risk, urban areas extension) matter. Abandoned channels also form wetlands that are ecological hotspots (Novitzky et al., 1996; Ward et al., 1999), serving as fish nurseries or endangered species reintroduction sites. Their infilling form archeological and quaternary paleo-climatic archives (van Dinter et al., 2017), where archeological artifacts can be found together with organic matter used for isotopic dating, pollens, fossils or sedimentary evidences of extreme events. Finally, heterogeneities formed in abandoned channels preserved in the fossil record influence the geological fluvial reservoir architecture and connectivity (Miall, 1996; Willis & Tang, 2010; Colombera et al., 2017; Cabello et al., 2018), with implications for natural resources exploitation.

1.2. Fluvial systems

Fluvial systems are formed by one or several active channels that are migrating in a floodplain. The floodplain corresponds to the domain that is flooded during overbank floods, while the area occupied by the channel path through time forms the channel belt. There are four main types of fluvial systems that form depending on the floodplain characteristics and the sediment supply: straight, braided, anastomosed and meandering (Leopold & Wolman, 1957; Rust, 1978; Church, 2006).

Straight channels develop along fault lines or on steep slopes, and in some deltas. They often incise a narrow and deep valley or a canyon (Fig. 1.1a). It is unusual for a straight channel to be absolutely straight for a distance greater than 10 channel widths, and they show only limited inflexion of their course (Leopold & Wolman, 1957). They develop a riffle and pool morphology (Fig. 1.2), with a spacing between riffles and pools approximately equal to 5 channel widths (Leopold & Wolman 1957, 1960). It is believed by Wolman & Leopold

(1957) that the mechanisms leading to channel meandering appear to occur in straight channel but that meandering is hindered by the valley slope or narrowness.

Braided systems sediment conduits are characterized by a single, low sinuosity channel at bankfull. At lower regime it consists of a network of channels separated by gravely banks, set in the conduit (Fig. 1.1b, 1.2; Leopold & Wolman, 1957; Miall, 1996). The gravel banks are generally unstable and are reworked and displaced during floods. When the floods are sufficiently frequent and no vegetation stabilizes the banks, channels can be highly mobile and unstable. Braided rivers are characterized by high width/depth ratios (W/D ratios) (>50) (Fig. 1.3a), steep slopes and low sinuosity (<1.3) (Miall, 1977; Bridge, 2003). Due to their steep slopes and general proximity to reliefs, braided systems carry a relatively coarse-grained sediment load.

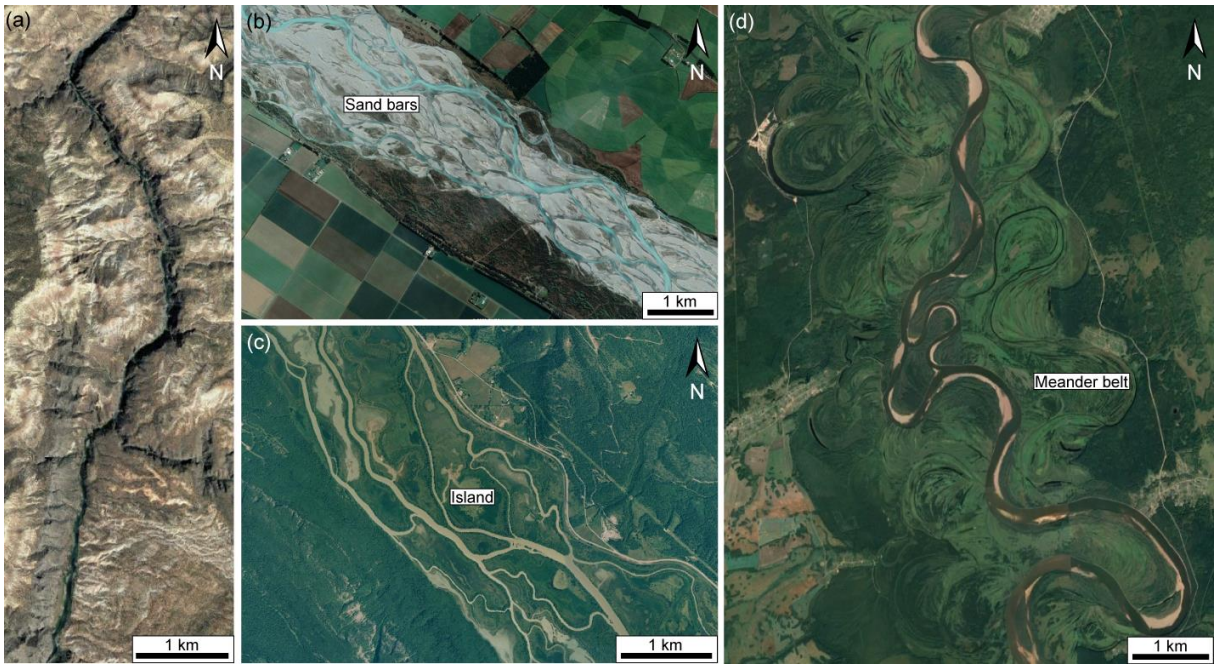

Figure 1.1: Satellite images of the four major types of fluvial systems. **(a)** Straight river (Gunnison River, USA). **(b)** Braided river (Rakaia River, South Island, New Zealand). **(c)** Anastomosed river (Columbia River, Canada). **(d)** Meandering river (Tchoulym River, Russia). Source: Google Earth Pro.

Anastomosed systems are formed by several, well differentiated channels separated by stretches of the floodplain, forming vegetalized, perennial islands that are not reworked during floods (Fig. 1.1c, 1.2). The channels are stable and can take several morphologies depending on the floodplain characteristics. They can be straight or sinuous, in which case they are deep and narrow, with very abrupt banks (Fig. 1.3b; Rust, 1978; Miall, 1996), or have a meandering pattern. Anastomosed threads have a low W/D ratio (<40) and a low slope, and dominantly carry fine-grained sediments. Anastomosed rivers were sometimes called anabranching rivers (Smith & Smith, 1980; Rust, 1981; Schumm, 1985), but the definitions

are variable, relying either on the stability or cohesiveness of the banks or the size of the islands. For instance, Nanson & Knighton (1996) integrated the notion of anabranching river in all types of fluvial systems, as rivers comprised of "multiple channels separated by vegetated semi-permanent alluvial islands excised from existing floodplain or formed by within-channel or deltaic accretion". As such the definition of anabranching river is very broad. To differentiate anabranching rivers from anastomosed rivers, Makaske (2001) proposes the following definition for anastomosed rivers: "Anastomosed systems are formed by two or more interconnected channels that enclose floodbasins", which couples channel pattern and floodplain geomorphology while excluding the braided systems.

Meandering systems generally form the distal part of the fluvial system. They are characterized by a single active, highly sinuous channel with some tributaries, notably chute channels (Fig. 1.1d, 1.2) (Allen, 1965; Miall, 1996; Bridge, 2003). They are set in low slopes environments and carry a mixed sediment load. Point bars are formed on the inner part of the meander bends in association with the migration and erosion towards the outer bank that generally occurs during floods (at least full bank, and also overbank). Channels are flanked by levees formed of silt and fine sand draping the edges of the channels during overbank flooding events (Fig. 1.3c; Allen, 1965, Miall, 1996). The levees can be breached, generally during floods (Slingerland & Smith, 2004) although bank failure, animal or debris dams, the formation of ice or log jams and the migration of bars downstream can lead to levee crevassing (Jones & Schumm, 1999). Part of the flow is diverted through the crevasse channel and this result in the formation of crevasse-splays, wide and thin sand-sheets that form on the floodplain (Allen, 1965; Smith et al., 1989). The deposits associated to the channel and its migration (i.e., point bars, levees, channel fill) form the meander belt, which is the part of the alluvial plain where the active channel migrates (Fig. 1.1d).

These major systems form the extreme poles in the classification. Yet the transition from one style to another is not sharp, and there are overlaps in conditions allowing two different styles. Thus some rivers share the characteristics of two of the main fluvial systems (Fig. 1.2), due to floodplain conditions such as slope, sediment erodibility or sediment supply falling at the limit between the ideal ranges for two distinct fluvial systems morphologies. Anabranching rivers, described earlier, regroup the characteristics of anastomosed and braided or meandering rivers (Nanson & Knighton, 1996). Wandering rivers are formed by one to two active sinuous channels hosting mid-channel bars, at the interface between braided and meandering rivers (Miall, 1996; Church, 2006) while low-sinuosity rivers can be found at the

interface between braided and anastomosed systems. In these low-sinuosity active channels, alternate bars are formed by lateral accretion before migrating downstream (Crowley, 1983; Miall, 1996).

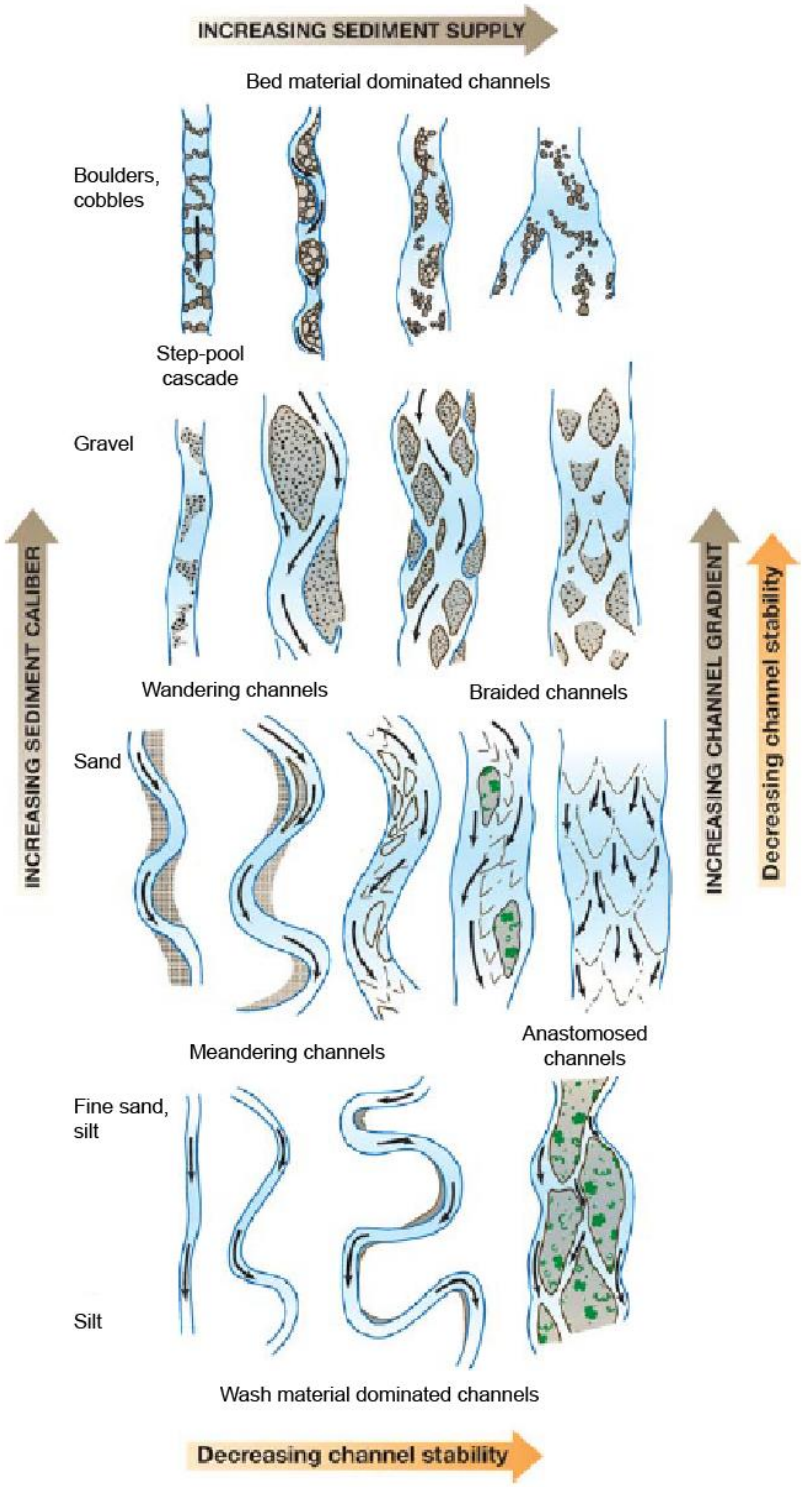

Figure 1.2: Diagram showing the variety of morphologies taken by rivers between the dominant types when the control factors vary. The main channel types are located at the appropriate positions within the diagram. Shading is intended to reflect sediment character. From Church (2006).

1.3. Floodplain dynamics and resulting sedimentary facies

Coarse sediments are mostly deposited and reworked during flooding events and the associated channel migration. Evolution of channel paths occurs by two major processes. The first is the channel migration by lateral erosion. In that case, when the floodplain is wide and the channels stable, migration is slow and the sand bodies are few and isolated. When migration is fast, channel abandonment is frequent and the sand bodies are numerous and interconnected (Miall, 1996). The second migration process is avulsion, when the river finds a new course. When avulsions are frequent, numerous, interconnected sand bodies will also be deposited.

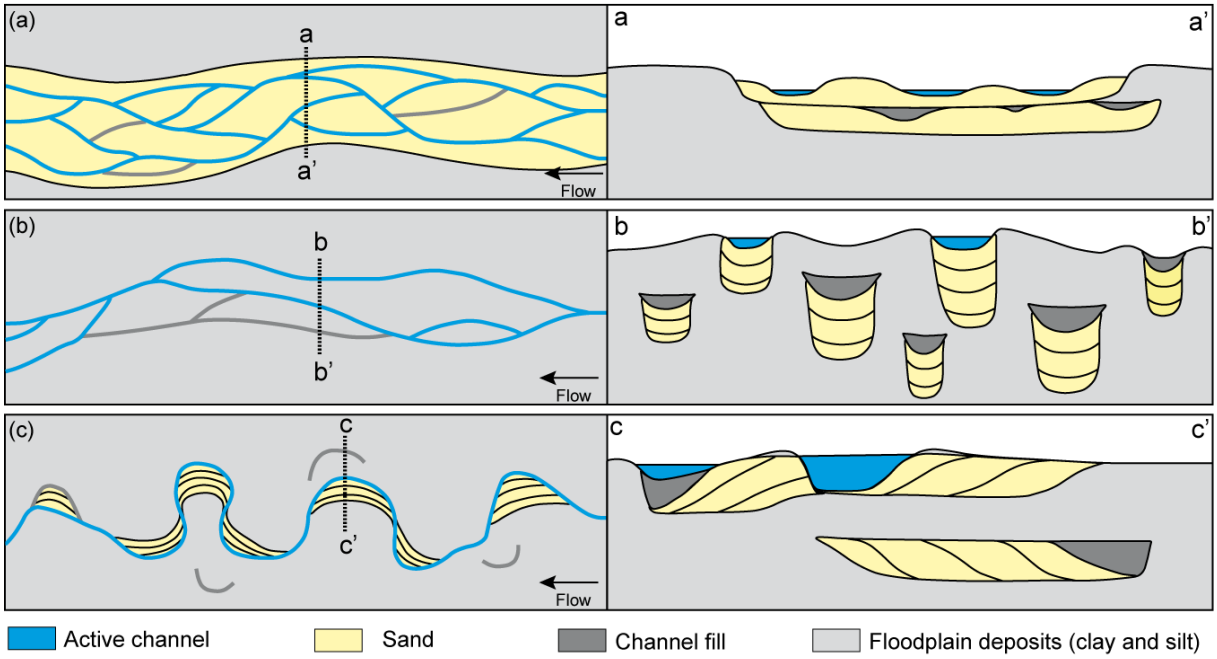

Figure 1.3: Representation of the typical planform and vertical geometry of the deposits formed by three major types of fluvial systems in aggrading setting. **(a)** Braided rivers. Low lateral mobility. **(b)** Anastomosed river. Lateral migration and avulsions. **(c)** Meandering river. Lateral migration. From Jerolmack & Mohrig (2007).

Channel migration and avulsion deposits sediments in a specific planform organization depending on the fluvial system type (Figs. 1.1 & 1.3). They also rework and erode previously deposited sediments, which in a graded system results in a near constant amount of coarse deposits in the floodplain as the material eroded at a point of the floodplain is deposited downstream at another point. When the system aggrades, the sand bodies stack vertically (Fig. 1.3; Miall, 1996). In the aggradation rate is high, the sand bodies can be vertically disconnected from each other. However, when the aggradation rate is appropriate, the combined lateral and vertical accumulation of coarse-grained fluvial deposits results in interconnected sand bodies that can form fluvial reservoirs (Fig. 1.4; Bridge, 2003). In this

intricate network of sedimentary bodies formed by the spatial and temporal evolution of the floodplain, the potential contrasts in physical properties, such as erodibility or permeability, between the deposits may impact both the future evolution of the floodplain and the reservoir properties. This section describes the architecture and facies of the sedimentary bodies found in the channel and alluvial plain, in relation to which abandoned channels are formed.

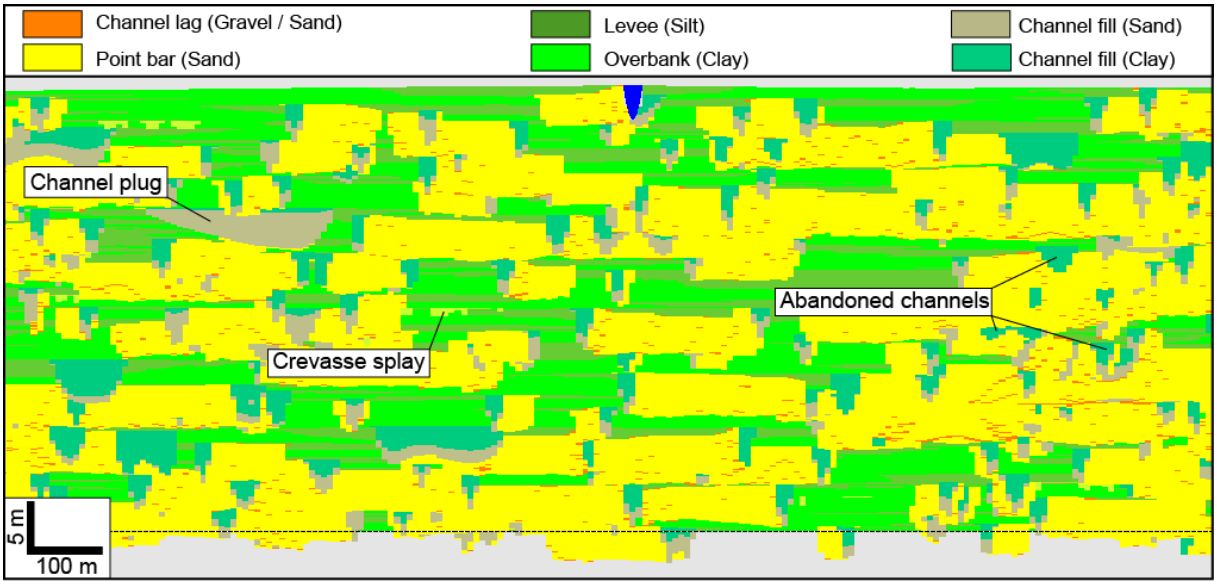

Figure 1.4: One example of floodplain cross section using a Flumy simulation (Lopez et al. 2008) that shows the spatial relationships between the abandoned channels and other lithofacies in a fluvial meandering reservoir.

1.3.1. Channel migration deposits and associated facies

Channel migration creates coarse-grained (gravels and sand) sedimentary bodies in floodplains by complex processes that are affected by both the channel evolution and geometry itself (Willis, 1989) and the complex flow dynamics in the channel (Leopold & Wolman, 1960; Allen, 1963, 1965, 1970a; Nanson, 1980; Robert, 2003; Fustic et al., 2012). Although they are generally considered to be good reservoir deposits, the resulting sedimentary bodies have a complex internal architecture with much heterogeneity at many different scales (Barton, 1994; Labrecque et al., 2011a; Deschamps et al., 2012). Channelized deposits can be divided in two groups: channel bed deposits and bars.

- **Channel lag deposits** form the channel bed. They correspond to channelized gravels or sands deposits with a convex erosive base and a fining-upward trend. They are generally formed by several successive sequences separated by erosion surfaces (Miall, 1996) and composed of massive sandstones or conglomerates whose thickness varies depending on the scale of the channel (Miall, 1996; Labrecque et al., 2011a, 2011b). They may offer a sharp lithological contrast with the surrounding sediments,

being generally deposited on clay, silts or finer sands, surmounted by finer sands and bracketed by clays (Figs. 1.4 & 1.5a; Donselaar & Overeem, 2008) and present many erosion surfaces that create yet more lithological contrasts inside the channel lag deposits.

- **Longitudinal sandbars** are dynamic structures that evolve within the channel. They can be found inside the channel of braided, straight or anastomosed systems, or anchored to the channel bank (Miall, 1977, 1996). They form thin and elongated fining-upward bodies formed by downstream accretion and lateral accretion on their edges (Miall, 1996). They form nodes that can capture dunes that were migrating downstream on the channel bed (Cant & Walker, 1978). Consequently these bars are formed by successive accretion layers of various grainsizes with different orientations and dips and some erosional surfaces, resulting in highly heterogeneous sedimentary bodies (Cant & Walker, 1978; Miall, 1996).
- **Point bars** are formed in association with the lateral migration of meander bends in meandering and anastomosed systems through erosion of the external bank of the bend (Allen, 1963; 1970a). On the internal bank they form accretion layers in a sigmoidal shape angling towards the channel with a 5 to 25° dip (Miall, 1979). Due to the varying effects of the channel shape on sediment deposition along the point bar length, point bars may have a very complex internal architecture. Macro-scale heterogeneities are formed by the fining-upward of the deposit across the whole point bar (Fig. 1.5a; Allen, 1970b; Walker, 1984), as well as the fining downstream and from the centre to the edge of the point bar (Fig. 1.5b; Bridge et al., 1995; Deschamps et al., 2012; Fustic et al., 2012; Durkin et al., 2015, 2017). Chute channels formed during floods (but not necessarily leading to chute cutoff) on top of the point bar that incise part of the point bar deposits (Fig. 1.5b) create erosion surfaces which are filled with heterogeneous material generally finer than the point bar deposits themselves (Deschamps et al., 2012; Colombera et al., 2017; Cabello et al., 2018). They form another set of heterogeneities inside of the point bar. Meso-scale heterogeneities inside the point bar are formed by changes in lithology or reworking of the deposits. During meander migration and rotation, part of the point bar is reworked, creating erosional surfaces overlain by new, discordant accretion sets that can have a different orientation, dip and grain size (Durkin et al., 2015). Furthermore, clay drapes forming permeability baffles can be deposited amongst the lateral accretion deposits in case of low-energy flow (Leopold & Wolman, 1960; Nanson, 1980; Robert, 2003; Pranter et al., 2007; Fustic et

al., 2012). These drapes are rare in point bars, except when a tidal effect reaches the meander bend (Deschamps et al., 2012). However they are more common in counter point bar deposits, the concave deposits connected to the downstream part of the point bar (Smith et al., 2011) where the flow energy is lower. Finally at the micro-scale grain size variations inside each set exist.

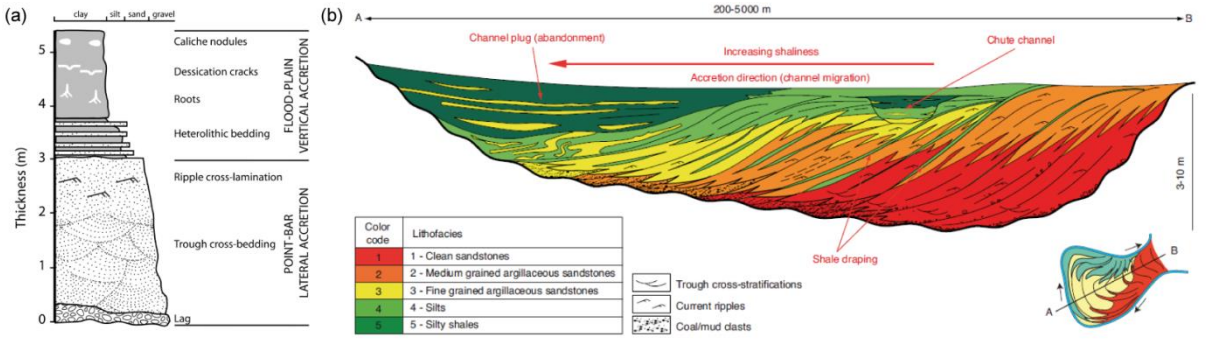

Fig. 1.5: Architecture, grainsize evolution and heterogeneities across a point bar. **(a)** Typical depositional sequence of meandering channel deposits (from Donselaar & Overeem 2008). **(b)** Internal architecture of a point bar displaying internal facies heterogeneities (from Deschamps et al. 2012).

1.3.1. Overbank deposits and associated facies

Most of the floodplain deposits are overbank deposits formed during flooding event. They are finely-grained sediments that become finer when the distance to the active channel increases. Overbank facies form a significant amount of the floodplain deposits in meandering and anastomosed systems, whereas the braided system channel network tends to occupy most of the floodplain (Miall, 1996). Two types of overbank deposits exist:

- The coarse-grained deposits form the **levees** and **crevasse splays**. Levees are deposited on the edge of the channels during overbank floods when suspended sediments overspill (Figs. 1.2; 1.4). They form a wedge-shaped deposit whose thickness and grain size decreases with the distance from the channel (Smith et al., 1989; Miall, 1996). Levees are formed by the aggregation of thin layers with a grainsize typically ranging from fine sands to silts. Paleosoils as well as animal and/or vegetal bioturbation can typically be found in the levees. Crevasse splays form when the flow breaches the levees, creating a crevasse channel. The crevasse channel itself forms sand ribbons with cross stratification and current ripples (Miall, 1996). When the flow reaches the floodplain it spills out and loses energy, inducing sediment settling forming thin lobe-shaped deposits with an important horizontal extension (Smith et al., 1989; Miall, 1996). Crevasse splays grainsize decreases vertically and

towards the floodplain, going from medium to fine sands with silts to clays sheets (Smith et al., 1989; Miall, 1996). The top part of the lobes is often bioturbated and is incised by the crevasse channels that supply them and keep building the lobe.

- Fine-grained deposits are formed in the floodplain by the decantation of flood waters at the end of the flooding event. This process deposits very thin sheets of silts and clays over large areas (Willis & Behrensmeyer, 1994; Miall, 1996). The horizontal sheets can mark either successive flooding events or a continuous sedimentation in swamps. Paleosoils and evaporites can be observed in these deposits (Miall, 1996), as well as desiccation cracks and bioturbation and organic-rich swamp deposits. These deposits are often incised or covered by coarser overbank deposits or channel migration facies.

1.3.3. Relation to abandoned channels

The sediments deposited by the active channels throughout their evolution in the floodplain have a close relation with the abandoned channels. First, they form the substrate in which channel abandonment will occur and with which the channel fill will interface. Secondly, the processes by which they are formed, i.e., lateral migration, levee crevassing and overspill, are amongst the processes that initiate channel abandonment. Finally, channel migration facies form the first stages of abandoned channel infilling when bedload is deposited due to the loss of energy in the abandoned channel during its progressive hydraulic disconnection, while overbank facies actively contribute to the abandoned channels infill by being regularly brought in the abandoned channel during the overbank floods occurring after the channel hydraulic disconnection.

1.4. Channel abandonment processes

Channel abandonment is a frequent event in the floodplain. It exists in every type of fluvial system. Three major processes can lead to channel abandonment: avulsions, the disconnection of part of one thread in an anastomosed system, and cutoffs. This section describes these processes and the spatial relationship between the abandoned channels and the previously described features of the floodplain.

1.4.1. Avulsions

An avulsion is the abandonment of a part or the whole of a meander belt by a stream for some new course at a lower elevation on the floodplain (Allen, 1965, Mohrig, 2000). The area of the floodplain where avulsions are frequent forms an avulsion belt (Smith et al. 1989; Smith & Pérez-Arlucea, 1994). There are many ways to classify avulsions: depending on (i) the proportion of the discharge that is steered away from the initial channel (Stouthamer, 2001; Slingerland & Smith, 2004), (ii) the avulsion site location (Leeder, 1978), (iii) the scale of the avulsion (Heller & Paola, 1996; Aslan & Blum, 1999) or (iv) the duration of the stage when the two channels are active (Berendsen & Stouhamer, 2000).

1.4.1.1. Avulsion types

An avulsion can be total, in which case the initial channel is abandoned, or partial, when only part of the discharge is diverted towards the avulsion channel. Avulsions can be nodal, i.e., meaning that all avulsions originate from the same location, the avulsion node (e.g., the apex of an alluvial cone) (Ganti et al., 2016a) or random, i.e., occurring at any point along the active channel. Regional avulsions are large scale avulsions where the initial channel is totally abandoned downstream of the avulsion point and a new channel is formed in the floodplain. Local avulsions create new channels that join the initial channel downstream. Finally some avulsions will reoccupy a channel abandoned during a previous avulsion (Aslan & Blum, 1999; Mohrig et al., 2000; Stouthamer, 2005) or capture another active channel nearby (Bernal et al., 2012). These avulsion modes (Fig. 1.6) are not mutually exclusive: an avulsion can be total, regional and nodal or partial with reoccupation. Avulsions can also occur very suddenly (Qian, 1990; Slingerland & Smith, 2004) or last several centuries (Stouthamer & Berendsen, 2001). Avulsions often follow o hierarchical scale: a large scale avulsion upstream can form new channels that will themselves undergo small scale avulsions (Slingerland & Smith, 2004).

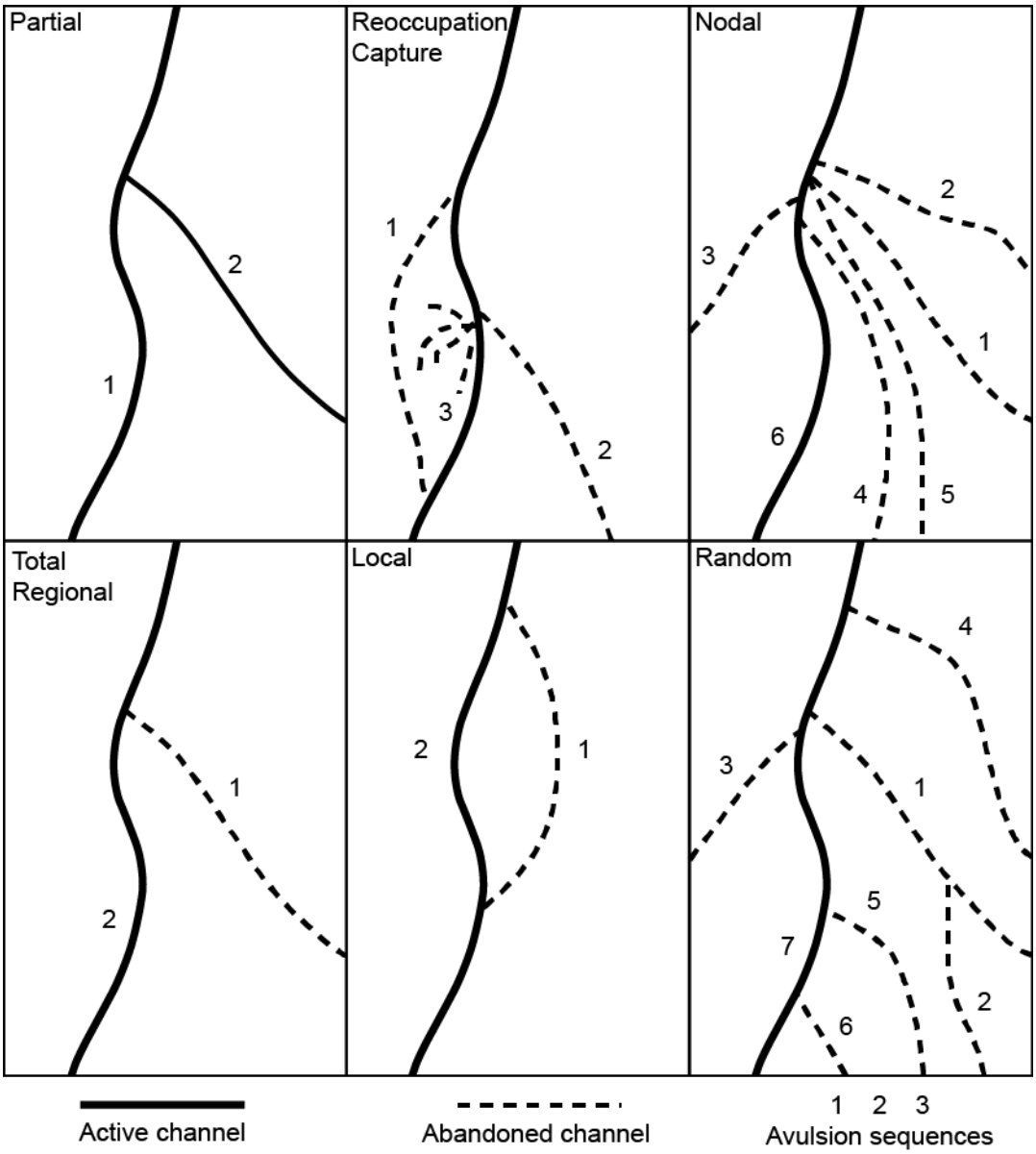

Figure 1.6: Avulsion types. From Stouthamer (2000), Slingerland & Smith (2004) and Bernal et al. (2012).

1.4.1.2. Avulsion initiation

An avulsion takes place when a trigger occurs in a favorable setup. Local setups leading to avulsions are a higher aggradation rate in the channel than in the levees, leading to a significant slope differential between the channel and a crevasse in the levee (Bridge & Leeder, 1979; Törnqvist, 1994; Bryant et al., 1995; Heller & Paola, 1996; Ethridge et al., 1999; Jerolmack & Mohrig, 2007) or a well-drained floodplain (Mohrig et al., 2000). A larger scale these local parameters are controlled by the sedimentary load, the discharge and the topography (Törnqvist, 1994; Ethridge et al., 1999; Jones & Schumm, 1999; Berendsen & Stouthamer, 2000; Stouthamer & Berendsen, 2001; Slingerland & Smith, 2004), base level elevation (Berendsen & Stouthamer, 2001; Giosan & Bhattacharya, 2005), or tectonics

(Stouthamer & Berendsen, 2001; Giosan & Bhattacharya, 2005; Lamb et al., 2012; Nittrouer et al., 2012; Reitz et al., 2015; Ganti et al., 2016a). The trigger event will form a crevasse that can lead to an avulsion when the crevasse connects the channel to low area with a sufficient slope advantage and drainage. When it is not the case, the avulsion fails (Slingerland & Smith, 2004). The triggers are often floods (Jones & Schumm, 1999; Blum et al., 2000; Ganti et al., 2016a, 2016b) but can also be dams formed by vegetal debris (Makaske et al., 2002; Montgomery & Piégay, 2003; Rodrigues et al., 2006; Sear et al., 2010) or ice (Gay et al., 1998; Ethridge et al., 1999; Makaske et al., 2002), the consequence of animal activities such as beaver dams (John & Klein, 2004) or hippopotamus trampling (Jones & Schumm, 1999), bank erosion (Schumann, 1989; Ethridge et al,. 1999) or the migration of bars that will temporary dam or plug a channel (Jones & Blakey, 1997; Edmonds et al., 2009).

1.4.1.3. Avulsion styles

Three major avulsion styles exist:

- **Avulsion by channel capture or reoccupation** occurs when a new course joins another active channel or when an abandoned channel is reoccupied (Fig. 1.7a, b). The newly joined channel might be too narrow to accommodate the new discharge, in which case water will overflow or the channel will widen (Smith et al., 1998; Pérez-Arlucea & Smith, 1999), or it can be too wide in which case the channel will narrow by the formation of lower benches anchored to the embankments (Sorrells & Royall, 2014; Reynolds & Royall, 2020). Preexisting channels in the floodplain are perfect mediums to redirect the flow and sediments from the avulsion point as they form well-drained topographic lows in the floodplain. The efficiency of the preexisting channels in flow capture coupled to their general abundance in floodplain ensure that channel reoccupation and capture is a widespread avulsion mode (Aslan & Blum, 1999; Smith et al., 1998; Mohrig et al., 2000; Morozova & Smith, 2000; Stouthamer, 2001) that occurs when aggradation rate is low, as in this case abandoned channels form the best topographic differential with the active channel (Aslan & Blum, 1999; Stouthamer, 2001).
- **Avulsion by incision of a new channel** occurs when following a levee breach the flow spills into the floodplain and, while draining along the most favorable slope in the floodplain, naturally seeks to connect low elevation areas. While doing so it incises the obstacles between such areas, connecting them, until it connects again with an active channel (Fig. 1.7a; Mohrig, et al. 2000). Initial flow path incision is

accompanied by the upstream erosion of a knickpoint (Fig. 1.7a) until the new channel can accommodate the discharge (Schumann, 1989; McCarthy et al., 1992; Smith et al., 1997). This type of avulsion occurs in flat, well drained floodplains that are sparsely vegetalized, which prevents the deposition of sediment and facilitates incision (Mohrig et al., 2000).

- **Avulsion by progradation** builds new channels above the floodplain. Flow that exits the initial channel and spills in the floodplain will slow, spread out and lose its transport capacity. It forms a crevasse splay (Smith et al., 1989) and progrades in the floodplain. If the crevasse doesn't heal, the lobe will eventually develop a dominant channel (Fig. 1.7b; Aslan & Blum, 1999; Mohrig et al., 2000; Morozova & Smith, 2000). The lobe can have a significant extension and contribute to a regional avulsion (Smith et al., 1989; Pérez-Arlucea & Smith, 1999) or its dominant channel can quickly join another active channel. This type of avulsion occurs when the floodplain is poorly drained, i.e., when the slope is low, the vegetation dense and the water table high, helping the formation of ponds in which the flow will deposit its sediments.

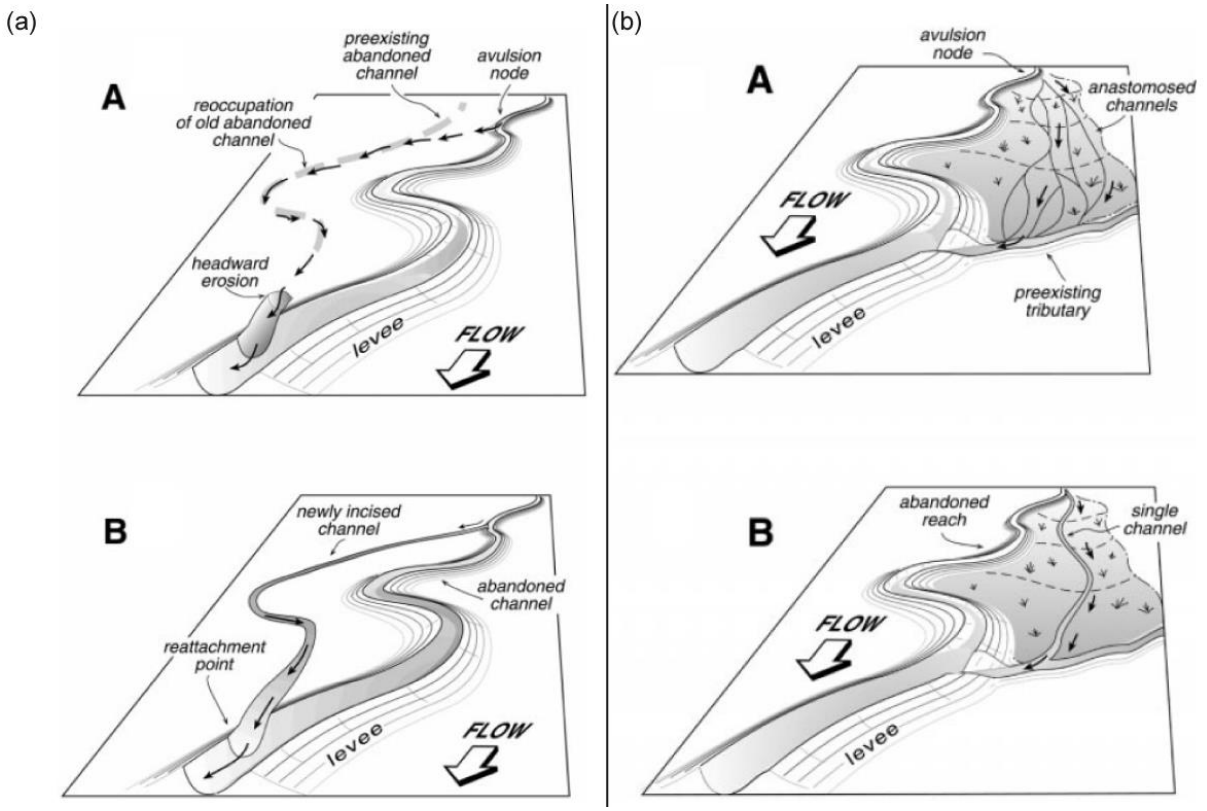

Figure 1.7: Models for avulsions by incision **(a)** and progradation **(b)**. Both panels show partial reoccupation of either an old abandoned channel **(a)** or an active tributary **(b)**. From Mohrig et al. (2000).

1.4.2. Chute cutoffs

Chute cutoffs are mostly associated with meandering, and in some cases with braided rivers, and occur when the river shortens its course and thus locally increases its slope (Fisk, 1947; Allen, 1965). Chute cutoffs are prominent features in highly mobile rivers (Lewis & Lewin, 1983). Cutoff is a process that shortens river length by one (Fisk, 1947; Allen, 1965) to several meander bends (Allen, 1965; Lewis & Lewin, 1983). Cutoff frequency increases with the channel sinuosity index (Allen, 1965) and their occurrence depends on flood frequency (Knighton, 1998), channel slope (Schumm & Khan, 1972) and substrate erodibility (Harrison et al., 2015; Schwendel et al., 2015), with specific factors combinations leading to different geometries.

Originally two types of cutoffs were described by Fisk (1944, 1947) in the Mississippi River floodplain: chute cutoffs and neck cutoffs. This distinction was made using the cutoff formation processes that resulted in distinct geometries. More recent classifications were expended to at least 5 categories, based on the processes that lead to cutoff formation (Fig. 1.8), and gathered under the term "chute cutoff" with Fisk's neck cutoff being one subtype of chute cutoff (Grenfell, 2012). Chute cutoffs are created by the formation of a new channel across the banks or the point bar of a meander bend (Fig. 1.8), either by incision or erosion between the bend arms or by occupation of the scroll sloughs (Fisk, 1947; Grenfell et al., 2012; van Dijk et al., 2014). Chute cutoffs are generally a prolongation of the bend just upstream of the disconnected loop (Fisk, 1947).

Three main categories of cutoffs are distinguished. Cutoffs by over-bar or overbank incision regroup three cutoff types (Fig. 1.8a-c) and appear to form roughly half of the cutoffs (Lewis & Lewin, 1983). This type of cutoff takes place when the local slope is steep (Lewis & Lewin, 1983) and requires high water levels and high rates of bedload transport (Lewis & Lewin, 1983; Howard, 1996; Ghinassi, 2011; Zinger et al., 2011). Cutoffs formed by over-bar or overbank incisions are formed by the downstream extension of an erosional embayment (Constantine et al., 2010b), by scroll slough process, i.e., the incision and widening of a swale of the point bar (Fisk, 1947; Grenfell et al., 2012) or by headward erosion (Gay et al., 1998):

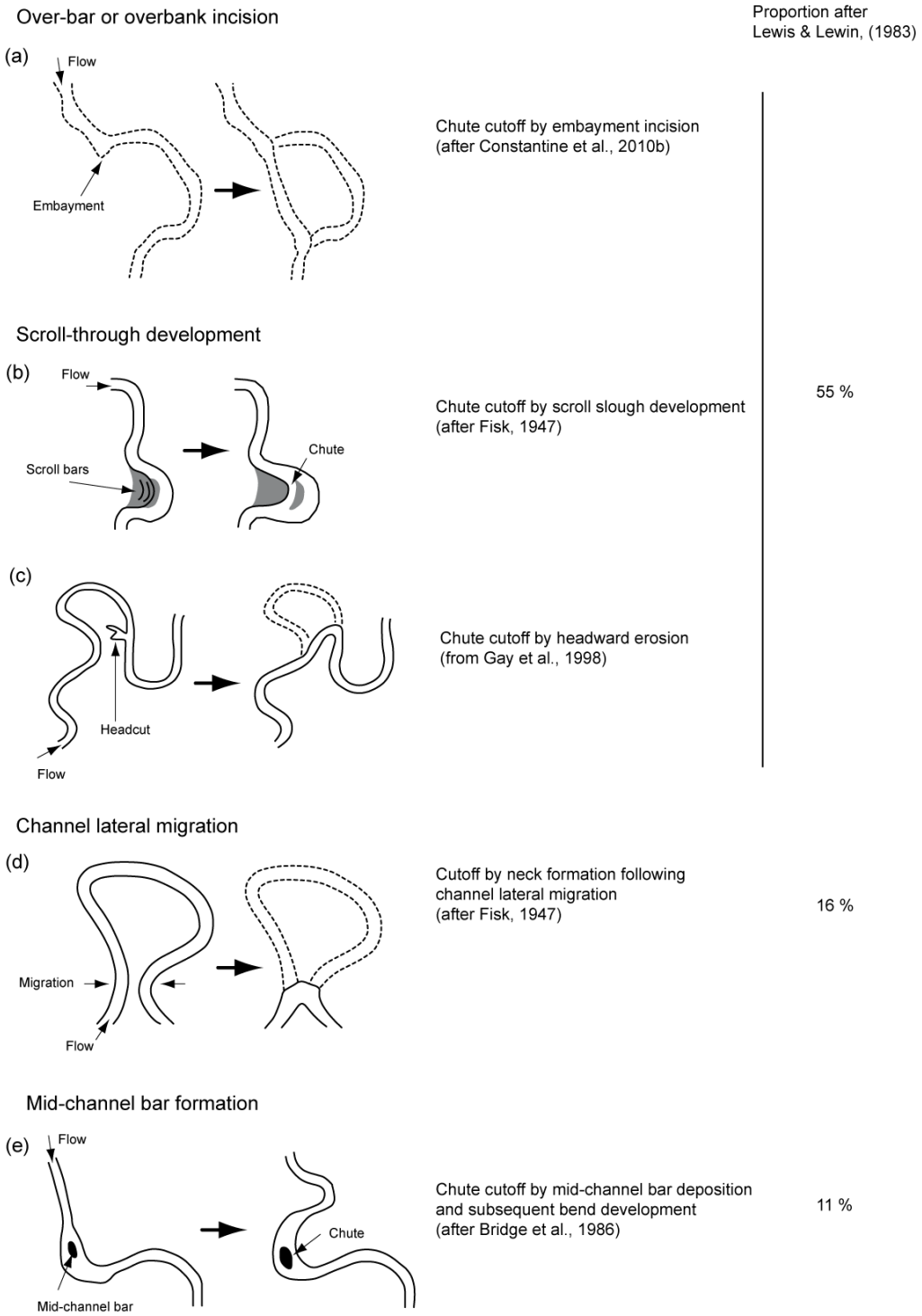

Figure 1.8: Cutoff mechanisms and geometries. **(a)** Headward erosion. **(b)** Embayment incision. **(c)** Scroll slough. **(d)** Neck formation. **(e)** Mid-channel bar formation. Adapted from Grenfell (2012). Proportions were taken from Lewis & Lewin (1983) after a study of 145 cutoffs in gravel bed rivers of Wales. The missing 18 percents are multi-loop (13%) and artificial cutoffs (5%).

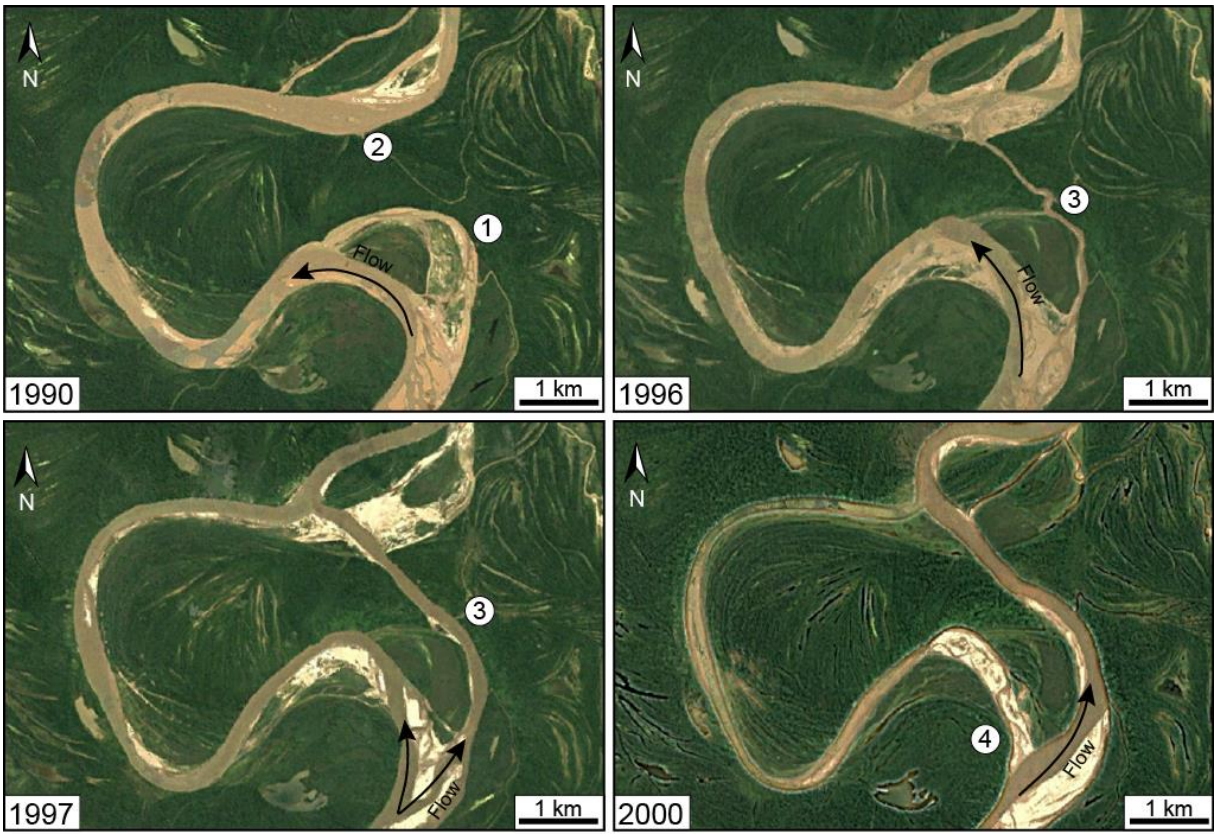

Figure 1.9: Satellite images showing chute cutoff initiation and evolution on the Ucayali River, Peru. Chute is initiated by incision of part of the point bar between two abandoned channels (1996) (1&2), leading to their widening (1997) (3). They become dominant by 2000 and the disconnected channel narrows quickly and a sand plug forms on its upstream part (4).

- Cutoff by erosional embayment is initiated by the erosion of the outer bank of the upstream reach of the meander (Constantine et al., 2010b). The erosion is at first local and then progresses downwards during successive floods. It forms an embayment (Fig. 1.10a) that can trigger chute cutoff. This type of chute cutoff appears to be controlled by the steepening of the floodplain slope and/or widening of the floodplain, the thinning of the vegetation and the reduction of sediment load all leading to an increase in the flow erosive power (Hauer & Habersack, 2009; Constantine et al., 2010b).
- Cutoff by swale widening occurs when a change in sediment load or inflow energy leads to the flooding of the point bar swales with enough erosive power to rework the point bar deposits (Grenfell et al., 2012). The flow is channelized through the swale and erodes its banks, leading to deepening and widening of the swale (Fig. 1.10b). If a swale becomes wide and deep enough it can capture most of the discharge and become the dominant channel (Fisk 1947; Grenfell et al., 2012).

- Cutoff by headward erosion requires superelevation of the water facilitating overbank flow across the point bar (Keller & Swanson, 1979; Thompson, 2003). This generally occurs due to the formation of dams (log-jams, ice-jams…) on the upstream part of the meander bend (Gay et al., 1998; Constantine et al., 2010b; Zinger et al., 2011) but can be due to an increase in sediment deposition that partially clogs the channel (Thompson, 2003). As the water spills back into the channel after following the steeper slope downstream it can incise the bank at the downstream part of the meander bend (Fig 1.11a). The resulting gully then propagates upwards (Fig. 1.11b, c, d) if high stage is maintained until it reaches the upstream part of the point bar. The two parts of the channel are then connected and a chute channel is created (Constantine et al., 2010b; Zinger et al., 2011). Headward erosion velocity depends on the overbank flow power relative to the erodibility of the bank, i.e., its cohesiveness and whether the ground is frozen or not (Gay et al., 1998; Constantine et al., 2010b).

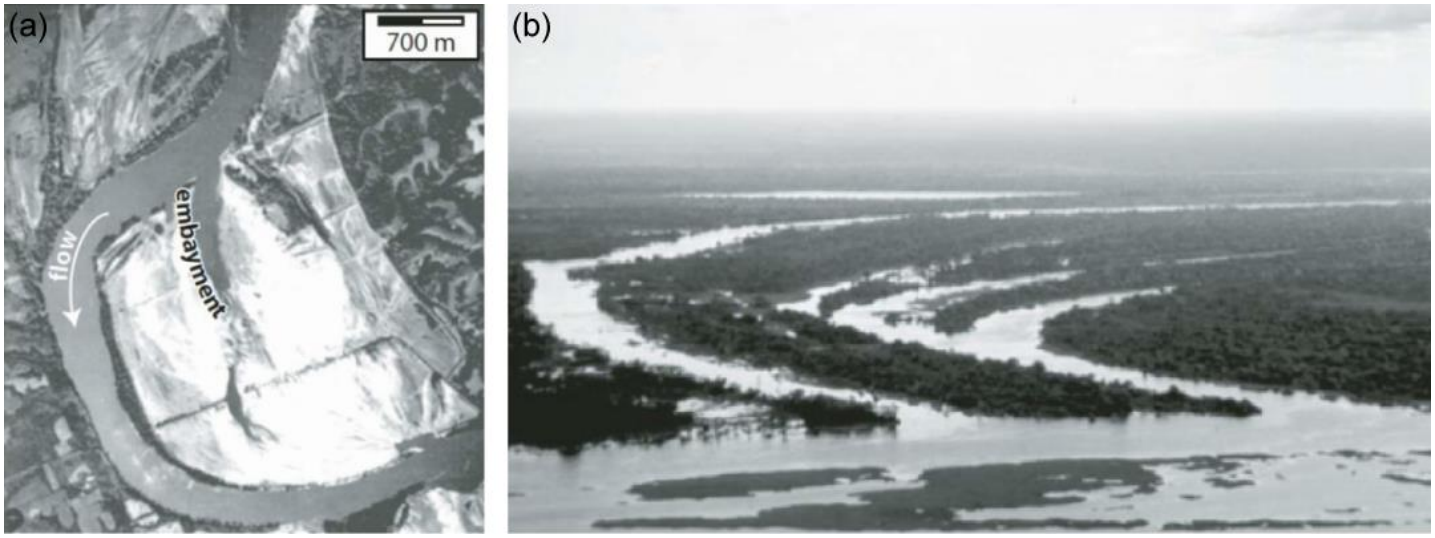

Figure 1.10: Cutoff formation processes. **(a)** Embayment formation on a meander bend of the Missouri River, USA. **(b)** Flooded swales in the Amazonian floodplain. Pictures from Constantine et al., 2010b.

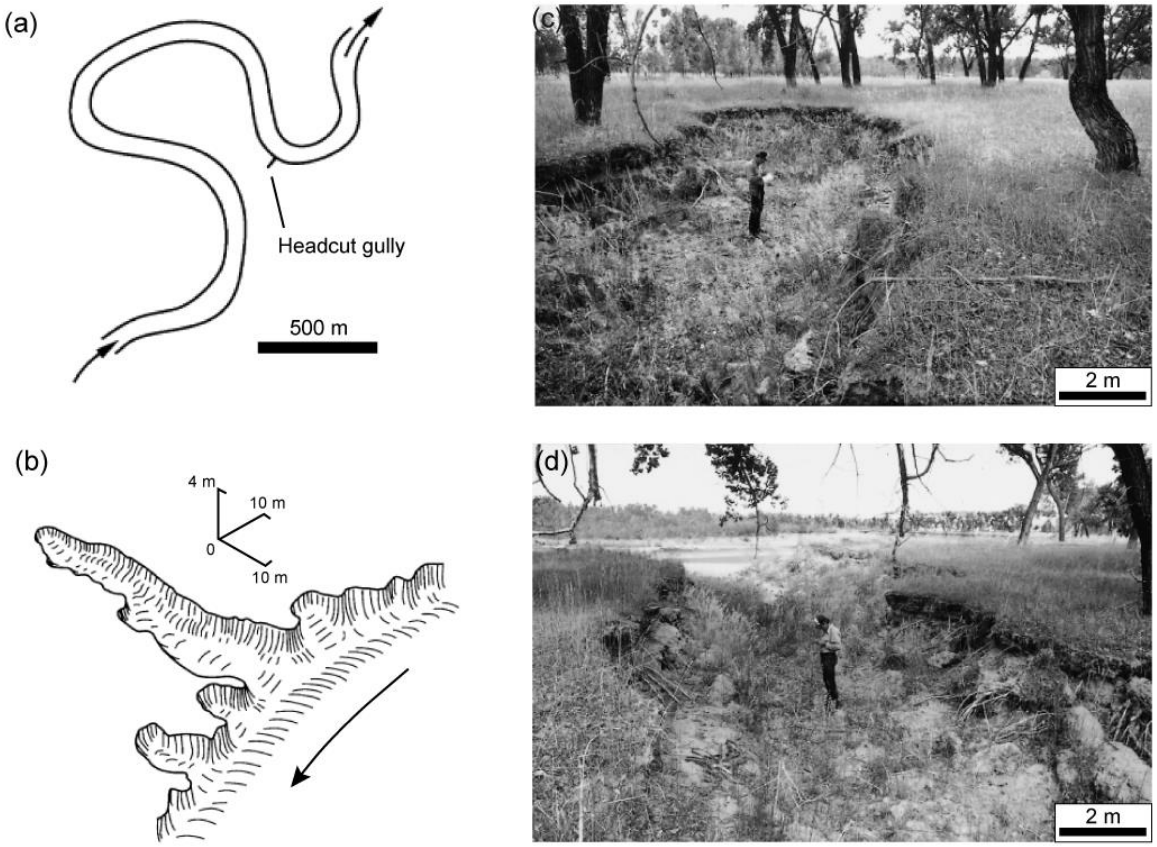

Figure 1.11: Sketch and pictures of headward erosion processes (Powder River, Montana, USA). **(a)** Schematic representation of the meander bend in 1985. **(b)** Isometric drawing of the gully. **(c-d)** Pictures of the gully facing upstream (c) and downstream (d). Adapted from Gay et al., 1998.

Cutoffs by channel lateral migration tend to form neck cutoffs (Fig. 1.8d), occurring late in the mature meander evolution (meander loop), either when the two opposite arms of the same bend join one another due to lateral migration (Fig. 1.12; Fisk, 1947; Gagliano & Howard, 1984), or when one meander bend migrates into another one (Gagliano & Howard, 1984). This drastically shortens the active channel as one or several entire meander bends are entirely removed. Due to the length of the channel that is bypassed by neck cutoff formation, an important slope difference between the newly connected upstream and downstream parts of the channel is created when the cutoff occurs (Gagliano & Howard, 1984). This induces local knickpoint regression due to the slope break, resulting in the upstream part of the abandoned channel being surelevated relatively to the active channel once equilibrium is reached. Neck cutoffs occur in low slope floodplains (Lewis & Lewin, 1983) as the low gradient favors the meander lateral mobility.

Figure 1.12: Satellite images showing neck cutoff initiation and evolution on the Ucayali River, Peru. The upstream arm of the bend migrates northward (1985-2014) until it joins the downstream arm of the bend, disconnecting the apex of the meander bend (2015).

Finally mid-channel bar formation can induce cutoff formation (Fig. 1.8e). This occurs by depositional processes, instead of erosion or incision as observed in the previous 4 categories of cutoffs. Channel widening and flow expansion lead to the formation of a stable mid-channel bar. The diversion of water by the stable mid-channel bar leads to the erosion of the channel banks and in some cases the development of a bend with a chute channel (Seminara, 2006; Bolla Pittaluga et al., 2009). Change in flow orientation at this bend favors the shorter channel, leading to disconnection (Bridge et al., 1986). This phenomenon appears to be the least common (Lewis & Lewin, 1983; Ashmore, 1991).

1.5. Current models for abandoned channels fill

During the disconnection process, the energy of the flow in the channel wanes, inducing a reduction in the grainsize of the sediments brought into the disconnecting channel, from coarse to very fine. Channel fill is formed by a mix of these sediments organized in a specific architecture depending on the channel geometry. The first studies to describing abandoned channel fills specified explicitly that abandoned channels are not exclusively filled by clays (Fisk, 1947; Allen, 1965; Bridge et al., 1986; Jordan & Pryor, 1992). Since then, many studies focused on the massive, homogeneous and sometimes laminated clay bodies found in abandoned channels (Bridge, 2003; Schwendel et al., 2015). Other studies focused on the coarse-grained fraction of the channel fill (Johnson & Paynter, 1967; Toonen et al., 2012; Cabello et al., 2018), and showed that many aspects of the channel fill deposition and architecture are still poorly understood (Donselaar & Overeem, 2008; Willis & Tang, 2010; Colombera et al., 2017; Cabello et al., 2018). This section will review the current knowledge on channel fill nature, formation and architecture as well as the factors and processes controlling the channel infilling.

1.5.1. Channel fill nature and geometry

Part of the abandoned channel fill is inherited from its active phase during which coarse channel lag deposits and bars are deposited. During the disconnection process the energy wanes in the channel and it loses its sediment transport capacity. A channel plug starts forming at the bifurcation with the dominant active channel (Fisk, 1947; Gagliano & Howard, 1984; Hooke, 1995), which further limits the flow capacity in the abandoned channel. This channel plug is described as a wedge-shaped body of fining-upwards coarse sediments. Two formation processes are proposed. The first considers that the channel plug is a sand (or gravel) bar located at the bifurcation that grows during successive flood events until it plugs the channel (Bridge et al., 1986; Plint, 1995; Bridge, 2003). The second plug formation

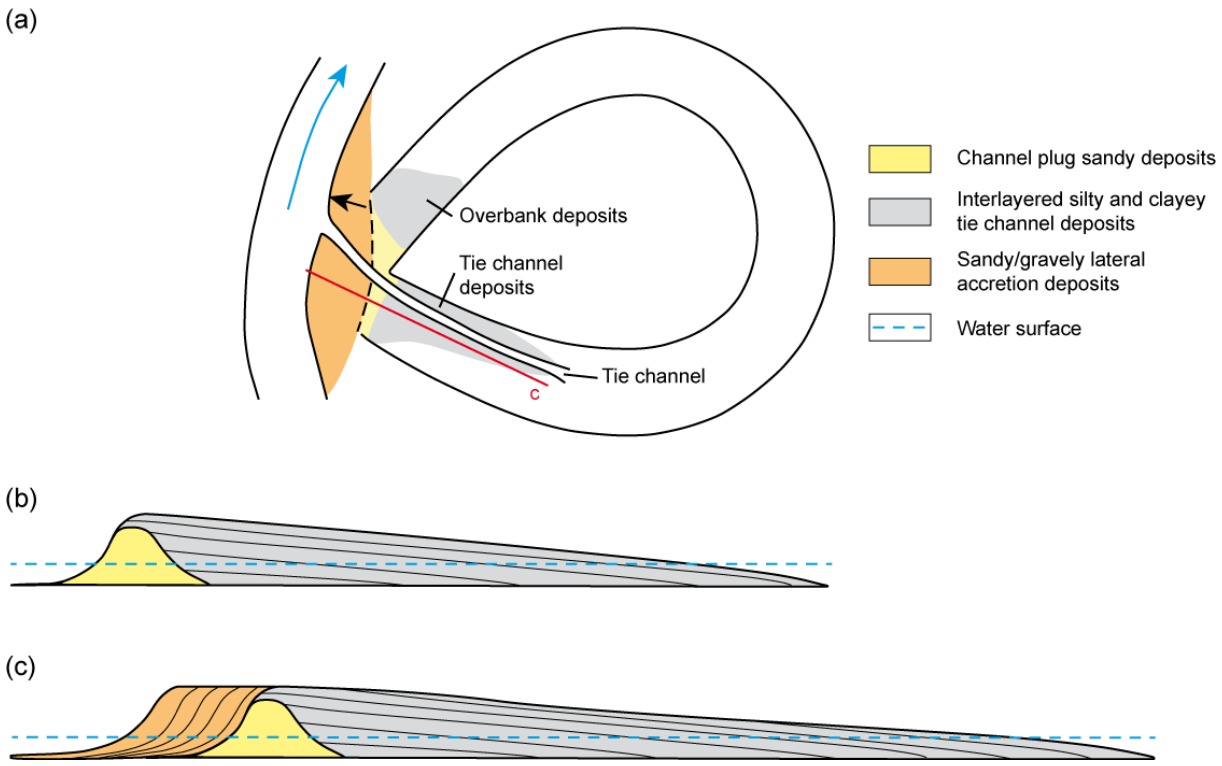

Fig. 1.13: Conceptual sketch illustrating the abandoned channel shape after disconnection **(a)** and channel plug architecture immediately after disconnection **(b)** and after the active channel migration **(c)**. After Rowland et al., (2005) Not to scale.

process describes it as having a thick and short coarse part in its upstream section similar to a sandbar that will be incised by a tie channel, i.e., a narrow channel that connect the active and abandoned channels through the channel plug (Fig. 1.13a) (Blake & Ollier, 1971). The tie channel can supply large volumes of suspended load sediments to the abandoned channel (Blake & Ollier, 1971; Rowland et al., 2005). These sediments form heterolithic deposits on and downstream of the channel plug when deposited (Fig. 1.13b-c). These heterolithic deposits form an extensive delta-like sedimentary body that extends the plug in the abandoned channel (Rowland et al., 2005). Mapping using historical aerial pictures and OSL dating of tie channels levees in different rivers showed that the resulting delta-like features progradation rate was dependent on abandoned channel dimensions ("deltas" in the larger ones need more sediments to advance), sediment supply and water-surface gradient between the active and abandoned channel (Rowland et al., 2005). The channel is abandoned when the tie channel is itself plugged or disconnected from the active channel. Tie channels can be frequent features in lowland rivers (Rowland et al., 2005). Abandoned channels can also fill from downstream when a secondary circulation going upstream from the confluence with the active channel is established during floods and can ultimately build another plug on the downstream part of the channel (Citterio & Piégay, 2009).

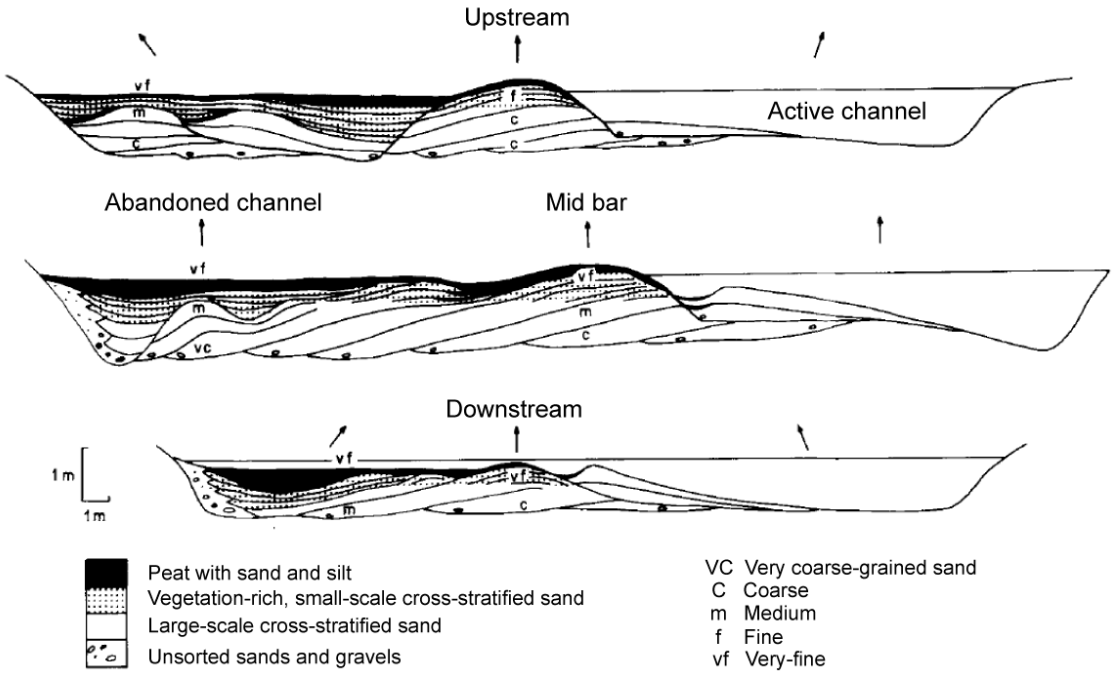

Figure 1.14: Channel fill deposits model for cross-sections along a channel bend. Arrows show the relative orientations of the active channel and bars. Bridge et al. (1986).

In the early years after channel disconnection, heterolithic deposits can still be formed in the channel thanks to overbank deposition (Citterio & Piégay, 2009), bank failure (Gautier et al., 2007) or downstream supply (if no downstream plug is formed or in tidal systems) (Piégay et al., 2008; Fernandes et al., 2016; Ganti et al., 2016b). As the distance with the active channel increases due to its migration, the overbank sediments supplied to the channel become finer and reach it less frequently (Piégay et al., 2008). Fine-grained sediments form in the channel thanks to these overbank events, runoff and the establishment of bogs forming peat. Heterolithic and fine-grained sediments fill the channel by draping the existing topography (Bridge et al., 1986) and gradually reduce the channel depth and width (Bridge et al., 1986; Toonen et al., 2012) until filling it completely (Fig. 1.14).

Thus, although most of the sediment deposited in the abandoned channel after channel plug formation are fine-grained, several processes can supply heterolithic deposits to the abandoned channel. Indeed, several studies have found that the channel fill can be very heterogeneous and even include sands (Fig. 1.15; Fisk, 1947; Bridge et al., 1986; Toonen et al., 2012; Cabello et al., 2018). Recent studies point out that the existence of coarse deposits in important proportions in some abandoned channels necessitates more studies focused on spatial heterogeneities in abandoned channels fills in order to gain a better understanding of their occurrence, formation processes and influence on the reservoir properties (Donselaar &

Overeem, 2008;Willis & Tang, 2010; Toonen et al., 2012; Colombera et al., 2017; Cabello et al., 2018).

Filling rates in abandoned channels vary in time. In the first stages of disconnection bedload can still enters the channel and coarse sediments are deposited, sometimes accounting for up to 40% of the sediment volume stored (Dieras et al., 2013). The channel plug growth, as well as the presence or absence and size of tie channels connecting the active and abandoned channels, are controlling the amount of sediment that can reach the disconnected channel (Rowland et al., 2005; Constantine et al., 2010a). After disconnection the channel fill rate depends on the proximity with the active channel and the magnitude and frequency of flooding events (Rowland et al., 2005; Piégay et al., 2008; Constantine et al., 2010a).

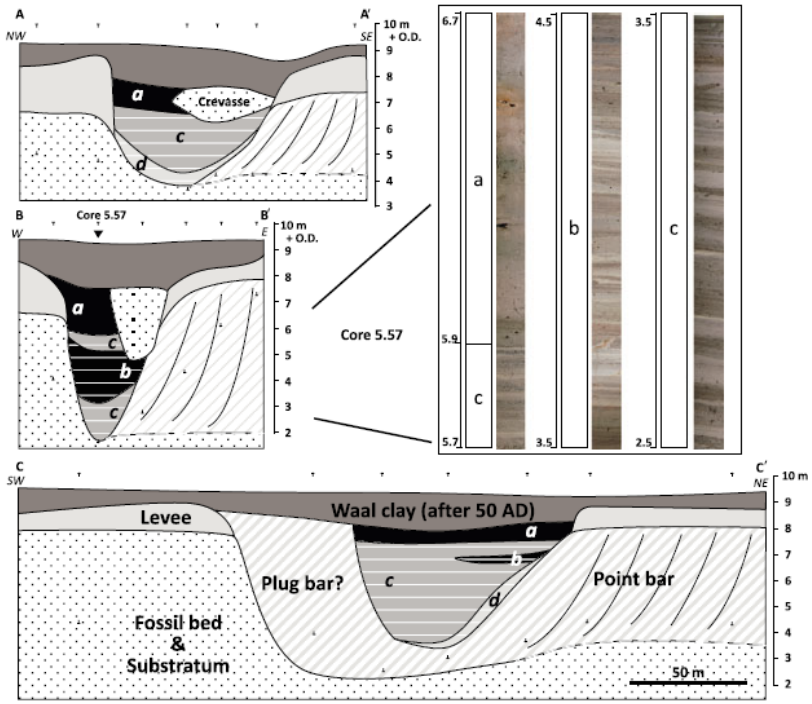

Figure 1.15: Example of detailed architecture analysis in an abandoned channel fill in a Rhine River cutoff (Netherlands). a: laminated clays. b: clayey silts. c: silts. d: silty sands (Toonen et al., 2012). Based on their observations the authors proposed that the channel fill grainsize evolution translates a global decrease in energy in the abandoned channel, with some flood-related coarser deposits intertwined in the fill.

Channels fill nature and geometry also appears to be controlled by the bifurcation and abandoned channel geometry, such as curvature, and disconnection process (Fig. 1.16):

- In the case of avulsions, a coarse channel plug thinning downstream forms at the bifurcation (Fig. 1.16a; Toonen et al., 2012; Dieras et al., 2013). When the avulsion is slow or when the bifurcation remains stable for some time before disconnection, the channel can adapt its width to its new, reduced, discharge by forming coarse lateral

accretion deposits (Sorrells & Royall, 2014; Reynolds & Royall, 2020). The remainder of the channel is filled with finer sediments brought during floods when the active channel overspills in the abandoned one (Stouthamer, 2001; Castanet, 2008), although some coarse deposits may also be found amongst the finer ones due to small channel reactivations (Stouthamer, 2001).

- During chute cutoffs events bedload continues to circulate in the channel during the early disconnection stages. Similarly to what happens in the case of avulsions, it form coarse deposits by lateral accretion when flow energy decreases (Fig. 1.16b; Fisk, 1947; Allen, 1965; Gibling, 2006; Toonen et al., 2012). Once the channel is fully disconnected from bedload supply from the active channel it is filled only by overbank deposits that most often supply fine sediments but sometimes coarser ones when the bedload spills in the floodplain (Fig. 1.15; Toonen et al., 2012).
- In the case of neck cutoffs the channel plugs appear to form very quickly at both extremities of the channel and the remainder of the channel is filled by overbank deposits during floods (Fisk, 1947; Allen, 1965). The overbank events drape clays in a concentric manner around the pre-existing geometries (Fig. 1.16c; Schumann, 1989; Gibling, 2006).

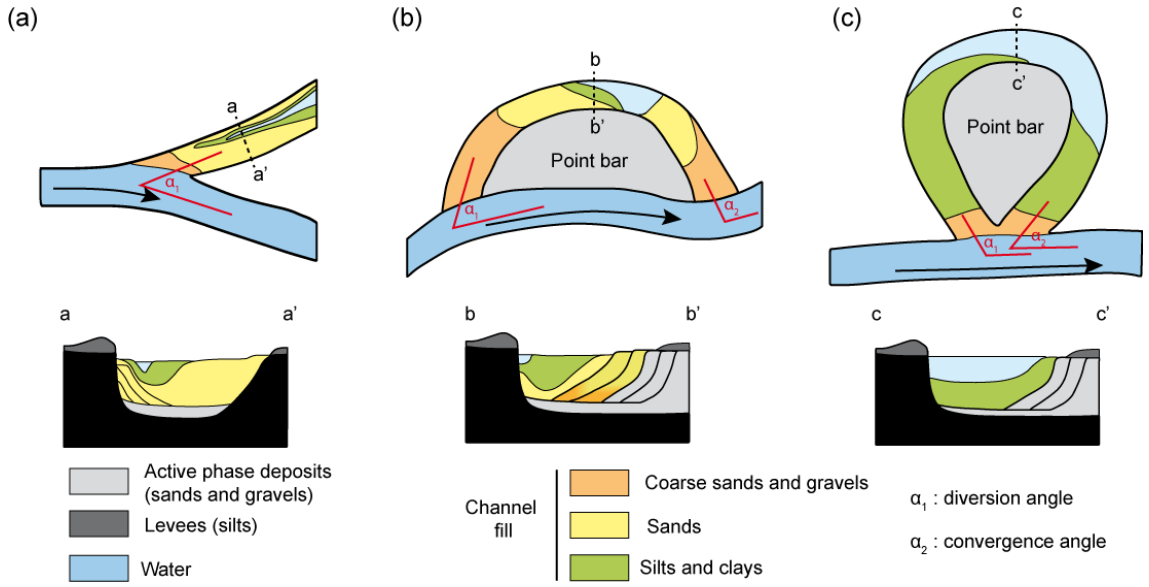

Figure 1.16: Conceptual sketches displaying the geometry and lithology of the channel fill depending on the disconnection type. **(a)** Avulsion. **(b)** Chute cutoff. **(c)** Neck cutoff. After Toonen et al. (2012) and Dieras (2013).

1.5.2. Current knowledge on processes controlling channel infilling

When abandonment occurs it can be separated in two phases (Jordan & Pryor, 1992): (i) the disconnection phase, or open abandoned channel stage during which the bedload becomes progressively disconnected from the channel to be abandoned and lasts years to decades (Fisk, 1947; Allen, 1965; Toonen et al., 2012; Richards & Konsoer, 2020), and (ii) the closed abandoned channel stage, which lasts centuries to millennia (Gagliano & Howard, 1984; Toonen et al. 2012; Ishii & Hori, 2016) and during which sediment is supplied without direct bedload connection to the active channel. In the following, the factors controlling bifurcation formation, their geometrical controls on disconnection and channel fill and the processes by which a closed abandoned channel is filled will be described.

1.5.2.1. Regional controls on channel abandonment and fill

Global and regional-scale factors control the creation of setup and trigger for the formation of bifurcations that can lead to channel abandonment according to the floodplain substratum lithology as well as the river type, its sinuosity and the global supply in sediment and water to the active channel and floodplain (Fig. 1.18). At the floodplain scale bifurcation formation is controlled by regional, long-term tectonics, local hydraulic regime and vegetation through the control of the regional sediment supply by the catchment geomorphology and the runoff. In turns this determines the floodplain geomorphology and the nature of the floodplain substratum. Alongside the vegetal cover (Micheli & Larsen, 2011; van Dijk et al., 2014) and the nature of the sediment available in the catchment, the catchment geomorphology and the runoff control floodplain sedimentation and thus bank erodibility, which in turn partially controls channel migration and sinuosity (Smith et al., 1998; Aslan et al., 2005; Schwendel et al., 2015) and thus the potential formation of bifurcations in the floodplain by cutoff or avulsion formation (Fig. 1.18; Jones & Hajek, 2007; Harrison et al., 2015). Global or local base level variations impact whether the channel is incising the floodplain or aggrading, thus impacting bifurcation formation (Stouthamer & Berendsen, 2000, 2001). Moreover, close to standing bodies of water, backwater effects (Chow, 1959) can elevate the channel water-surfaces upstream of the body of water, creating a perturbation zone – the backwater zone – along which the water surface slope is reduced and no longer parallel to the channel bed (Fig. 1.17). This promotes sediment deposition and can create backfilling deposition in the channel (Edmonds et al., 2009; Hoyal & Sheets, 2009; Chatanantavet et al., 2012; Nittrouer et al., 2012; Wilson & Goodbred, 2015; Fernandes et al., 2016).

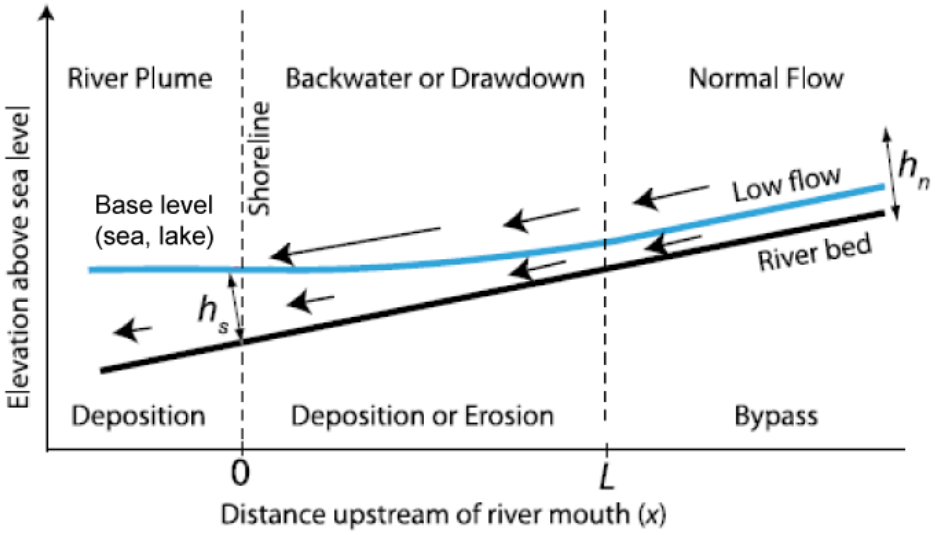

Figure 1.17: Illustrative sketch of backwater effects on channel water-surface elevation. x>L: Normal flow. 0<x<L: transitional region. x<0: offshore river plume. h_s: water depth at the shoreline. h_n: normal flow depth. Adapted from Lamb et al. (2012).

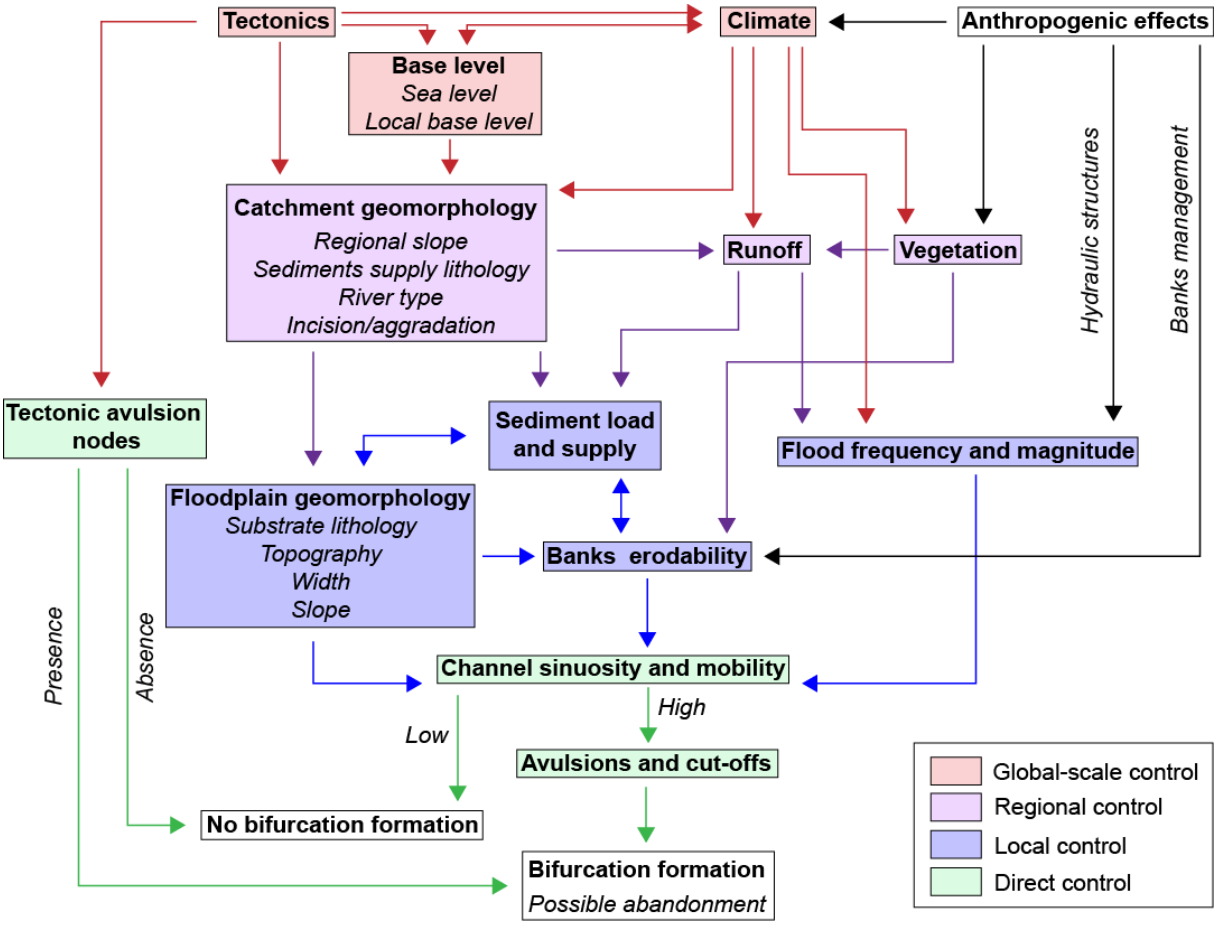

Figure 1.18: Diagram representing the scales, interactions and effects of the controls on bifurcation formation.

Global and regional-scale factors also control the overall quantity and grainsize of the sediment available for channel infilling. In the catchment and the floodplain, the sedimentary load available, i.e., the frequency and magnitude of floods able to mobilize it (Erskine et al., 1992) and the quantity of sediment as well as its repartition between suspended load and bedload (Gray et al., 2016), are the primary controls on the infilling nature and rate of abandoned channels, as mixed and suspended load rivers will be able to supply sediments to the abandoned channel long after it is disconnected from bedload supply (Hooke, 1995; Citterio & Piégay, 2009). The overall availability of the sediments for channel fill is controlled by several factors:

- The climate, including its regional high frequency periodic oscillations such as El Niño events (Aalto et al., 2003), control the frequency and magnitude of the floods (Berendsen & Stouthamer, 2000; Stouthamer & Berendsen, 2000; Ghinassi, 2011; Sidorchuk, 2001; Gouw, 2007) during which channels migrate and most of the sediment, notably the bedload, is transported and deposited in abandoned channels (Nicholas & Walling, 1997; Piégay et al., 2008; Sidorchuk et al., 2009; Ganti et al., 2016b). Climate also controls the catchment and floodplain vegetal cover. When present, the vegetation roots stabilize the banks and reduce their erodibility, decrease the runoff in the floodplain, reducing flood magnitude, and trap the finely-grained sediments before they reach the channel, reducing its filling rate (Makaske, 2001; Liébault & Piégay, 2002; Piégay et al., 2004; Rodrigues et al,. 2006; Wren et al., 2008; Micheli & Larsen, 2011; van Dijk et al., 2014; Harrison et al., 2015;).
- On the long term, tectonics variations also control,s the discharge and sediment supply, mostly by modifying the regional slope and relief of the catchment and floodplain (Heller & Paola, 1996; Stouthamer & Berendsen, 2000, 2001; Gouw, 2007; Reitz et al., 2015). Relief and slope increase positively impact the floodplain runoff and draining, which partially control the magnitude of the floods as well as the amount and nature of sediments eroded and supplied to the floodplain (Leddy et al., 1993). Tectonics also have a more direct control on bifurcation formation as avulsion nodes are potentially created by tectonic tilting or faulting (Schumann, 1989; McCarthy et al., 1992; Smith et al., 1997; Aslan & Blum, 1999; Ethridge et al., 1999; Morozova & Smith, 2000; Stouthamer & Berendsen, 2000).

Since human activities started modifying the soil occupation and reworking the river networks these phenomenons have been perturbed. Runoff and soil erosion have mostly been increased by the changes in soil occupation brought by agriculture, and deforestation and in some rare cases decreased by afforestation (Jacobson & Coleman, 1986; Gomez et al., 1998; Liébault & Piégay, 2002; Walling et al., 2003; Piégay et al., 2004, 2008; Shi et al., 2010; Micheli & Larsen, 2011; Erkens et al., 2011; Dutu et al., 2014). In the rivers, discharge and sediment supply have been reduced (Lecce, 1997; Liébault & Piégay, 2002; Piégay et al., 2004; Dutu et al., 2014), generally due to river damming, discharge regulation or banks protections in urban areas (Ethridge et al., 1999; Shi et al., 2010; Dépret et al., 2017).

1.5.2.2. Bifurcation dynamics and its control on disconnection

Once a bifurcation is formed, channel abandonment is dependent upon the stability of the bifurcation. In stable bifurcations, water and sediment partitioning at the bifurcation point is adjusted to downstream channel geometry and their resulting transport capacity (Fig. 1.19). The channels can remain stable for durations ranging from a few days in the case of some neck cutoff (Gay et al., 1998) to several years or decades in the case of chute cutoff or avulsions (Stouthamer & Berendsen, 2001; Toonen et al., 2012), before a perturbation destabilize them. At unstable bifurcations the water and sediment partitioning is not (or no longer) adapted to the channels morphologies. When the discharge and sediment load partitioning at the bifurcation results in a channel being sediment starved, the eroding capacity of the flow increases and it will start eroding the substrate, gaining in width and/or depth. However, when a channel receives more sediment than it can accommodate, bedload deposition is initiated, leading to its disconnection (Wang et al., 1995; Bolla Pittaluga et al., 2003), due to the formation of a channel plug. Thus at the bifurcation scale channel abandonment is controlled by the discharge and sediment load partitioning between the two channels and their capacity to accommodate it. The ability of a given channel (i) to adapt their morphology to discharge and sediment partitioning are controlled at the bifurcation scale by geometric and hydraulic factors: the channel width W_i, the channel depth D_i, and the resulting Width-Depth ratio (W_i/D_i *ratio*), the diversion angle α, the channel slope S_i, the water discharge Q_{wi} and sediment supply Q_{si} and the substrate erodibility E (Fig. 1.19).

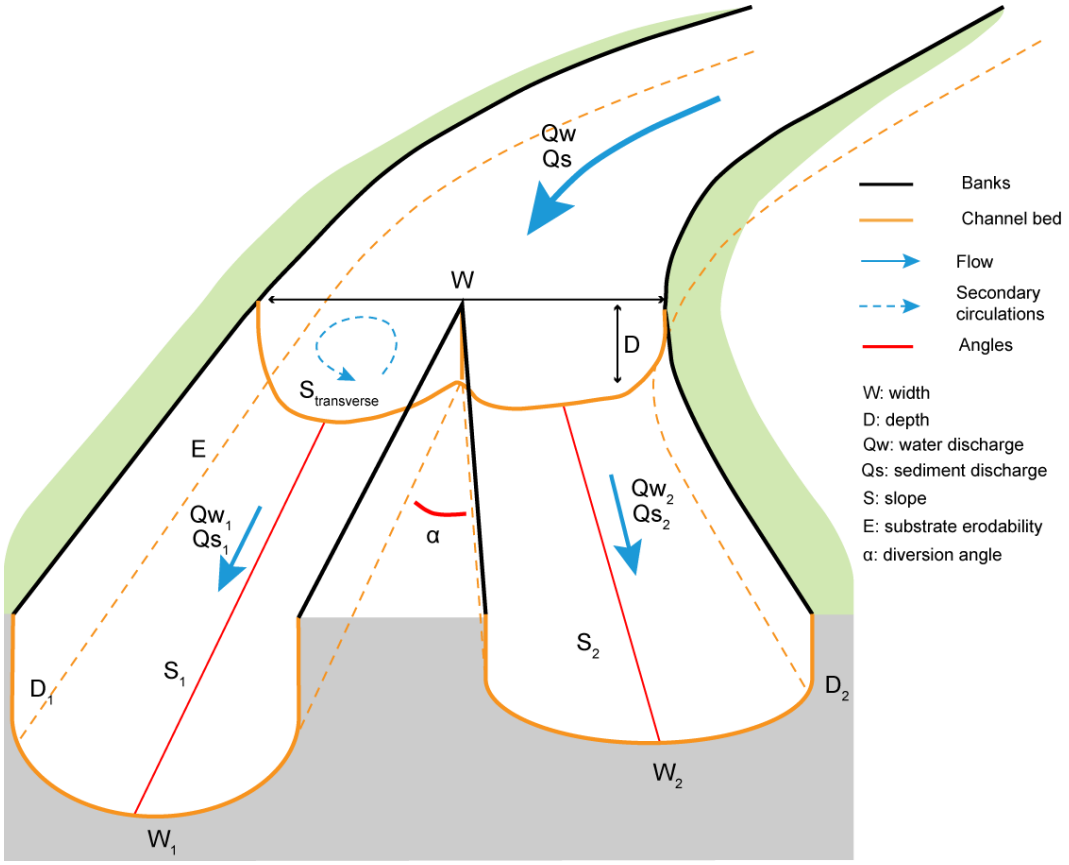

Figure 1.19: Sketch of a bifurcation highlighting the geometric and hydraulic factors controlling bifurcation stability.

These factors are controlled by global and regional parameters as described above (Fig. 1.18) but at the local scale they effectively control the bifurcation stability (Fig. 1.23) and thus the early stages of channel infilling when a bifurcation is destabilized and bedload deposition starts, forming the channel plug. Local modifications of the bifurcation geometry, such as the migration of a sandbar that adjusts the bifurcation angle (Bertoldi, 2012), have a strong impact on bifurcation stability that generally overcomes regional controls. In order to study the sediment distribution and stability of a bifurcation in a 1D morphodynamic model, Wang et al. (1995) determined that it was necessary to define a nodal-point relation. In their model, where a river bifurcates into two branches flowing into a lake, they determine that the ratio between specific sediment transport rates Q_s in each distributary is proportional to a power of the discharge ratio Q_w and the channel width W as follows:

$$\frac{Q_{s_1}}{Q_{s_2}} = \left[\frac{Q_{w_1}}{Q_{w_2}}\right]^k \left[\frac{W_1}{W_2}\right]^{1-k} \qquad (k > 0) \qquad Eq.\,1.1$$

Their exponent k appears to vary from case to case. Wang et al. (1995) determined that two equilibrium configurations exist for the bifurcation, one unstable with only one channel

remaining active (small *k*) and one where both channels remain open (large *k*). They verified their theoretical conclusions using numerical simulations.

Later on, this nodal-point concept has been expanded for a better understanding of the parameters controlling the discharge partitioning (van de Mark & Mosselman, 2012; Marra et al., 2014; Bolla Pittaluga et al., 2015; Schielen & Blom, 2018), or the study of braided river bifurcation through a quasi 2D model (Bolla Pittaluga et al., 2003). It was found that more possible equilibrium configurations exist, between three to five depending mostly on the nature of the bedload sediment supplied (sand, gravel, mixed), the Shields number of the upstream channel, the *W/D ratio* and the bed slope (Bolla Pittaluga et al., 2015; Schielen & Blom, 2018). These studies also pointed that the nodal-point relationship as determined can easily be perturbed in natural cases by the presence of bars, a gradient advantage in one channel or the upstream curvature of the channel, banks cohesiveness variations or bend sorting (Bolla Pittaluga et al., 2015; Schielen & Blom, 2018).

The dimensionless Shields number is used to calculate the initiation of sediment movement in a fluid. It is defined as:

$$\tau_* = \theta = \frac{\tau}{(\rho_s - \rho)gD} \qquad Eq.\,1.2$$

With τ the shear stress of the flow on the channel bed (kg m^{-1} s^{-2}), g the gravity (m s^{-2}), ρ and ρ_s respectively the water and sediment density in kg m^{-3} and D the sediment diameter in meters.

Field and flume studies suggest the importance of the Shields number on bifurcation stability through the control of the *W/D ratio* (Wang et al., 1995; Bertoldi et al., 2009b; Bolla Pittaluga et al., 2015). Similarly, the presence of bars in the channel is thought as a destabilizing factor for bifurcations (Fig. 1.23; Bertoldi & Tubino, 2007; Bertoldi, 2012). Indeed the presence of migrating bars usually increases with the W/D ratio. Bars can steer the flow and bedload in one channel or another, change the local longitudinal or transverse slope and modify the bifurcation diversion angle (Kleinhans et al., 2008; Bertoldi, 2012; van Dijk et al., 2014; Costigan & Gerken, 2016). The bars mobility and thus temporary presence can create a dynamic equilibrium at the bifurcation, but also sometime permanently destabilize it, leading to channel abandonment (Fig. 1.23).

Sediment partitioning was found to be proportional to the downstream channel elevation, as the suspended sediment concentration decreases exponentially upwards (Slingerland & Smith, 1998). In the case of a differential bed elevation between the downstream channels of the bifurcation, the channel with the lower bed elevation will draw both the bedload and the lower part of the water column which carries more suspended sediments, whereas the channel with the more elevated bed will draw water from the upper part of the water column that contains less suspended sediment (Slingerland & Smith, 2004). Similarly, channel slope is often different between each distributary and the upstream channel (Fig. 1.19) and the downstream channel with the higher slope (longitudinal or transverse) receives a more important part of the discharge and bedload (Fig. 1.20) (Slingerland & Smith, 1998; Bolla Pittaluga et al., 2003; Miori et al., 2006; Kleinhans et al., 2008, 2013). The slope of the abandoned channel also partially controls the channel filling rate once it is disconnected (Gagliano & Howard, 1984). The effect of the slope can be compensated or increased by an upstream curvature of the channel as the water inertia will favor the channel that stems from the external bank of the bend (Fig. 1.20) (Kleinhans et al., 2008, 2011, 2013; Hardy et al., 2011).

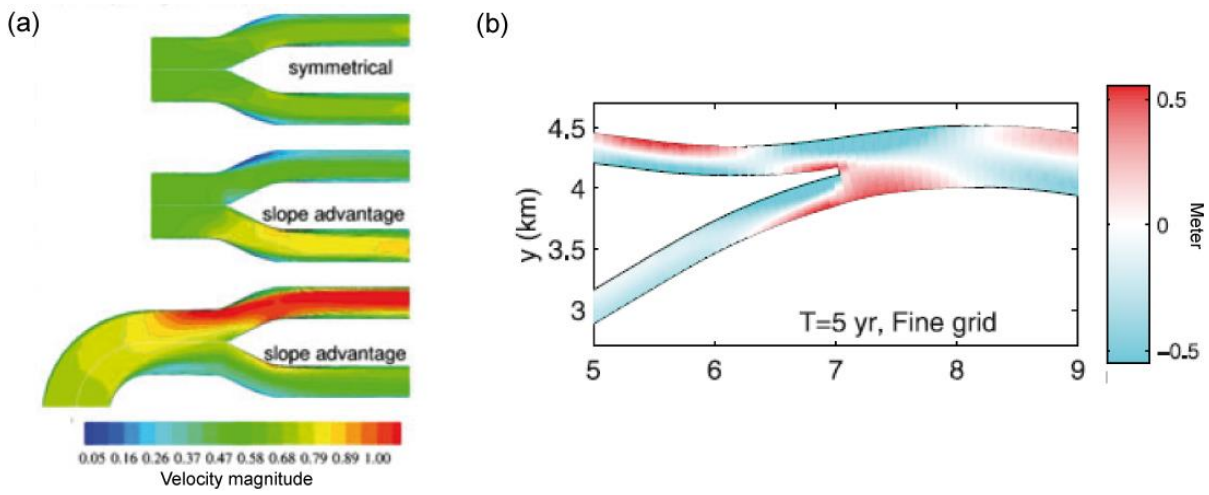

Figure 1.20: Effect of the upstream slope advantage and curvature on flow (a) and sediment erosion or deposition (b). From Kleinhans et al., 2008 & 2013.

The water-surface slopes in the channels, and the ratio of the water-surface slopes in both channels, have a significant influence on channel disconnection and sedimentary fill (Grenfell, 2012). Through numerical modeling and field study, Edmonds & Slingerland (2008) showed that an increase in the water surface slope in a distributary increases the shear stress and encourages bedload transport through the channel, whereas deposition is encouraged in the other distributary. Indeed, Slingerland & Smith (1998, 2004) demonstrated that the water slope ratio controlled the channel capacity to capture discharge, and that a

water-surface slope ratio advantage of 4 to 5 led to total capture of the flow and disconnection of one of the channels. The water surface slope ratio between the channels is linked to the channel bed slope and length. In cutoff cases, when both channels separate and link back downstream, the bed – and water surface – slope ratio can be estimated using the length ratio between the channels. Indeed, the elevation differential between the bifurcation and the confluence are the same for both channels and thus the slopes are controlled by the length of the channels. With the slope measured as follow:

$$S = \frac{(z_b - z_c)}{L} \qquad Eq.\,1.3$$

With S the channel slope, L the channel length and z_b and z_c the bed – or water – elevation at the bifurcation and confluence, respectively (Fig. 1.21). Thus the slope ratio S_2/S_1 can be estimated as:

$$\frac{S_2}{S_1} = \frac{\frac{(z_b - z_c)}{L_2}}{\frac{(z_b - z_c)}{L_1}} = \frac{(z_b - z_c)}{L_2} * \frac{L_1}{(z_b - z_c)} = \frac{L_1}{L_2} \qquad Eq.\,1.4$$

Consequently, in cutoff cases the relative slope ratio between the channels can be estimated using the channels length, even when no elevation data is available, such as in aerial pictures or maps. This is a useful tool for the study of abandoned channel fill deposits, as demonstrated by Dieras (2013) who linked the ratio of slopes to oxbow lakes infilling rate by a linear relationship, using a similar method. However, this assumes the absence of slope-breaks or knickpoints in the channels.

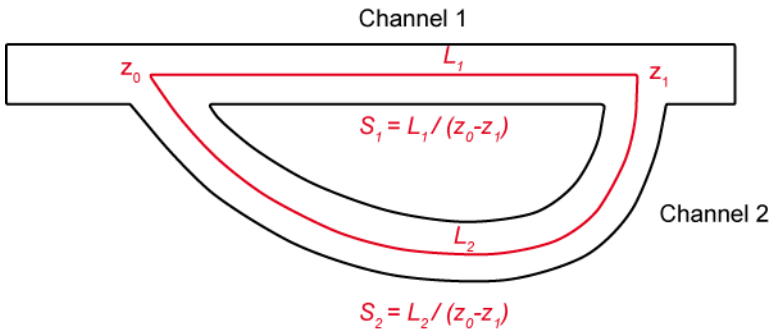

Figure 1.21: Sketch illustrating the relationship between length and slope ratios in cutoff cases that allows slope ratio measurement without having access to elevation data.

Finally, the diversion angle, whose value is controlled by the banks erodability (Federici & Paola, 2003; Bertoldi & Tubino, 2007; Kleinhans et al., 2008, 2013), the upstream geometry of the channel (Kleinhans et al., 2008, 2011, 2013; Hardy et al., 2011; Bertoldi, 2012) and the presence of bars (Slingerland & Smith, 1998; Federici & Paola, 2003; Bertoldi & Tubino, 2007; Kleinhans et al., 2008; Bertoldi, 2012; Miori et al., 2012) is the final geometrical control on discharge and bedload partitioning at the bifurcation as it creates secondary circulations at the bifurcation and in the downstream channels (Figs. 1.19 & 1.22a) (de Heer & Mosselman, 2004; Le Coz et al., 2010; Constantine et al., 2010a; van der Mark & Mosselman, 2012) that affect the discharge and sediment partitioning (Fig. 1.23). These secondary circulations can steer the flow and bedload towards one channel and their width is controlled by the diversion angle value. Bulle (1926) and de Heer & Mosselman (2004) have shown that an important part of the bedload is steered towards the channel with the highest diversion angle compared to the upstream channel as the flow near the channel bed is naturally steered towards the internal part of the bend whereas the surface flow is steered towards the external bend. This Bulle effect (Bulle, 1926; de Heer & Mosselman, 2004) is however inhibited by a high *W/D ratio* (de Heer & Mosselman, 2004).

Through the secondary circulations, the diversion angle is believed to be directly responsible of channel abandonment as the higher the diversion angle, the larger the *flow separation zone* (Fig. 1.22b-c), a zone on the external bank of the channel just downstream of the bifurcation point where the flow loses its energy and sediment is deposited (Bulle, 1926; de Heer & Mosselman, 2004; Constantine et al., 2010a; Le Coz et al., 2010). The flow separation zone width is also controlled by the shape of the bifurcation as a sharp wedge forming the angle between the two channels results in a thinner flow separation zone than a blunted one (de Heer & Mosselman, 2004; Le Coz et al., 2010). It is theorized that the value of the diversion angle controls the abandonment speed (Fisk, 1947; Lindner, 1953; Allen, 1965; Shields & Abt, 1989; Piégay et al., 2008; Constantine et al., 2010a; Micheli & Larsen, 2011; Toonen et al., 2012; Dutu et al., 2014; Costigan & Gerken, 2016; Dépret et al., 2017), possibly through this flow separation zone value, but it was never formally quantified (Constantine et al., 2010a). This would explain the differences observed in the fillings of chute and neck cutoffs and avulsions (Fig. 1.16; Fisk, 1947; Allen, 1965; Toonen et al., 2012).

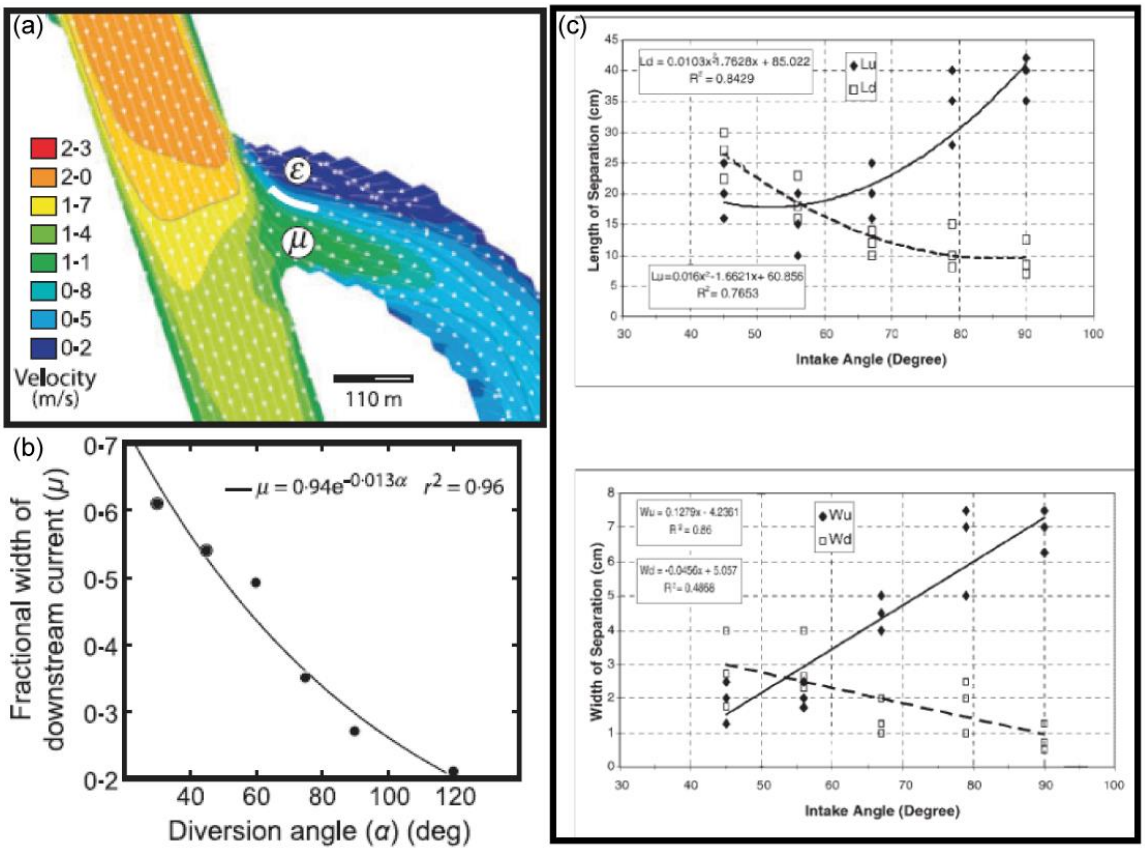

Figure 1.22: Effects of the diversion angle on the flow separation zone. Flow velocity modeling for a 60° bifurcation. μ: fraction of the total abandoned channel width occupied by the downstream flow cross-section. ε: flow separation zone **(a)**. Relationship between the diversion angle value and the flow separation zone width **(b)**. **(a-b)** from Constantine et al. (2010b). Relationship between the diversion angle value and the flow separation zone length and width at the upstream and downstream entrances of a water intake. *Lu*: length upstream. *Ld*: length downstream. *Wu*: width upstream. *Wd*: width downstream. From Keshavarzi & Habibi (2005) **(c)**.

The bifurcation is a dynamic geomorphic feature whose stability cannot be guaranteed in time as the temporal and spatial evolution of both the upstream channel and the bifurcation itself can at any moment create a perturbation that will destabilize it. In answer to this destabilization, the bifurcation will adapt its stability configuration and geometry, potentially leading to channel abandonment (Fig. 1.23). It is interesting to note that symmetrical bifurcations (with an equal partitioning of water and sediment in each channel) are not stable nor found in nature (Bolla Pittaluga et al., 2003, 2015: Schielen & Blom ,2018) and that stable bifurcations are asymmetrical (unequal partitioning of water and sediment, unequal width and depth (Fig. 1.19), the most extreme state of asymmetry being when one channel is fully disconnected from the active channel.

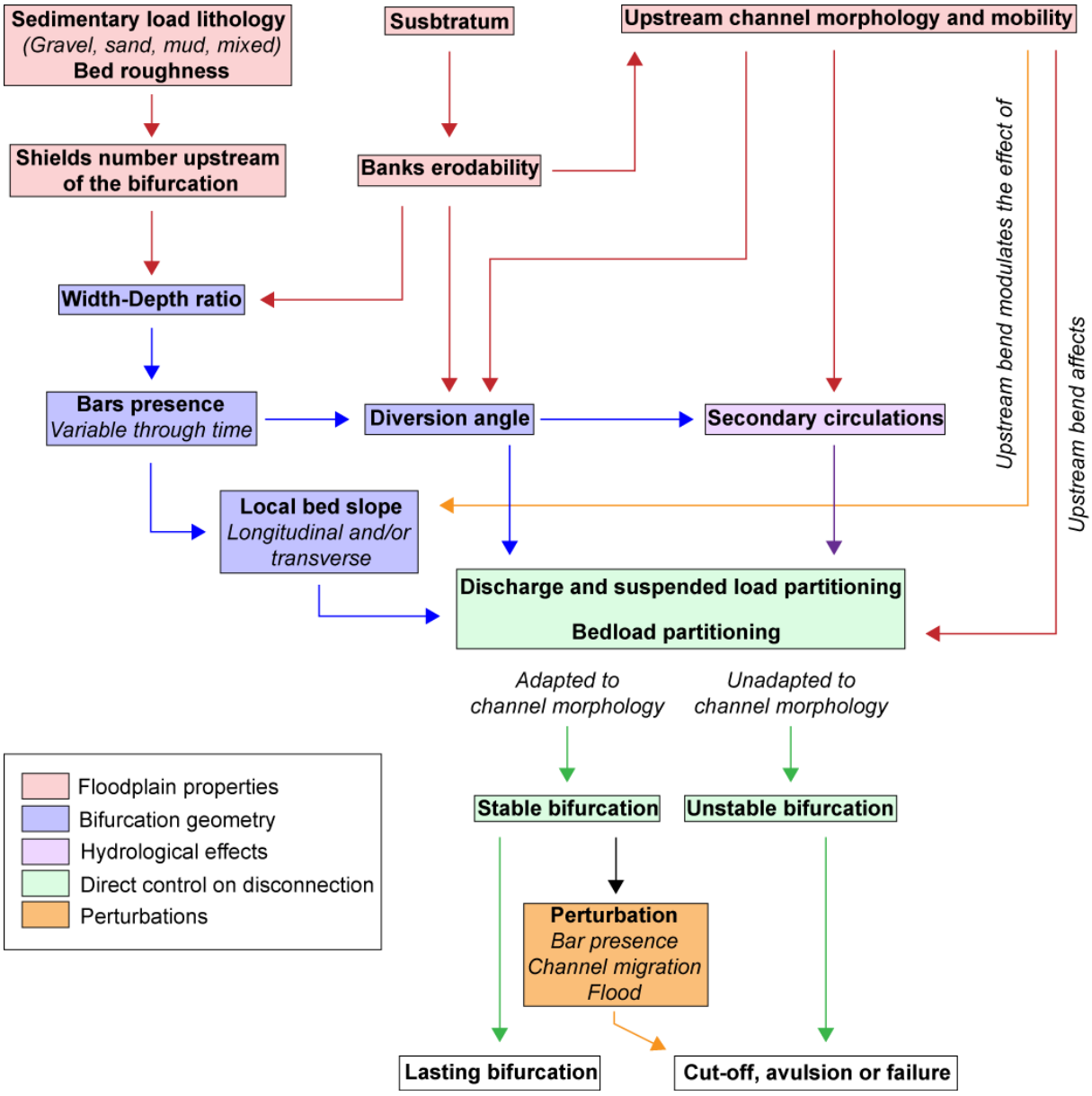

Figure 1.23: Diagram representing the local and geometric factors controlling bifurcation stability and their interactions.

1.5.2.3. Closed-stage channel filling processes

Once the abandoned channel is disconnected from bed- and suspended load by the formation of the channel plug, its sediment supply is limited to overbank sediments (Jordan & Pryor 1992). The farther away the active channel is the finer and rarer the sediment supply will be (Erskine et al., 1992; Nicholas & Walling, 1997; Makaske et al., 2002; Piégay et al., 2008; Wren et al., 2008; Citterio & Piégay, 2009; Gray et al., 2016). A transitional stage may correspond to the development of a tie channel supplying intermediate grainsize deposits (Fig. 1.13). When the abandoned channel is isolated, it forms an area of still water that is filled by

the occasionally supplied fine-grained, suspended material, or accumulation of organic matter and carbonate from the organisms living in the still water. Thus both the abandoned channel filling rate and the grainsize of fill sediments are determined by the type of connectivity between the active and abandoned channel (Amoros, 2001; Sutton et al., 2004; Latterell et al., 2006; Citterio & Piégay, 2009; Gray et al., 2016; Coffey & Shaw, 2017). A simple classification by Amoros (2001) describes three types of connectivity, based on distance from the active channel and/or flood magnitude and frequency:

- Connectivity to the active channel inexistent or rare, only during centennial floods. In this case the channel is filled by finely-grained overbank deposits.
- Connection during annual or decennial floods. The channel is filled by fine and sometimes coarser overbank deposits.
- Permanent connection from downstream, supplying bedload during floods. In rare cases the connection can be permanent from upstream and the downstream part is the plugged channel (Fisk 1947; Saucier, 1994; Citterio & Piégay, 2009).

The distance from the active channel varies in time as it migrates in the floodplain. It is generally accepted that the more filled an abandoned channel is, the older the abandonment is and that the amount of deposited sediment increases with time but the filling rate decreases with distance from the active channel (Shields & Abt, 1989; Erskine et al., 1992; Hooke, 1995; Piégay et al., 2008; Wren et al., 2008; Citterio & Piégay, 2009), although some exceptions of closely connected yet still almost empty channels can be observed (Fisk, 1944). The amount of sediment stored is dependent on the abandoned channel volume (Vella et al., 2005; Gray et al., 2016).

Abandoned channels can be reoccupied after their disconnection, either by their reactivation or their capture by another channel of the floodplain (Smith et al., 1998; Aslan & Blum, 1999; Mohrig et al., 2000; Stouthamer, 2001; Makaske et al., 2002; Aslan et al., 2005; Gray et al., 2016; Reitz et al., 2010; Toonen et al,. 2012). Thus sometimes several phases of sediment deposition are observed in abandoned channel fills, separated by erosional surfaces that mark the channel reactivation (Fisk, 1947; Makaske, 2001; Stouthamer & Berendsen, 2001; Aslan et al., 2005).

1.6. Conclusion

The earlier descriptions of channel fills, as made by Fisk (1947), Schumm (1960) and Allen (1965) were comprehensive descriptions that represented channel fills as heterogeneous sedimentary bodies composed of a coarsely-grained fraction deposited in the early stages of the disconnection, and fine-grained sediments that fill the channel after its abandonment. (Fig. 1.24a). Although more and more studies have shown that the channel fills were complex structures incorporating significant volumes of coarsely-grained sediments (Johnson & Paynter, 1967; Bridge et al., 1986; Hooke, 1995; Donselaar & Overeem, 2008; Toonen et al., 2012; Colombera et al., 2017; Cabello et al., 2018), the channel fill architecture is often simplified to massive clay deposits for modeling purposes (Fig. 1.24b) (e.g., Parker et al., 2011).

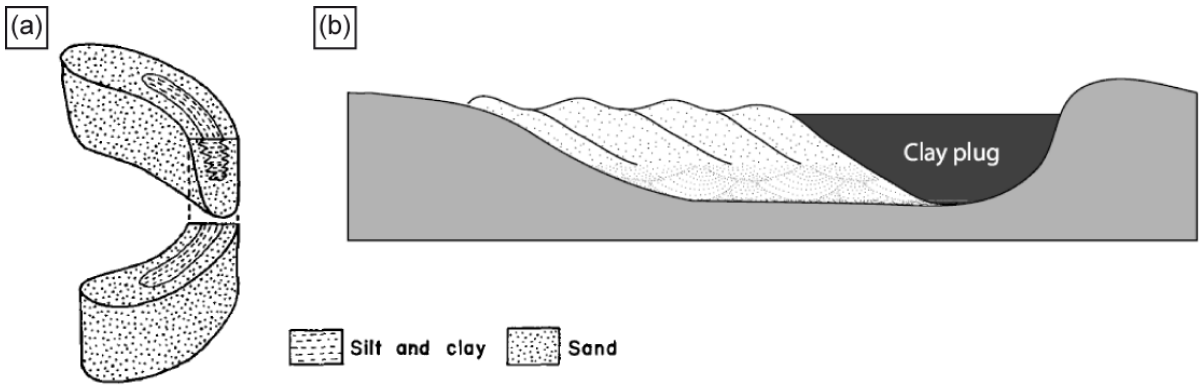

Figure 1.24: Channel fill deposits as described by Allen (1965) after the works of Fisk (1947) and Schumm (1960) **(a)** and representation of a channel fill cross-section filled by clays as commonly described, as pointed out by Donselaar & Overeem (2008) (**b**). Allen (1965) and Donselaar & Overeem (2008).

The deposition processes – and resulting architectures – of the coarse-grained part of the channel fill remain poorly understood. Indeed, bifurcations can remain stable for several years before being suddenly disconnected, or form unstable and be very quickly abandoned. Thus observation of the actual disconnection initiation and of the early stages of fill deposition can be difficult to achieve as a constant, potentially year-long monitoring of the bifurcation can be necessary. The study of the coarse-grained deposits is further complicated by their rapid covering by finer sediments or vegetation, making the determination of their architecture difficult.

Consequently many questions still surround abandoned channel bedload fill deposits. For instance, are the coarse-grained bars found in the channel formed during the disconnection phase when the energy in the channel wanes, and thus part of the channel fill, or are they

channel bed or lag deposits? Similarly, the channel plug definition needs to be precised on an architectural level. Although most studies describe it as a wedge-shaped body thinning toward the abandoned channel (Fisk, 1947; Allen, 1965; Rowland et al., 2005), what is exactly the channel plug made of? In the description made by Rowland et al. (2005), is it the whole composite body formed during the connection to the active channel via direct connection or tie channel, or is it only the coarse upstream part (Fig. 1.13)? Is it really wedge-shaped or akin to a levee? Similarly, the factors controlling the deposition, architecture and spatial distribution of these coarse deposits have not been determined yet.

This study focuses on the coarse-grained deposits of the channel fill to propose relationships between the bifurcation geometry, depositional processes and resulting architecture. In the following, the coarse-grained sediments deposited after the initiation of the disconnection phase are considered as channel fill, to differentiate bed load deposits from the active and abandonment phase deposits.

Chapter 2: Bedload dynamics and deposition in abandoned channels using an experimental bifurcation setup

Ce chapitre présente des experiences de laboratoire modélisant une bifurcation afin de tester les contrôles sur l'abandon de chenaux (angle de bifurcation, pente initiale du lit, variations des pentes des surfaces libres ou la présence d'un lit érodable) et une détermination de leurs effets sur la longueur, le volume et les processus de formation du bouchon sableux. La première section (2.1), qui est la retranscription d'un article publié dans Earth Surface Dynamics (https://esurf.copernicus.org/articles/8/275/2020/), se concentre sur l'angle de bifurcation.

La seconde section (2.2) décrit des expériences similaires réalisées dans le but de déterminer les effets de la présence d'un lit érodable et de la modification des pentes des surfaces libres sur la géométrie du bouchon sableux.

This chapter introduces flume experiments conducted in a bifurcation setup to test controls on channel abandonment (bifurcation angle, initial bed slope, varying free surface slope and the presence of an erodible sand bed) with a specific focus on their effect on sand plug length, volume and deposition processes. The first section (2.1), which is the transcript of an article published in Earth Surface Dynamics (https://esurf.copernicus.org/articles/8/275/2020/), focuses mostly on the bifurcation angle:

> SZEWCZYK, L., GRIMAUD, J.-L., COJAN, I., 2020. Experimental evidence for bifurcation angles control on abandoned channel fill geometry. Earth Surface Dynamics, 8, 275-288. https://doi.org/10.5194/esurf-8-275-2020.

The second section (2.2) describes similar experiments that were conducted in the aim of determining the effects of different forcings, i.e. the presence of an erodible sand bed and the modification of the free surface slope in one distributary channel, on the sand plug geometry.

2.1. Experimental evidences for bifurcation angles control on abandoned channel fill geometry

2.1.1. Abstract

The nature of abandoned channels' sedimentary fills has a significant influence on the development and evolution of floodplains and ultimately on fluvial reservoir geometry. A control of bifurcation geometry (i.e., bifurcation angle) on channel abandonment dynamics and resulting channel fills, such as sand plugs, has been intuited many times but never quantified. In this study, we present a series of experiments focusing on bedload transport designed to test the conditions for channel abandonment by modifying the bifurcation angle between channels, the flow incidence angles and the differential channel bottom slopes. We find that disconnection is possible in the case of asymmetrical bifurcations with high diversion angle (≥ 30) and quantify for the first time an inverse relationship between diversion angle and sand plug length and volume. The resulting sand plug formation is initiated in the flow separation zone at the external bank of the mouth of the diverted channel. Sedimentation in this zone induces a feedback loop leading to sand plug growth, discharge decrease and eventually to channel disconnection. Finally, the formation processes and final complex architecture of sand plugs are described, allowing for a better understanding of their geometry. Although our setup lacks some of the complexity of natural rivers, our results seem to apply at larger scales. Taken into account, these new data will improve fluvial (reservoir) models by incorporating more realistic topography and grain size description in abandoned channels.

2.1.2. Introduction

Abandoned channels are ubiquitous features of the alluvial plain, which have a huge impact on the fluvial system evolution and properties. First, abandoned channels form local topographic lows that trap sediments (Aalto et al., 2008; Lauer & Parker, 2008; Dieras et al., 2013) and host wetlands (Novitzky et al., 1996; Ward et al., 1999). Second, the fine-grain fraction of their filling may influence active channels migration, as clays are more resistant to erosion than sandy sediments (Howard, 1992; Smith et al., 1998; Berendsen & Stouthamer, 2000; Schwendel et al., 2015). Last, abandoned channels are filled with sediments of varied permeability, which may impact flow path in active alluvial plains (Flipo et al., 2014) and ultimately in the resulting geological reservoir (Miall, 1996; Willis & Tang, 2010; Colombera et al., 2017; Cabello et al., 2018). Indeed, recent studies have shown that sedimentary fills are

complex bodies and may contain coarser sediments than initially assumed (Hooke, 1995; Toonen et al., 2012; Dieras et al., 2013). When integrated to reservoir flow simulations, these coarse deposits may drastically change the connectivity of otherwise isolated sand bodies (e.g., point bars; Donselaar & Overeem, 2008).

Currently, abandoned channels are studied on the field (Hooke, 1995; Constantine et al., 2010a; Dieras et al., 2013) but less so in numerical models and experiments. Different styles of abandonment are observed in fluvial systems (i.e., cutoffs, avulsions), implying the formation of sedimentary fills of various grain sizes and geometries (Allen, 1965; Toonen et al., 2012; Fig. 2.1). A common thread to existing models is that abandonment is the consequence of the formation of a wedge-shaped sand plug in one of two channels shortly after a bifurcation (Fig. 2.1). Disconnected channels are then mostly filled by fine-grained overbank flood sediment (Bridge et al., 1986; Plint, 1995; Bridge, 2003). The coarse deposits are introduced beforehand as bedload, i.e., as long as there is a connection with the active channel. The dynamics at the bifurcation during the disconnection phase have therefore a key control on the sediment architecture of later abandoned channels (Bertoldi, 2012; Bolla Pittaluga et al., 2015; Constantine et al., 2010a; Kleinhans et al., 2013).

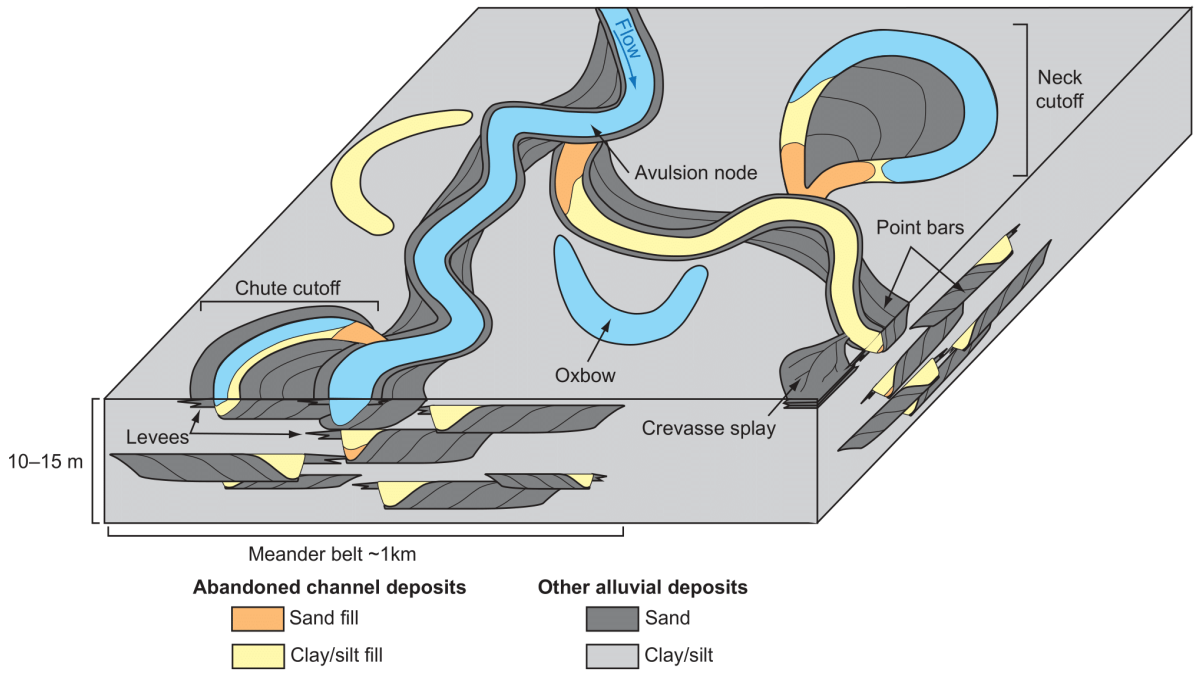

Figure 2.1: 3-D sketch showing the occurrences of deposits associated with abandoned channels in an alluvial plain.

Based on field studies, the geometry of the bifurcation, particularly the upstream bifurcation angle, is thought to control the duration of (dis)connection and therefore sand plug accretion and geometry (Fisk, 1947; Shields et al., 1984; Shields & Abt, 1989), but most authors agree that bifurcations remain overlooked in alluvial plains (Constantine et al., 2010a; Kleinhans et al., 2013).

Existing numerical and experimental studies focus on the parameters controlling discharge and sediment partitioning at bifurcation (Bulle, 1926; de Heer & Mosselman, 2004; Kleinhans et al., 2008, 2013; Salter et al., 2018, 2019) and bifurcation (in)stability (Bertoldi & Tubino, 2007; Bolla Pittaluga et al., 2003, 2015; Iwantoro et al., 2019). To our knowledge, no study currently exists that focuses specifically on quantifying the condition(s) for abandoning channels at a bifurcation and on the resulting sediment architecture.

In this work, we study experimentally and quantify for the first time the influence of bifurcation geometry, specifically the diversion angle, on fluvial channel abandonment. We focus on (1) abandonment potential and the associated processes and (2) the extent and geometry of the sedimentary bodies formed by bedload deposition in abandoned channels, i.e., sand plugs and sandbars.

2.1.3. Methods

2.1.3.1. Experimental design

Experiments were carried out in the Geomorphic Lab of the Centre de Géosciences of MINES ParisTech, Fontainebleau. A modular flume with fixed walls was built. It was composed of three branches: one inlet and two distributary channels connected through a bifurcation area (Fig. 2.2). Each channel had a width W of 4 cm and a length of about 75 cm. The global slope of the experiment was 1.48% while the slopes in distributaries 1 and 2, respectively, $S1$ and $S2$, varied with the configuration (Table 2.1). The bifurcation area was modular to allow different angles between the inlet and the distributary channels. Three angles were considered (Table 2.1, Fig. 2.2). The bifurcation angle α was the angle between the two distributaries. The incidence angles β_1 and β_2 were the angles between the inlet channel and the stream-left and -right distributaries, respectively (Fig. 2.2). When $\beta_1 = 0$, $\beta_2 = \alpha$ and corresponded to a diversion angle, as usually defined.

The experiments started in an empty flume and typically lasted 90 to 100 min. Input water and sediment discharges were constantly fed at rates of 300 and 0.6 Lh^{-1}, respectively. Both fluxes

were calibrated beforehand to allow formation of sedimentary structures without filling the flume too quickly, allowing observations to be made. The water was delivered through a head tank to reduce turbulence in the incoming flow. The water was dyed in blue using food colorant in order to enhance contrast in pictures. The sediment was a well-sorted, rounded to sub-angular, fine (d_{50}= 209 μm) Fontainebleau sand. Sediment traps allowed quantifying the volume of sediment that bypassed the distributaries.

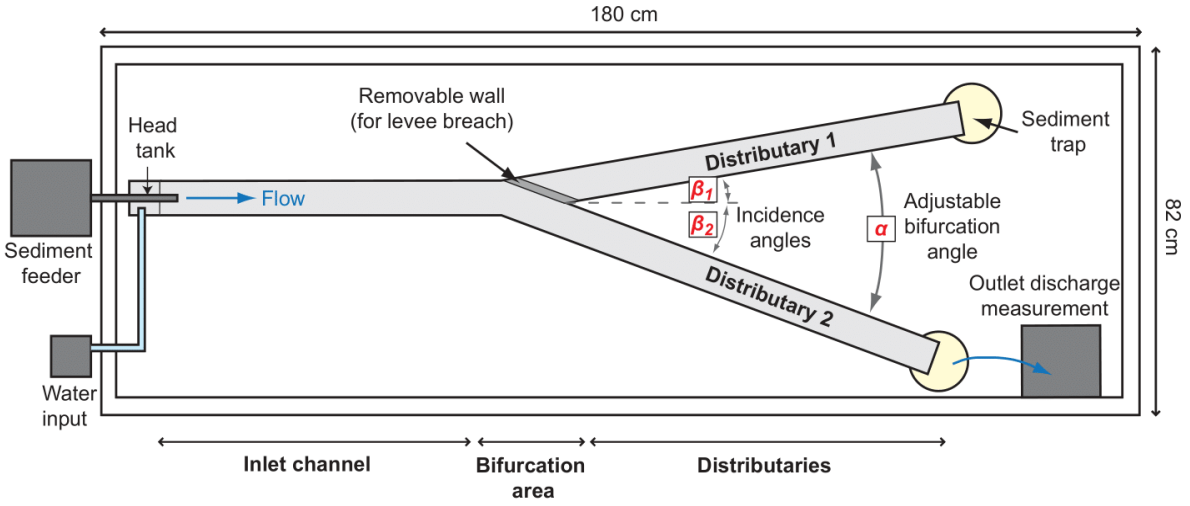

Figure 2.2: Overhead view of the experimental setup together with the different angles considered and the levee breach setup.

Experiment	Bifurcation angle α (°)	Distributary 1				Distributary 2			
		$\beta 1$ (°)	Bed slope S1 (%)	Equilibrium water discharge ($L\,h^{-1}$)	Shields parameter θ	$\beta 2$ (°)	Bed slope S2 (%)	Equilibrium water discharge ($L\,h^{-1}$)	Shields parameter θ
1	30	10	1.468	–	0.213	20	1.418	–	0.123
2*				–	0.213			–	0.082
3		15	1.443	153.4	0.209	15	1.443	146.6	0.209
4*				150.6	0.209			149.4	0.084
5		0	1.48	250	0.172	30	1.312	50	0.114
6*				262	0.214			38	0.076
7	45	22.5	1.405	150.6	0.204	22.5	1.405	149.4	0.204
8*				161.4	0.204			138.6	0.244
9		0	1.48	299	0.172	45	1.193	1	0.138
10*				274.2	0.214			25.8	0.069
11	60	30	1.312	181.5	0.190	30	1.312	118.5	0.114
12		0	1.48	270.1	0.214	60	0.98	29.9	0.085
13*				294.3	0.214			5.7	0.085
14	90	45	1.193	193.6	0.138	45	1.193	106.4	0.207
15		0	1.48	294.3	0.172	90	0	5.7	0.116
16*				258	0.214			42	0.058
17				299	0.214		1	1	0.087
18				294.3	0.214		1.282	5.7	0.149
19				291.6	0.214		2.56	8.4	0.074

Table 2.1: List of experiments and associated parameters.

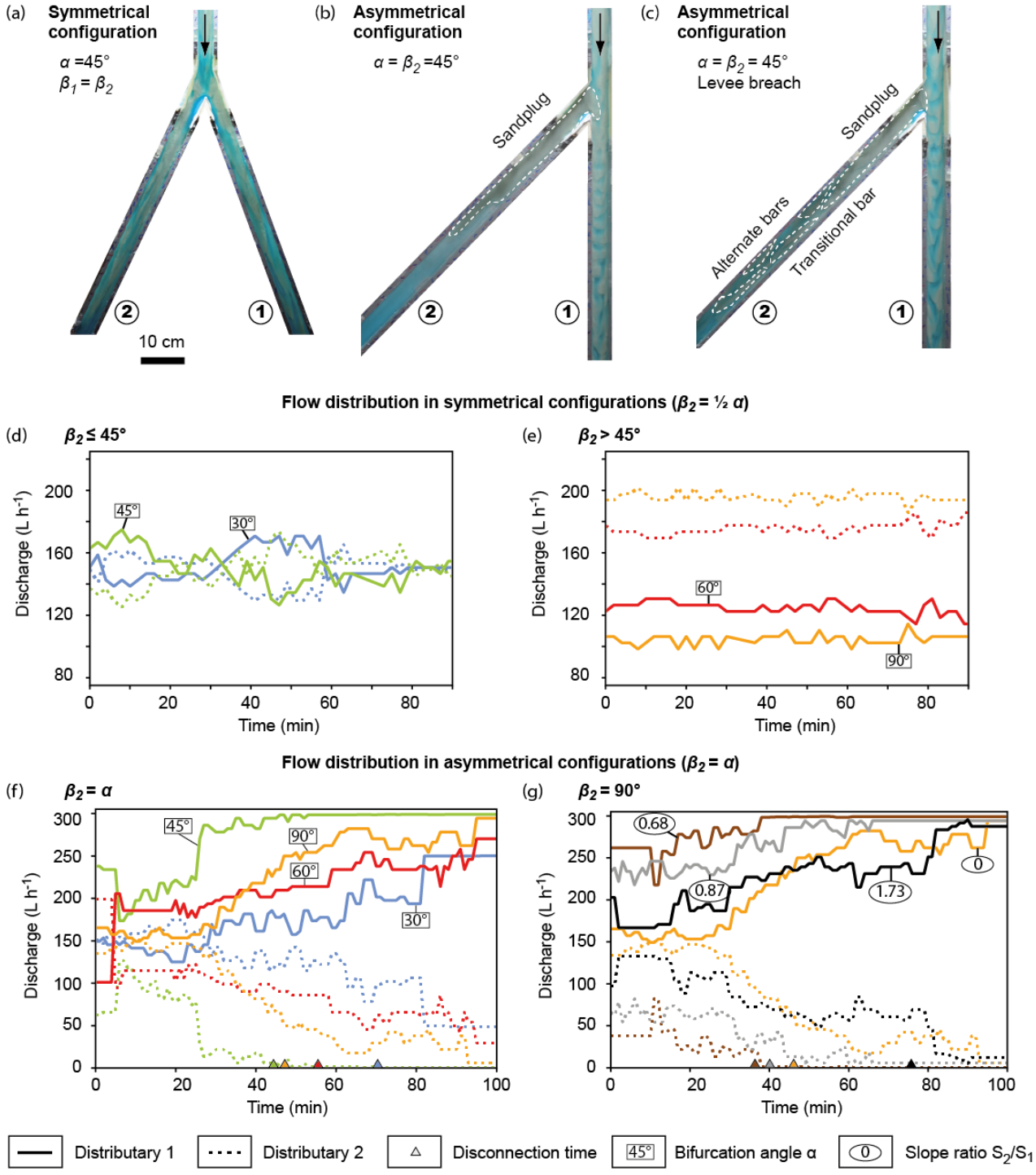

Figure 2.3: Evolution of the experiments. **(a-c)** Overhead pictures of the setup for the symmetrical **(a)** and asymmetrical configurations without **(b)** and with levee breach **(c)**. **(d-f)** Evolution of water discharge measurement at the output of the distributary channels for symmetrical **(d-e)** and asymmetrical **(f-g)** configurations. **(g)** Asymmetrical 90° configurations with varying slope ratios S_2/S_1.

A total of 16 experiments were designed to explore the influence of bifurcation angle α values ranging from 30 to 90° and β_1 and associated β_2 values ranging from 0 to 90° (Exps. 1 to 16) (Table 2.1). A first set of four symmetrical ($\beta_1 = \beta_2 = 1/2\alpha$, Exps. 3, 7, 11 and 14) (Fig. 2.3a) and five asymmetrical ($\beta_1 \neq \beta_2$, Exps. 1, 5, 9, 12 and 15) (Fig. 2.3b) configurations was built. A second set of seven experiments (Exps. 2, 4, 6, 8, 10, 13 and 16) replicated the configurations of the first set (except for Exps. 11 and 14) with the addition of a removable wall placed at the entrance of distributary 1 parallel to the orientation of distributary 2 (Figs. 2.2 & 2.3c) (Appendix A). The wall was removed after the system had reached equilibrium (identical input and output sediment discharges) to simulate a levee breach (Fig. 2.3c). In all asymmetrical configurations (except for Exps. 1 and 2), distributary 1 was straight ($\beta_1 = 0$) so that β_2 was a diversion angle (Table 2.1).

A final set of three experiments (Exps. 17, 18 and 19) was designed to determine if the observed effects of a given diversion angle could be counterbalanced by a slope variation in the deviated distributary. The experiments had the same planar geometry as Exp. 15 ($\alpha = \beta_2 = 90°$, slope ratio $S_2/S_1 = 0$), but the slope at the bottom of distributary 2 was modified so that three additional different slope ratios S_2/S_1 could be tested (i.e., respectively, 0.68, 0.87 and 1.73 in Exps. 17, 18 and 19).

2.1.3.2. Data acquisition

Free surface elevation was periodically measured in all channels. Water discharge was measured out of the two distributaries using a system similar to that of Salter et al. (2019). Water was flowing out of the channel into a cylinder with a hole at the bottom small enough to allow variation of the level in the cylinder. The weight evolution was measured within the cylinder using a digital scale and converted into discharge using a calibration curve. Figure 2.3d, e, f and g show the resulting water discharge partitioning for experiments without removable wall. Pictures of the flume were taken every minute by an overhead camera to observe sand bodies' formation and measure their length. The sand body's total length, i.e., including both subaerial and submarine parts, was measured from pictures. Sand plug construction was reported by increments of 15 min for asymmetrical configurations without levee breach (Fig. 2.4). Sand plug length was measured at the last location where it extended over the whole channel width and at its downstream limit. In the following, the mean of these two measurements is used to speak of sand plug length (Fig. 2.4). The final digital elevation models (DEMs) of the deposits were computed from 3-D photogrammetric surveys taken by two cameras mounted on a mobile rail using the Agisoft PhotoScan Professional v1.4

software (Fig. 2.5). The DEMs (precision of 0.4 to 0.5 mm) were used to produce mean longitudinal elevation profiles and to measure the longitudinal slope of sediment deposited in disconnected channel 2 (Fig. 2.6). Finally, sand plug volume calculated from DEMs and sand plug length L– divided by channel width W – were compared to bifurcation angles and slope ratios (Fig. 2.7).

2.1.3.3. Sediment transport law

A sediment transport law was calibrated to compare the experimental results with theory using the methods of Seizilles et al. (2013) and Delorme et al. (2017). A series of runs were carried out with constant water and sediment feed rates in a 3 cm wide flume. The experiment was repeated with different sediment discharges Q_s, and the equilibrium slope was measured each time after 10–15 h to estimate the associated Shields parameter θ (Fig. 2.8a). A critical Shields parameter θ_c – where a threshold of motion (i.e., qs=Qs/W > 0 g s^{-1} m^{-1}) was attained (Fig. 2.8a) – was estimated using

$$\frac{Q_s}{W} = q_0\,(\theta - \theta_c) \qquad Eq.\,2.1$$

The critical Shields parameter was then used to estimate channel slope at threshold (see Métivier et al., 2017 and references therein):

$$S = \left[\sqrt{\mu}\left(\frac{\theta_c(\rho_s - \rho)}{\rho}\right)^{\frac{5}{4}}\sqrt{\frac{\kappa\left[\frac{1}{2}\right]2^{\frac{3}{2}}}{3C_f}}\right]Q_*{}^{-\frac{1}{2}} \qquad Eq.\,2.2$$

Where $Q_* = Q/\sqrt{g d_s^5}$ is the dimensionless discharge, ρ and ρ_s the densities of water and sediment, μ the friction angle, C_f the turbulent friction coefficient and $\kappa[1/2]\approx 1.85$ a transcendental integral. In our setup, ρ = 1000 kg m^{-3}, ρ_s = 2650 kg m^{-3} and $\mu \approx 0.7$. C_f varied between 0.02 and 0.1 as an uncertainty estimate (Fig. 2.8b).

In experiments where a disconnection was observed, Q values were measured 2 min before disconnection to compare sand plug slope with Q_* according to the threshold theory (Fig. 2.8b). Finally, a run was performed for about 10 h in a 4 cm wide flume with a 1.48 % bottom slope to mimic the inlet channel conditions. The resulting bed slope was compared to the theory (Fig. 2.8b).

2.1.4. Results

Each experiment began with a short (15–20 min) phase of progradation of the sediment down to the bifurcation point. The sediment started forming a sandbar downstream of the sediment feeder and then split into alternate bars that migrated through the inlet channel. Once the sediment reached the bifurcation, it was partitioned into the distributaries, except when a removable wall was present. After an adjustment period, water discharge was considered at equilibrium when it remained constant – or slightly varied around a constant value – in each channel (Fig. 2.3). The associated water partitioning could be equal (i.e., identical in both branches) or unequal (i.e., different discharges in both branches). Sediment bypassing each distributary channel at equilibrium was roughly proportional to discharge partitioning. A distributary channel was considered disconnected when no bedload movement was observed. Usually, such disconnection occurred before water discharge equilibrium was attained (Fig. 2.3f and g).

2.1.4.1. Bifurcation geometries allowing channel disconnection

In the case of symmetrical bifurcations (Fig. 2.3a, d and e), no disconnection occurred. For low bifurcation angle ($\alpha \leq 45^{\circ}$, Exps. 3 and 7), a stage of soft avulsions (as defined by Salter et al., 2018) was observed initially (Fig. 2.3d). In this case, equilibrium with equal water partitioning was attained after both distributaries had been filled with sediment.

For high bifurcation angles ($\alpha \geq 60°$, Exps. 11 and 14), unequal water discharge partitioning lasted from the beginning of the experiment (Fig. 2.3e), and no soft avulsion stage was observed. The degree of such discharge asymmetry increased with bifurcation angle (Fig. 2.3e). Discharge partitioning in replicates of experimental runs 11 and 14 showed that the favored distributary channel was randomly chosen due to the interaction between the flow, the upstream alternate bars and the wedge of the bifurcation point. This indicated that the unequal water partitioning was not due to a tilt in the experimental setup.

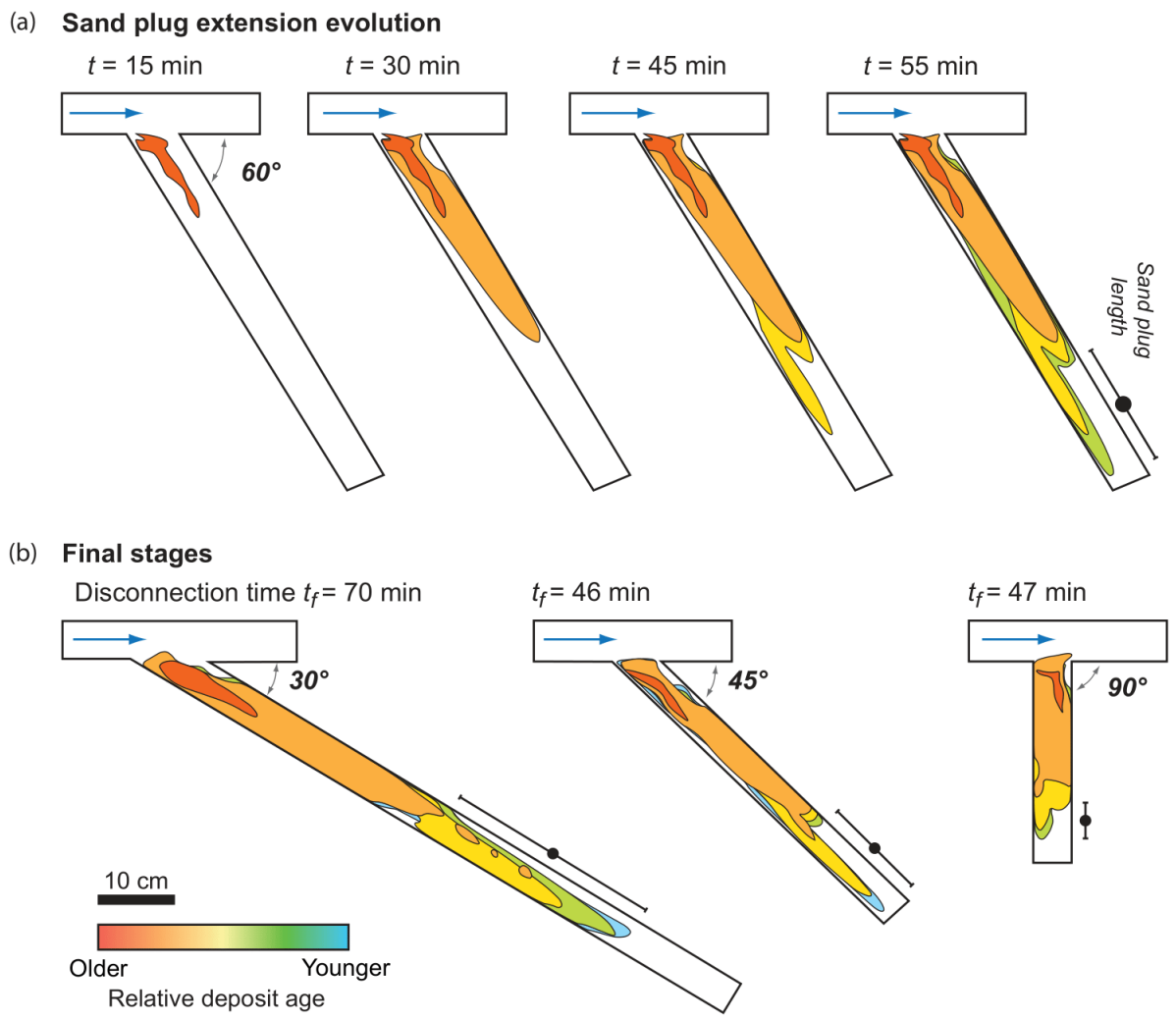

Figure 2.4: Planar growth of sand plug from overhead pictures. **(a)** Consecutive growth phases of the sand plug for β_2 = 30°. **(b)** Final states of the sand lug for different β_2 angles. Contours are drawn every 15 min. The mean sand plug length is represented with a black circle, together with uncertainties.

All asymmetrical configurations reached equilibrium with unequal water discharge partitioning (Fig. 2.3f and g). In Exps. 1 and 2 ($\beta_1 = 10°, \beta_2 = 20°$), no disconnection was observed. In the other asymmetrical experiments (i.e., Exps. 3, 4, 9, 10, 12, 13 and 15 to 19), disconnection was always attained and a sand plug formed (Fig. 2.3b and c). Water discharge partitioning was unequal between the two distributaries. A sand plug started to form in distributary channel 2 and as a response the straight distributary ($\beta_1 = 0°$) captured an increasingly important portion of the flow (Fig. 2.3f). Discharge asymmetry observed at equilibrium was globally proportional to β_2. In Exp. 9 ($\beta_2 = 45°$), disconnection was reached very quickly (50 min) due to the development of an additional sandbar on top of the sand plug that steered the flow towards the first distributary (Fig. 2.3f). This was the only occurrence of such a phenomenon out of the 19 experiments. In all experiments, fluctuations of water

discharge were observed. Visual inspections showed that these fluctuations were linked to the migration of alternate bars in the inlet channel (Bertoldi & Tubino, 2007). A bar located stream right immediately before the bifurcation provided sediment to the distributary 2 and temporarily decreased its water discharge, favoring deposition and construction of the sand plug. A bar located stream left immediately before the bifurcation temporarily decreased sediment supply and increased water discharge to distributary 2, favoring sediment entrainment.

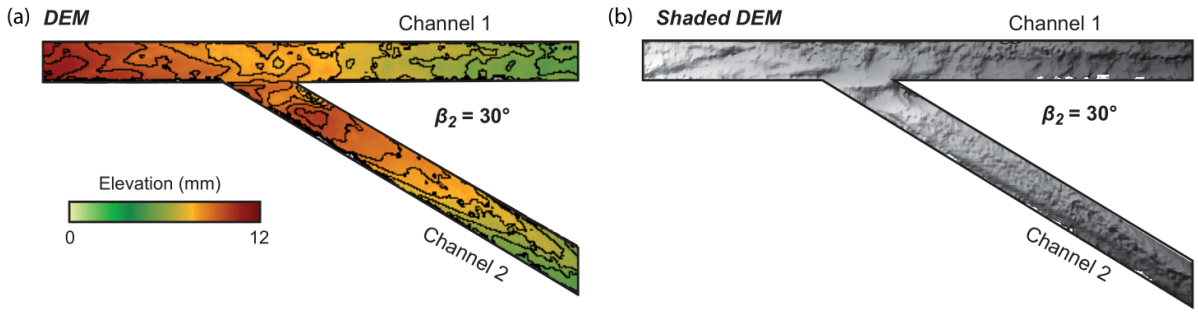

Figure 2.5: Final topography of Experiment 5 showing the active (1) and disconnected (2) channels. **(a)** Elevation DEM. **(b)** Shaded relief of the same DEM. Contour lines represent 1.5 mm elevation.

Levee breach experiments reached final equilibrium 5 to 10 min after distributary 1 was opened. Their final equilibrium state was very similar to that of the experiments made without levee breach in the same configuration (Fig. 2.3b and c). In asymmetrical experiments with levee breach (Exps. 6, 10, 13 and 16), sediment remained in transit through distributary 2 before the opening of distributary 1. This allowed the deposition of alternate bars (Fig. 2.3c) in distributary 2. In the asymmetrical experiments without levee breach (i.e., Exps. 5, 9, 12, 15, 17, 18 and 19), all sediment that entered distributary 2 was deposited to form a sand plug (Figs. 2.3b & 2.5b).

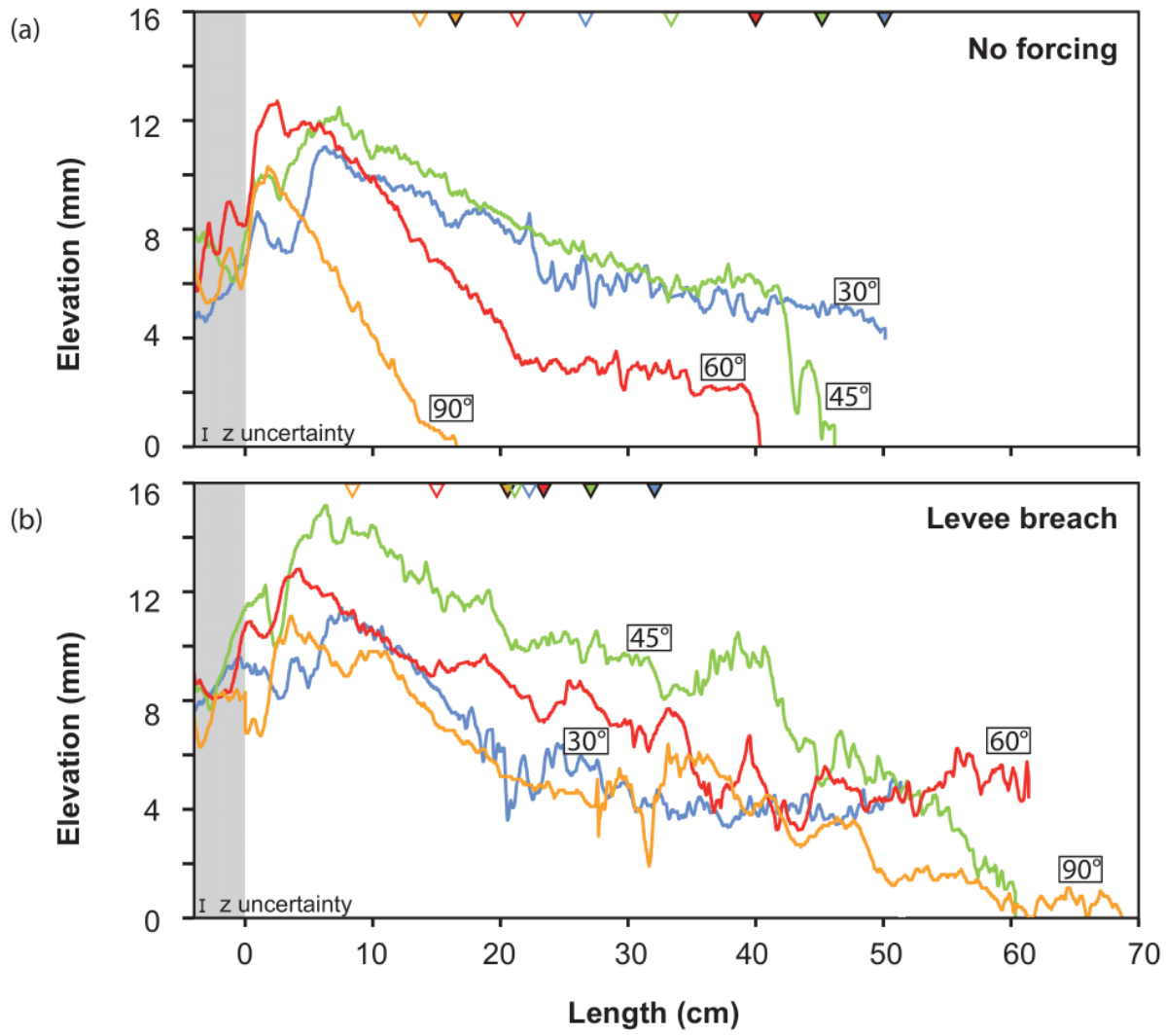

Figure 2.6: Mean longitudinal elevation profiles of the sand plugs for increasing β_2 angles without **(a)** and with levee breach **(b)**. Profiles were corrected for bottom slope to facilitate comparisons. The grey area corresponds to the active channel. Empty triangles correspond to the furthest location where the sand plug occupies the entire channel width, while full triangles indicate the subaqueous extremity of the sand plug.

Figure 2.3g shows discharge partitioning under varying slope ratios S_2/S_1 (0, 0.68, 0.87 and 1.73) for the same bifurcation angles ($\beta_1 = 0°$, $\alpha = \beta 2 = 90°$). In each case, the same final steady state ($Q_{w1} \approx 290\ L\ h^{-1}$, $Q_{w2} \approx 10\ L\ h^{-1}$) was reached and distributary channel 2 disconnected (Fig. 2.3g). A sand plug thus formed, albeit at a different speed. Overall, the time required to reach disconnection increased with slope ratio (Fig. 2.3g). Experiment 15 ($S_2/S_1 = 0$) did not strictly follow the trend and showed the slowest sand plug building rate of the four experiments.

2.1.4.2. Sand plug formation dynamics and architecture

During sand plug formation, discharge gradually decreased in distributary channel 2, until a constant value was attained (Fig. 2.3f) and no more sediment motion was observed. Sand plug growth processes and final architecture were very similar in all these experiments, regardless of the incidence angle (Fig. 2.4).

The formation of the sand plug initiated on the external side of the diverted channel, immediately after the bifurcation (Fig. 2.4). Visual inspection showed that in this area flow velocity was the lowest, allowing the deposition of sand that initiated the first fixed sandbar. This first bar anchored to the external bank of the channel and quickly grew downstream and towards channel centerline (Fig. 2.4a). It then widened and lengthened until its growth stopped. Other bars then formed from the sides of previously formed sandbar(s) and stretched downstream, resulting in a composite sand plug (Figs. 2.4a & 2.8). When sand was deposited over the entire width of the channel, a thalweg formed across the sand plug. It allowed sediment transfer downstream until it was buried by a sandbar that disconnected the whole channel. Overall, a slight decrease of sand plug growth speed with diversion angle is observed.

In the case of levee breach experiments (Exps. 6, 10, 13 and 16), alternate bars formed in distributary 2 before the opening of distributary 1 (Fig. 2.3c). After the levee breach, the discharge abruptly decreased in distributary 2, initiating the rapid (2–5 min) formation of the sand plug. In the meantime, a transient knickpoint formed along the inlet channel to allow for bed slope adjustment. Parts of the existing alternate bars at the bifurcation were thus reworked (Fig. 2.8). A small plug, mostly consisting of the reworked deposits, formed rapidly at the entrance of distributary channel 2.

Sand plug long slope increased with the diversion angle (from 2.5 % to 7.8 %; Table 1). This was the most visible in the no-forcing scenarios, as there was no interference from previously deposited alternate bars (Fig. 2.6a). Bars after the plug itself showed the shallower slopes (Fig. 2.6b). In the case of a levee breach, the sand plug slope was slightly steeper when the diversion angle was lower than or equal to 45° (Table A1). Figure 2.8b shows that sand plug slopes are overall consistent with the threshold theory when compared to the dimensionless discharge, with deviations towards lower or steeper slopes than the theory depending on the forcing scenario. The upstream end of the sand plug was about 4 to 8 mm more elevated than the active channel bed (Figs. 2.5a & 2.6a) and was slightly elevated compared to the water

elevation in the active channel, similarly to a levee in natural systems. In the case of a levee breach, the inherited geometry caused by the alternate bars is preserved, resulting in a sand plug with a roughly equal maximum elevation but a higher overall elevation (Fig. 2.6b).

2.1.4.3. Controls on sand plug length and volume

Relationships between incidence angle β_2 and sand plug length and volume, as well as between differential bottom slope and sand plug length and volume were found in asymmetrical configurations (Fig. 2.7). Above a 30° threshold value of β_2 required to form a sand plug, sand plug length linearly decreased with β_2 (Fig. 2.7a). In the case of a levee breach, sand plugs were shorter for a given β_2 value (Fig. 2.7a). In fact, the regression lines calculated in the cases without and with levee breach returned coefficient values of about –0.11 and– 0.08, respectively. This induces a slow convergence of sand plug lengths towards higher angles and shows that the sand plugs formed by a levee breach are slightly less affected by the β_2 value.

Without levee breach, the sand plug was the only bedload deposit in the disconnected distributary (Exps. 5, 9, 12 and 15) (Figs. 2.3b & 2.5b). Its volume steadily decreased with β_2, following a roughly linear relationship (Fig. 2.7b). With a levee breach (Exps. 6, 10, 13 and 16), the total volume of sediment also decreased linearly with β_2, but was globally higher. Indeed, in the levee breach experiments the sand plug accounts for only part of the sand volume deposited in the distributary, the rest being accounted for by the alternate bars formed during the channel active phase. When only the volume of the sand plug itself is taken into account, sand plug volume was thus lower than in the no-forcing cases (Fig. 2.7b). Figure 2.7c indicates that the length and volume of the sand plug was also slightly affected by the slope ratio. The sand plug became more elongated and thinner as the slope increased in distributary 2 and consequently sand plug slope overall decreased with an increase of the slope ratio, from 0.68–0.87 (Exps. 15 and 17) to 1.73 (Exp. 19).

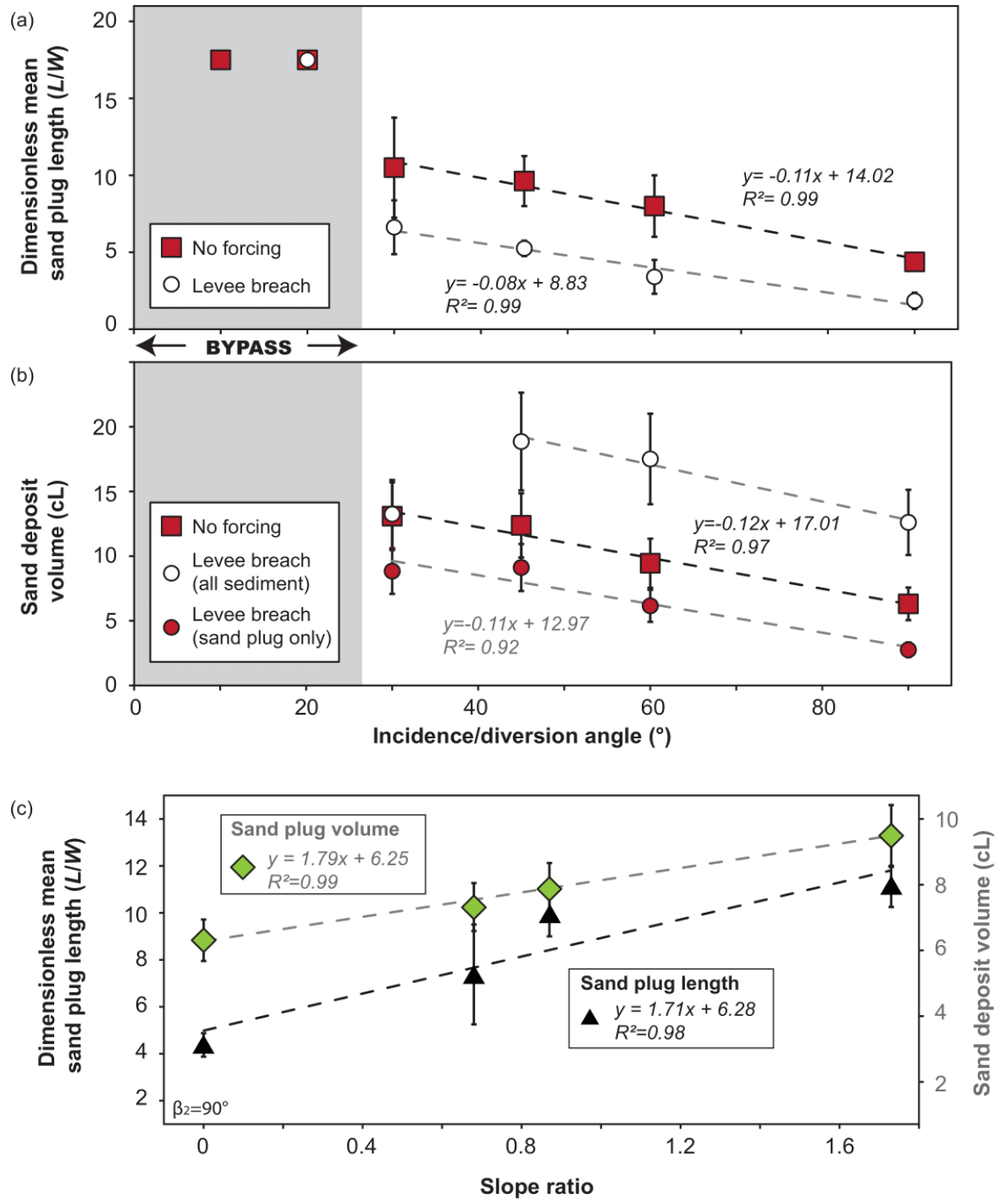

Figure 2.7: Relationships between the sand plug length and volume, and the incidence angle β_2 **(a, b)** and slope ratio S_2/S_1 for $\beta_2 = 90°$ **(c)**. The regression line for total sediment in panel **(b)** was not calculated since only three points were aligned.

2.1.5. Discussion

2.1.5.1. Bifurcation angle control on abandonment

In this study, channel disconnection was possible for highly asymmetrical bifurcation (i.e., $\alpha = \beta_2$ *and* $\beta_2 \geq 30°$) (Exps. 5, 6, 9, 10, 12, 13 and 15 to 18). In symmetrical configurations, no disconnection was observed although an effect on discharge partitioning occurred. Such discharge imbalance can be attributed to the bifurcation angle value alone, since the slopes of both distributaries are equal. Experiments 1 and 2 demonstrated that even in asymmetrical cases, no disconnection is possible if the diversion angle is too low ($\beta 1, \beta 2 < 30°$) or the bifurcation not asymmetrical enough. Hence, bifurcation geometry indeed controls the disconnection of channel as proposed by Fisk (1947), Shields et al. (1984) and Shields & Abt (1989). Moreover, our results suggest that disconnection is more sensitive to incidence angle value than bifurcation angle value alone. In essence, the value of the flow deviation from its original trajectory has more impact than the value of flow divergence between the distributaries. The fact that disconnection was observed despite slope advantage in the diverted distributary channel (Figs. 2.3g & 2.7c) (Table 2.1) is another strong argument in favor of planar geometry control on bifurcation (dis)equilibrium.

In symmetrical experiments, water discharge shifted from a soft avulsion regime with roughly equal partitioning (e.g., Salter et al., 2018) to an unequal partitioning as bifurcation angle α increased (Fig. 2.3d and e). Considering the trend in Fig. 2.3d and e, we may hypothesize that abandonment would have occurred at some point if the bifurcation angle α had been increased further. In a comparable set of experiments, Bertoldi & Tubino (2007) and Salter et al. (2019) showed that disconnection may also be possible for low-angle symmetrical configurations (respectively, 30° and 16°). Their work focused on delta networks, where bifurcations can be considered stable with two active distributaries of a width inferior to that of the upstream channel. In their experiments, Bertoldi & Tubino (2007) and Salter et al. (2019), respectively, had a ratio of 0.66 and 0.7. In that case, the downstream migration of an alternate bar at equilibrium with the upstream channel into a narrower distributary may easily lead to sand plug formation. In our fluvial-channel-focused experiments, where an avulsion generally led to channel abandonment in favor of the other, the ratio between the width of each distributary and the width of the upstream channel was 1 (Fig. 2.2). The distributaries could accommodate the alternate bars' migrations, preventing disconnection. Furthermore, Bertoldi & Tubino (2007) and Salter et al. (2019) demonstrated that discharge asymmetry is largely a function of flow aspect ratio upstream of the

bifurcation. In our experiment, upstream water depth was usually 4 mm; thus, aspect ratio was about 10, which is propitious to equal flow partitioning in symmetrical bifurcation geometry (Salter et al., 2018).

2.1.5.2. Bifurcation angle control on sand plug extent

Numerous field studies intuited a relationship between the incidence angle and the length of the sand plug, stating that a low incidence angle produced a longer sand plug (Fisk, 1947; Allen, 1965; Gagliano & Howard, 1984; Shields et al., 1984; Shields & Abt, 1989; Dieras et al., 2013). This was explained by the fact that bedload is easily diverted into the channel at low angles and on a longer distance before deposition. With increasing bifurcation angles, a smaller fraction of the bedload enters the channel, resulting in shorter and smaller sand plugs. Our experiments show that bedload partitioning is proportional to discharge partitioning and that final discharge partitioning is controlled by the diversion angle (Fig. 2.3). As a result, sand plug volumes and lengths linearly decrease with diversion angle (Fig. 2.7a–b). Sand plug volumes and lengths are also modulated by the slope of the abandoned channel (Fig. 2.7c). Sudden events such as levee breaching create shorter and less voluminous sand plugs, as less bedload material is mobilized to build the sand plug due to the faster disconnection (Fig. 2.7a and b).

The fast disconnection and limited sand plug length and volume observed in the case of a levee breach (Fig. 2.7a-b) can also be explained by the rapid entrenchment of the flow in channel 1. The newly opened channel 1 has a slope advantage as no aggradation occurred during the first phase of the experiment. As the result of incision and knickpoint retreat, a threshold that prevents part of the bedload to enter distributary 2 is created (Slingerland & Smith, 2004) and the flow is preferentially funneled in the distributary channel 1. It is worth noting that the effect of levee breaching on sand plug length and volume decreases slightly when the incidence angle increases (Fig. 2.7a-b), with a slight convergence towards higher angles. The slight difference in regression line values between the no-forcing and levee breach scenarios also hints that although the sand plug extent and volume are controlled by the diversion angle, different triggers might initiate sand plug formation depending on the scenario.

As bedload partitioning varies with discharge partitioning in our setup, a smaller fraction of bedload enters the deviated distributary and this fraction diminishes in time with discharge, until disconnection. In a flume with comparable geometry, Bulle (1926) measured the bedload

partitioning in distributaries and found that around 90 % of the bedload was steered in the deviated distributary for angles ranging from 30 to 150°. However, this was at the cost of maintaining the discharge equal in both distributaries, by adjusting water slope using sluice gate elevation at the end of each distributary (Bulle, 1926; Lindner, 1953). The resulting water-surface slope ratios were likely far above the ones we used, since we did not observed equal discharge partitioning (i.e., Fig. 2.3g). Hence, a comparison of sediment partitioning between Bulle (1926) and the present work does not seem relevant.

2.1.5.3. Mechanism for channel abandonment

Beyond the influence of the bifurcation angle, other mechanisms have been invoked to explain channel disconnection: the Shields number of the system upstream of the bifurcation and its effects on the aspect ratio (Wang et al., 1995; Bertoldi et al., 2009b; Bolla Pittaluga et al., 2015) and bars' presence (Bertoldi & Tubino, 2007; Bertoldi, 2012), as well as the sinuosity upstream of the bifurcation and the slopes in each distributaries (Kleinhans et al., 2013; Van Dijk et al., 2014). Based on the results of this study, one may argue that it is the difference of channel bed slope associated with the bifurcation geometry – and not the bifurcation geometry itself – that leads to abandonment. The experiments presented in Fig. 2.3g show that this is not the case in the experiments with asymmetrical bifurcations, as a high diversion angle is a sufficient condition for hydraulic disconnection. Having a reasonable slope advantage to the diverted channel does not reverse the final outcome; it only affects the time needed to disconnect the channel and the extent of the deposits.

Another proposed mechanism is that low discharge in one channel induces sedimentation, which would in turn further reduce the discharge in the channel by plugging it or by changing the bed slope, creating a feedback loop leading to disconnection (Zolezzi et al., 2006; Bertoldi, 2012). Based on this study, this is discounted as abandonment would have been observed when discharge partitioning was unequal from the beginning in symmetrical configurations with incidence angles above the 30° threshold (Fig. 2.3e). The sand plug does create a feedback loop that helps disconnection, but the timing of the discharge decrease in distributary 2 during the asymmetrical experiments shows that it is not the discharge imbalance that initiates the sand plug formation. It is rather the formation of the sand plug that induces the change in discharge partitioning (Fig. 2.3f), leading to disconnection.

Eddies were observed on the external bank of the channel, immediately downstream of the bifurcation, in which water was slowed and sediment deposited. Bulle (1926) observed that

these eddies were produced by flow separation at the bifurcation. These eddies were also found in numerical modeling by de Heer and Mosselman (2004) and van der Mark and Mosselman (2012), and observed by Constantine et al. (2010a) on the Sacramento River and were named the “flow separation zone”. The latter authors observed that the width of the flow separation zone increases with the incidence angle value. In our experiments, the wider flow separation zone in the diverted channel led to the formation of the first stage of the sand plug against the external bank of the diverted channel just downstream of the bifurcation (Fig. 2.4). This in turn led to a further reduction of the flow diverted in the channel, favoring deposition and growth of the sand plug, until the channel got disconnected. At low values of β, this flow separation zone was too narrow to initiate the feedback loop. When β reached 30°, it became wide enough to create a larger and higher sandbar and start the feedback loop.

2.4.5.4. Comparison with field cases and upscaling

Although our model represents a very simplified setup, it has been purpose built to study the influence of bifurcation geometry on disconnection and on bedload deposits partitioning and geometry in abandoned channels. As such, it complements previous studies focusing on equilibrium configurations relative to water and sediment flows (Bolla Pittaluga et al., 2003, 2015; Bertoldi & Tubino, 2007; Edmonds & Slingerland, 2008; Bertoldi et al., 2009b; Salter et al., 2018, 2019). River channel section and slope are thought to adjust to water discharge (see Métivier et al., 2017 and references therein). For instance, Lacey's law states that river width scales with the square root of water discharge (Lacey, 1930). Both the equilibrium slope of the inlet channel and the slopes of disconnected channels observed in the experiment are consistent with the threshold theory and remain within the uncertainty range (Fig. 2.8b). However, in the case of a levee breach, equilibrium slopes are gentler than the theoretical equilibrium slope, and in the case of no-forcing scenarios, slopes are steeper. These deviations would confirm that abandonment trigger was dominated by channel entrenchment in the former case and by plug construction in the latter. As our experimental observations are compatible with Lacey's law and the threshold theory, even in such constrained settings (i.e., fixed wall), they are likely to apply in nature.

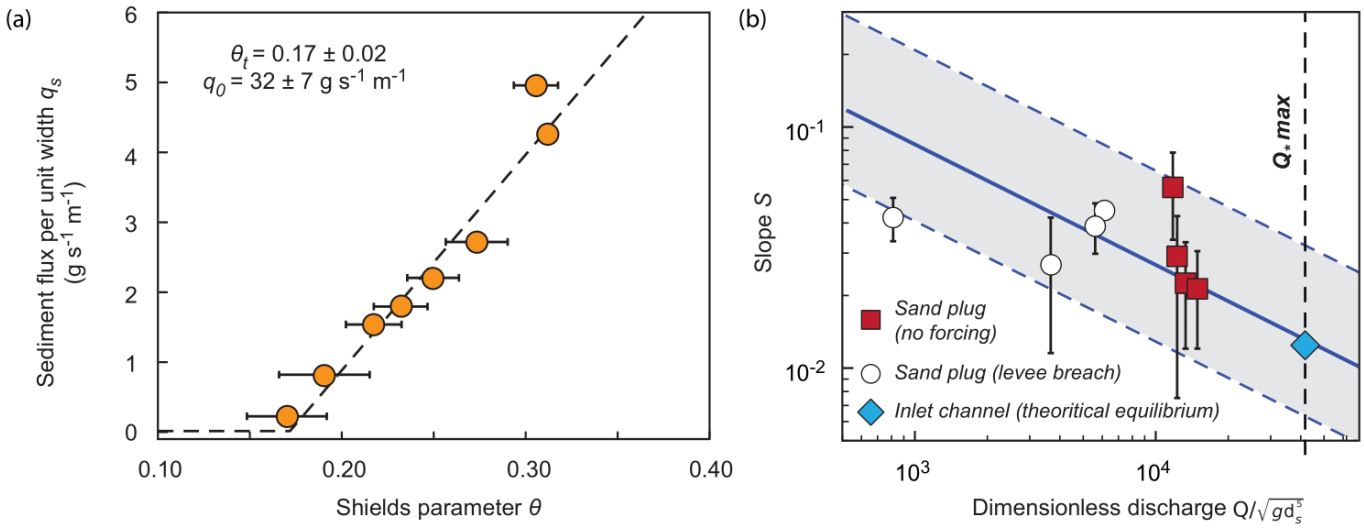

Figure 2.8: Transport law. Volumetric flux per unit width, as a function of Shield parameter θ. The dashed line corresponds to Eq. (1) fitted to the data **(a)**. Regime relationship between dimensionless discharge Q_* and slope measured in the experiments. The solid blue line corresponds to the threshold theory (Eq. 2, θ_t = 0.17 and C_f = 0.06). The shaded area and dashed lines indicate uncertainty based on varying friction coefficient C_f value **(b)**.

An intermediate scale between our flume experiment and natural systems is the irrigation system channels, which also have fixed width. Intake plugging is an issue that many water management engineers face, and the question of optimal diversion angle value has been intensively studied. Novak et al. (1990) and Munir (2011) state, for instance, that a 30 to 45° diversion angle is desirable to limit silting up of the channel, whereas a 90° angle is "the least desirable one". This statement is consistent with the present study where channels with high diversion angles are easily plugged and disconnected. Neary et al. (1999) observed sedimentation patterns similar to this study (i.e., a sandbar anchored on the external bank of the deviated channel immediately downstream of the bifurcation) in a 90° lateral intake adjoining the Ohio River, both in the actual intake and numerical simulations. Hence, the first-order observations made in this study seem to apply at larger scales such as larger waterways.

In natural cases, avulsion and disconnection are usually accompanied by the enlargement of the new dominant channel path (Kleinhans et al., 2008) and eventually change of bifurcation angle with time (Bertoldi, 2012). Both impact sand plug construction. In our experiments, channel walls were fixed and the dominant flow immediately occupied a channel equal in width to the inlet channel. As a result, disconnection rates were likely faster than when the channel could erode its bank to adjust its shape, similarly to natural systems. Such delay would probably favor the building of larger sand plugs in abandoned channels. To our

knowledge, no relationship between diversion angle and sand plug length has been quantified on the field yet. Constantine et al. (2010a) found no significant correlation between the incidence angle and the emerged length of the sand plug based on aerial photographs. However, they did find a negative correlation between incidence angle and gravel fill depth below water measured at the apex of abandoned meanders. Such measurements are more comparable to our results (i.e., taking into account the submerged part of the sand plug) and seem to be adequate when investigating on the field for a relationship between incidence angle and bedload deposits. The fact that the subaerial plugs length in abandoned channels is not related to bifurcation angles may be due to fine-grain deposition over the sand plug after disconnection. More field investigations would be required to test this hypothesis.

2.1.5.5. Sand plug architecture integration to reservoir modelling

The sand plug formation processes observed experimentally in this study are the same independently of the bifurcation geometry and occurrence or absence of levee breach (Figs.2. 4 & 2.9). Sand plugs are not simply sediment wedges deposited at the mouth of the disconnected channels (Fisk, 1947; Allen, 1965) but complex bedload features formed by bars amalgamation (Fig. 2.9). Sand plugs have a major slope break separating the thicker upstream part that actually plugs the channel and the downstream part and lateral width variation on the downstream part (Fig. 2.9). Inherited topography affects the sand plug final architecture (Fig. 2.6b). For instance, alternate sandbars may be found isolated in the channel. During disconnection, the sand plug may rework some of the previously deposited bars to form transitional bars (Figs. 2.3c & 2.9). Together, they form a consistent coarse-grain plug that extends inside the paleo-river path.

In natural cases, the successive episodes of construction would imply the presence of grain-size variations in the internal structure of the sand plug. These heterogeneities would include permeability baffles formed at the interface between sandbars during low energy phases and possible erosional surfaces formed during phases of high energy, increasing permeability. In these cases, the internal structure of a sand plug could be comparable to that of a complex point bar (Deschamps et al., 2012; Cabello et al., 2018) and thus form a good reservoir in itself.

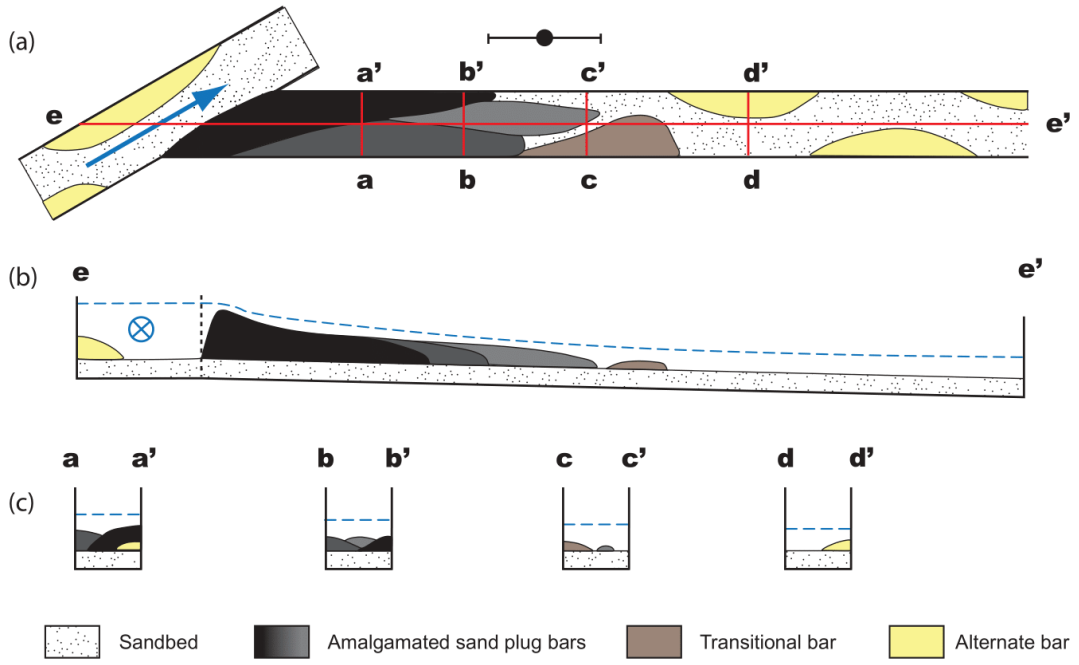

Figure 2.9: Conceptual architecture of sand plug derived from experimental observations: overhead view **(a)**, longitudinal profile **(b)** and transverse sections **(c)**.

Finally, the presence of bedload deposits in disconnected channels demonstrates how the abandoned channel fills could be connectivity bridges rather than permeability barriers, especially in the upstream part of abandoned channels (Larue & Hovadik, 2006; Donselaar & Overeem, 2008). This could have a significant impact on fluvial river models. Indeed, common models for meandering channels migration (e.g., Parker et al., 2011) usually assume that abandoned channels are 100 % filled by mud plug, with consequences on the erodibility of alluvial plains and thus channel migration (Howard, 1996). Using a dependence of sand plug length and volume on diversion angles will influence the overall connectivity in reservoir modeling (i) at the scale of channel fills and potentially (ii) at the scale of channel belts. For instance, sand plug lengths vary between 5 and 12 W in the present study (Fig. 2.7a). The latter is in the range of the wavelength for typical meandering rivers (Williams, 1986) and would allow a connection between about three to four point bars. This suggested length of bedload deposits is consistent with the presence of bedload deposits mapped in low sinuosity avulsion channels by Stouthamer (2001) and Toonen et al. (2012) three to five meander bends downstream of the bifurcation point. Exploring the ranges of sand plug lengths is therefore a promising research area for reservoir characterization in the future. For instance, the construction and amalgamation of plug bars may be different in curved channel than in the straight channels used in this study.

2.1.6 Conclusion

Based on the series of experiment designed to force channel abandonment under constant water and sediment discharge, we find the following:

- Above a diversion angle threshold of 22.5°, discharge partitioning becomes unequal. Disconnection occurs when the diversion angle is greater than or equal to 30°.
- Sand plug length and volume linearly decrease with the diversion angle.
- The incidence angle controls the width of the flow separation zone in the diverted channel. When the incidence angle is high enough, sand plug formation begins in this zone and its presence creates a feedback loop leading to further deposition until disconnection occurs.
- The sand plug is a complex structure formed by amalgamated and interconnected sandbars of various lengths, widths, elevation and slope, which may increase the connectivity of fluvial reservoirs, in particular between otherwise isolated point bar deposits.

2.2. Influence of additional forcing parameters on plug geometry

This section details two sets of experiments performed in the modular avulsion flume. The effects of two forcings were investigated: (i) the presence of an erodible sand bed in both channels and (ii) the rise of base level inducing the formation of a backwater zone in distributary channel 2 where abandonment took place.

2.2.1. Erodible sand bed

In this set, two additional experiments (Exps. 20 and 21) were conducted to investigate the impact of an erodible bed (sand bed) in comparison with the previous experiments run in a context of a fixed-bed (Plexiglas) channel (Section 2.1). These experiments (Exp 20 and 21) replicated experiments 7 and 9 (bifurcation angle 45°), with one symmetrical ($\beta_1 = \beta_2 = 1/2\alpha$) and one asymmetrical ($\beta_2 = \alpha$) run, respectively (Table 2.2). The flume was filled with a 0.5 cm thick layer of the same sand than the one delivered to the flume during the experiment. The channel bed was flattened before the start of the experiments. Additionally, a 0.5 cm high piece of Plexiglas was set up at the downstream extremities of the flume to prevent regressive erosion of the channel bed material. The experiments were conducted and monitored following the exact same protocol as described in Section 2.1 (Fig. 2.10). The outcome and deposit evolution in the additional experiments were compared to the ones described in Section 2.1 (Figs. 2.11 & 2.12). Comparable results were obtained with this new set of experiments (Table 2.2): no abandonment in the symmetrical experiment and formation of a sand plug in the asymmetrical experiment leading to the disconnection of distributary 2.

Exp	Bifurcation angle α (°)	Distributary 1			Distributary 2			Sandplug			
		β1 (°)	Bed Slope S1 (%)	Shields parameter θ	β2 (°)	Bed Slope S2 (%)	Shields parameter θ	Dimensionless length	Sandplug volume (cL)	Disconnection time (min)	Sandplug slope (%)
7	45	22.5	1.405	0.2040	22.5	1.405	0.2040	-	-	-	-
20				0.244			0.285	-	-	-	-
9		0	1.48	0.1720	45	1.193	0.1380	9.625	12.38	46	2.7/1
21				0.214			0.173	5.98	8.06	44	3/0.5

Table 2.2: List of sand bed experiments and associated parameters. Sand bed volume is not accounted in sand plug volume.

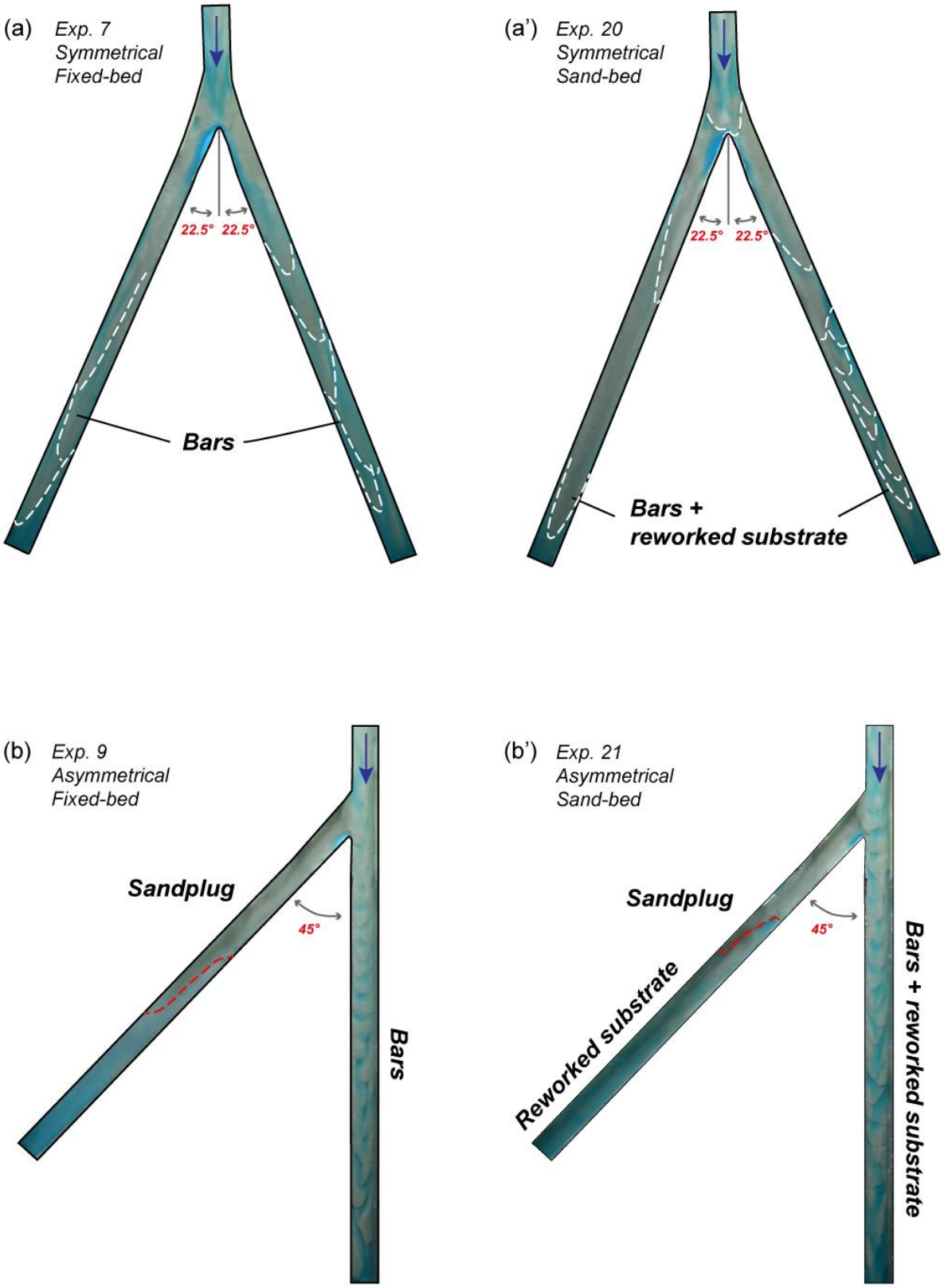

Figure 2.10: Final interpreted overhead pictures of the fixed-bed experiments **(a, b)** and of the sand bed experiments **(a', b')**.

Experiments ended up with sand bodies of comparable architecture with those of the previous set (Figs. 2.10, 2.11 & 2.12): migrating sand bars in symmetrical experiments, and the formation of a sand plug on the channel bed of distributary 2 with mobile sand bars in distributary 1 in asymmetrical experiments. In the case the sand bed, we observed reworking processes in all channels. They stopped in distributary 2 once a sand plug formed. These reworking processes developed downstream migrating bars incorporating sediment from the sand bed and bed load. Although some erosion processes occurred, the sand bed was never totally eroded, excepted at the bifurcation in Exp. 21 due to the eddies formed by the bifurcation wedge. When the bifurcation geometry allowed it (i.e., during Exp. 21), the sand plug formed on top of these partially reworked deposits. The sand plugs longitudinal elevation profiles were similar in Exps. 9 and 21, with the only significant difference being a vertical translation of the deposits roughly corresponding to the initial sand bed thickness (Fig. 2.11). When compared to Exp. 9, the resulting sand plug (i.e., the deposits newly formed on top of the sand bed) was shorter by roughly a third (Table 2.1; Figs. 2.10, 2.11 & 2.12), and its volume was also lower by a third (Table 2.2).

Despite these differences between fixed-bed and sand-bed experiments, in Exp. 21 the sand plug formed in a way similar to Exp. 9 (Fig. 2.12): deposition started in the flow separation zone, followed by bar amalgamation progressing both transversally and downstream. Although the time needed to attain disconnection was almost identical in both experiments (Table 2.2), the initial growth rate of the sand plug was faster during Exp. 21 (Fig. 2.12). Growth rate then slowed and the plug attained a final length similar to that of Exp. 9 in the same amount of time. The fast initial growth phase was encouraged by the reworking of the sand bed that supplied sediment to build the plug in the disconnecting channel from the beginning of the experiment, whereas in fixed-bed experiments the sediment had to propagate downstream up to the bifurcation first (Section 2.1).

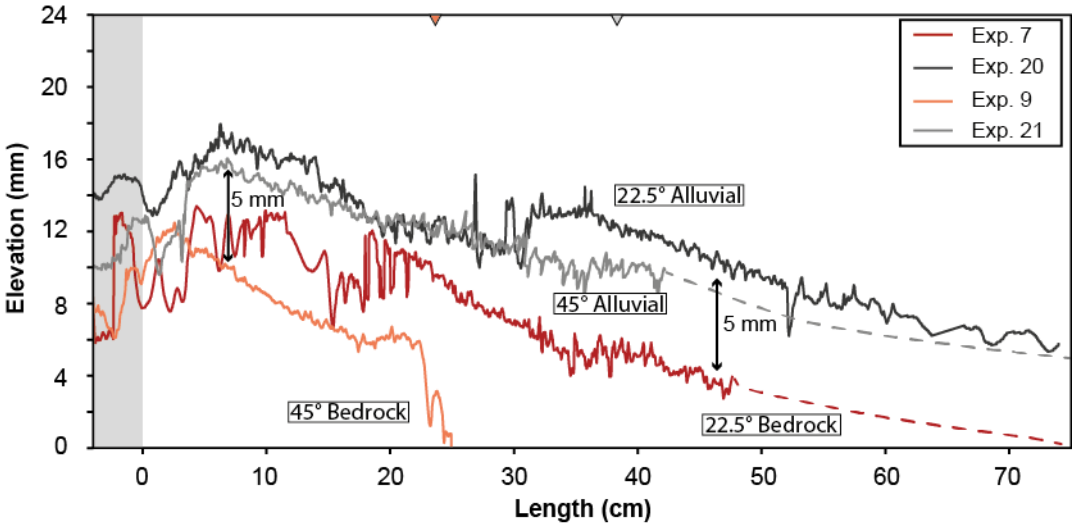

Figure 2.11: Mean longitudinal elevation profiles of the sand deposits for the sand bed (Exp. 20, 21) and fixed-bed (Exp. 7, 9) experiments. The grey area corresponds to the active channel. Triangles indicate the length of the sand plug in asymmetrical experiments cases.

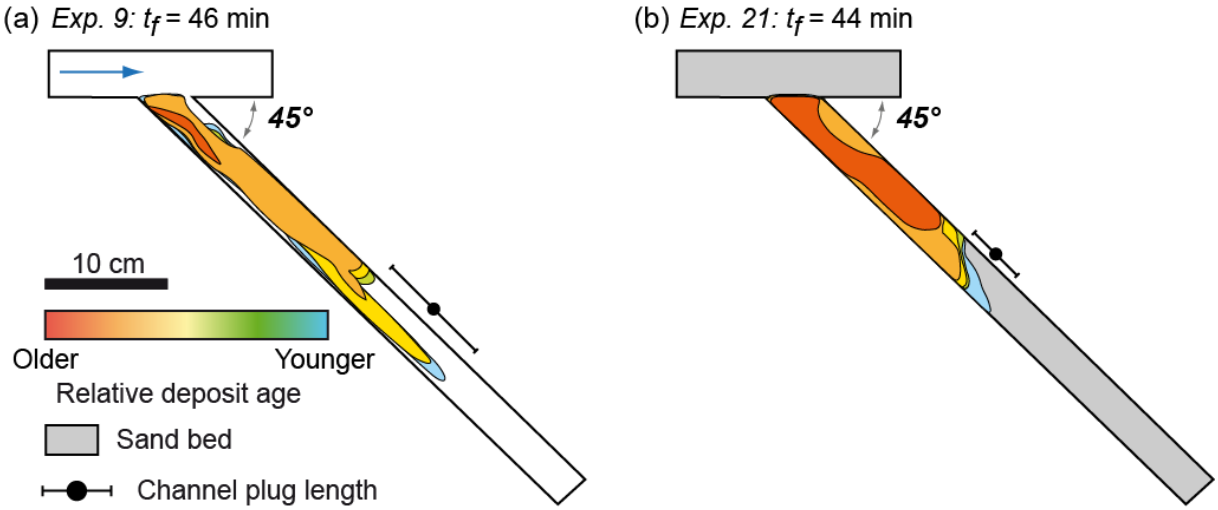

Figure 2.12: Plan view of final states of sand plugs for Exps. 9 **(a)** and 21 **(b)**. Growth stages are indicated by the colours.

2.2.2. Differential base level and associated backwater dynamics

2.2.2.1. Experimental design

In this set, ten additional experiments with fixed-bed (Plexiglas bed) were performed to look at the impact of increased base level in one distributary on (i) bifurcation stability and (ii) architecture of associated bedload deposits. Local base level elevation was obtained by fixing a 0.5 or 1 cm high weir at the outlet of distributary channel 2. The 10 experiments replicated Exps. 1, 3, 5, 7, 9, 12 and 15 presented in section 2.1. Bifurcation angles α ranged from 30 to

90° and incidence angles β_1 and associated β_2 values ranged from 10 to 90° (Exps. 22 to 31) (Table 2.3). The tested bifurcation configurations were therefore:

- 2 symmetrical configurations ($\beta_1 = \beta_2 = 1/2\alpha$), weir of either 0.5 cm (Exps. 24 and 27) or 1 cm (Exps. 25 and 28).
- 1 slightly asymmetrical configuration ($\alpha = 30°$, $\beta_1 = 10°$, $\beta_2 = 20°$), weir of either 0.5 cm (Exp. 22) or 1 cm (Exp. 23).
- 4 highly asymmetrical configurations ($\beta_2 = \alpha$), weir of 0.5 cm (Exps. 26, 29, 30 and 31).

Experiment	Bifurcation angle α (°)	Distributary 1			Distributary 2				Sandplug				
		β1 (°)	Bed Slope S1 (%)	Shields parameter θ	β2 (°)	Base level (cm)	Bed Slope S2 (%)	Shields parameter θ	Dimensionless length	Volume (cL)	Disconnection time (min)	Slope (%)	Backwater zone length (cm)
1	30	10	1.468	0.2130	20	0	1.418	0.1230	-	-	-	-	-
22				0.170		0.5		0.206	-	-	-	-	35.3
23				0.213		1		0.452	14.4	14	189	4	77.6
3		15	1.443	0.2090	15	0	1.443	0.2090	-	-	-	-	-
24				0.167		0.5		0.084	-	-	-	-	67.6
25				0.209		1		0.418	-	-	-	-	69.3
5		0	1.48	0.1720	30	0	1.312	0.1140	10.5	13.09	70	2.5/1	-
26				0.2140		0.5		0.2660	5.2	13.98	73	1.8	53.4
7	45	22.5	1.405	0.2040	22.5	0	1.405	0.2040	-	-	-	-	-
27				0.163		0.5		0.285	-	-	-	-	42.7
28				0.163		1		0.448	13.75	14.9	153	2.2	78.3
9		0	1.48	0.1720	45	0	1.193	0.1380	9.625	12.38	46	2.7/1	-
29				0.214		0.5		0.3460	4.75	10.2	87	6.8	83.8
12	60	0	1.48	0.2140	60	0	0.98	0.0850	8	9.45	55	4.3/0.6	-
30				0.214		0.5		0.227	4.5	9.81	65	5/12	81.6
15	90	0	1.48	0.1720	90	0	0	0.1160	4.375	6.31	47	7.8/3.4	-
31				0.129		0.5		0.203	3.25	8.47	77	13.6/8	94.6

Table 2.3: List of base level variation experiments and associated parameters.

Base level rise created a backwater zone in distributary 2. *Backwater* effect (*sensu* Chow 1959) corresponds to the adjustment (elevation) of the free surface height in response to the downstream presence of a standing water body. It is thus associated with a reduced slope of the water-surface in the affected channel. The backwater effect is known for inducing sediment deposition and promoting avulsion and channel abandonment in river systems (Nittrouer et al., 2012; Chatanantavet et al., 2012; Wilson & Goodbred, 2015; Fernandes et al., 2016 ; Ganti et al., 2016a, b). In the experiments, the theoretical length of the backwater zone – i.e., the upstream limit where water surface slope diverges from the channel bed slope due to backwater effect – was calculated using the backwater length L_b defined by Paola & Mohrig (1996):

$$L_b = \frac{H}{S_{ws}} \qquad \text{Eq. 2.3}$$

where H is the mean channel depth measured along the diverted channel and S_{ws} the water surface slope in normal flow conditions. Here, the bed slope was used assuming that in the

free flow zone the channel and water surface slopes were roughly parallel, an assumption frequently used to estimate backwater zone length (Paola & Mohrig 1996; Chatanantavet et al. 2012; Lamb et al. 2012; Chatanantavet & Lamb 2014). In Exp. 31, with a 90° diversion angle the mean of distributary 2 and the inlet channel bed slopes was used to calculate backwater length to account for its extension upstream of the inlet channel. In experiments without weirs, as no standing body of water existed, no backwater zone was formed. Backwater lengths are indicated in Table 2.2 and their upstream limits are represented in Figure 2.13. The part of the channel unaffected by backwater effect was called free flow zone.

2.2.2.2. Results

When base level was increased by 0.5 cm (Exps. 22, 24, 26, 27, 29, 30 and 31), the experiments outcomes were similar to the no-forcing cases (with either fixed- or sand beds): (i) no disconnection for symmetrical or slightly asymmetrical experiments and (ii) disconnection for highly asymmetrical experiments with a diversion angle equal or larger to 30°. In the latter, the backwater zone reached the bifurcation, with the exception of the 30° experiment (Exp. 26) (Table 2.3). However, disconnection time was longer than in the no-forcing scenarios and the sand plugs were shorter (Table 2.3; Fig. 2.13), once again with the exception of Exp.26. Sand plugs volume was not significantly impacted by differential base level elevation (Fig. 2.16). When base level was increased by 1 cm (Exps. 23, 25 and 28), the experiment outcomes were more strongly affected: disconnection occurred in cases with incidence or diversion angles equal or larger to 20°, either in symmetrical or slightly asymmetrical cases, for which the backwater zone reached the bifurcation (Table 2.2).

In this set of experiment (base level rise), when disconnection occurred (Exps. 23, 26, 28, 29, 30 and 31), initiation of sand plug followed the same processes as described in Section 2.1 (Fig. 2.12): sediment deposition initiated in the flow separation zone, which was still present even when the backwater zone reached the bifurcation. The first bar produced by sediment deposition in the flow separation zone was of similar shape and length in both sets of experiments (Fig. 2.13). In Exp. 26, the construction of the following bars was at first similar to what was observed in the no-forcing experiment counterpart (Exp. 5): bars grew downstream from the first bar that was anchored to the external bank of the channel and widened (Fig. 2.13). In Exp. 5, this depositional pattern resulted in elongated bars that did not occupy the whole channel width at the downstream part of the sand plug (Fig. 2.13a). However, in Exp. 26 the bedload deposits reached the upstream limit of the backwater zone

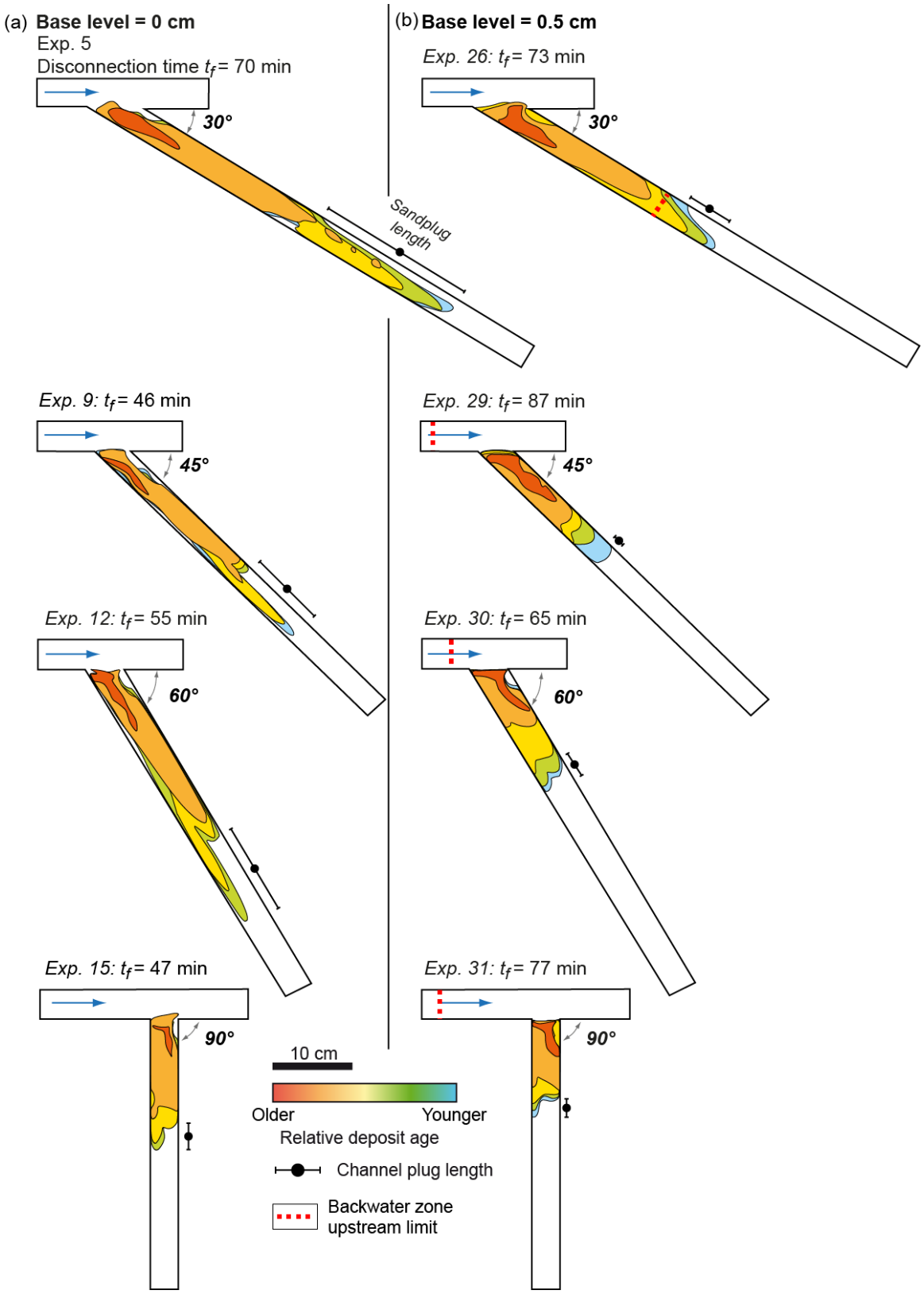

Figure 2.13: Plan view of final states of sand plugs for different β_2 angles with a base level of 0 cm **(a)** and with a base level rise of 0.5 cm **(b)**. Growth stages are indicated by the colours.

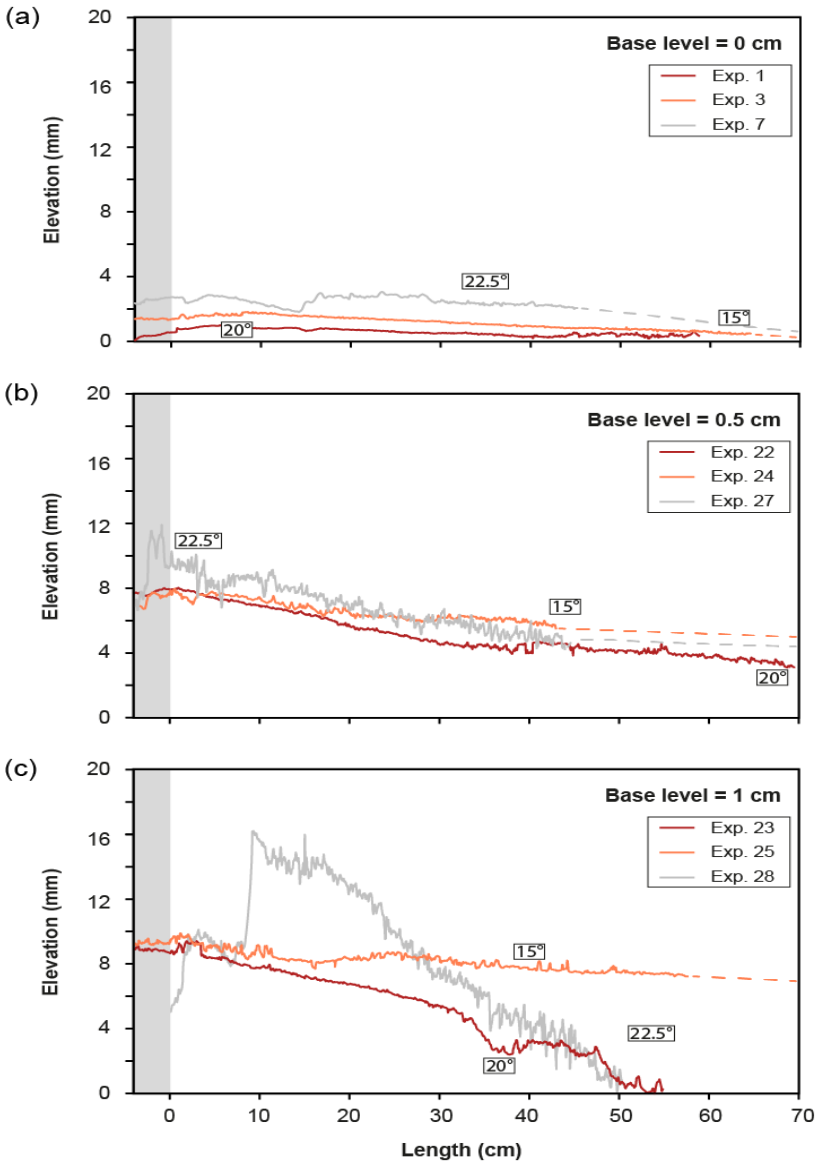

Figure 2.14: Mean longitudinal elevation profiles of the sand plugs for increasing β_2 angles in no-forcing **(a)** a base level elevation of 0.5 cm **(b)** and a base level elevation of 1 cm **(c)** scenarios for low diversion angles (15 to 22.5°), symmetrical or slightly asymmetrical experiments. Profiles were corrected for bottom slope to facilitate comparison. The grey area corresponds to the active channel.

that formed a still body of water, modifying the surface slope and the water depth in the distributary. Visual observation showed that the velocity (and thus kinetic energy) of the flow and its transport capacity were reduced. Upon reaching this limit the sedimentation pattern changed. A single body occupied the whole width of the channel and prograded. Consequently, plug downstream growth rate slowed (Fig. 2.13b). This sedimentation pattern by progradation of the sediment rather than longitudinal sand bars construction and migration, appeared akin to that of a delta. In Exps. 29, 30 & 31, where the backwater zone upstream limit was upstream of the bifurcation point, this prograding sedimentation pattern immediately took place after the first bar was formed in the flow separation zone (Fig. 2.13b).

In symmetrical or slightly asymmetrical experiments (Exps. 1, 22, 23, 3, 24, 25, 7, 27 and 28) the global thickness of the plug deposits increased with the base level rise (Fig. 2.14a-c). In

cases where no disconnection occurred despite differential base levels (Exps. 22, 24, 27 & 25), the bedload deposits formed a sand bed with a thickness roughly equivalent to the base level increase (Fig. 2.14b-c). When the base level was increased by 1 cm, the backwater zone reached the bifurcation for incidence angles superior or equal to 20° (Exps. 23 & 28), and disconnection occurred (Table 2.3), forming sand plugs (Fig. 2.14c). Sand plugs thickness decreased downstream, forming a wedge (Fig. 2.14c).

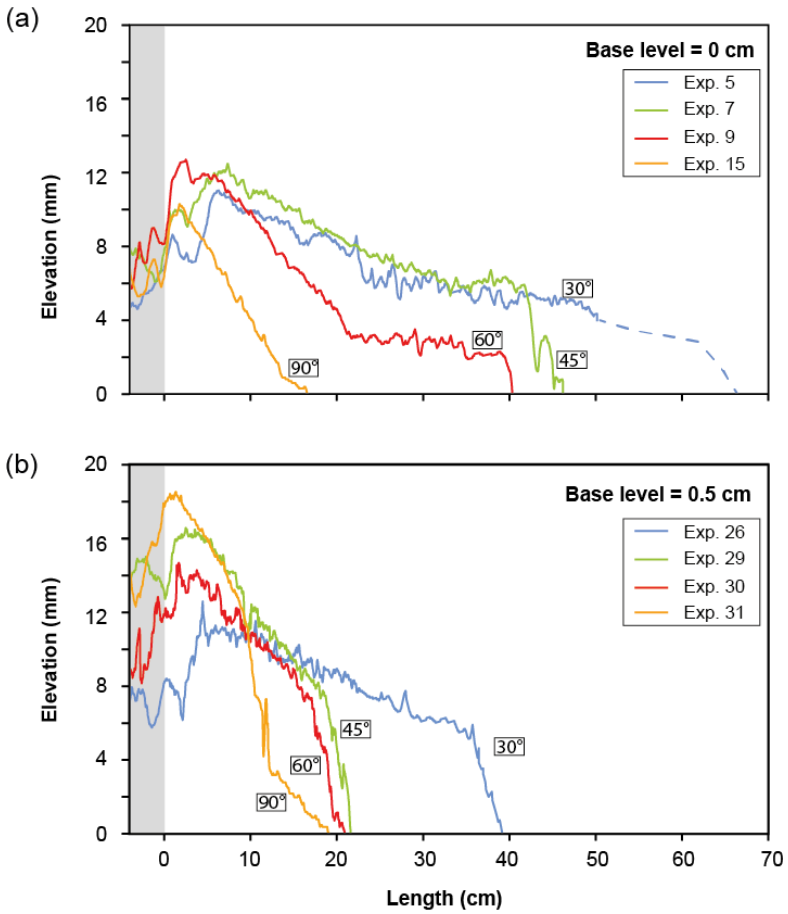

Figure 2.15: Comparison between mean longitudinal elevation profiles of the sand plugs for increasing β_2 angles in no-forcing **(a)** and base level elevated by 0.5 cm **(b)** scenarios. Profiles were corrected for bottom slope to facilitate comparison. The grey area corresponds to the active channel.

In all highly asymmetrical experiments (Exps. 5, 26, 9, 29, 12, 30, 15 and 31), a sand plug formed (Table 2.3). In no-forcing scenarios the upstream parts of the sand plugs were thick and their well-developed downstream parts were thinner and had a gentle slope (Fig. 2.15a). The sand plugs formed in raised base-level scenarios had a different profile, with the exception of Exp. 26, for which the sand plug geometry was almost identical to Exp. 5, albeit being shorter (Fig. 2.15). When the backwater zone reached the bifurcation (Exps. 29, 30 & 31), the upstream part of the plug was also well-developed and generally higher than in no-forcing scenarios and the sand plugs slopes were steeper (Table 2.3; Fig. 2.15). However, the downstream part of the plug was not developed and the sand plugs downstream extremity ended abruptly (Fig. 2.15b). Similarly to the no-forcing scenarios, the sand plugs slope increased and their length shortened when the incidence angle increased (Figs. 2.13, 2.15).

In no forcing scenarios, sand plug length decreased linearly when the diversion angle increased (Fig. 2.16a; Section 2.1). When the base level was elevated by 0.5 cm, sand plugs lengths were less strongly affected by the diversion angle (Figs. 2.16a & 2.17). Indeed, when the base level was elevated by 0.5 cm the sand plugs were formed in the backwater zone, or in the case of Exp. 26 reached the backwater zone (Figs. 2.13 & 2.17). When the sand plugs formed in the backwater zone, their length appeared instead linked to the raise in base level (Fig. 2.17), with lengths roughly equal to 5 times the channel width when the base level was raised by 0.5 cm (Fig. 2.16a). Sand plugs lengths in no-forcing cases and base level raise of 0.5 cm converged at high angles (Fig. 2.16a). Sand plugs volumes did not seem to be significantly affected by backwater effects (Fig. 2.16b), as shown by an overall linearly decreasing trend of sand plugs volume – formed under the different scenarios – when the incidence angle increased (Table 2.2; Fig. 2.16b).

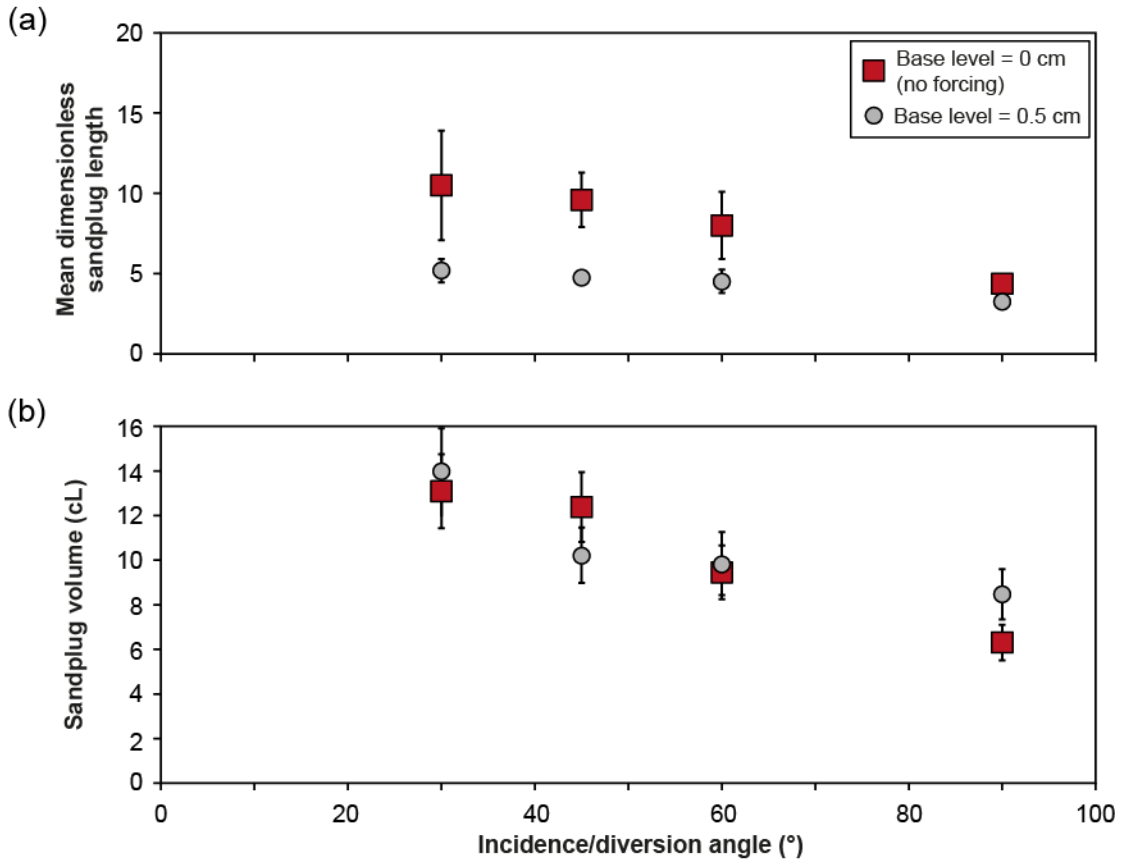

Figure 2.16: Plots of sand plug length **(a)** and volume **(b)** and the incidence angle β_2 for highly asymmetrical bifurcations.

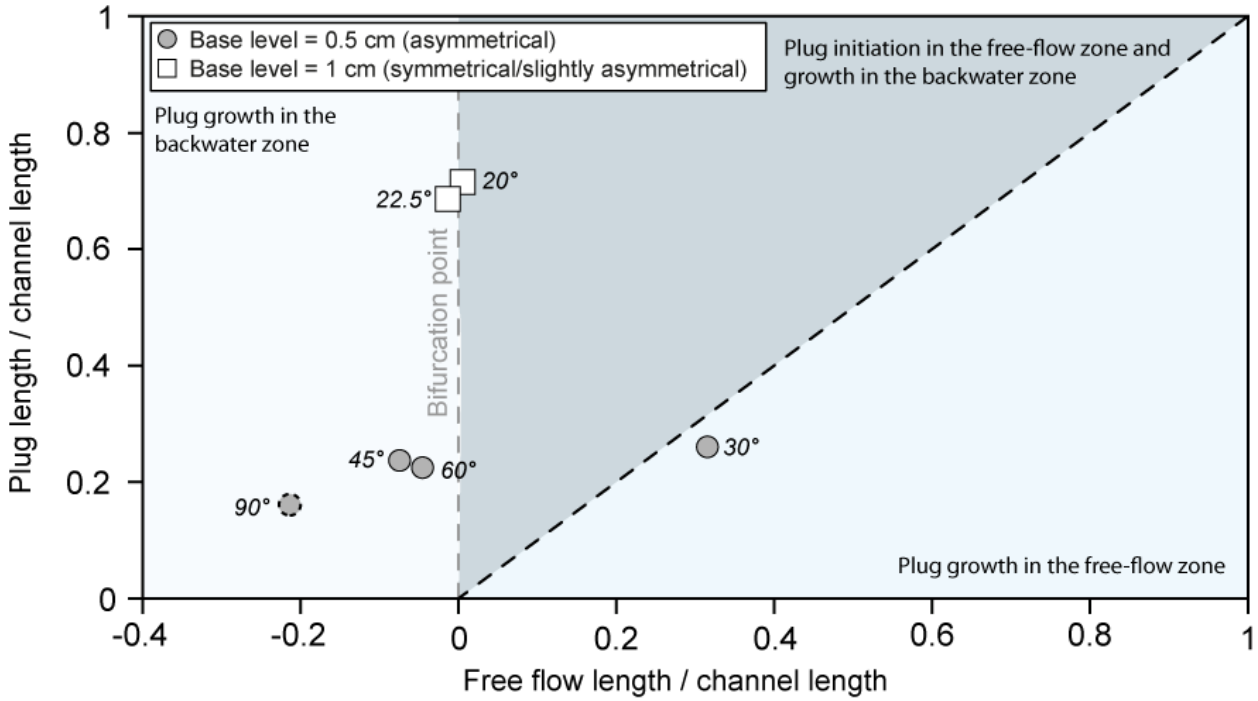

Figure 2.17: Plot of sand plug length on free flow zone length. Dashed point indicates that backwater zone length was calculated as the mean of distributary 2 and the inlet channel slope as distributary 2 was flat.

Finally, the time required for sand plug formation and disconnection of distributary 2 increased with base level elevation (Fig. 2.18). For a given base level, the disconnection times of the different experiments are modulated by the diversion angle, but all were within 25 minutes of each other (Table 2.2; Fig. 2.18).

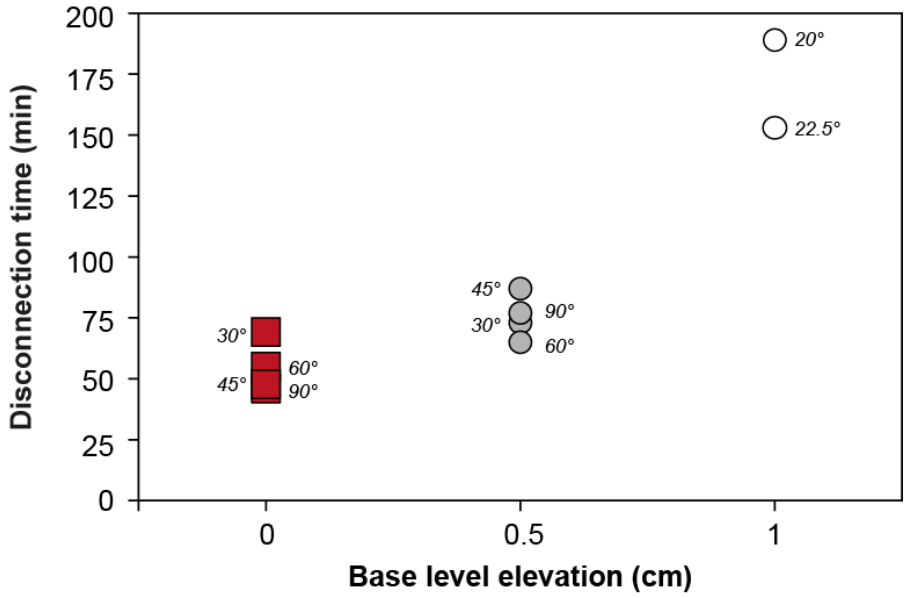

Figure 2.18: Plot of disconnection time and base level elevation.

2.2.3. Interpretation

The results of the two experiments with erodible beds showed no major effect on bifurcation stability, bedload dynamics or disconnection time. The setup bifurcation geometry (bifurcation and diversion angles and channel slopes) remained the main control in the tested settings. However, although the deposition processes and final architecture of the sand plugs in both experiments were similar, the sand plug deposited on top of the sand bed was shorter and consequently less voluminous. As the disconnection time was the same, it is probably due to a different sediment supply. Indeed at first sand plug construction was fast as sediment was readily available thanks to the sand bed reworking and the upstream supply. However the growth rate of the sand plug decreased quickly. When the plug formed it limited both the amount of sediment that could enter distributary 2 and the discharge. Consequently the discharge increased in distributary 1, causing channel entrenchment which further reduced the bedload supply to distributary 2 due to the topographic step thus formed between the channel and the sand plug (Slingerland & Smith, 2004; Richards & Konsoer, 2020), in a process similar to what was observed in levee breach experiments in Section 2.1.

Base level experiments showed that abandonment becomes possible for previously stable bifurcations when the backwater zone associated to the base level raise reaches the bifurcation point (Fig. 2.13). In such cases disconnection becomes possible at incidence angles ≥20°, lowering the threshold observed in the previous set of experiments (≥30°, Section 2.1). Indeed, Nittrouer et al. (2012), Chatanantavet et al. (2012), Wilson & Goodbred (2015), Fernandes et al. (2016) and Ganti et al. (2016a, b) found that backwater effects facilitate avulsion and are a major control on avulsion nodes position. In our case, when the backwater zone reached the bifurcation the flow became deeper and its velocity decreased, as the water-surface slope in distributary 2 decreased. Sediment deposition was thus encouraged. As only one distributary was affected by the backwater effect, the bifurcations became further unbalanced in their discharge and sediment partitioning, eventually leading to channel abandonment. However, the opposite effect can be achieved by artificially steepening the water-surface slope in the diverted distributary, as demonstrated by Bulle (1926) who used this process to force equal discharge partitioning in both distributaries of his experimental asymmetrical bifurcation.

As the asymmetrical bifurcations were already unstable due to their geometry, the outcome of these experiments (i.e., whether disconnection occurs or not) was not affected by the fact that the backwater zone reached the bifurcation and distributary 2 was disconnected. However, if

our setting had had longer distributaries, the decrease in water-surface slope induced by the base level rise would have been less significant, and the backwater zone may not have reached the bifurcation. Thus the sand plug growth and length would have remained unaffected by it, leaving the control of its length to the diversion angle.

When disconnection occurred, whether it was in symmetrical or asymmetrical configurations, the initiation processes of sand plug formation (first bar position, width and length) were still controlled by the flow separation zone width and thus the diversion geometry (Fig. 2.13) as described in Section 2.1. However, the deposition processes that followed the formation of the initial bar were affected by the deeper and slower flow when the sand plug reached the backwater zone, as in Exp. 26, or when it formed totally inside it (Exps. 23, 28, 29, 30 & 31). Consequently, the elongated, downstream migrating bars that were anchored to the sand plug and grew downstream in the free flowing channels of the no-forcing experiments, as described in Section 2.1, did not form. Instead, the sand plug grew by forming a progradation front, which led to the formation of shorter and more rectangular sand plugs (Fig. 2.15).

The experiments introduced in this section showed the influence of free surface slope modification related to base level elevation – in one distributary channel – on plug formation. The experimental setup did not allow accurate measurement of the water-surface along the channels, thus the water-surface slopes and their slope ratio between both distributaries could not be calculated. Instead, backwater length was estimated (Eq. 2.3). When backwater occurred, its effects were tentatively quantified using a dimensionless number that represents the fraction of the distributary channel outside of the backwater zone – thus located in the free flow zone (Fig. 2.17). Currently, with the limited set of experiments available, much remains to be known on these effects. For instance, Exps. 23 & 25 give precious insight on the destabilizing effect of the backwater zone on previously stable bifurcations but determining relationship between a base level increase and plug length is not possible. New sets of experiments with both 0.5 and 1 cm base level rise would be required using for instance geometries similar to those of Exps. 26, 29, 30 & 31.

Curiously, base level variation does not impact significantly the sand plug volume, which appears to be more strongly affected the diversion angle (Fig. 2.16b). Indeed, although the raise in base level decreased the sand plug length, it also resulted in sand plug thickening, occupying the whole channel width and adopting a more rectangular shape instead of a wedge-shaped one (Fig. 2.15) as they formed in the backwater zone (Fig. 2.17). This

phenomenon can be compared to the findings of Sahoo et al. (2020), which demonstrate that in a confined channel backwater effects induce vertical stacking of sedimentary bodies until aggradation deconfines it, leading to an avulsion. In our setup this would lead to important vertical aggradation along the sand plug, making it thick and rectangular, until it completely plugged the channel, effectively disconnecting it and completing the avulsion. This vertical aggradation and new shape of the sand plug allowed maintaining a roughly equivalent volume of the sand plug with the no forcing experiments despite their shortened length (Fig. 2.16).

2.3. Conclusion

The flume experiments presented in this chapter showed that – with water and sediment discharge maintained constant and fixed channel banks – channel abandonment is influenced by the bifurcation asymmetry and associated slope changes. These experiments allowed monitoring the formation of sand plug formation leading to channel abandonment through the amalgamation of migrating channel bars (Fig. 2.9).

Typically, a bifurcation becomes unstable when the diversion angle is ≥30°. The value of the diversion angle controls the width and length of a flow separation zone, which controls the inception of the sand plug. Sand plug length and volume inversely correlate with diversion angle. Levee breaching modulates the results without disrupting the general trends. Additional experiments – with fixed 90° diversion angle and varied bottom slope in the diverted channel – produced abandonment despite slope (dis)advantage, supporting an impact of diversion angle alone.

The presence of a sand-bed does not impact the sand plug deposition processes nor its architecture. However the resulting sand plugs are shorter and less voluminous due to a reduced sediment supply following the active channel entrenchment. When free surface slopes are modified in response to base level rise in one distributary channel, the resulting sand plugs formation processes and geometry are modified. The modification of the water surface slope can destabilize a stable bifurcation, leading to channel abandonment and lowering the diversion angle threshold for disconnection to 20°.

Chapter 3: Experimental abandonments in curved channels geometries: insights on the architecture of cutoff bedload fills

Ce chapitre se concentre sur le dépôt de sédiments de charge de fond dans des chenaux courbes abandonnés expérimentalement. L'objectif est de reproduire certains des processus majeurs ayant lieux durant les recoupements de méandres afin de déterminer les effets respectifs de (i) la largeur du chenal nouvellement incisé, (ii) la valeur de l'angle de diversion et (iii) les variations de la pente de la surface de l'eau sur la géométrie des bouchons de chenaux formés à la fois à l'amont et à l'aval du chenal abandonné.

This chapter focuses on bedload deposition in experimentally-abandoned curved channels. The objective is to reproduce some of the major processes at play during cutoffs (neck and chute) in order to decipher between the effects of: (i) cutoff channel width, (ii) diversion angle and (iii) water-surface slope variations on the geometry of both the upstream and downstream plugs in curved channels.

3.1. Introduction

Experiments presented in Chapter 2 allowed the quantification of a negative relationship between the channel plug length and volume and the diversion angle in a fixed bed and bank setup, and then investigated the backwater effect on channel plug geometry. These experiments showed that the initial deposition model could be challenged with the modification of the water-surface slope, a process that occurs in association with cutoffs. Chute cutoffs shorten and straighten channel paths by carving a path through the inner part of a meander. The stream flow is captured either by a swale between scroll bars or by headward erosion propagating upstream through the meander loop or when the channel intersects its own path. The associated curved channels often consist of low gradient channels that are active during floods. In time, the new channel path widens and deepens enough to capture most of the flow until the old channel is abandoned. The cutoff channel has a steeper gradient than the old meander channel, which results in a fast diversion of the river due to the quick regressive erosion that isolates the old meander loop. As cutoff events shorten the river length (Fisk, 1947; Allen, 1965; Lewis & Lewin, 1983), the elevation differential between the bifurcation and the confluence point remains the same and the slope of the newly formed cutoff channel is steeper than in the old channel. Due to the generally important difference in length between neck cutoff abandoned channel and its cutoff channel compared to other chute channel configurations, the modification of water-surface slope is comparatively more important in neck cutoff configurations than in other cutoff configurations.

In natural systems, the initial cutoff channel is generally narrower and shallower than the curved channel. Channel widening leads to increased discharge, which in turn results in channel deepening (Zolezzi et al. 2006). Theoretical modelling using the nodal point condition (Wang et al., 1995) found that the water and sediment partitioning at a bifurcation depend on the downstream channels width, the wider branch capturing a larger fraction of both. This assumption has been confirmed by field studies on several bifurcations (Zolezzi et al. 2006). As such channel bank erodibility and channel widening rate are key factors in bifurcation stability and channel abandonment (Kleinhans et al. 2013). Federici & Paola (2003), Miori et al. (2006) and Van Denderen et al. (2018) found that bifurcation stability depended on the ability of the channels to adapt their width and that stable bifurcations are highly asymmetrical, with one branch being larger and receiving more water and sediment. Miori et al. (2006) found that only this configuration was stable in settings with highly erodible banks. However, Miori et al's model do not take into account the local effects of bar

migration through the bifurcation, which can drastically modify the discharge and sediment partitioning and potentially lead to stable configurations with one branch completely abandoned, as demonstrated by Bolla Pittaluga et al. (2003) and Bertoldi et al. (2009). Indeed, the presence of bars can increase the slope advantage in favour of the channel that receives the larger portion of the discharge (Miori et al. 2006; Zolezzi et al. 2006; Bertoldi et al. 2009; Kleihans et al. 2013), leading to channel abandonment.

When abandonment occurs and the banks are cohesive, the lower rate by which the new channel widens results in long-lasting stable bifurcation. Simultaneously discharge and sediment supply are slowly reduced in the curved channel, resulting in progressive channel shallowing (Zolezzi et al., 2006) and narrowing by bedload deposition along the channel banks (Constantine et al. 2010a; Sorrells & Royall, 2014; Reynolds & Royall, 2020). Although bank cohesion plays a role in neck cutoff formation by modulating channel migration, narrowing is less likely to take place as neck cutoffs do not form lasting bifurcations. This results in fewer bedload deposits in the abandoned channel (Fisk, 1947, Allen, 1965).

Field observation on channels abandoned by cutoff processes showed that the coarse part of the channel plugs, formed by bedload deposits, tends to be longer in case of chute cutoffs than neck cutoffs (Fisk 1947; Allen 1965). Neck cutoff channels also tend to have higher diversion angles than chute channels (Fisk 1947). These observations have led to the theory that the diversion angle between the active and disconnected channels controls the lengths, volume and geometry of the coarse-grained bedload deposits in abandoned channels (Fisk 1947; Bridge et al. 1986; Shield & Abt 1989; Hooke 1995), although no clear relationship between channel plug length and diversion angle has been quantified on the field (Piégay et al., 2008; Constantine et al., 2010a). Section 2.2 thus provided an alternative explanation that the difference observed in plug geometry could as well be the result of hydraulic processes.

3.2. Methodology

3.2.1. Experimental design

The experiments were realized on the same frame as the ones presented in Chapter 2, at the Geomorphic Lab of the Centre de Géosciences of MINES ParisTech, Fontainebleau. They were designed by LS and JLG, and conducted by Armand Crouzet and Pierre Maria, two students of second year in the CESI engineer school in Nanterre. The walls of the flume were fixed and the setting was composed of two parts: an upstream straight inlet channel (rectangular section –Plexiglas) followed by a curved channel carved in a piece of Styrofoam (rectangular section) (Fig. 3.1), which simulated overbar through (thereafter named 'open geometry configurations) and neck cutoff configurations (thereafter named 'closed geometry configurations) (Fig. 3.1). The Styrofoam block was set at a global slope of 1.48%. Consequently the straight channel had a slope of 1.48%, while the curved channel slope was lower and varied along its length depending of its curvature and orientation relative to the global slope. In some experiments simulating neck cutoffs configurations the Styrofoam bed slope in the curved channel can locally be positive before the experiments reach equilibrium. Despite this, the overall slope of the curved channels – i.e., the difference in elevation of the curved channel bed between the bifurcation and confluence divided by the curved channel length – was 1.22% for the open geometry configurations and 0.14% for the closed geometry configurations. Each configuration was reversible, allowing testing two sets of bifurcation (β_b) and confluence angles (β_c) per geometry. The straight channel length was 142 cm from the inlet to the outlet while the curved channel length varied from 68 cm (open-meander geometry) and 88 cm (closed-meander geometry). Length ratios between the curved and straight channels (L_1/L_2 *ratio*) – measured between the bifurcation and confluence points – were thus 0.83 for open-meander geometry experiments and 0.1 for closed-meander geometry experiments. Channel width was constant at 4 cm in any straight or curved channel, with the exception of two experiments during which the straight channel width was reduced to 2 and 3 cm (simulating the chute cutoff channel) between the bifurcation and confluence points (Table 3.1).

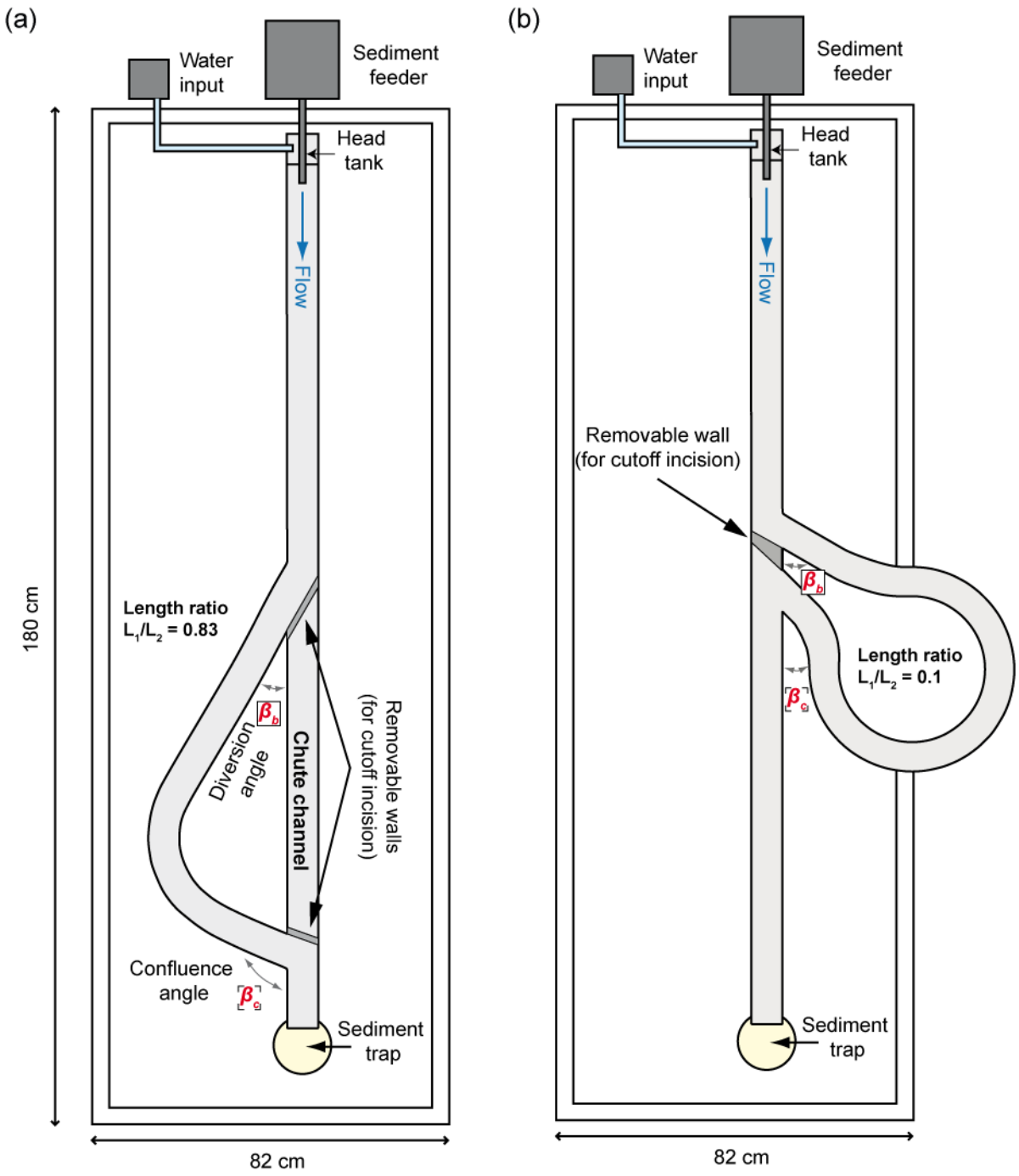

Figure 3.1: Overhead view of the experimental setup showing the open- **(a)** and closed- **(b)** meanders configurations as well as the walls that were removed to simulate incision. Each configuration was reversible.

Exp	Parameters	Upstream				Downstream				Theoretical backwater length (cm)	Equilibrium water-surface slope ratio S_2/S_1	Remarks
		Diversion angle	Mean dimensionless sandplug length	Immersion/Emersion ratio	Bedload volume (cL)	Confluence angle	Mean dimensionless sandplug length	Immersion/Emersion ratio	Bedload volume (cL)			
AR-OM1	Avulsion with reconnection - Open meander	25	10,6	-	15,8	120	1,4	-	0,1	57,4	0,71	Pool at the apex outer bank
AR-OM2	Avulsion with reconnection - Open meander	60	6	1,2	12,2	155	2,1	-	4,1	49,2	0,66	Sediment deposition at the apex outer bend - no deposition at the inner bend
AR-CM1	Avulsion with reconnection - Closed meander	60	2,5	1,3	5,6	45	2,9	7	5,0	148,8	0,25	Upstream plug abrupt dip - Downstream plug tapered
AR-CM2	Avulsion with reconnection - Closed meander	135	1,5	1,2	2,0	120	1,6	-	2,0	128,5	0,1	Upstream plug abrupt dip - Downstream plug tapered
E1	Avulsion with reconnection - Open meander - Straight channel 2 cm	25	-	-	-	120	-	-	-	-	-	No disconnection
E2	Avulsion with reconnection - Open meander - Straight channel 3 cm	25	-	-	-	120	-	-	-	-	-	No disconnection - Slower equilibrium
S1	Scroll slough cutoff incision	25	8,3	-	11,5	120	0,3	-	1,1	57,4	0,8	Fast disconnection - Plug shaped by inherited topography
S2	Scroll slough cutoff incision	60	3,3	1,9	11,1	155	0,9	-	0,9	57,4	0,53	Fast disconnection - Plug shaped by inherited topography - Plug and bars emmersion
N1	Neck cutoff incision	60	0,9	1	0,8	45	1,4	1,5	2,1	121,8	0,15	Fast disconnection - Plug shaped by inherited topography - Plug and bars emmersion
N2	Neck cutoff incision	135	1,4	1	0,5	120	1,4	-	1,4	115,0	0,31	Fast disconnection - Plug shaped by inherited topography - Plug and bars emmersion

Table 3.1: List of the experiments and resulting channel plug characteristics.

Input water and sediment discharges were constantly fed at rates of 300 and 0.6 L h^{-1}, respectively, as in Chapter 2. The water was delivered through a head tank to reduce the flow turbulence and was dyed blue to enhance contrast in pictures. The sediment was a well-sorted, rounded to sub-angular, fine (d_{50}=209 µm) Fontainebleau sand. A sediment trap at the outlet of the experiment was used to quantify the volume of sediment that bypassed the channels during experimental runs. The experiments started in an empty flume and lasted until equilibrium was reached, which was defined as when the flux measured in the sediment trap was the same as the input flux.

A set of 10 experiments were designed with two different configurations that had different planform geometries and bifurcation angle β_b values of 25, 60, 60 and 135° and corresponding confluence angles β_c values of 120, 155, 45 or 120° (Table 3.1). The bifurcation and confluence angles were measured as the angle between initial direction of the flow and the new branch. The first set of experiments had an open-meander geometry (Fig. 3.4a-b), with respective β_b and β_c values of 25 and 120° in one configuration (Exps. AR-OM1, & S1) and of 60 and 155° when reversed (Exps. AR-OM2 & S2). Experiments AR-OM1 and AR-OM2 were performed with the cutoff channel in place since the beginning. In contrast, experiments S1 and S2 simulated cutoff incision (Fig. 3.1). Similarly to Chapter 2, the walls were removed after the system reached equilibrium where bedload deposition allowed the adjustment of the channel bottom slope. Additionally, experiments E1 and E2 were performed using the same geometry as Exp. AR-OM1, but with modification of the width W_1 of the straight channel (Fig. 3.5a-b) to respectively 2 and 3 cm (Table 3.1).

The second set had a closed-meander geometry (Fig. 3.4c-d). The associated experiments had respective β_b and β_c values of 60 and 45° in one configuration (Exps. AR-CM1 & N1) and of 135 and 120° when reversed (Exps. AR-CM2 & N2). Experiments AR-CM1 and AR-CM2 were performed with the cutoff channel in place since the beginning while Experiments N1 and N2 simulated incision using removable walls (Fig. 3.1) similarly to Experiments S1 and S2 (Table 3.1). Due to material constraints the closed-meander experiments represent simplified geometries as no upstream or downstream curvature were modeled, resulting in less realistic geometries of the inlet and outlet parts of the flume. Although imprecise, the experiments allow comparison of the bedload deposits and their geometrical controls in varied cutoff geometries.

3.2.2. Data acquisition

Data acquisition was mostly similar to that presented in Chapter 2. During experiments, overhead pictures of the experimental runs were taken every 30 seconds with a camera while 3D photogrammetric surveys were made every 30 minutes (Fig. 3.2) (see Chapter 2 for details). The DEMs had a minimal precision of 0.4 to 0.5 mm.

The overhead pictures were analyzed using a Python script to automatically differentiate between the underwater sand from the emerged one – using pixels blue band intensity (from the dyed water) and saturation thresholds – to identify the Plexiglas or Styrofoam channel-bed, the emerged bars and the underwater sediment (Fig. 3.3). The method is inspired from Tal et al. (2012). It allowed for computing curved channel area that was empty or occupied by either the underwater or emerged bedload deposits for each overhead picture, as well as fill evolution curves through time (Figs. 3.4, 3.5 & 3.6). The overhead pictures were also used to monitor and report at regular intervals the sand deposit evolution and their spatial extent for all experiments where disconnection occurred (Table 3.1), allowing the creation of the deposit evolution maps (Fig. 3.7). Additionally, free surface elevation was measured along both channels at regular intervals during the experimental runs. It was then plotted for both channels against the channel longitudinal length (Fig. 3.8). Measurements were made using millimetric scales drawn on the Styrofoam bank of the channels with a precision of ± 0.5 mm. The scales were placed at key locations regularly spaced along the channels. 9 measurement points were selected in the open-meander configurations and 21 in the closed-meander configurations. The free surface elevation measurement was a time consuming process that required two operators in order to be accurate while still being able to observe the sedimentation dynamics. Thus this measurement was introduced during the internship of Armand Crouzet and Pierre Maria who conducted the observations.

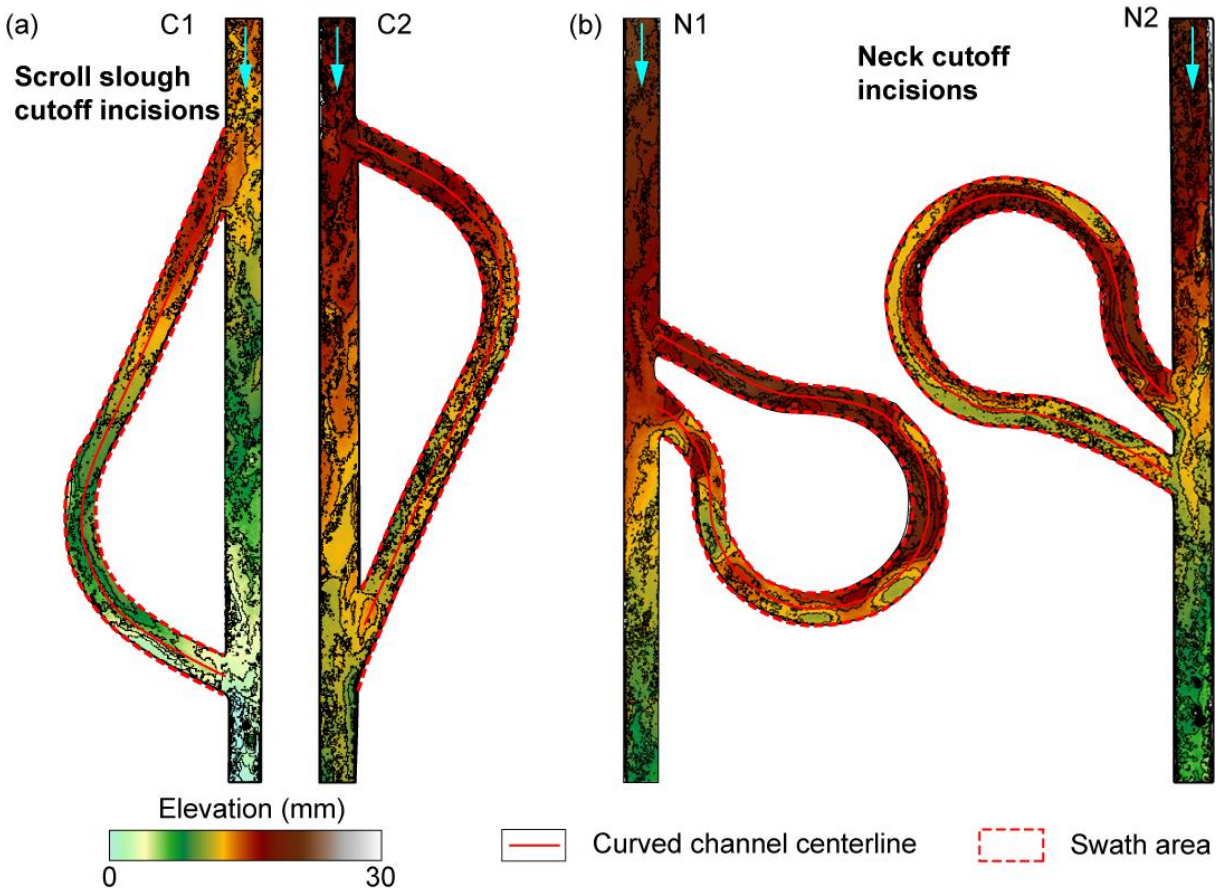

Figure 3.2: Final deposits DEM of experiments S1 & S2 **(a)** and N1 & N2 **(b)** illustrating the swath method used to build the deposits longitudinal mean elevation profiles. Contour line are spaced by 2 mm.

The whole length of sand bodies (both the emerged and underwater parts) was first measured using direct measures during the experimental runs and then using the overhead pictures. Channel plug length was measured between the diversion point and the last location where it extended over the whole channel width (minimal plug length) and at its downstream limit for the upstream channel plugs (maximal plug length). In the following, the channel plug corresponds to the mean of these two measurements. Plugs that developed from the confluence point were measured in a similar way. In cases with cutoff incision only the deposits that formed during the cutoff phase are included in channel plug measurements. The DEMs were used to produce the mean longitudinal elevation profiles of the bedload deposits in the curved channels (Fig. 3.9). These longitudinal elevation profiles were corrected for the variable slope of the curved channel induced by the channel curvature in the fixed-slope setting by drawing segments along the curved channels length in empty 3D scans of the experiments, measuring their slope and using it to correct the deposits elevation along the same segments. Several control points measured manually during the experimental runs were used to validate these corrections. Total bedload deposits volumes were measured after

extraction of the sediment from the curved channel at the end of the experiments, while individual channel plug volumes were calculated from the DEMs and longitudinal profiles using the same method as in Chapter 2. When comparable, the channel plug volume data shows that the 3D measurements underestimate the channel plug volume by 2-10%. The channel plug length and volume were then plotted against diversion angles and compared with data from experimental runs made in the avulsion setting with variable base level in Section 2.2 (Fig. 3.10). The water surface slope ratios S_2/S_1 were measured at equilibrium for each experiment (Table 3.1) and compared with channel plug extent and volume (Fig. 3.11). Water discharge could not be precisely monitored in each channel as in Chapter 2, so flow dynamics in the channels was estimated using visual observation of floating objects.

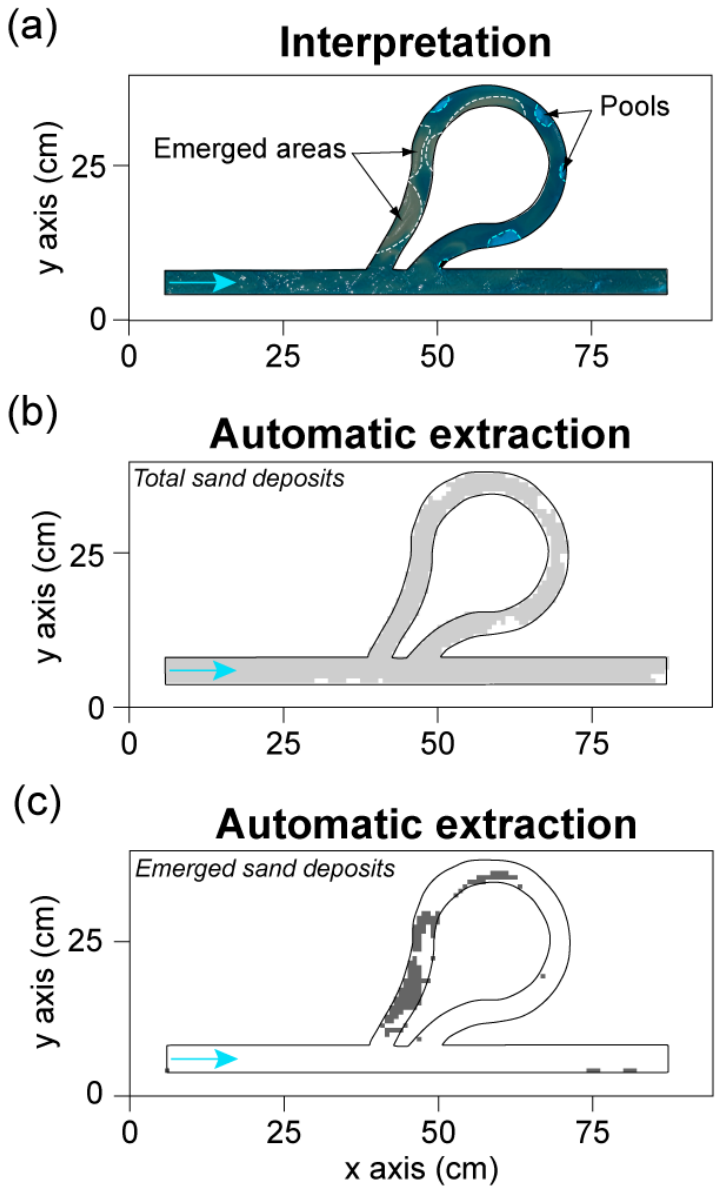

Figure 3.3: Interpreted overhead photograph **(a)** and total sand deposits **(b)** and emerged sand deposits **(c)** mapped using color and saturation computer treatments of the picture.

3.3. Results

Experiments began with a very short (1-2 min) phase of downstream sediment progradation in the inlet channel up to the bifurcation area, followed by the propagation of the sediment in the open channel(s). The sediment partitioned similarly to what was observed in Chapter 2. Sedimentation in the straight channel followed a downstream migrating bars pattern, whereas in the curved channel the sedimentation had a mixed pattern of downstream migrating bars from the bifurcation point and lateral accreting ones at the channel apex. In the cutoff incision experiments, the walls were removed after a first equilibrium within the curved channel was reached, then the experiment was conducted until a new equilibrium within each of the two open channels was reached.

3.3.1. Bedload deposits in the case of local avulsions

All curved channels were disconnected in experiments with pre-existing cutoff channels in place (Exps. AR-OM1/AR-OM2, AR-CM1/AR-CM2) (Table 3.1; Fig. 3.4). Bedload sediment progressively deposited from the bifurcation point, forming a channel plug. Automatic extraction of sand area from pictures showed that most of most of the sand surface was under water. Furthermore, the rate of growth of the plug slowed over time and reached a plateau (Fig. 3.4). The area of the meander loop occupied by sediments decreased when the diversion angle β_b increased (Fig. 3.4, Exps. AR-OM1 & AR-OM2, AR-CM1 & AR-CM2). A stronger effect of channel geometry (i.e., open- vs closed-meander) was observed (Fig. 3.4): bedload deposits occupied 50 to 80% of the surface of the curved channel in the case of open-meander geometries and only 20-30% in closed-meander geometries. This control of the channel geometry over diversion angle was confirmed by experiments AR-OM2 & AR-CM1, which had an identical diversion angle but a different geometry. In Exp. AR-OM2 (*Open-meander geometry*, $\beta_b = 60°$) the curved channel surface was occupied at 60% by sediments whereas in Exp. AR-CM1 (*Closed-meander geometry*, $\beta_b = 60°$) the surface was reduced to 30%. Similarly, the time needed to reach disconnection and equilibrium was controlled by both the diversion angle and the channel geometry. Indeed it increased from around 70-80 minutes with a 25° diversion angle to 100-110 minutes with a 135° diversion angle, and despite having the same diversion angle than Exp. AR-OM1 (60°), Exp. AR-CM1 reached equilibrium 20 minutes faster (Fig. 3.4 a-b).

The sedimentation patterns in the curved channels were modulated by the channel geometry (Fig. 3.7a-d). The channel plug started its formation anchored at the internal bank of the

curved channel just downstream of the bifurcation, in the flow separation zone, where visual inspection using floating devices showed flow velocity to be the lowest. In open-meander configurations it then extended downstream while increasing its width until it occupied the whole channel width (Fig. 3.7a-d). The channel plug grew by a succession of downstream migrating bars, each anchored to upstream ones, forming an amalgamated sedimentary body. The first bars of the channel plug that reached the apex were deviated towards its external bank (Fig. 3.7a-b). For closed-meander geometries, the channel plugs grew by progradation and their channel plugs were shorter and did not reach the curved apex.

In each case, a channel plug also formed at the downstream extremity of the curved channel (Fig. 3.7a-d). It also started its formation on the internal bank of the channel relative to the flow in the straight channel, just upstream of the confluence, and grew upstream and laterally. It occupied only a portion of the channel width during Exp. AR-OM1 (Fig. 3.7a). In that particular case, the partial plug length was measured with the lower value being null, and the upper value its maximal extent. For the 3 other experiments the downstream channel plug spanned the whole width of the channel (Fig. 3.7b-d). Downstream channel plug formation started only after the upstream plug started occupying the whole channel width and the subsequent decrease of discharge in the curved channel, and it kept growing for a few minutes from downstream after the upstream plug stopped growing (Fig. 3.6c, e & g).

In these local avulsion modeling experiments, the upstream and downstream channel plugs formed the only deposits in the curved channels. For open-meander geometry (Exps. AR-OM1 & AR-OM2), the upstream channel plugs had roughly the same elevation and their downstream slope increased with the diversion angle (Fig. 3.9a). Both the upstream and downstream plugs were wedge-shaped with a slope break at their extremities, resulting in an abrupt lee face. For closed-meander geometry (Exps. AR-CM1 & AR-CM2), the elevation of the upstream channel plug lowered when the diversion angle increased and channel plugs had a more rectangular shape (Fig. 3.9b).

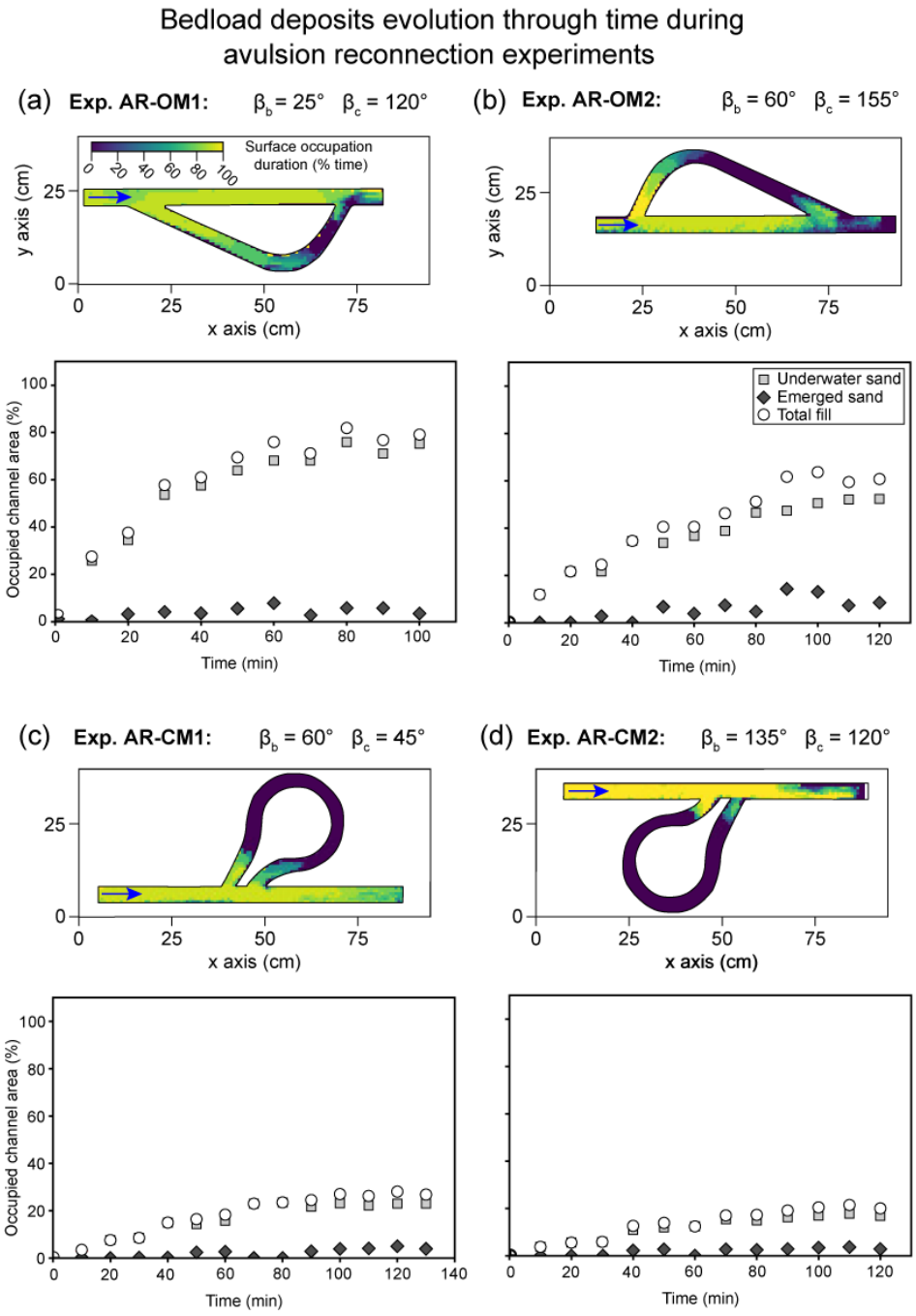

Figure 3.4: Final occupation maps and temporal occupation of curved channels for the reoccupation experiments. Experiment AR-OM1 **(a)** Experiment AR-OM2 **(b)** Experiment AR-CM1 **(c)** Experiment AR-CM2 **(d)**.

In these experiments, both the upstream diversion angle and curved channel geometry affected water-surface elevation in the straight and curved channels (Fig. 3.8). For open-meander geometries, where the curved channel length was 1.2 times the length of the straight channel (Fig. 3.1a), the water surface elevation increased by around 1 mm across the whole channels length when the diversion angle increased from 25 to 60°. In these experiments, the

curved channel water surface elevation was lower over most of its length than in the straight channel (Fig. 3.8a). However, just upstream of the confluence point the water surface elevation became slightly higher in the curved channel than in the straight channel (Fig. 3.8a). In both channels the water surface slope decreased gently, and the curved channel had a slightly lower gradient than the straight channel, resulting in water-surface slope ratios S_2/S_1 of 0.66 (β_b = *25*°) and 0.71 (β_b = *60*°) (Table 3.1). For closed-meander geometries, the straight channel was 10 times shorter than the curved channel (Fig. 3.1b), and the global water surface elevation between the bifurcation and confluence points was roughly constant in the straight channel but in the curved channel it decreased by around 5 mm when the diversion angle increased fom 60 to 135° (Fig. 3.8b). In this configuration, the water surface elevation in the curved channel was for the most part higher or equivalent than that of the straight channel down to the confluence point (Fig. 3.8b). The water surface slope in the curved channel was very low due to its length, resulting in slope ratios S_2/S_1 of 0.10 (β_b = *155*°) and 0.25 (β_b = *60*°) (Table 3.1).

3.3.2. Effects of cutoff channel width on bifurcation (un)stability

Experiments E1, E2 and AR-OM1 (*open-meander geometries*, β_b = *25*°, β_c = *120*°) were designed to look at the effect of the cutoff channel width variation, from half the width of the curved channel up to equal widths. In these experiments no disconnection was attained as long as the cutoff channel width was narrower than the curved channel width (Exps. E1, W_1 = *2cm* & E2, W_1 = *3 cm*) (Fig. 3.5a-b). While 90% of the curved channel surface was occupied by sediments at the end of both E1 and E2 experiments (100 min), it took longer to reach this state in Exp. E2 (55-70 min) than in Exp. E1 (40 min) (Fig. 3.5a-b). Sediment also occupied a smaller length of the cutoff channel between the diversion and confluence points in Exp. E1 than in Exp. E2. When the curved channel was disconnected during Exp. AR-OM1 (W_1 = W_2 = *4 cm*), sediments occupied only 70-80% of its surface (Fig. 3.5c). Unlike in Exps. E1 & E2, where deposition occurred in the curved channel at a very regular rate before stopping (Fig. 3.5a-b), their deposition rate slowed over time and (Fig. 3.5c) and an equilibrium plateau was reached after 70 to 80 minutes. Bedload deposits formed over the whole surface of the narrow part of the cutoff channel. In all three experiments sand emersion was null.

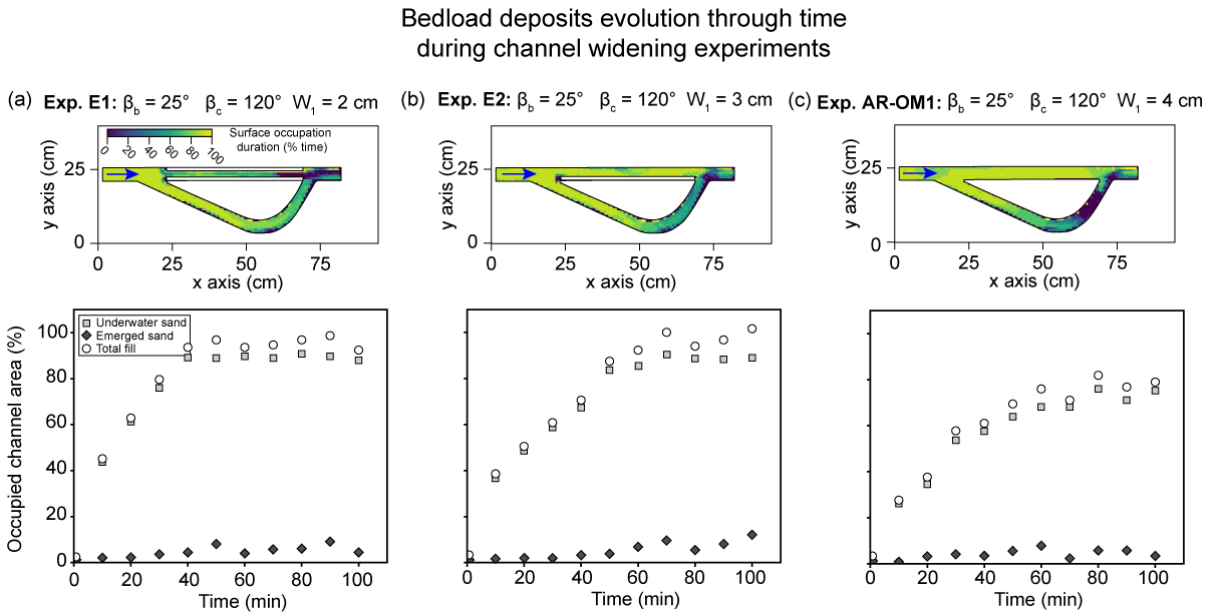

Figure 3.5: Final occupation maps and temporal occupation curve of the curved channels for straight channel experiments with modified width E1 & E2 **(a-b)** up to the upstream channel width (AR-OM1) **(c)**.

3.3.3. Bedload deposits in the case of cutoff incision

In cases of cutoff incisions (Exps. S1, S2, N1 & N2), bedload sediments were deposited in the curved channel in two phases. The first phase, before the removing of the walls, simulated deposits in the curved channel in an equilibrium stage with the flow. The curved channel was progressively occupied by downstream migrating and laterally accreting the bedload sediments along the channel, until equilibrium was reached (Fig. 3.6a-d). During this initial phase, 60 to 80% of the curved channel area was occupied by underwater bedload. Initiation time for channel filling and the fill rate depended on both the curved channel geometry (Fig. 3.6a & c) and the diversion angle (Fig. 3.6 a-b & c-d). Similarly to experiments without cutoff incision, the filling rate was higher and equilibrium attained faster for open-meander geometries (30 to 50 minutes) than for closed-meander geometries (100 to 130 minutes). Additionally, sediment area growth rate decreased when the bifurcation angle β_b increased (Fig. 3.6). Due to the length of the bend channel in closed-meander geometries, the time needed to reach equilibrium during both phases of experiments N1 and N2 was noticeably longer than in open-meander geometries (Fig. 3.6c-d).

The second phase started when the walls were removed. Flow and sediment responses were similar in both configurations after the wall removal, but with a different response time. The wall removal connected the upstream and downstream parts of the straight channel that induced an immediate and important decrease in water elevation in the curved channels, resulting in the immediate emersion of part of the bedload deposits accumulated during the

first phase of the experiments with no sediment transport or erosion (Fig. 3.6). These emerged deposits were preferentially located at the internal bank of the channel mouth, partially plugging the channel, and at the channel apex inner bank (Figs. 3.6 & 3.7e-h).

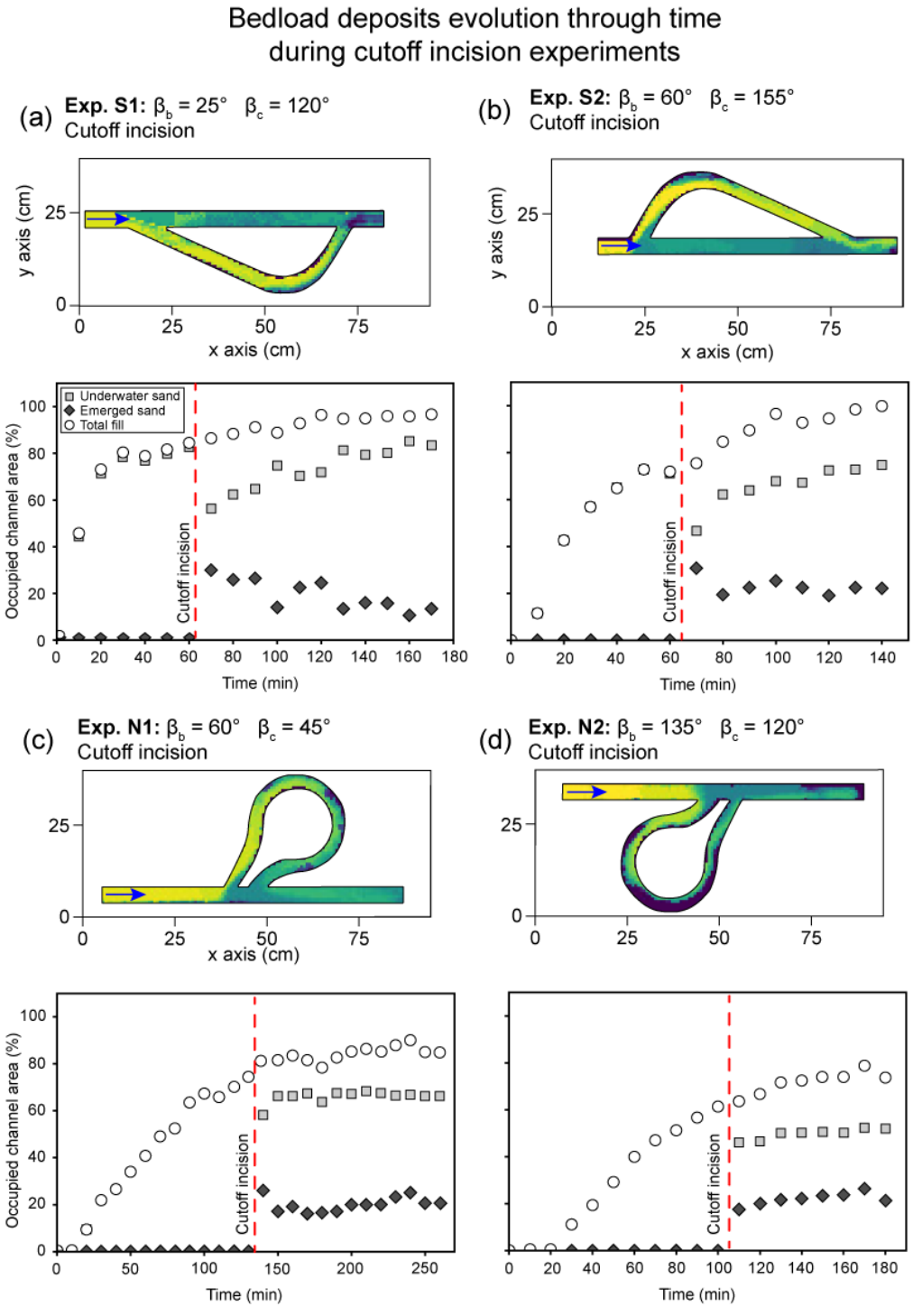

Figure 3.6: Final occupation maps and temporal occupation curve of the curved channels for cutoff incision experiments. **(a)** Experiment S1. **(b)** Experiment S2. **(c)** Experiment N1. **(d)** Experiment N2.

Simultaneously, a transient knickpoint was formed in the straight channel and migrated upstream in the inlet channel from the bifurcation area, resulting in an adjustment of the slope in the inlet channel. Consequently, sediment deposition started in the straight channel between the bifurcation and confluence points, forming a sand bed thanks to sediment progradation. The sand bed deposition prompted water surface elevation in the straight channel, and then in the curved channel. This resulted in a relative decrease of the subaerial deposits surface, compensated by a relative increase of the submerged deposits surface (Fig. 3.6). This process lasted between 50 and 80 minutes for the scroll slough cutoff configuration experiments (Fig. 3.6a-b) and only 5 to 10 minutes for the neck cutoff configuration experiments (Fig. 3.6c-d). The difference was due to the cutoff channel being 5 times shorter in neck-like configurations. Over time the total fill area of the curved channels increased slightly due to the slow deposition of new sediments in some areas of the channel left unoccupied during the first phase, mostly pools at the apex and thalwegs at the bifurcation and confluence areas (Fig. 3.7e-h). In cutoff incision experiments, the curved channel disconnected faster than in avulsion and reconnection experiments (Figs. 3.4 & 3.6). In experiments with incision, 80 to 100% of the surface of curved channel was filled, noticeably larger than for the corresponding experiments without incision (Figs. 3.4 & 3.6). These final fill areas were smaller for neck cutoff configurations experiments and only slightly affected by the diversion angle (Fig. 3.6).

In case of cutoff incision, sediment preferentially deposited along the inner bank of the three channel bends during the first phase of the experiments (Fig. 3.7e-h). Once the cutoff channel was opened, the shallow part of these deposits became emerged due to the decreased water elevation. The flow energy also decreased and sedimentation immediately started in the thalweg formed during the first phase of the experiments. New deposits formed several bars that migrated in the topographic lows and then aggraded at the bifurcation point, plugging the thalweg and forming a channel plug that incorporated the deposits accumulated prior to the cutoff initiation (Fig. 3.7e-h). Similarly, the downstream extremity of the curved channel was plugged by sediments transported by the downstream flow in the straight channel that penetrated in the bent channel. Sedimentation started once the sediments progressing in the straight channel reached the confluence area.

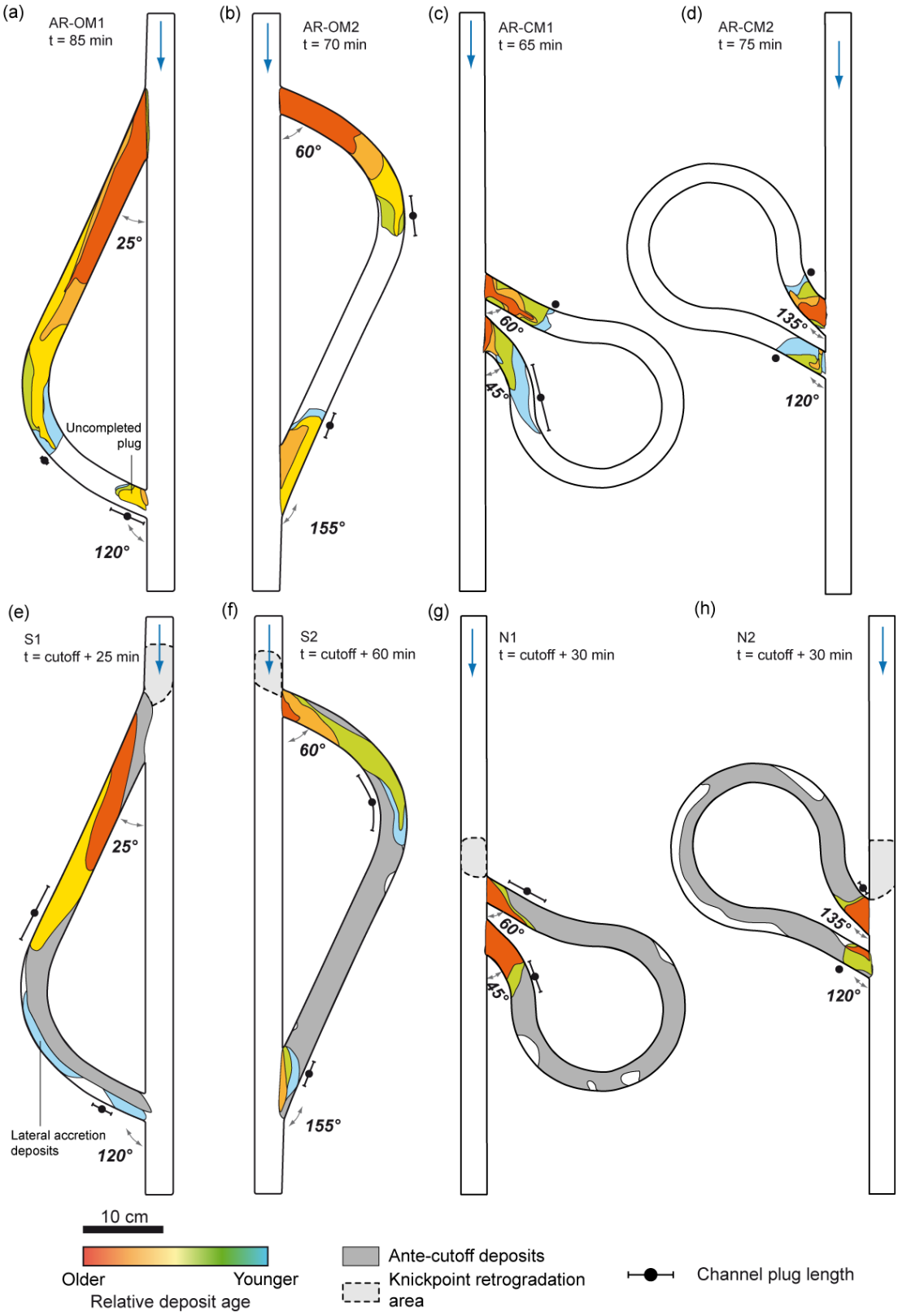

Figure 3.7: Planar growth of the bedload deposits in the curved channels through time for avulsion with reconnection **(a-d)** and cutoff incision experiments **(e-h)**. Contour lines were drawn at regular intervals. The mean channel plug lengths are represented with a black circle together with uncertainties.

The upstream channel plugs were shorter and with a steeper or equivalent slope in the cutoff incision experiments (Exps. S1 & S2) than in the avulsion experiments (Fig. 3.9a) in open-meander geometries. On the contrary, in closed-meander configurations the plugs formed during cutoff incision experiments were longer than those formed during avulsion experiments (Fig. 3.9b). Between the upstream and downstream plugs, bedload deposits formed a sand bed (Exps. S1 & S2) or sandbars (Exps. N1 & N2) (Fig. 3.9). In all experiments, the channel plugs formed on average the thickest deposits of the curved channel, and upstream plug deposits were thicker than the downstream plugs (Fig. 3.9). Some lateral accretion deposits that formed during the active phase of cutoff incision experiments were thicker than channel plug deposits in neck cutoff configurations, but they thinned rapidly towards the channel centerline, resulting in a smaller mean thickness across the channel.

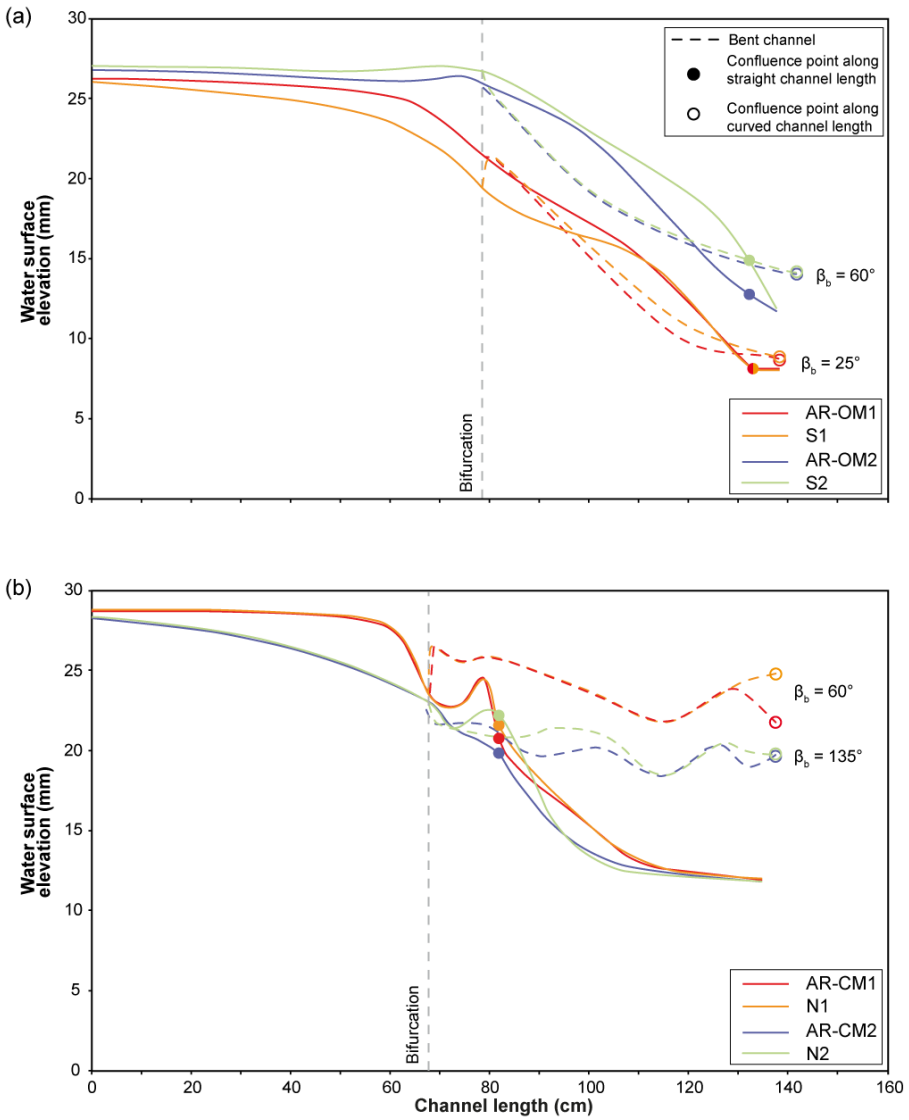

Figure 3.8: Equilibrium water surface elevation along the straight and curved (dashed line) channels for open **(a)** and closed-meander **(b)** experiments.

Both the upstream diversion angle and curved channel geometry strongly affected water surface elevation in the straight and curved channels (Fig. 3.8). Indeed, cutoff incision events appeared to have little effect on the final water surface elevation at equilibrium and the water surface elevation followed the same trend independently of the timing of the cutoff channel development (Fig. 3.8). For scroll slough incision simulations, the free surface elevation in the curved channel were lower than in the straight channel for most of the curved channel length (Fig. 3.8a), resulting in free surface slope ratios S_2/S_1 that were 0.53 ($\beta_b = 60°$) and 0.8 ($\beta_b = 25°$) (Table 3.1). In neck cutoff configurations, the water surface elevation was higher in the curved channel than in the straight one during Exp. N1 (Fig. 3.8b), with a slope ratio of 0.15 ($\beta_b = 60°$) (Table 3.1). The opposite was observed during Exp. N2 (Fig. 3.8b), and the water-surface slope was slightly steeper, resulting in a slope ratio of 0.31 ($\beta_b = 135°$) (Table 3.1). When comparing avulsion and cutoff incision experiments, Figure 3.7 shows that the equilibrium water-surface elevation was the same for a given geometry, but changed with the diversion angle or channel geometry, indicating that each configuration had a single hydraulic equilibrium. Finally, both in avulsion and cutoff incision cases, the curved channel geometry had a major importance on the water-surface slope (Fig. 3.7). Indeed, the water elevation was higher in both the inlet and curved channel in closed-meander geometries than in open-meander geometries, even when the upstream diversion angle was the same (Exps. AR-OM2/S2 and AR-CM1/S1).

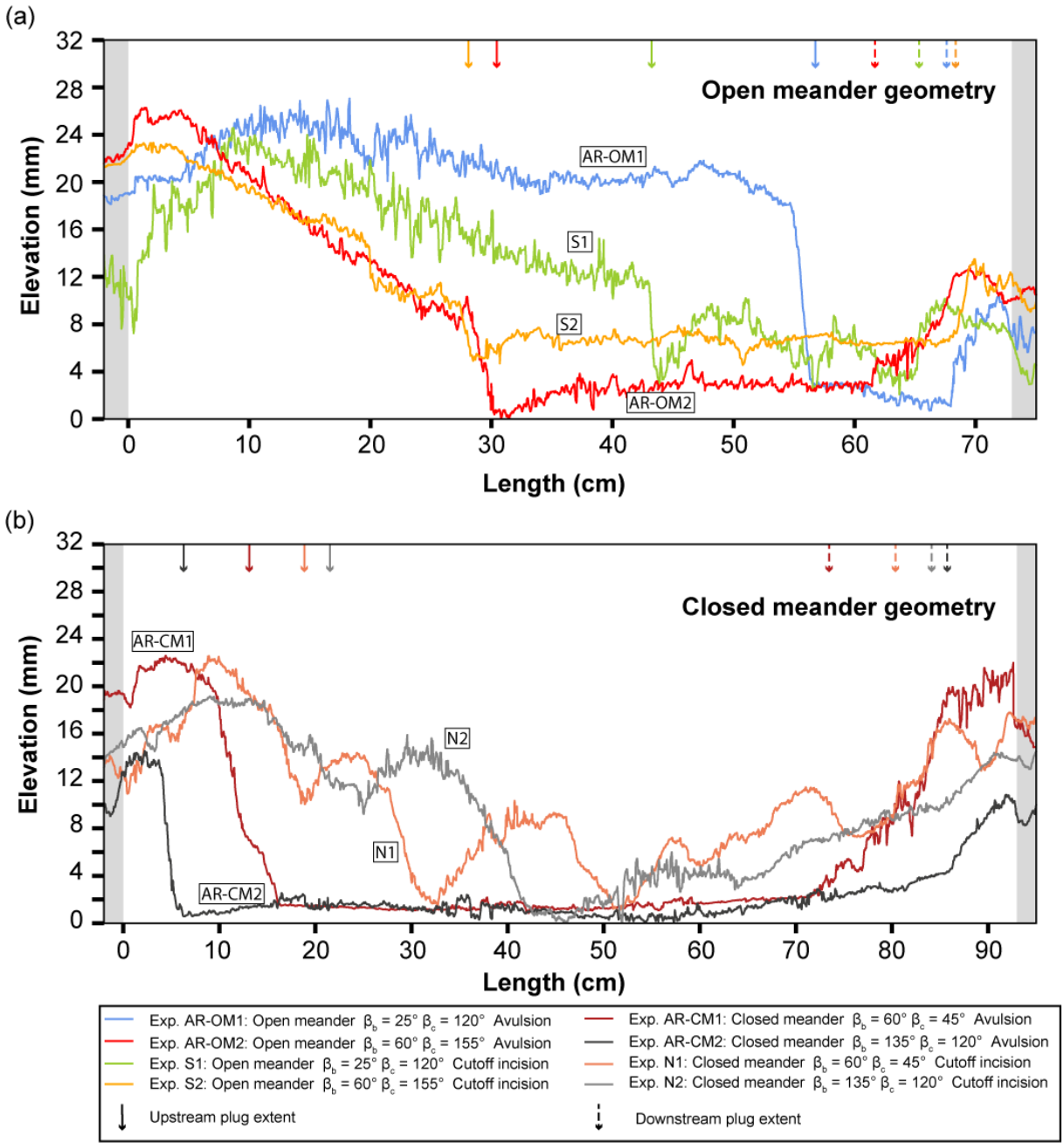

Figure 3.9: Longitudinal mean elevation profiles of the bedload deposits in the curved channels as measured using the method illustrated in Figure 2. **(a)** Open-meander geometries. **(b)** Closed-meander geometries. Grey boxes indicate the active channel. Full arrows indicate the extremities of the upstream channel plugs and dashed arrows the extremities of the downstream channel plugs.

3.3.4. Controls on channel fill architecture

When compared to the diversion angle, curved channel plugs length and volume had very distinct behaviors depending on whether they formed in open or closed-meander geometries (Fig. 3.10). At angles < 90°, a negative relationship was established between diversion angles and channel plug length for open-meander geometries, comparable to that of the avulsion experiments conducted without base level rise (*BL = 0 cm*) presented in Section 2.1 (Fig. 3.10a). This relationship was not observed at high diversion angles (Fig. 3.10a). Cutoff incision processes shortened the overall channel plug but their length still followed this pattern, with a similar channels plug lengths at high angles (Fig. 3.10a). For closed-meander geometries, a low slope decreasing relationship was discernible, as the plug length decreased very slightly when the diversion angle increased (Fig. 3.10a). This, in turn, was comparable to what was observed for avulsion experiments that had an elevated base level (Fig. 3.10a), resulting in water-surface slope perturbations reaching the bifurcation point (Section 2.2). In cutoff incision scenarii, channel plug lengths were shorter than in the simple geometry experiments and followed the same trend for angles ≤ 60°. For the large angles (≥ 120°), the plug lengths were similar and did not show any trend (Fig. 3.10a). A relation between diversion angle and channel plug volume was observed in open-meander geometry experiments, and was comparable to the relation observed in avulsion cases with base level elevation in Section 2.2 (Fig. 3.10b). This relation was not observed in closed-meander geometry experiments cases. The total volume of bedload deposits in the curved channel, including the deposits made during the first phase of the experiment, was larger in the neck cutoff configurations than in scroll slough cutoff configurations. In both cases it decreased when the upstream diversion angle increased (Fig. 3.10b).

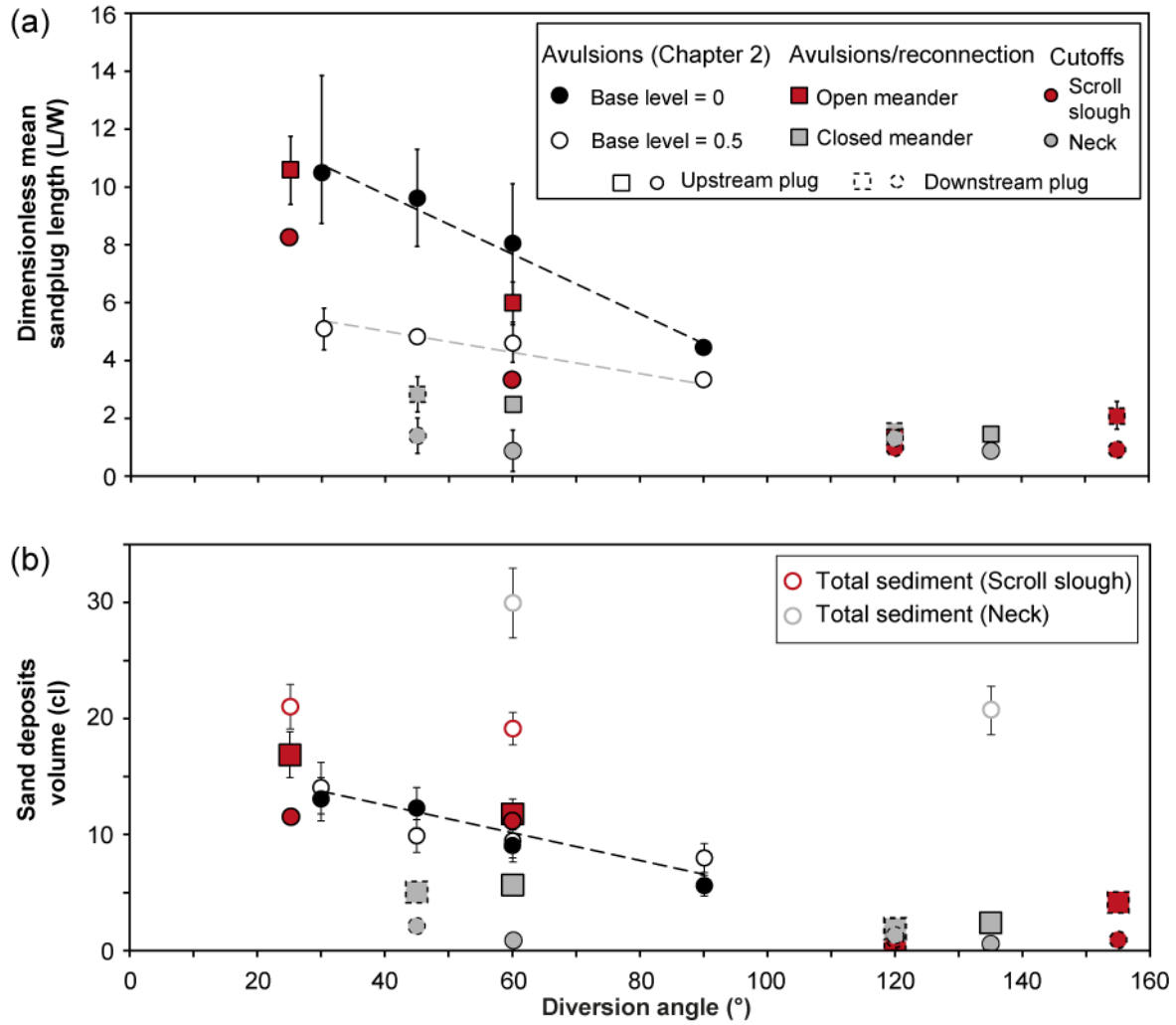

Figure 3.10: Effects of the diversion angle on the channel plug deposits length **(a)** and volume **(b)** for the cutoff and avulsion (Section 2.2) experiments at different base level elevations.Total sediment volumes indicated for cutoff incision experiments are indicated only in view of the upstream diversion angle. Dashed lines represent relationships between the sandplugs length and volume and the diversion angle defined in Chapter 2.

Channel plug length was unaffected by the fact that it was formed at the upstream or downstream extremity of the curved channel (Figs. 3.7 & 3.10a), with the possible exception of Exp. S1 where the downstream plug was not fully formed (Fig. 3.7a). However, the upstream channel plug were always thicker than the downstream ones, albeit only slightly in neck cutoff cases (Fig. 3.9). This resulted in upstream channel plugs that were generally more voluminous than the downstream ones, even when they were slightly shorter (Fig. 3.10b).

Results from experiments AR-OM2 & AR-CM1 and S2 & N1 conducted with the same diversion angle (60°) illustrate the differential controls exerted by the cutoff disconnection process on channel plug length and volume. Indeed for scroll slough cutoff experiments (S2), channel plugs were longer and had a larger volume than for neck cutoff experiments (N1)

(Fig. 3.10). The main difference between these experiments was the curved channel slope, and thus the S_2/S_1 slope ratio and location of the upper limit of the water-surface slope modification. In open-meander geometries, which had S_2/S_1 slope ratio > 0.5, the water-surface slope modification did not reach the bifurcation point whereas it exceeded it in closed-meander geometries. Consequently the channel plug formation initiation was unaffected in open-meander geometry cases, although the downstream extremity of the plugs could have formed under hydraulic effects influence. In closed-meander geometry cases, which had a S_2/S_1 slope ratio < 0.5, the whole length of the channel plug was influenced by water-surface slope modification.

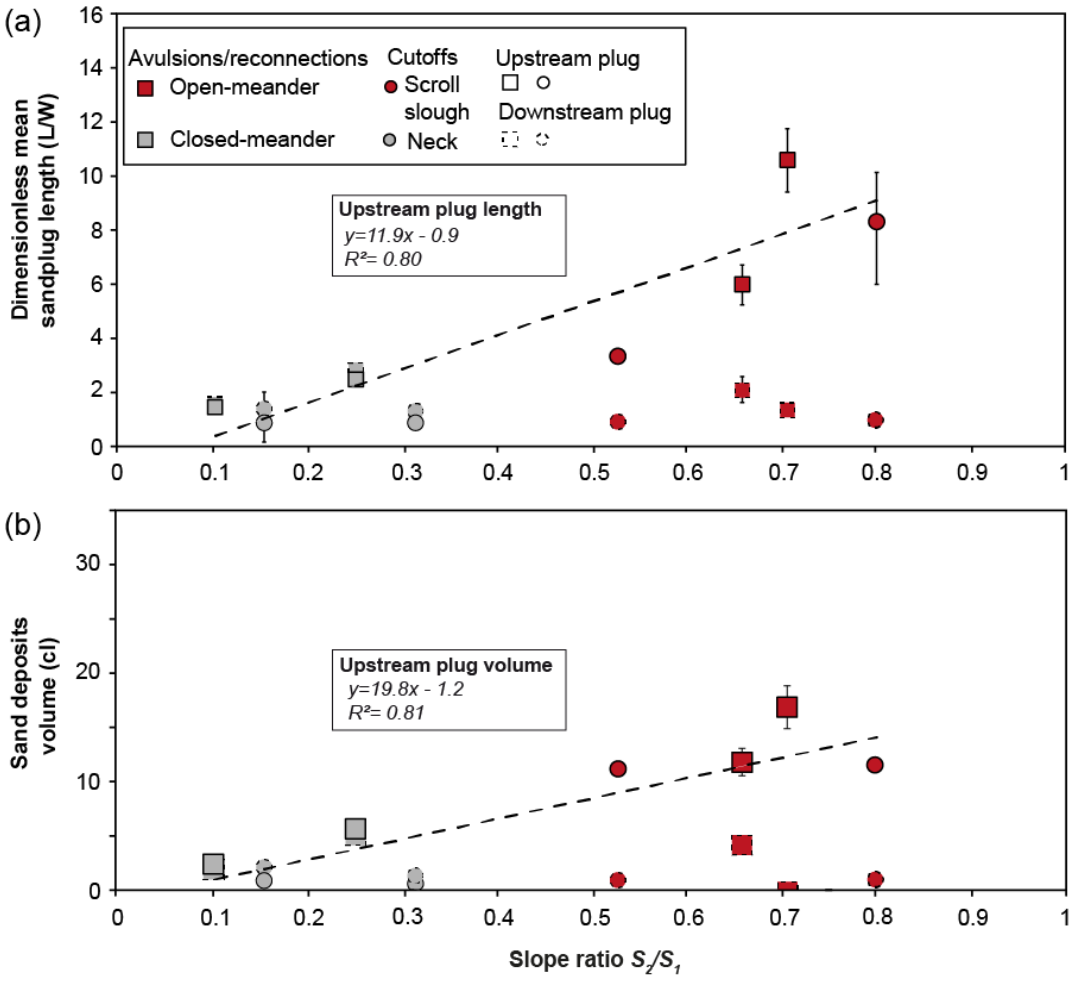

Figure 3.11: Relationships between the slope ratio S_2/S_1 and channel plug length **(a)** and volume **(b)**.

The differential control of the channel planform geometry on channel plug length and volume therefore appears linked to the S_2/S_1 ratio. In cutoff geometries, when both channels separate and then link again, a low slope ratio means that one channel is significantly longer than the other, and thus its slope is gentler. Consequently, this channel is more likely to be affected by downstream hydraulic effects, as the water-surface slope modification zone length is linked to the channel slope. Figure 3.11 shows the relationship between the slopes ratio S_2/S_1 and the channel plugs length and volume of the cutoff experiments shown in Figure 3.10. It illustrates the clear differences in slope ratios between the two geometries and shows a clear positive and linear relationship between the upstream channel plug length and the slope ratio (Fig. 3.11a). A similar but weaker trend exists for the channel plug volumes (Fig. 3.11b). However, the slope ratio does not seem to impact downstream plugs length or volume which remain constant around 1-3 channel width and 1-5 cL, respectively (Fig. 3.11).

3.4. Discussion

3.4.1. Geometrical controls on channel equilibrium

Results of this chapter showed that the bifurcation stability appears to be strongly influenced by its planform geometry. For instance the final equilibrium state of the free surface elevation along both channels suggests that a stable hydraulic equilibrium may be found for a given geometry of the channels and bifurcation, independently of the process initiating this bifurcation (i.e., through avulsion channel or cutoff incision) (Fig. 3.8). Also, during cutoff incision experiments, the time needed to reach equilibrium, i.e., the time needed for the knickpoint to balance the slope in the straight channel, was directly linked to the length of the straight cutoff channel (Fig. 3.6), as only after this was done was the curved channel plugged. These geometric controls likely exert their influence through the water-surface slope ratio. One may argue that it is comparable to backwater effects that were demonstrated as capable of destabilizing an otherwise stable bifurcation in Section 2.2.

While the final architecture of the deposits in cutoff incision experiments can be considered realistic (albeit in a non-erodible bank and bed setting) due to the first phase of the experiments allowing the channel slope to reach equilibrium, the experiments conducted in avulsion with reconnection cases are different from natural settings where for instance inlet channels are curved and rivers banks adjust. However, these experiments allowed the detailed

description of channel plug formation dynamics, and notably of the downstream channel plug deposition processes and timing.

Exps. E1 & E2 (Fig. 3.5) support that, all other parameters being constant, water and sediment partitioning at a bifurcation depend on the downstream channel width, with the wider branch capturing a larger fraction of both, as modelled by Wang et al. (1995) and confirmed by field studies by Zolezzi et al. (2006). In the experiments, channel plug formation was prevented in the curved channel, despite important sediment deposition on the channel bed. This likely occurred due to increased discharge in the curved channel. This observation demonstrates that the cutoff channel evolution and rate of widening partially controls the amount of sediment that will be deposited in the curved channel (Fig. 3.5). Consequently, in natural cases, cutoff channel evolution, stability and widening rate probably modulate the extent and volume of bedload deposits in an abandoned channel. This venue of research deserves future experimental work.

Disconnection occurred only in experiments where both channels had the same initial width. In that case, channel narrowing and shallowing due to bedload deposition in the curved channel ultimately led to channel disconnection. The initial sediment deposition was due to the presence of the flow separation zone at the channel mouth whose width is controlled by the diversion angle (Constantine et al. 2010a). It created secondary circulations that reduced the discharge in the diverted channel, which generally led to channel abandonment (Miori et al., 2006; Zolezzi et al., 2006). Thus when both channels had the same width, channel plugging was controlled by the bifurcation geometry (i.e., in our case the slope ratio and the diversion angle), by reducing the flow in the diverted channel and favouring bedload deposition (see Chapter 2). However, in cutoff incision experiments, the cutoff channel was opened at its maximal width and also at its maximum depth. Thus, the cutoff channel could initially accommodate a larger part of the discharge than it would in natural settings, where the flow progressively incises it. Consequently in this experimental setup equilibrium was possibly achieved faster than it would have in a more complex setting with erodible bed and banks allowing a progressive deepening and widening of the cutoff channel. Thus it is possible that while the global trends determined using these experiments reflect natural phenomenons, the channel plugs length and volume are possibly slightly underestimated compared to field cases.

Furthermore, in natural cases the fate of disconnecting channels changes when the channels or bifurcation geometries are modified (Bertoldi, 2012). Consequently, the fixed banks of our experimental setup may force channel disconnection, as channel stability is encouraged by channel width adaptation (Federici & Paola, 2003). Recent modelling using the nodal point condition have found that more equilibrium solutions existed when the channel banks were erodible instead of being fixed (Schielen & Blom, 2018), with different permutations of channels sharing more or less equally the discharge, leading to two stable bifurcations with both branches open and three with one branch closed. Thus it is possible that from the same starting geometry, these experiments with erodible banks would lead to longer lasting bifurcations, stable bifurcations with two open channels or even cutoff failures in some cases. However these equilibrium solutions are dependent on the Shields parameter and thus the sediment load. In bedload dominated cases, the nodal point condition has 3 equilibrium solutions (Bolla Pittaluga et al., 2003), with either both branches open or one of each branch closed. In cases of mixed load settings, more configurations could be found (Bolla Pittaluga et al., 2003).

3.4.2. Deposition process and architectural elements of abandoned channel fills

In all experiments where abandonment occurred, the most prominent bedload deposits features were the upstream and downstream channel plugs. Both plugs had similar architecture, i.e., an assembly of several amalgamated bars whose first bar was anchored at the bifurcation (or confluence) point and grew downstream (or upstream), with the subsequent bars anchored to the first one(s), forming a complex sedimentary body (Figs. 3.7 & 3.9). This geometry is similar to what was observed at the downstream extremity of a meander abandoned by neck cutoff abandoned meander of the Arkansas River by Richards & Konsoer (2020). In all experiments the channel plug formation processes were comparable to those described in Section 2.1 during experimental avulsion cases, i.e., deposition initiated in the flow separation zone followed by the plug assembly downstream growth. However, their shape was modified when the plug reached a zone in which the water-surface slope was modified the extreme case being for neck-like geometries (Figs. 3.7 & 3.9). Similarly to what was described in Section 2.2, the channel plugs were wedge-shaped when they formed freely and roughly rectangular when formed completely under downstream hydraulic effects influence (Fig. 3.9). In open-meander cutoff incision experiments, the bar and pool architecture of the bedload channel fill is similar to what was observed in erodible banks flume experiments by Han & Endreny (2014) and in the field by Richards & Konsoer (2020).

This demonstrates that our observations are likely to apply in nature despite having been realized in fixed-walls conditions.

In experiments with cutoff incision, incision and knickpoint retreat in the straight channel section as well as pre-existing deposits in the curved channel led to the formation of a topographic step at the curved channel mouth (Miori et al., 2006; Zolezzi et al., 2006; Richards & Konsoer, 2020). As a result, the bedload supply to the curved channel was reduced (Slingerland & Smith, 2004; Richards & Konsoer, 2020). This topographic step can explain the faster disconnection of the curved channel in cutoff incision cases (Figs. 3.4 & 3.6). The associated decrease in sediment supply was responsible for the slower construction rate of the channel plug (Fig. 3.7), which was then shorter and less voluminous (Fig. 3.10). Thus in cutoff incision cases, channel plug deposits were shorter and grew in the former topographic lows of the active phase deposits, which resulted in a composite plug formed by the amalgamation of active and disconnection phase deposits. In natural cases, this would result in a strong connectivity between the channel plug deposits and both the coarse channel lag and point bar deposits (Cabello et al. 2018). The composite nature of the channel plugs implies that their internal architecture is complex due to its amalgamation. In natural cases, as the grain-size range is wider and the flow energy in the channel decreases in time due to the channel plug build-up, this complex architecture would result in global fining-upward and fining-downstream trends and sharp grain-size variations inside the channel plug (Donselaar & Overeem, 2008; Toonen et al., 2012).

Observation of the downstream channel plug growth processes showed that it was formed by the same processes as the upstream channel plug (Fig. 3.7). The experimental runs further suggest that the sediment forming the downstream channel plug originated from downstream (i.e., from the cutoff channel) and not the curved channel. Indeed, in experiments with a pre-existing cutoff channel, no bedload deposits were observed in most of the curved channel but in each experiment a downstream channel plug was formed regardless (Fig. 3.7). Furthermore, the upstream elongation of the downstream channel plug suggests sediment supply from downstream. Such a backflow creeping upwards in channels disconnected at their upstream end was observed during floods by Shields & Abt (1989). Additionally, Le Coz et al. (2010) and Costigan & Gerken (2016) observed large zones of flow stagnation and recirculation – which encouraged sediment deposition – at the downstream ends of disconnecting channels. These zones appeared similar to the upstream flow separation zone and were also positioned at the external bank of the channel relative to the confluence (Fig.

3.7). This is probably how the downstream channel plugs formed in our experiments, at least in open-meander geometries where the downstream plugs are thinner than the upstream plugs (Fig. 3.9a). Indeed our experiments are in a constant flood regime in order to transport bedload. The downstream channel plugs formation was initiated only after the upstream channel plug occupied the whole width of the channel, which reduced drastically the upstream flow. Thus the backflow coming from the cutoff channel was stronger than the normal flow at the downstream extremity of the curved channel, allowing it to steer bedload upslope and form the downstream channel plug. However, in closed-meander geometries, both the upstream and downstream parts of the curved channel tended to go down slope for Exps. AR-CM1 & N1 and upslope for Exps. AR-CM2 and N2 (Fig. 8). In Exps. AR-CM1 & AR-CM2 the downstream plugs are almost as thick as the upstream plugs, but in Exps. N1 & N2, where the slope in the curved channel was at normal equilibrium due to bedload deposition in the first phase of the experiments the downstream plugs are also thinner than the upstream ones (Fig. 3.9b). Thus we can conclude that when the bed slopes in both channels are at equilibrium, the downstream channel plug construction is controlled by backflow effects.

3.4.3. Controls on bedload fill deposits geometry and volume

The decrease of the total bedload deposits volume with diversion angle in the experimental cutoff experiments (Fig. 3.10b) is coherent with the observations of Fisk (1947) and Allen (1965) based on field studies. Indeed they linked the volume of bedload sediments in the abandoned channel to the bifurcation longevity, which is itself linked to the channel diversion angle. As low angle chute cutoff channels bifurcations tend to remain stable a long time, channel narrowing occurs and deposits start filling the channel before the plug starts its formation (Sorrells & Royall, 2014; Reynolds & Royall, 2019), generally resulting in a high fraction of coarse channel fill (Fig. 3.10b; Fisk, 1947; Allen, 1965; Bridge et al. 1986). On the other hand, with the exception of the channel plugs, coarse fill deposits are almost non-existent in neck cutoff channels (Fisk, 1947; Allen, 1965). In our experimental setup the important amount of bedload deposited in the curved channel during Exps. N1 & N2 (Fig. 3.10b) is attributed to the bed levelling phase, and thus are not considered as abandoned channel fill deposits, with the exception of the small channel plug deposits. Thus the cutoff incision experiments give insight on the spatial and geometrical relationships between coarse channel plug and point bar deposits.

Channel fill bedload deposits exhibit similar deposition dynamics and processes in all experiments (Fig. 3.7). In open-meander geometries channel plug length and volume appear

controlled by the diversion angle (Fig. 3.10), similarly to what was described in Chapter 2. However at diversion angles ≤ 90° major variations in channel plug length and volume are observed between open and closed-meander geometries (Fig. 3.10). Indeed in closed-meander geometries a diversion angle increase affects only weakly channel plug length and volume (Fig. 3.10). This demonstrates that although the diversion angle can be held responsible for channel disconnection due to its control on sedimentation initiation (Section 2.1), it does not control alone the channel plug extent and volume. This difference in behavior between different experiments types suggests that the other control on channel plug length is linked to the channel geometries. The slope ratio S_2/S_1 is strongly affected by the channel planform geometry, and a linear relationship between the length and volume of the upstream channel plugs and the channels slope ratio, encompassing all channel geometries, was tentatively determined (Fig. 3.11). The relationship between channel plug length or volume and slope ratio S_2/S_1 can tentatively be approximated using the length ratio L_1/L_2 (Eq. 1.4). In the experiments, only 2 length ratio were tested. A fit of the data is attempted in Figure 3.12 and shows a trend similar to the slope ratio, but with a slightly different slope. Although being crude, such relationship is easier to apply on the field to study abandoned channel fill, for instance with aerial imagery. More tests using different length ratio would be required to refine the relationship.

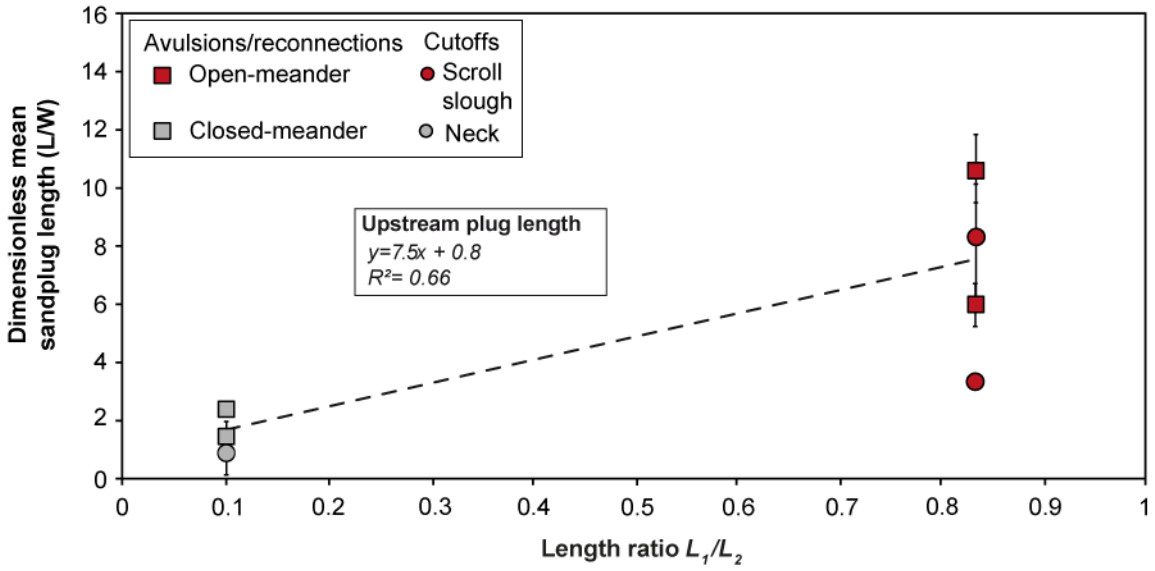

Figure 3.12: Relationships between the length ratio L_1/L_2 and upstream channel plug length.

Figure 3.11 also shows that the slope ratio influences the channel plug shape, with more rectangular channel when the slope ratio is < 0.5, i.e., in our case, in closed-meander geometry. This more rectangular shape observed in closed channel geometries can be explained by the vertical aggradation induced in confined channels by the water-surface slope modification (Sahoo et al., 2020). Combined with the almost fixed length in closed channel geometries cases, this rectangular shape results in channel plug volumes that are also unaffected by the diversion angle for a given geometry (Fig. 3.10b), similarly to what was observed in avulsion settings in Section 2.2 (Fig. 3.10b).

While this relationship between slope ratio and channel plug length and volume works well for the upstream plug, it does not explain the downstream plugs extent and geometry. Their position at the confluence exposes them to strong hydraulic effects. Their length and volume are thus probably controlled by the backflow strength relative to the normal flow (Costigan & Gerken, 2016). However, as the downstream plug is built the backflow strength and sediment supply from downstream decreases, leading to the interruption of its construction. As the backflow is weaker than normal flow due to the channels and water-surface slopes, a thinner plug can be sufficient to disconnect the channel from downstream flow. Furthermore, at the time of the downstream plug formation the active channel can be entrenched (Chapter 2) (Richards & Konsoer, 2020), preventing bedload to spill in the abandoned channel. Thus, downstream plug construction must be tied to the discharge intensity, sediment supply and the downstream diversion angle value. Indeed the diversion angle also controls the flow separation zone width and length downstream, albeit with a negative relationship (Keshavarzi & Habibi, 2005).

Thus, as the relationship between diversion angle and channel plug extent and volume is superseded by hydraulic effects controlled by the channels slope ratio when they reach the bifurcation, a simple linear relationship may be used to link the slope ratio to channel plug length and volume. Furthermore, the slope ratio allows to determine under which flow regime the plugs are (or were) formed, which in turn allows to determine their shape. Indeed, although more testing is required, preliminary observations suggest that a slope ratio < 0.5, or ≤ 0.4 indicates that water-surface slope reach the bifurcation in both avulsion and cutoff cases, resulting in the formation of rectangular channel plugs instead of the wedge-shaped ones observed when the slope ratio was > 0.5 (Fig. 3.11).

Results of this study also put a new perspective as to why a relationship between diversion angle and channel plug length has not been quantified on the field. A commonly advanced explanation is that it is difficult to measure the total length of the channel plug in the field as part of it is underwater and possibly covered by finer-grained sediments, and channel plug study is often made using aerial photographs of historical maps (e.g., Greco & Alford, 2003; Constantine et al. 2010a). The competition between diversion angle and channels slope ratio observed in this study is another explanation for this lack of clear relationship.

3.1.4. Experimental predictive model for channel plug length and volume

Chapters 2 & 3 established several geometrical relationships linking channel geometry and upstream channel plug deposition. The first relationships found determined that the channel plug length and volume decreased when the diversion angle increased (Fig. 2.7). However, these relationships varied with the water-surface slope ratio between the abandoned and active channels (Fig. 2.16) and the relationships based on the diversion angle were thus affected by the channels geometry (Fig. 3.10). Linear relationships fitting all cutoff experiments were found linking the water-surface slope ratio between the channels (L_{exp_S}), which can be estimated using the channels length ratio (L_{exp_L}), and channel plug dimensionless length (Figs. 3.11 & 3.12):

$$L_{\exp\_S} = 11.9 * (S_2/S_1) - 0.9 \qquad Eq.\ 3.1$$

$$L_{\exp\_L} = 7.5 * (L_1/L_2) + 0.8 \qquad Eq.\ 3.2$$

These relationships work for channel plugs regardless of the channels geometry. They are established for water-surface slope ratio (or channels length ratio) values ranging between 0.1 and 0.8, which is the range of water-surface slope or channels length ratio expected in abandoned channels as in most cases the longer channel is abandoned.

The channel plug volume in m^3 was also linked the water-surface slope ratio by a similar relationship, also valid for the length ratio:

$$V_{\exp} = 0.0002 * (S_2/S_1) - 1.10^{-5} \qquad Eq.3.3$$

However, this specific relationship works for this experimental setup but is dependent on its dimensions such as width and plug height. Using the observations made on channel plug geometry, Eqs. 3.1 & 3.2 can be used to estimate the channel plug theoretical volume (Fig. 3.13). Channel plugs are wedge-shaped in free-flow conditions and those formed under the

influence of downstream hydraulic effects are more rectangular (Figs. 2.15 & 3.9). Their theoretical volume can be measured as:

$$V_{theo} = \frac{L * W * h}{d} \qquad Eq.3.4$$

With V_{theo} the theoretical channel plug volume, W the channel width at the bifurcation, h the channel plug height at the bifurcation point and d a coefficient used to approximate the channel plug shape, varying between 1 when it is a rectangle and 2 when it is a perfect triangle. L can be calculated using Eqs. 3.1 or 3.2 and W measured, but the values of h and d must be determined.

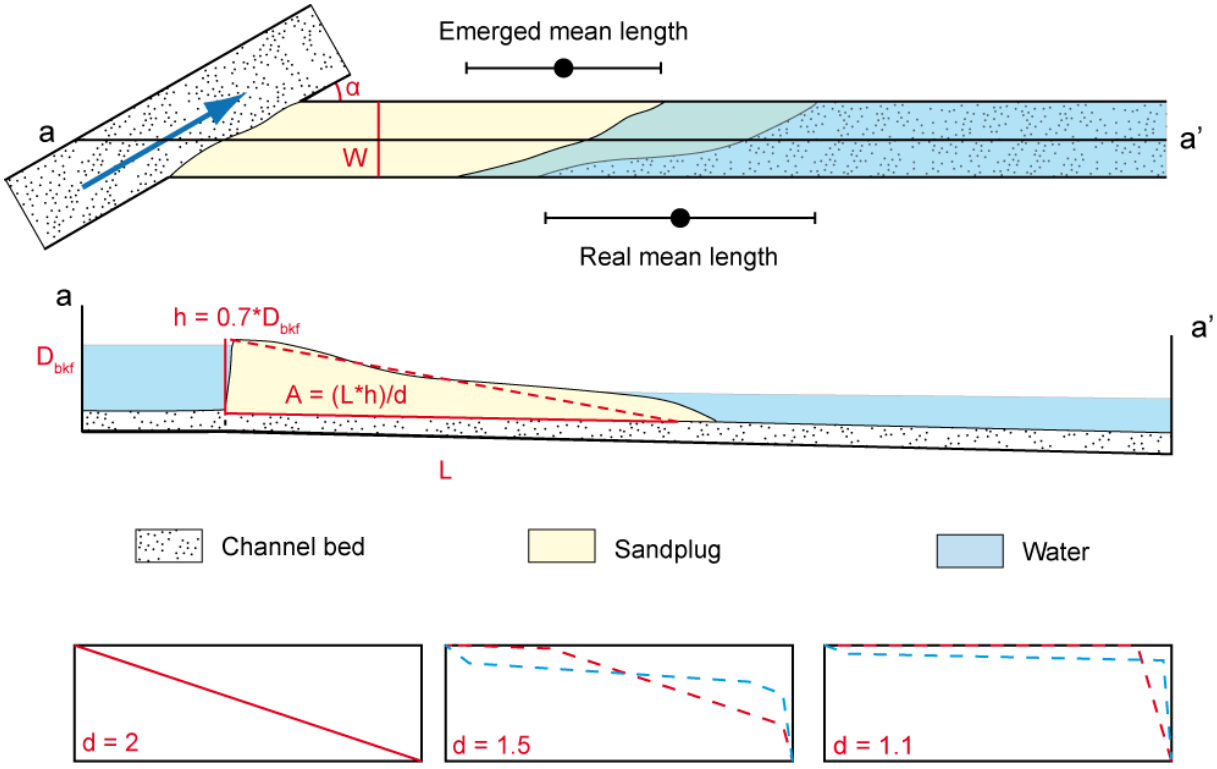

Figure 3.13: Geometrical parameters used to measure the theoretical channel plug volume.

h can be expressed as a fraction of the mean bankfull channel depth D_{bkf}, as the coarse part of the channel plug is built during high water stages. Measurements of the channel bankfull depth and of the plug thickness at the bifurcation using both direct measurements at the end of the experimental runs and the elevation profiles (Figs. 2.6, 2.15 & 3.9) determined that h corresponded to roughly 0.7 times the mean bankfull depth.

V_{theo} values with h = 0.7 and d values varying between 1 and 2 were tested in Eq. 3.4, using both Eqs. 3.1 and 3.2 to determine the channel plug length. These values were then compared

to the volume experimentally measured for these S_2/S_1 values (Table 3.1) in order to calculate the Root-mean-square deviation (RMSE) between the theoretical and measured values for each *d* tested. RMSE is used to measure the differences between values predicted by a model and the values observed. The lower a RMSE value is, the closest the model fits to the data. This allowed the calibration of the *d* parameter based on the experimental data. RMSE calculations determined that the best value of *d* was 1.1 when using Eq. 3.1 to estimate the length and 1 when using Eq. 3.2. This expresses the fact that channel plugs are not triangular but gently thin downstream before diving abruptly (Figs. 2.6, 2.15 & 3.9). Thus, using Eq. 3.1 and the values of *h* and *d* determined above, Eq. 3.4 becomes:

$$V_{theo} = \frac{(11.9 * (S_2/S_1) - 0.9) * W^2 * 0.7}{1.1} \qquad Eq. 3.5$$

Or

$$V_{theo} = (7.5 * (L_1/L_2) + 0.8) * W^2 * 0.7 \qquad Eq. 3.6$$

With *W* squared to give results in m^3 as the length is dimensionless. These theoretical relationships based on the plug length and geometry were then compared with the experimental results measured during Chapter 3 experiments (Fig. 3.14). The theoretical relationship underestimate channel plug volume at water-surface slope ratios > 0.6 compared to the experimental results (Fig. 3.14), probably due to uncertainties on the parameters used to represent plug geometry (Fig. 3.13) whose effect scales with plug length.

Although Figure 3.14 indicates that the attempt to model the plug geometry with Eq. 3.4 is encouraging, the tentative prediction equations based on the water-surface slope ratio and channels length ratio were developed using data from only a few experiments. These relationships linking channels geometry to channel plug length and volume are promising, but more experiments are needed to refine them and their accuracy must be tested using field cases. Although coarse-grained channel fill volume is difficult to measure and data is lacking to verify Eq. 3.4, channel plug length data are readily to test the validity of Eqs. 3.1 & 3.2 on the field.

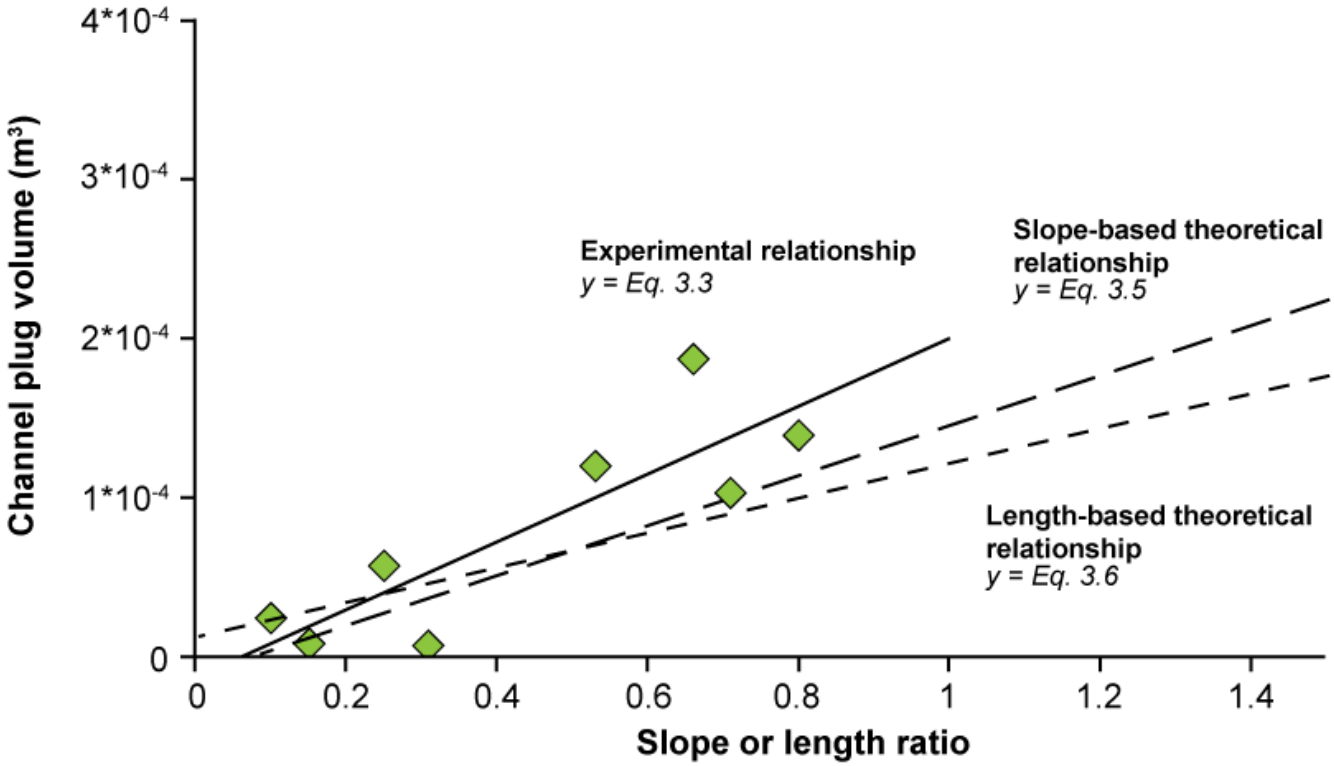

Figure 3.14: Relationships between the channels water-surface slope ratio or length ratio and the channel plug volume, compared with Chapter 3 experiments upstream channel plugs volume, assuming equivalence between both ratios (Eq. 1.4).

3.5. Conclusion

Increasingly complex flume experiments simulating avulsions and cutoff incision at constant water and sediment discharge with a varied range of bifurcation and confluence angles provided the opportunity to further study bedload deposition controls and architecture in curved abandoned channels. We found that:

1) Channel planform geometry has a major control on bifurcation dynamics shared between the diversion angle and channel geometry induced adjustments of the water-surface slope.
2) Two relationships depending on the channels slope ratio S_2/S_1 were found between the diversion angle and channel plug length and volume, while a single linear relationship was found between the channels water-surface slope ratio and the upstream channel plugs length and volume.
3) Out of the influence of water-surface slope variations, channel plug length and volume decrease as the diversion angle increases, especially for angles < 90°. When affected by the water-surface slope, their length and volume are much less affected by diversion angle. When the water-surface slope ratio is < 0.5 channel plugs have a more rectangular longitudinal shape.
4) The area occupied by channel plug deposits in abandoned channels is predominantly controlled by the presence (~ 20-30%) or absence (~ 50-70%) of downstream hydraulic effects, with a slight influence of the diversion angle.
5) Using the experimental results on channel plug length and architecture, tentative relationships are proposed to predict bedload channel plug length and volume.

Chapter 4: Gravel infill dynamics and depositional patterns in chute cutoffs channels of a gravel-bed river: the Ain River, France

Ce chapitre décrit les dépôts grossiers de remplissage observes dans des chenaux abandonnés dans l'Ain (France), qui est une rivière dominée par la charge de fond. Il est composé par un manuscrit en cours de préparation pour soumission à Earth Surface Processes & Landforms.

This chapter studies coarse-grained fill deposition in abandoned channels of the bedload dominated Ain River (France). It is composed of a manuscript being prepared for submission to Earth Surface Processes & Landforms:

> SZEWCZYK, L., GRIMAUD, J.-L., COJAN, I., PIÉGAY, H., *in prep*. Gravel infill dynamics and depositional patterns in chute cutoffs channels of a gravel-bed river: the Ain River, France. ESPL.

4.1. Abstract

Abandoned channels are efficient sediment sinks whose closure phase is dominated by bedload deposits (plug) and the abandoned-channel fill by fine-grained sediments (fill). The geometry and architecture of the bedload deposits accumulated during the channel disconnection remains overlooked. In particular, the respective roles of the various processes controlling the geometry of the bedload plugs still need to be quantified on the field. This study focuses on the mapping and characterization of the bedload deposits associated to the closure phase in three abandoned channels and the survey of the evolution of the channel fill in a fourth channel in the process of being disconnected in the bedload-dominated Ain River, France. We find that bedload fill sediments accumulate mainly by (i) an initial bar at the mouth of the abandoned channel in the flow separation zone thus reducing the flow (ii) lateral accretion of coarse-grained bars during channel narrowing downstream of the initial upstream bar and (iii) amalgamation of coarse-grained longitudinal bars that fine-upward as they migrate downstream. Channel plug grows downstream until it reaches its maximum length then it starts thickening. In this study, competition between the diversion angle and water-surface slope ratio induced downstream hydraulic effects resulted in the absence of clear control for channel plug length, although for most studied cases it is around 5 to 6 times the channel width at the bifurcation. Channel plug volume, area and final geometry are controlled by the channel morphology as well as local sediment supply that appear itself controlled by feedbacks created by channels disconnection along the river reach.

4.2. Introduction

Field studies on abandoned channel fills showed complex architectures resulting from evolving channel geometry, sediment fill and hydraulic processes: (i) deposition of a bed load forming a channel plug at one or both entrances of the abandoned channel, (ii) heterolithic deposition further away from the abandonment point, and (iii) fine overbank deposition filling the remaining space available in isolated areas (Fisk, 1947; Bridge et al., 1986; Plint, 1995; Hooke, 1995; Toonen et al., 2012). Bed load sediments accumulate during the closure phase with the initial formation of plug bars at the entrance of the channel, followed by the deposition of downstream bars during channel abandonment, while the suspended load contributes to the fine-grained filling, corresponding to the open-stage (channel closure phase) and closed-stages (after channel abandonment) (Jordan & Pryor, 1992). The experimental observations made on coarse-grained bedload deposits in the previous chapters are coherent

with these findings: an initial bar formed at the mouth of the abandoned channel in the flow separation zone thus reducing the flow, which led to the amalgamation of coarse-grained, downstream migrating, longitudinal bars. Although bedload dynamics and sand- and gravel-bars formation has been extensively described in active braided rivers (e.g., Ashmore 1987, 1988; Bridge & Glabel 1992; Joshi & Xu 2017), the formation processes and temporal evolution of these bedload deposits in abandoned channels remain relatively overlooked. Currently, it appears that although the channel plug formation have been recorded by several studies using direct observation (Bridge et al., 1986; Hooke, 1995) or aerial pictures (Gautier et al., 2007), much remains to understand about the respective roles of controlling parameters on the bedload geometry and architecture in disconnecting channels.

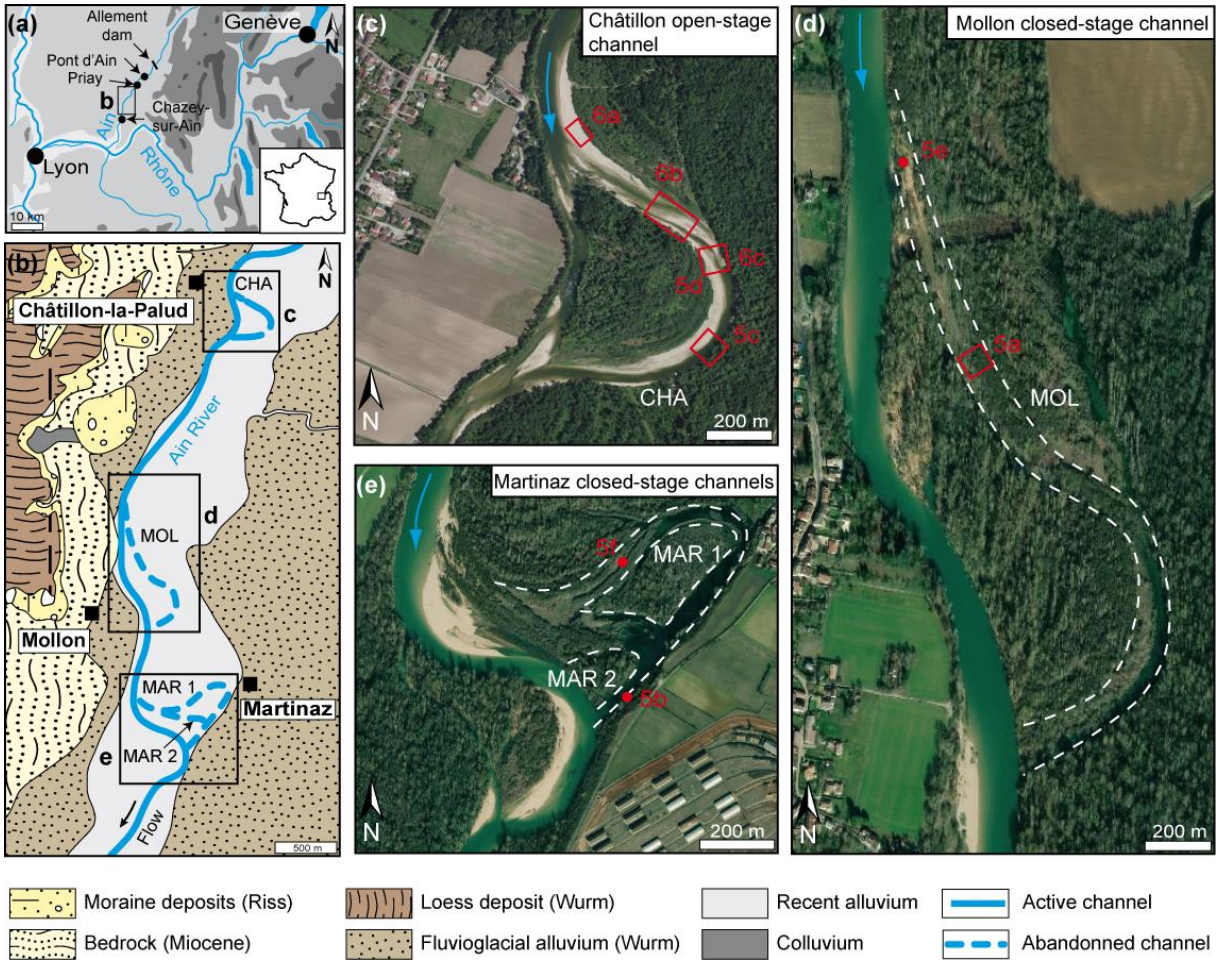

Figure 4.1: Location **(a)**, simplified geological map **(b)** of the study area and 2019 aerial photographs of the cutoffs (**c**, Martinaz; **d**, Mollon; **e**, Châtillon). Simplified 1/50000 geological map from Ambérieux-en-Bugey map, Kerrien et al. 1987. River course drawn on the geological map is that of 2017-2018, terrace contour has been modified accordingly to take into account river bank erosion and cutoffs. Red dots and boxes on the aerial photographs indicate the location of the pictures shown in Figs. 4.5 and 4.6.

One of the main controls invoked on abandoned channel bedload geometry is the duration of the disconnection process, which was linked by many field observations to the bifurcation geometry (Fisk, 1947; Allen, 1965; Gagliano & Howard, 1984; Shields et al., 1984; Shields & Abt, 1989). The experimental results in Chapters 2 did find geometrical controls on channel disconnection and channel plug geometry. The diversion angle was confirmed to control the initiation of the channel plug formation, through its control on the width of a flow separation zone at the bifurcation (Bulle, 1926; de Heer & Mosselman, 2004; Constantine et al., 2010a; van der Mark & Mosselman, 2012) which in turns controls the transport capacity of the flow in the disconnecting channel. Further experiments introducing more complex hydraulic effects (i.e., backwater effects) showed that plug formation was modified when it occurred under these downstream hydraulic effects influence (Chapter 2), and that both the channel plug length and volume were controlled by the water-surface slope ratio between the channels (Chapter 3).

Bedload dominated rivers that show a large migration rate offer the opportunity to investigate the controls on bedload sedimentation during channel disconnection as embayment incision and scroll-slough cutoffs occur frequently. Channel plug formation during the open stage takes a relatively short time (years to tens of years, Fisk, 1947; Bridge et al., 1986; Hooke, 1995), while the subsequent filling of the abandoned channel during the closed stage generally takes far longer (centuries to millennia; Gagliano & Howard, 1984; Toonen et al. 2012; Ishii & Hori, 2016). Thus, knowledge on the processes and resulting architecture of open-stage channel –which requires shorter timescale monitoring – allows us to deduce the subsequent channel clay plugging, as long as the channel is not reactivated.

Because of its rapidly changing morphology, the Ain River is adapted to study the channel evolution and associated deposits during cutoffs. In this study, four chute cutoff channels of the bedload dominated Ain River (eastern France) were studied. Three of them were formed by embayment incision and channel reoccupation while the last formed by scroll-slough processes. Using aerial photographs, a Digital Elevation Model (DEM), and on site surveys for sedimentary bodies mapping and grainsize measurements, the evolution, depositional processes and final architecture of bedload sediments are discussed in order to determine the controls on bedload sediments geometry, extent and volume in abandoned channels. Additional data from historical aerial photograph of five other channels of the Ain River were gathered.

4.3. Study area

4.3.1. Geomorphic setting

The Ain River rises from the Jura Mountains (eastern France) and flows into the Rhône River some 200 km downstream (Fig. 4.1a). The upper course of the Ain River stretches 160 km from its source down to the town of Pont d'Ain, mostly along the limestone reliefs of the Jura Mountains. The lower course of the Ain River, from Pont d'Ain to the confluence with the Rhône near Anthon, flows in a narrow, low-relief alluvial plain, shaped into sediments of fluvio-glacial origin (Fig. 4.1b). There, the valley slope is comprised between 1.2 and 1.8 ‰ (Piégay et al., 2002) and the development of a meandering pattern along long reaches of the lower Ain River allowed numerous channel cutoff occurrences (Piégay et al., 2000).

The Ain River catchment area is 3765 km². The natural discharge of the Ain River was typical of a fluvio-nival regime (with limited nival influence) although the hydraulic regime was largely modified by water management, especially since the mid-1960s with the construction of several dams for hydropower (electricity) (Rollet et al., 2005, Rollet, 2007). Over the 2000-2020 period, the average annual discharge was 120 m^3 s^{-1} at the Chazey-sur-Ain gauging station, 14 km upstream of the confluence with the Rhône (Fig. 4.2). High water stages commonly occurred during winter and early spring, with large flood discharge (QIX.2: 900 m^3 s^{-1}, QIX.5: 1200 m^3 s^{-1}, QIX.10: 1740 m^3 s^{-1}). Overall, very little fine sediments were deposited or preserved in the studied area (Dieras et al. 2013).

Before the construction of the dams, the upper course of the river supplied most of the sediment load in the form of limestone clasts, as most tributaries of the lower course convey much less sediment. Sediment storage by the dams resulted in a drastic reduction of sediment discharge (Rollet et al., 2013) and a wave of sediment starvation is now observed 1.5 km downstream of the town of Priay (Rollet et al., 2005, Rollet, 2007), inducing channel incision. To limit the effect of this sediment starvation on bank erosion, an experiment was conducted to reintroduce 95000 m^3 of gravel to the lower Ain between 2005 and 2010, in order to stabilize the river course and restore the abandoned channels ecological potential (Arnaud et al., 2015).

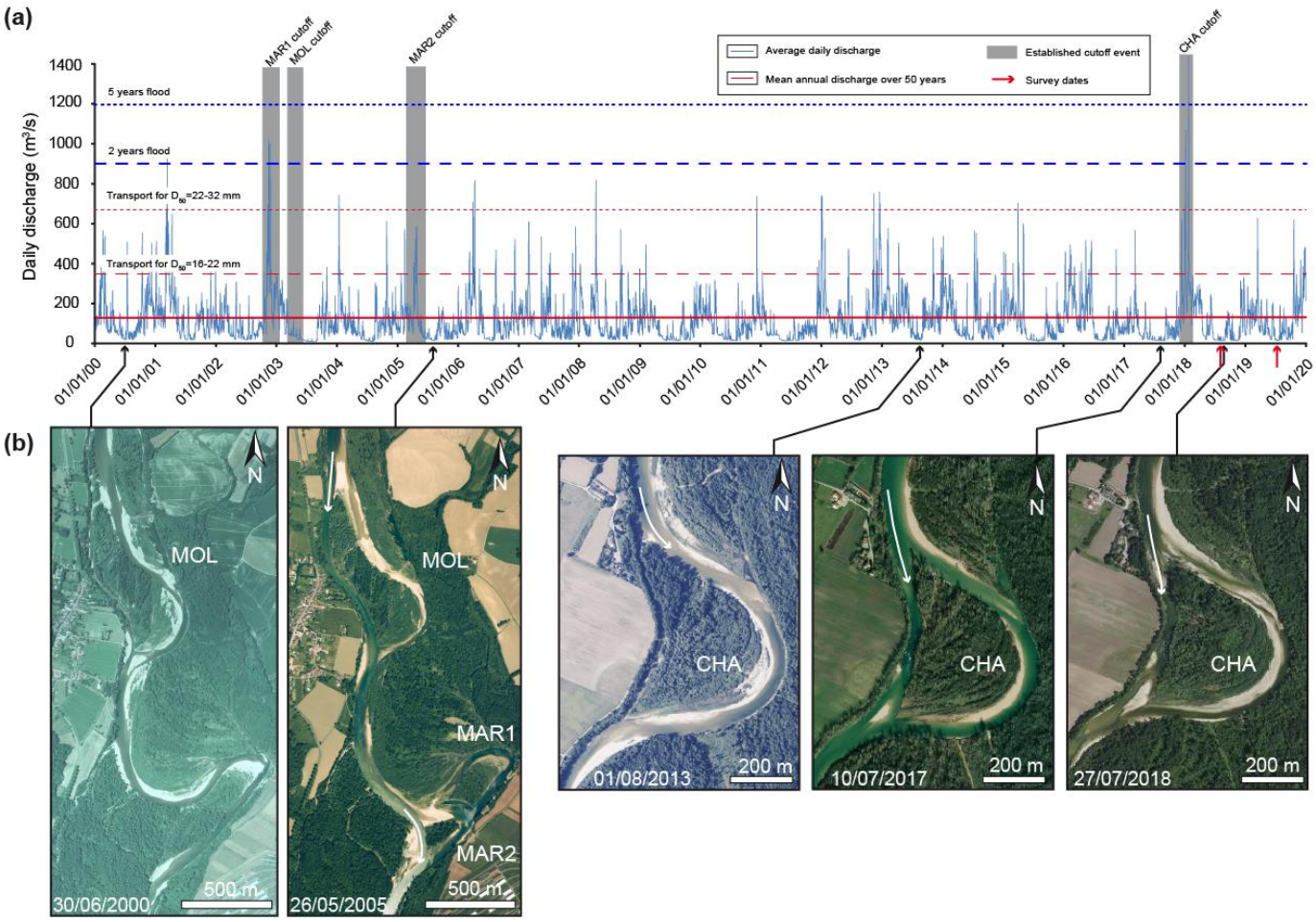

Figure 4.2: Dates of cutoff formation and average daily discharge at the gauging station of Chazey-sur-Ain (from January 1st, 2000 to February 1st, 2020) **(a)** and aerial views of channel morphology evolution **(b)**. Cutoff dates from Grenfell et al. (2012) and Dieras (2013) for Martinaz and Mollon cutoffs. Thresholds for sediment transport data are from Rollet (2007) and 2- and 5-years flood discharge from the Chazey-sur-Ain gauging station.

4.3.2. Studied channels

Our study focused on a segment of the lower part of the Ain River, some 15 km downstream of the Allement dam (Fig. 4.1a) and 4 km downstream of the town of Priay. Although bedload delivered to the study area was reduced due to the dam, the sediment starvation front did not propagate to the area in 2019; thus limited impact on the morphology was observed (Rollet et al. 2005; Dieras et al. 2013). Sediment sampled at the surface was well-sorted (D_{50} ~ 22 mm; Rollet, 2007; Lassettre et al., 2008; Dieras et al. 2013). The thresholds for sediment motion for the ranges of D_{50} 16-22 mm and 22-32 mm on this specific section of the river was determined by Rollet (2007) to be respectively 350 and 650 $m^3 s^{-1}$ (Fig. 4.2).

Four chute cutoff channels located between the villages of Châtillon-la-Palud and Martinaz were studied (Fig. 4.1b; Table 1): one open-stage channel and three closed-stage channels (*sensu* Jordan & Pryor, 1992). The Châtillon cutoff (CHA) (Fig. 4.1c) is the open-stage channel. A chute channel partially reoccupying the1969 Ain course formed since at least

2005, and both the Ain main channel and the narrow chute channel were active until October 2017. Between October 2017 and February 2018 the chute channel widened and the CHA meander bend began to fill (Fig. 4.2). The event responsible for this shift is likely the large flood that occurred the 23rd of January 2018 (1430 m^3 s^{-1}) (Fig. 4.2).

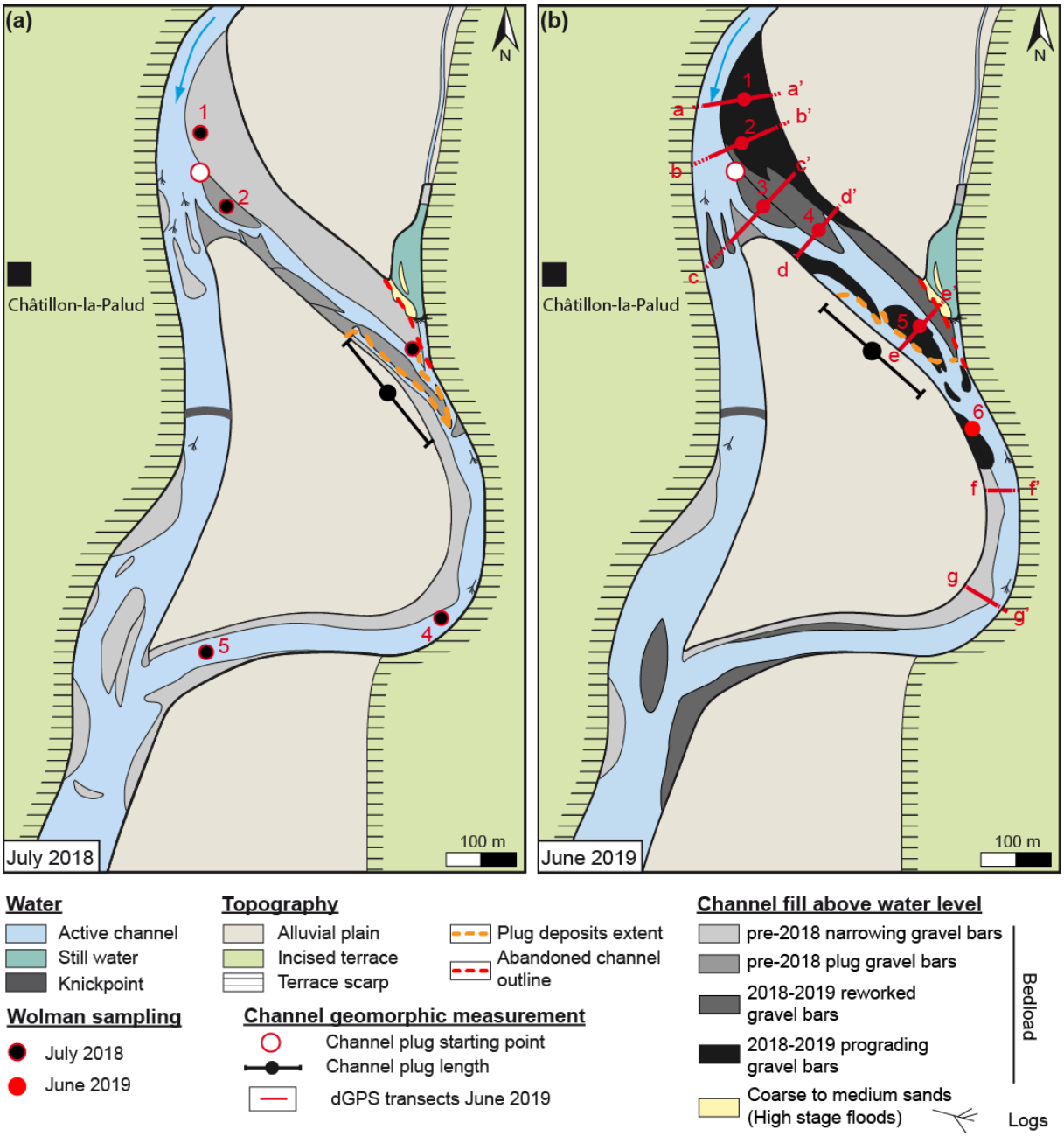

Figure 4.3: Evolution of the geomorphic features of a cutoff in open-stage after a major winter flood, the Châtillon (CHA) cutoff in July 2018 **(a)** and June 2019 **(b)**. (See Fig. 4.1 for site location and Fig. 4.2 for the duration and amplitude of the winter flood).

.

		CHA	MOL	MAR1	MAR2	HYE	M54	PLA	PGA	BRO
			From Dieras et al. (2013)			From Citterio & Piégay (2009)				
Chronology	Diversion	Between 2000 and 2005	1996	Between 10/2002 and 02/2003	Between 03 and 05/2005	Between 1954 and 1963	Between 1948 and 1954	Between 1948 and 1954	Between 1956 and 1965	Between 1956 and 1965
	Stable bifurcation	At least 13 years	Several years	A few months	-	-	-	-	-	-
	Channel narrowing	-	-	-	-	-	-	-	-	-
	Abandonment onset	10/2017	01/2003	02-03/2003	-	-	-	-	-	-
	Plug open stage	02/2018	-	-	-	-	-	-	-	-
	Plug closed stage	Not yet	≤2005 (Aerial picture)	≤2005 (Aerial picture)	≤2005 (Aerial picture)	≤1963 (Aerial picture)	≤1954 (Aerial picture)	≤1954 (Aerial picture)	≤1965 (Aerial picture)	≤1965 (Aerial picture)
	New channel path	Partial reoccupation of 1969 river course	Partial reoccupation of 1954 river course	Lateral migration then reoccupation of 1971 river course	Partial reoccupation of 1954 river course	-	-	-	-	-
Diversion angle		42 ± 2.5 °	22.5 ± 2.5 °	37.5 ± 2.5 °	57.5 ± 2.5 °	55 ± 2.5 °	40 ± 2.5 °	41 ± 2.5 °	50 ± 2.5 °	40 ± 2.5 °
Dimensionless channel plug length		5.8	14.2	6.3	2.1	6.1	7.3	5.8	6.8	6.4
Dimensionless channel plug area		0.56	0.69	0.63	0.58	0.60	0.56	0.51	0.58	0.52
Dimensionless channel plug volume		0.19	0.38	0.19	0.27	-	-	-	-	-
Slope ratio abandonned / active		0.47	0.84	0.26	0.41	-	-	-	-	-
Length ratio active / abandonned		0.49	0.85	0.24	0.42	0.66	0.81	0.41	0.64	0.47
Surveys	Dieras et al. 2013	-	2004-2008 Geomorphic survey 2008 Lidar 2010 dGPS	2004-2008 Geomorphic survey 2008 Lidar 2010 dGPS	2004-2008 Geomorphic survey 2008 Lidar 2010 dGPS	-	-	-	-	-
	This study	2018-2019 geomorphic surveys 2019 dGPS	2018 geomorphic survey	2018 geomorphic survey	2018 geomorphic survey	1963 aerial pictures	1954 aerial pictures	1954 aerial pictures	1965 aerial pictures	1965 aerial pictures

Table 4.1: Summary of the studied channels characteristics.

The Mollon cutoff (MOL) (Fig. 1d) was located at the edge of the floodplain, the right bank of the Ain River corresponding to Miocene bedrock and fluvio-glacial terrace (Figs. 4.1b & 4.4a). It initiated in 1996, partially reoccupying the 1954 course of the river. The channel closed between February and May 2003 (Grenfell et al., 2012, Dieras et al., 2013). In the Martinaz area, two closed channels could be observed. The first channel (MAR1) (Fig. 4.1e) was disconnected after a flood event that occurred between October 2002 and February 2003 (Fig. 4.2; Dieras et al., 2013). The second channel (MAR2) (Fig. 4.1e) was disconnected between March and May 2005 (Fig. 4.2; Dieras et al., 2013). The downstream limb of the meander is cutting the same fluvio-glacial terrace as that of the Mollon site (Figs. 4.1b & 4.4b). The MAR1 channel migrated laterally until it reoccupied the 1971 Ain River path, and was then disconnected by a chute cutoff on its scroll bar. The MAR2 event corresponded to a chute cutoff that reoccupied the 1954 Ain River course (Rollet, 2007).

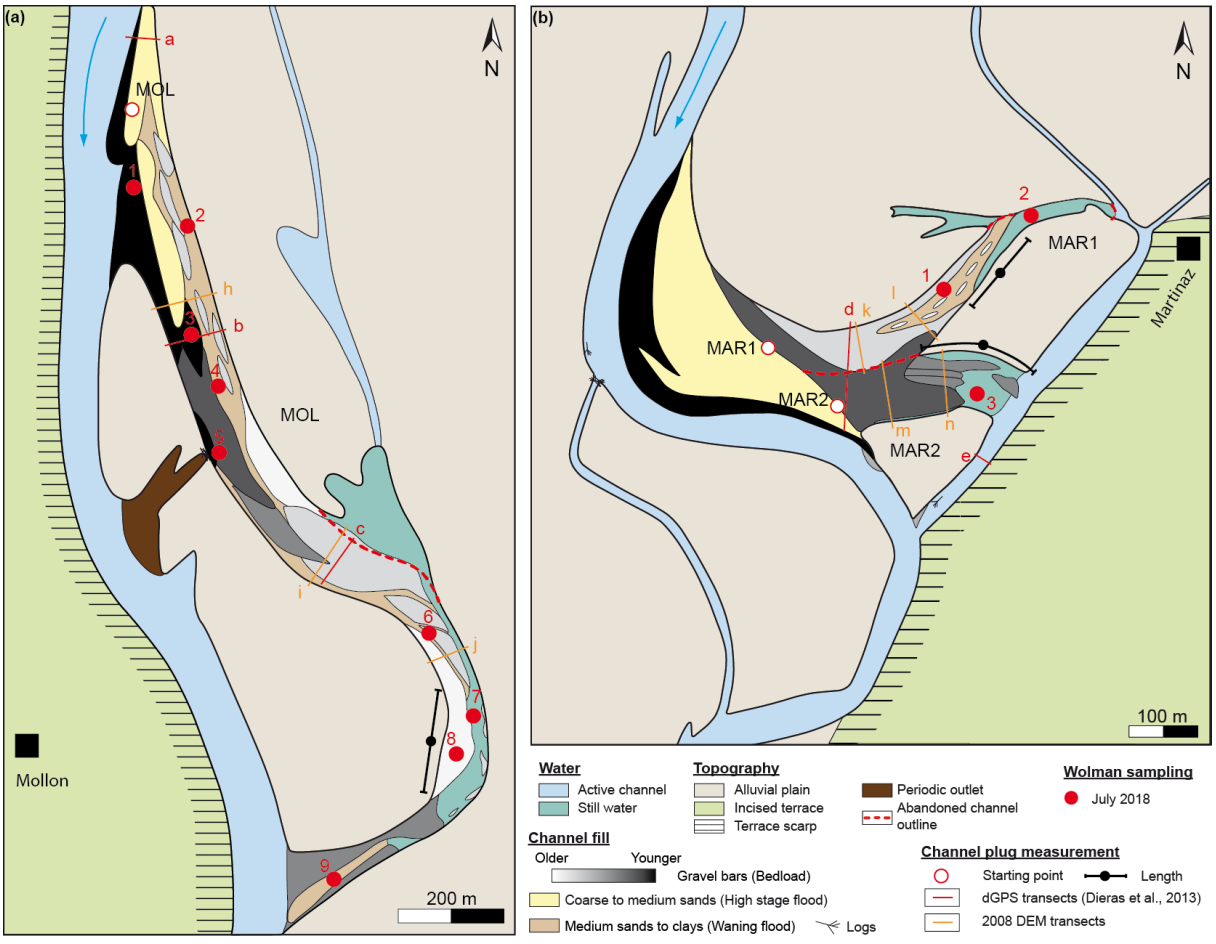

Figure 4.4: Geomorphic features of cutoffs in closed-stage, the Mollon (MOL) **(a)** and Martinaz (MAR1 & MAR2) **(b)** cutoffs as of July 2018.

4.4. Methods

4.4.1. Channel fill sedimentary bodies mapping

Mapping of the sedimentary bodies (Figs. 4.3 & 4.4) of the channel fills was based on DEM and aerial pictures analysis, and was completed by field surveys (Figs. 4.5, 4.6, 4.7 & 4.8).

4.4.1.1. DEM

A 2008 DEM of the area (horizontal precision: 25 cm, vertical precision: 1.5 cm), obtained from the ENS Lyon, was used to study the channel levees and fill topography of the then abandoned MOL and MAR sites, as well as to determine the slope ratios between the abandoned and active channels. As the abandoned channels in cutoff cases rejoin the active channel, the elevation variation is identical along both channels. Thus the slope ratios ($S_{abandonned}/S_{active}$) of the channels were compared to their length ratios ($L_{active}/L_{abandoned}$) and found to be very similar (Table 4.1). This allows, in cutoff cases, to use the length ratio to estimate the slope ratio between the channels when elevation data is missing, e.g., while using aerial pictures.

4.4.1.2. Aerial pictures analysis

Aerial pictures (IGN, geoportail.gouv.fr) were studied over the 2000-2020 period to investigate channel disconnection and channel fill growth timing (see also Dieras et al. 2013). The start of the diversion and initiation of the channel plug was obtained with a precision from a few months to a year depending on the aerial survey frequency. These data were also used to measure the diversion angle at the time of disconnection. Uncertainties on channels diversion angle were estimated from the precision of measurement, and from the fact that the diversion angle varied through time during plugging processes (Bertoldi, 2012). Length of channel plug deposits was measured from the bifurcation point to the point where: (1) the gravel bars occupied the whole channel width, (minimum plug length), and (2) only one or several sediment tongues extended downstream from the main body of the channel plug (maximum plug length) (Figs. 4.3 & 4.4) (Szewczyk et al., 2020). The mean channel plug length corresponds to the average between these measurements. Channel plug area and the associated uncertainties were estimated taking into account picture resolution and potential distortion of the maps.

Additionally, historical aerial photographs (IGN, remonterletemps.ign.fr) going back to 1948 were used to study the disconnection of 5 channels previously studied by Citterio & Piégay

(2009) using the same method (Table 4.1). These channels were abandoned along the Ain River, from Gévrieux, just downstream of the current CHA site, to the confluence with the Rhône River. The channels exact disconnection dates are unknown and the gap between two aerial pictures surveying was often several years. Consequently the historical photographs used to complement the dataset were selected as the first available showing the disconnected channels, before the channel plug was colonized by vegetation. Measurements of the channel plug length and area were made using the stark contrast in color between the lightly colored bedload sediments forming the plug and the rest of the channel. Using the length ratios between the channels, their slope ratios were estimated (Table 4.1). The same method was applied to 5 channels of the Allier River (France), another bedload dominated river. As the contrast between the bedload fill sediments and the rest of the channel is less marked on these pictures, only the channel plug length was measured. The Allier River and the selected abandoned channels are briefly presented in Appendix C.

4.4.1.3. Observations and data collection on the field

The CHA, MOL, MAR1 and MAR2 sites were surveyed at low flow –i.e. when the channels were the most accessible- in July 2018 in order to map the sedimentary bodies and collect grain size and elevation data. Contours of the sedimentary bodies inside each channel, and their elevation relatively to each other, were mapped to complement aerial pictures analysis (Figs. 4.3 & 4.4) in order to reconstruct the architecture of the deposits prior and during channel abandonment. The channels features – in particular the surface of the plug – were studied in detail in order to map accurately sedimentary bodies of different origin (Figs. 4.5 & 4.6). The spatial relationship between the sedimentary bodies, i.e., relative elevation and the nature of their contact (anchoring, covering, steering) were used to obtain a relative chronology of their formation (Figs. 4.3 & 4.4).

Grain size data were used to further differentiate channel fill and channel bed deposits: Wolman pebble counts (Wolman 1954) were performed along sections at the surface of gravel bars and/or at the channel bed to determine median grain size (Fig. 4.7; Table 4.3). In this study, Wolman counts likely missed coarser-grained channel bed deposit in the abandoned channels as they were covered by younger deposits. The average grain-size of the bedload fill deposits was thus potentially underestimated. Similarly, there is no information on the first plug deposits grain-size.

In June 2019, another survey focusing on the CHA site allowed the mapping of deposits and erosional features changes between 2018 and 2019 (Fig. 4.3), as well as the completion of grain size analyses (Fig. 4.3b; Table 4.3). Additionally, topographic profiles of channel cross-sections were measured using a Leica Zeno 20 differential-GPS (dGPS) along straight and curved reaches, at location chosen to intersect key features of the CHA channel fill such as channel plug or the pool at the channel apex (Figs. 4.3b & 4.8). The dGPS cross sections were measured by taking a point every meter, with an acquisition time of 90 seconds and at least 8-9 satellites visible, with an average vertical and horizontal precision of ± 2.5 cm. Data acquisition was interrupted in the channel when water depth was too important and risked damaging the antenna, or close to the riparian woods where the vegetation cover masked the satellites. In these cases, topographic profiles were completed as best as possible using visual observation, physical measurement and DEM (Fig. 4.8). Channel bankfull widths were measured following the classic field survey method along straight reaches and at the apex of the meander loops (Leopold & Maddock, 1953; Williams, 1978; Fitzpatrick et al., 1998), i.e., the width of the channel is determined on a section perpendicular to the channel orientation by the major slope break on the banks (Fig. 4.8).

4.4.2. Estimation of the bedload deposits in the abandoned channel

In order to estimate plug volume in the CHA abandoned channel, as the channel geometry prior to the initiation of the plug formation was not surveyed, we developed a method based on the classic hydrological relationships between the geomorphic parameters (bankfull width, mean bankfull depth, cross-sectional area) of meandering channels. This method was also used on the MOL and MAR channels to compare its results with prior measurements made by Dieras et al. (2013). First, abandoned channels were divided in segments based on their curvature, i.e., straight or bent. Channel bankfull width was measured along each of these segments and a cross-sectional area was estimated using hydrological relationships (Fig. 4.9a).

Along straight reaches, the cross sectional area ($A_{straight}$) defined by the product of the channel bankfull width ($W_{bkf\_straight}$) by the mean bankfull channel depth ($D_{bkf\_straight}$) was computed using the relationship between D_{bkf} and W_{bkf} developed by Williams (1986, equation 39) (Fig. 4.9a):

$$A_{straight} = W_{bkf\_straight} * D_{bkf\_straight} = 0.12 * W_{bkf\_straight}^{1.69} \quad \text{Eq. 4.1}$$

With

$$D_{bkf\_straight} = 0.12 * W_{bkf\_straight}^{0.69} \quad \text{Eq. 4.2}$$

with $W_{bkf\_straight}$ and $D_{bkf\_straight}$ (in meters).

Along curved segments, we computed the bankfull cross-sectional area using the relationship developed by Ethridge & Schumm (1977) based on the experiment of Khan (1971) (Fig. 4.9a):

$$A_{apex}1 = A_{bkf\_straight} * 0.8 \quad \text{Eq. 4.3}$$

We also used Khan's experimental results relating the maximum bankfull depth at the apex and the mean bankfull depth along straight reaches, to compute the cross-sectional area at the bend, approximated by a triangle (Fig. 4.9a):

$$A_{apex}2 = \frac{W_{bkf\_apex} * D_{bkf\_apex}}{2} = \frac{W_{bkf\_apex} * D_{bkf\_straight}}{1.17} \quad \text{Eq. 4.4}$$

A_{apex} was estimated using the two methods described above (Eqs. 4.3 and 4.4) and results were compared. The difference between the computed bankfull cross-sectional area before abandonment and the area computed from field measurements was considered to correspond to the plug fill area (Fig. 4.9b). This was used to measure the proportion of the cross-section occupied by bedload fill deposits (Fig. 4.9b), and plug volume was then estimated by multiplying cross-sectional fill area by segment length (Fig. 4.10c).

Volume uncertainties were estimated using analytical, extrapolation and methodological errors. In the CHA channel, the 2019 DGPs survey was used to measure both the channel width and the cross-sectional area. The dGPS measurements had an accuracy of ±2.5 cm, but some of the profiles were not complete due to the channel depth (Fig. 4.8). Consequently the cross-sectional areas measured for these profiles were less precise, although the channel bankfull width measurements were confirmed by other measurements (i.e., field measurements and aerial pictures). In the MOL and MAR channels, both the empty volumes of the channels and the 2008 cross-sectional area were computed using the method described above with transversal elevation profiles made on the 2008 DEM along the MOL and MAR channels (Fig. 4.4). These profiles, as well as transversal elevation profiles made by Dieras et al. (2013) using a dGPS (precision of ±2.5 cm) (Fig. 4.4), were used to produce several estimates of the cross-sectional area occupied by bedload deposits forming the channel plugs of the MOL and MAR sites as of 2008 and 2010 (Fig. 4.9b). Across the three sites, the dGPS and DEM profiles as well as the profiles from Dieras et al. (2013) were used with the plugs

length to propose an estimation of the channel plug volumes using the method described above (Fig. 4.10c). These factors result in a deviation from mean value for the volume estimated to 5-7% in the MOL and MAR1 channels and 20% in the MAR2 channel. The estimated volumes, together with length and area were plotted against bifurcation angles for comparison (Fig. 4.10). Measurements were made dimensionless to ease comparison with other studies: plug length was divided by channel width, plug area was divided by the total area of the abandoned channel and plug volume was divided by initial, empty channel volume. However, this method assumes that the computed cross-sectional area is the same along the whole length of the segments used to estimate the bedload channel fill volume, which leads to miscalculation of the volume (Lane et al., 1995; Fuller et al. 2003). Despite this, the method described above is to be able to provide an estimate of the empty volume of the channel in order to make channel fill measurements as accurate as possible when lacking data on the empty geometry of the channel, as is the case for the CHA site.

The results obtained in the MOL and MAR channels were compared with the volumes computed by Dieras et al. (2013) to test the validity of our method. They used different methods (Fig. 4.10c) that compared measurements with a reference longitudinal profile surveyed prior to cutoff incident. Their first method was similar to ours, using the cross-sections evolution through time (2004-2008) to make a morphologic budget approach, although the width of their cross-sections was shorter than the bankfull width. Their cross-sectional profiles were used to make a comparison between their measurements and those obtained while using the bankfull width (Fig. 4.9b), and the influence it had on channel fill volume estimation (Fig. 4.10c). Being similar to ours, this method suffers from the same drawback of not considering topography changes between cross-sections. Their second method was based on differences in elevation of the emerged deposits in the channels between two DEMs (2008 and 2010). Finally they used the deepest portion of the submerged surface of the channels in 2010 as the reference for the empty channel bed elevation, and measured the elevation difference between this surface and the 2010 channel fill to estimate the aggradation within the submerged portions of the channels. This was used to provide a minimal estimation of sediment volume in the parts of the channels that were submerged in 2010. This method could then be integrated with the second one to provide estimates of the deposits thickness across the whole surface of the channel. Overall, the combination of their second and third method appears more accurate than their first method as it does not rely on extrapolating data along the channel. Dieras et al. (2013) used a combination of their three

methods to estimate sediment deposition in the channels after cutoff, which was used for comparison with our method in Figure 4.10c.

4.5. Results

4.5.1. Channel facies description and interpretation

Based on the geomorphic features and Wolman pebble counts in the CHA, MOL and MAR sites, five sedimentary fill facies were identified in the channels (Table 4.2).

	Facies	Position in abandoned channels	Measured grain-sizes range	Interpretation
F-I	Coarse to very coarse gravels and pebbles with cobbles and boulders	Thalwegs and pools	2-256 mm	Channel lag deposits
F-II	Medium-grained accreting gravel bars	Inner side of the channel bends, dipping towards the channel	2-90 mm	Lateral accretion deposits
F-III	Medium-grained, progressively fining prograding gravel bars	Upstream reach of the channels, prograding downstream and aggrading	2-128 mm	Downstream migrating fill bars
F-IV	Coarse to medium sands	On top of gravel bars close to the bifurcation point	0.5-2 mm	Proximal portion of high stage flood deposits
F-V	Fining upwards medium sands to clays	Channels topographic lows	< 0.5 mm	Distal portion of high stage flood deposits

Table 4.2: Sedimentary facies.

F-I) Coarse to very coarse gravels and pebbles

These were found in the topographic lows (i.e., thalwegs, pools) of the main river channel and at the thalweg of the abandoned channels (Fig. 4.5a, b). They formed extensive deposits (Fig. 4.5a) that were found over the whole length of the abandoned channel and showed a wide grain-size distribution range (Table 4.3, MAR 1-3, MOL 9, CHA 2018 4, 2019 4). Among these deposits the grain-size distribution range varied along the channel depending of the thalweg topography: In the still partially active CHA site the gravels were finer (D_{50} = 22-32 mm) at the channel riffles (Fig. 4.3; Table 4.3 CHA 2018 5) than at the bottom of the pools (D_{50} = 45-64 or 64-90 mm, Table 4.3 CHA 2018 4, CHA 2019 4). In the disconnected channels, the grain-size also varied from gravels in the thalweg (D_{50} = 22-32 mm; Table 4.3 MOL2, 4, 6, 7) to pluri-decimetric boulders in the pools (Fig. 4.5b). These sediments were interpreted as channel lag deposits formed prior to disconnection (Facies F-I).

F-II and F-III) Medium gravels

Gravel deposits formed bars that were either attached to the inner bank of the channel bends (Fig 4.5c) or formed elongated bodies within the channel (Fig. 4.5d). The former (Facies F-II) followed the outline of the channel bends for several hundreds of meters with a maximal width of a few tens of meters (Figs. 4.3 & 4.4). They were gently dipping towards the channel (Fig. 4.5c). Aerial photographs showed that they grew laterally from the bank towards the channel (Fig. 4.2; Appendix B), without channel lateral migration. They laid directly on top of the channel lag deposits as indicated by the sharp contrast in grain size at their interface (Fig. 4.7b & Table 4.3 CHA 2018 4), without erosive base observed. They showed a narrow grain-size distribution and a D_{50} of around 16-22 mm (Table 4.3, MOL 8, CHA 2018 4). They were interpreted as lateral accretion deposits, i.e., point-bars in the active channel and deposits made to adjust the channel width in the disconnecting channel.

The second type of gravel bars (Facies F-III) were found within the surveyed channels. They formed elongated bodies in the channel (Fig. 4.5d) of about 100-200 m long and 10-50 m wide (Figs. 4.3 & 4.4) with a gentle slope toss face and steep slope lee face (Fig. 4.6a, b). They were interpreted as downstream migrating bars. These bars sometimes laid directly on top of the channel lag deposits (Fig. 4.6c), creating a sharp contrast in grain-size at their interface (Table 4.3, CHA 2019 4), or migrated on top of each other or on top of the lateral accretion deposits. The bars appeared to be gently prograding on the coarser lag deposits. In the still active CHA channel some of these bars were reworked or migrated downstream between the 2018 and 2019 surveys. The grain-size distribution range of these bars was wider (<2 to 128 mm, Table 3) and their D_{50} decreased from the bars deposited on top of the channel lag deposits (D_{50} = 22-32 mm) to the ones on top of other elongated gravel bars (D_{50} = 16-22 mm) (Fig. 4.6a; Table 4.3 CHA 2018 2 &3, CHA 2019 3& 4). These bars were interpreted as downstream migrating gravel fill bars.

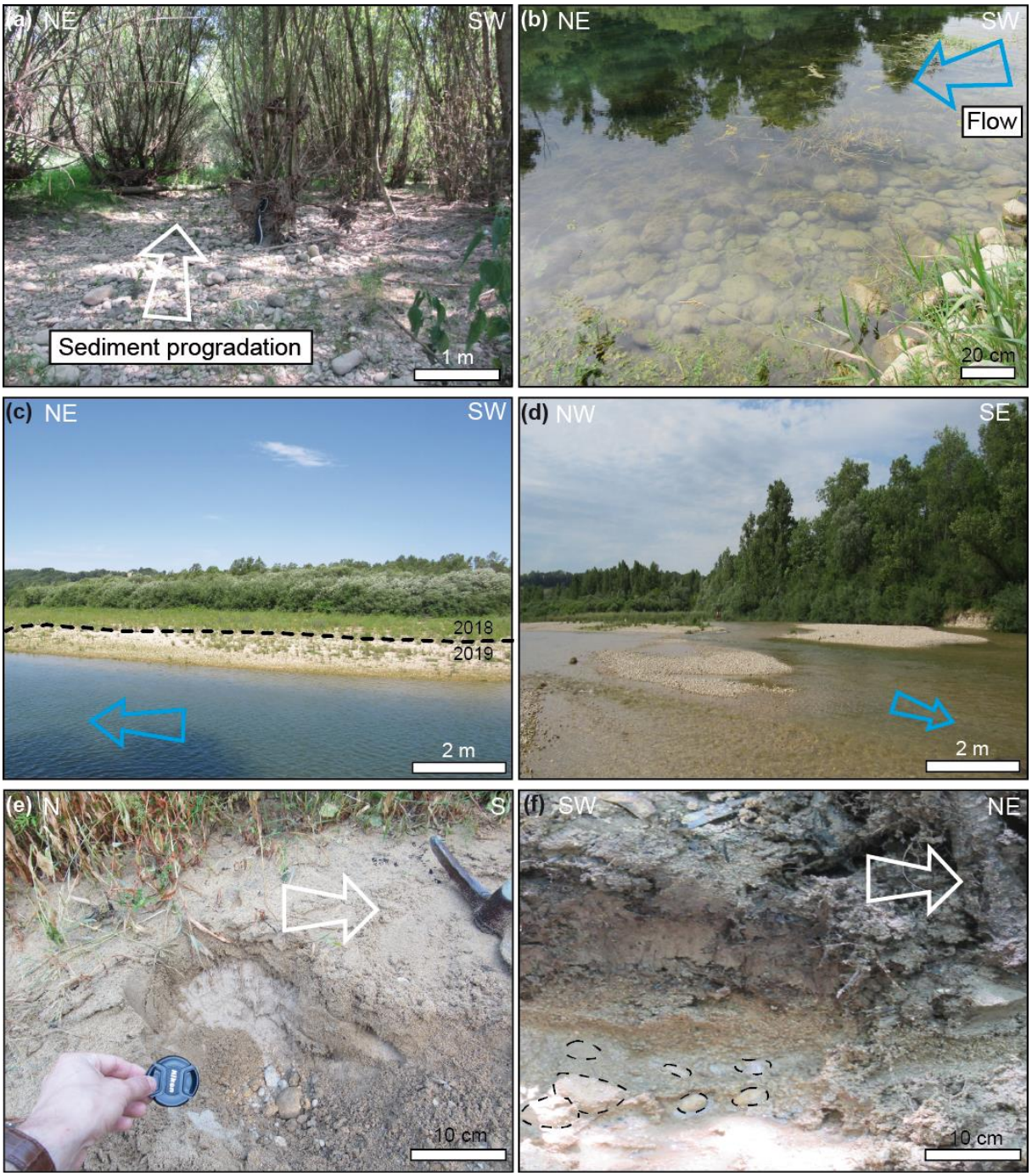

Figure 4.5: Channel fill elements. **(a)** Channel lag deposits in the thalweg on the upstream part of the channel plug (Mollon) (Fig. 4.1d). **(b**) Channel lag deposits in the downstream active part of the channel (Martinaz) (Fig. 4.1c). **(c)** Laterally accreting and **(d)** downstream migrating gravel bar deposits (Châtillon). The bar on (c) was vegetalized between 2018 and 2019, with the dashed line indicating the 2018 limit of vegetation extension. **(e)** Sandy flood deposits covering a gravel bar near the bifurcation of the Mollon channel (Fig. 4.1d). **(f)** Sandy to clayey fining upward deposits overlying gravels preserved in the topographic lows of the channel plug (Martinaz) (Fig. 4.1c).

F-IV) Coarse to medium sands

These sandy sediments corresponded to 0.2 to 0.3 m thick layers of clean, coarse to medium sands (Fig. 4.5e). They were deposited on top of gravel bars in the upstream portion of the channels, close to the bifurcation point and no erosional features were observed (Fig. 4.4a). A sharp contrast in grain size was observed between these deposits and the underlying ones. These were interpreted as the coarser portion of the high stage flood deposits that spilled over the topographic threshold created by gravel deposition at the mouth of the abandoned channel (Facies F-IV).

F-V) Medium sands to clays

Finally, a 0.05 to 0.2 m thick layer of fining-upwards medium sands to clays (Fig. 4.5f) deposited in some of the topographic lows of the closed-stage abandoned channels, covering in some places the channel lag deposits and the lower parts of the gravel bars (Fig. 4.4). These deposits were interpreted as the distal part of high stage flood deposits in areas further away from the bifurcation point and in topographic lows that favored preservation of the fine-grained deposits (Facies F-V).

4.5.2. Channel fill architecture in the studied channels

The channels at the MOL and MAR sites and the 5 channels studied using historical photographs were disconnected and corresponded to the closed-stages defined by Jordan & Pryor (1992) (Appendix B), meaning that only fine-grained sediments brought by overflow events were deposited in the abandoned channels. The CHA channel site was still in the open-stage in 2019, i.e., bedload material still accumulated in the channel and deposits length, area and volume are those of the June 2019 survey.

4.5.2.1. Open-stage channel: the CHA site

Disconnection process was not over at the CHA site and the channel fill plug was still under construction. At the bifurcation point located close to the apex of a meander bend, the point bar growth slightly modified the channel course since the beginning of disconnection process (Fig. 4.2b). In the upstream part of the disconnecting channel, elongated downstream migrating gravel bars (Facies F-II) were attached to the point bar or to the outer bank of the bend (Fig. 4.3). Individual bar dimensions ranged from 50 to 100 m in length and 20 to 30 m in width. They were amalgamated and prograded on top of each other, resulting in aggradation. This amalgamated body occupied the upstream part of the channel (Fig. 4.3 &

4.6a) and nearly clogged the channel just downstream of the bifurcation, leaving only a narrow thalweg (Figs. 4.3b & 4.6c). Other gravel bars grew downstream of this plug, down to the confluence with the small tributary coming from the north (Fig. 4.3b). These bars spatial distribution resulted in a pool and riffle topography from the bifurcation point almost to the bend apex. Further downstream of the bifurcation, laterally growing gravel bars (Facies F-II) were attached to the inner bend of the channel loop and other were attached to both banks close to the downstream extremity of the disconnecting channel (Fig. 4.3b). The bar construction at the channel bend apex and its downstream extremity resulted in a significant narrowing of the channel width, which was more marked at the channel apex (Fig. 4.3).

Comparison between data from the 2018 and 2019 surveys showed the progradation of the new longitudinal gravel bars on top of the point bars or previously deposited longitudinal plug bars (Fig. 4.3b), both corresponding to Facies F-III. A slight remobilization of part of the 2018 deposits was also noticed (Fig. 4.3a, b). The most recent longitudinal bars had a finer grain-size range distribution (Fig. 4.6a; Table 4.3 CHA 2018 1, CHA 2019 1). The migration of these bars on top of the previously deposited ones between 2018 and 2019 resulted in the formation of a 0.3-0.4 m topographic step at the end of the amalgamated bodies (Figs. 4.3b, 4.6a, c). Between 2018 and 2019, new, finer-grained (D_{50} = 16-22 mm, Table 4.3 CHA 2019 6) gravel bars (Facies F-III) formed some 80-100 m downstream of the topographic step (Figs. 4.3b & 5d). These bars were isolated and less extensive than the bars of the amalgamated deposits (~80 m long, 10-15 m wide). They were located on the inner bend of the apex, partially overlying lateral accretion deposits (Fig. 4.3b). The lateral accretion deposits at the inner part of the bend (Facies F-II) slightly extended in the downstream part of the channel (Fig. 4.3b) and were vegetalized between 2018 and 2019 (Fig. 4.5c). The underwater part of these deposits was clean in 2018 but draped by a thin layer of mud in 2019. No fill deposits were found on the outer bend of the pool. At the time of the surveys, the water elevation in the pool was around 1.8 m and large clasts (up to 180 mm, Table 4.3) were found on the channel tahlweg (Facies I). The depth of water in the downstream riffle at the time of the surveys was 0.1 to 0.4 m (Fig. 4.6d). The water surface slope ratio between the active and disconnecting channel was 0.47.

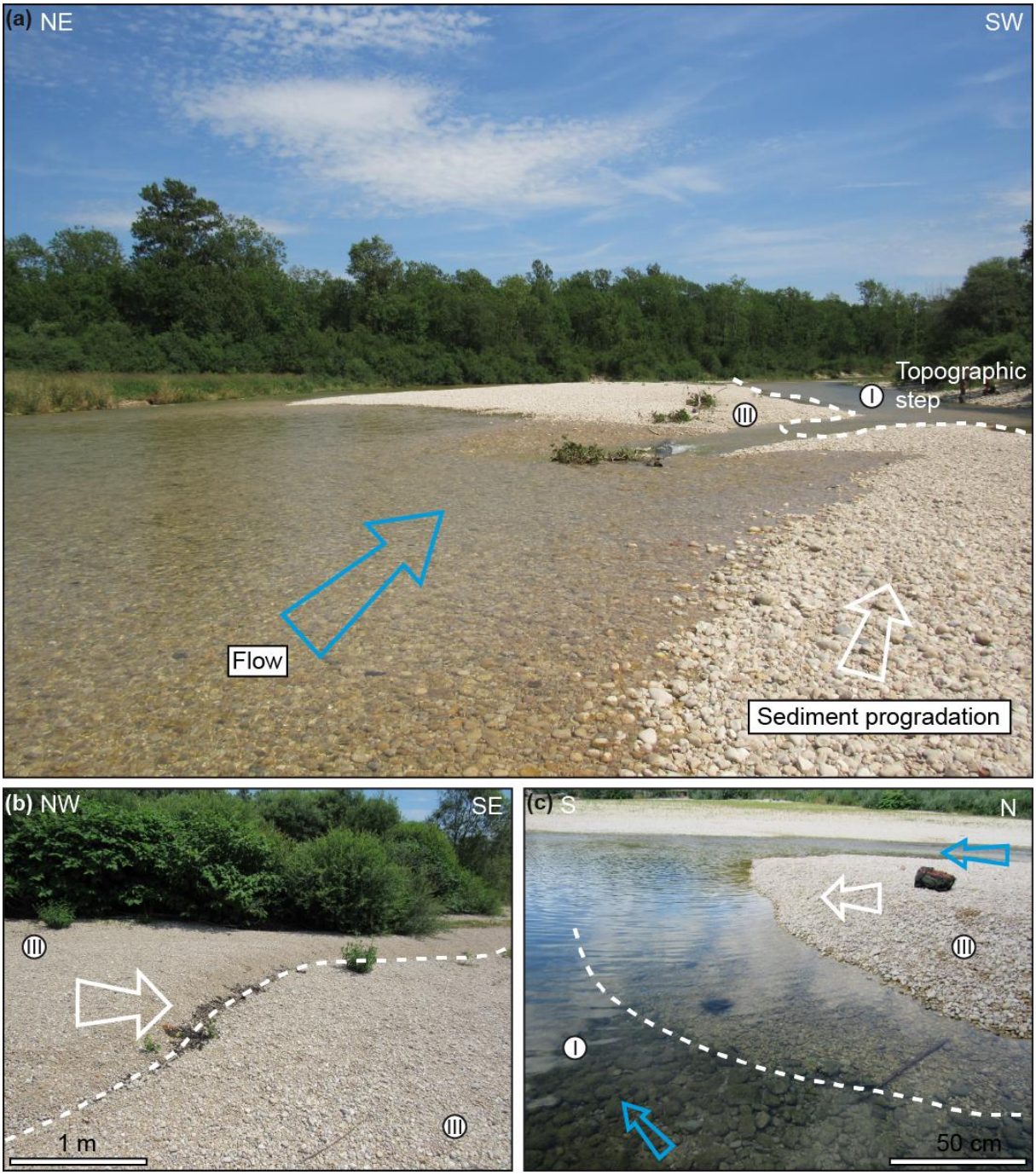

Figure 4.6: Notable disconnection features of the Châtillon cut off. **(a)** Characteristic geometry of a prograding gravel bar during the early stage of the plug (facies F-II). The crest between the gently sloping toss face and the steep lee face creates an undulating topographic step across the channel reach reflecting migration process by lobes as the prograding bar (facies F-II) overlies the channel lag deposits of the former active channel (facies F-I) (Fig. 4.1e). **(b)** Finer grained gravel-bar (facies F-III) that migrated on the early plug deposits (facies F-II) during the high waterstage of winter 2018-2019 (Fig. 4.1e). **(c)** Toe of the prograding gravel bar (facies F-II) (medium grain size) below water level, toe contour is drawn based on the grain size contrast with the coarse channel lag deposits (facies I), it is considered as the downstream limit of the channel plug deposits (Fig. 4.1e).

Cut-off	Sample	Sampled body	Distance from bifurcation (m)	Distribution mode	D_{50} range (mm)	Distribution range (mm)	Facies
MOL	MOL 1	Gravel plug	50	Unimodal	22-32	6-90	III
	MOL 2	Channel lag	90	Unimodal	22-32	2-90	I
	MOL 3	Gravel bar	240	Unimodal	16-22	2-90	III
	MOL 4	Channel lag	320	Unimodal	22-32	6-90	I
	MOL 5	Gravel bar	440	Unimodal	16-22	8-126	III
	MOL 6	Gravel bar	850	Unimodal	22-32	11-90	III
	MOL 7	Channel lag	980	Unimodal	22-32	4-128	I
	MOL 8	Lateral accretion deposits	1040	Unimodal	16-22	4-64	II
	MOL 9	Channel lag	1280	Unimodal	32-45	11-180	I
MAR	MAR 1	Channel lag	200	Unimodal	16-22	6-90	I
	MAR 2	Channel lag	440	Unimodal	16-22	8-256	I
	MAR 3	Channel lag	190	Unimodal	22-32	8-90	I
CHA	CHA 2018-1	Point bar	-50	Unimodal	22-32	<2-90	II
	CHA 2018-2	Gravel plug	50	Unimodal	22-32	6-128	III
	CHA 2018-3	Gravel bar	300	Unimodal	22-32	<2-128	III
	CHA 2018-4	Lateral accretion deposits / channel lag	650	Bimodal	16-22/45-64	6-180	I/II
	CHA 2018-5	Downstream gravel bar	1000	Unimodal	22-32	8-90	III
	CHA 2019-1	Gravel bar on point bar	-100	Unimodal	16-22	4-90	III
	CHA 2019-2	Gravel bar on point bar	-30	Unimodal	16-22	6-90	III
	CHA 2019-3	Gravel plug	50	Unimodal	16-22	4-64	III
	CHA 2019-4	Gravel plug/channel lag	120	Bimodal	16-22/64-90	4-128	I/III
	CHA 2019-5	Gravel bar	300	Unimodal	22-32	6-128	III
	CHA 2019-6	Gravel bar	450	Unimodal	16-22	8-64	III

Table 4.3: Wolman Pebble Counts sampling data.

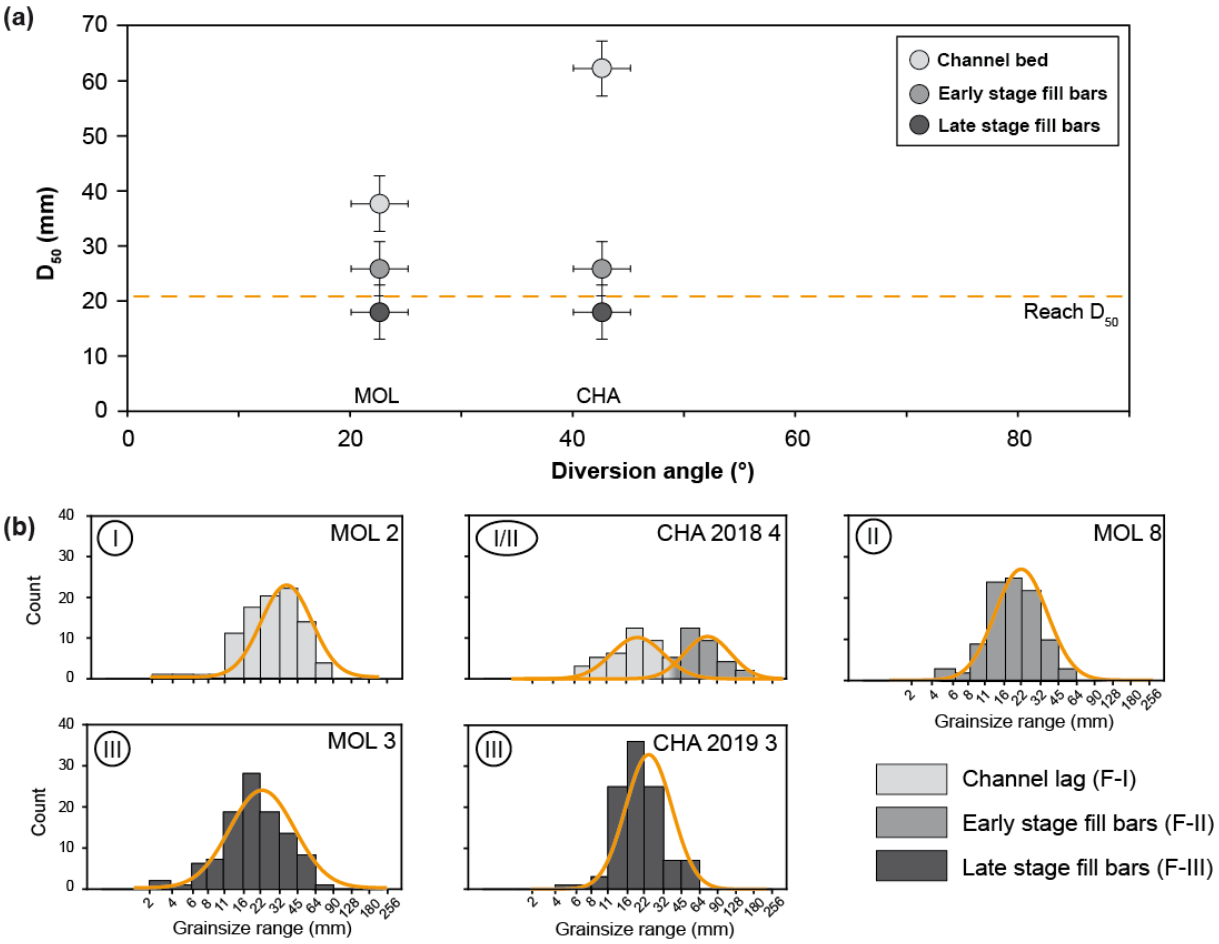

Figure 4.7: Contrast in grain-size between active channel lag and the different generations of fill bars for the mature closed-stage MOL site and open-stage CHA site **(a)**. Examples of grainsize distribution of samples from channel lag, early and late stage fill bars **(b)**. Wolman counts designation refers to Table 1 and Fig. 3 and 4. Roman numerals refer to the facies of Table 2 sampled as shown in Fig. 6. MAR sites values are not displayed as the number of samples do not allow meaningful comparison. Reach D_{50} value comes from Rollet (2007).

The dGPS cross sections surveyed in this channel (Figs. 4.3b, 4.8) showed the change in sedimentation pattern along the channel length. In the upstream part of the channel the bedload fill deposits formed by downstream migrating longitudinal bars (Facied F-II) (Fig. 4.3) and occupied roughly 35-45% of the cross-sectional area (Fig. 4.9b). Near the bend apex, the fill deposits were mostly formed by lateral accretion processes (Facies F-III) (Fig. 4.3) and occupied roughly 5 to 14% of the cross-sectional area (Fig. 4.9b).

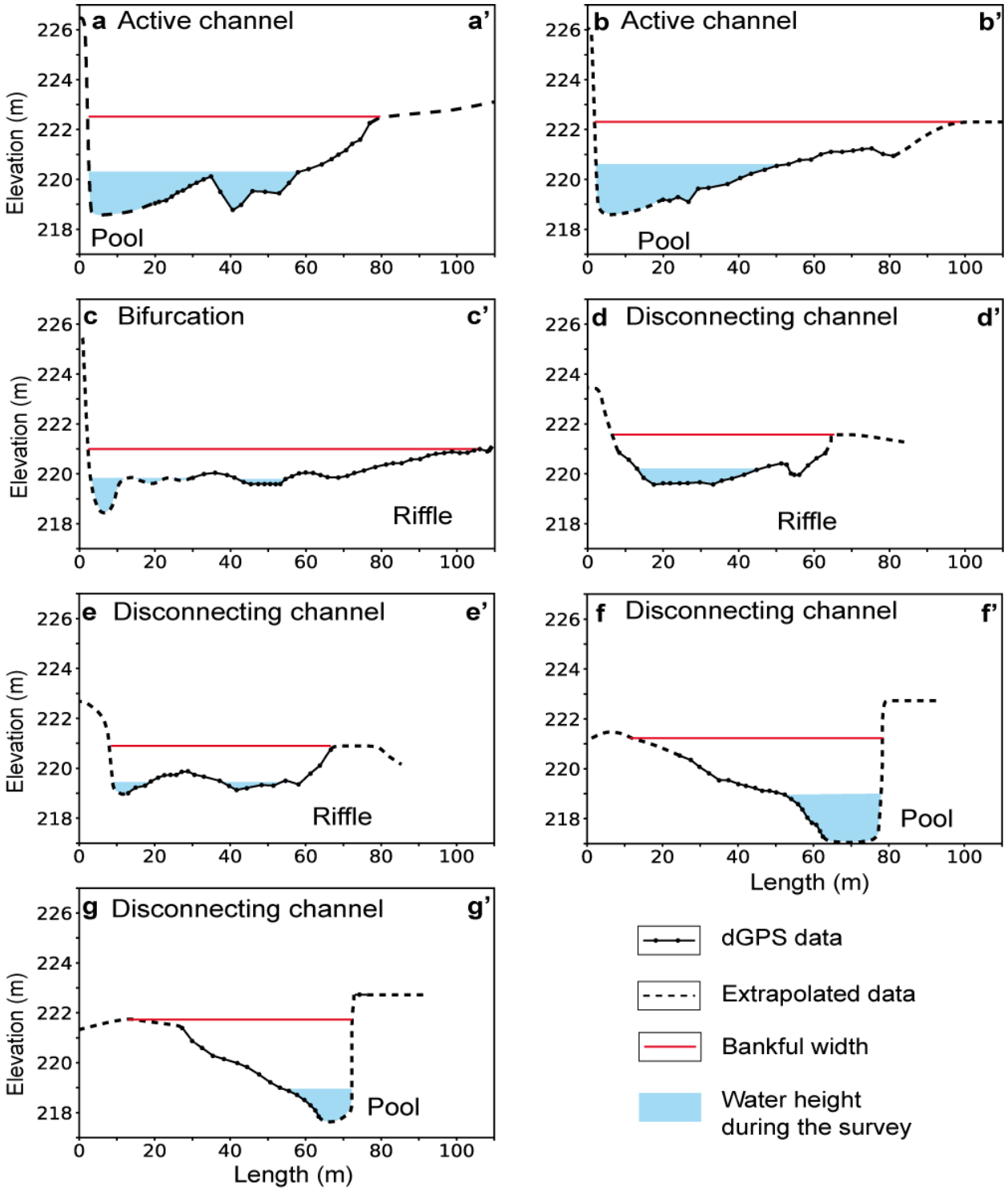

Figure 4.8: Cross sections of the bed topography of the CHA cut-off. (see Fig. 3 for section location).Data come from dGPS and DEM and physical measurements data along segments that could not be surveyed.

4.5.2.1. Closed-stage channels

a) Upstream plug, free downstream confluence: MAR1 & MAR 2 sites

The MAR1 and MAR2 channels were disconnected from the active channel by the formation of upstream channel plugs that were rapidly vegetalized. The downstream reaches of the channels were still connected to the Ain River in 2019. The MAR1 channel plug consisted of several low longitudinal bars (Facies F-II). The plug length was 250-400 m. A progressive decrease of about 2 m of plug elevation was observed from the disconnection point to the toe of the plug. Downstream of the plug toe, channel lag deposits (Facies I) were observed, with short (15-20 m) and thin (0.5 m) bars (Facies F-II) regularly spaced in the thalweg. These bars appeared to be the first ones to have formed in the earlier stages of channel disconnection as they have been covered by other bars during the channel plug growth. The downstream part of the plug and the channel lag deposits were covered by fining-upward fine-grained deposits (Facies F-V), interpreted as deposits of high stage flows that could overflow in the plug and were preserved in the topographic lows of the plug. Downstream of the plug, a pool of still water was observed upstream of the confluence with two small creeks. Flow from the creeks was sufficient to maintain running water in the downstream part of the abandoned channel (Fig. 4.4b). The slope ratio between the active and abandoned channel was 0.26.

The MAR2 cutoff occurred in 2005, after the MAR1 abandoned channel was already in the closed-stage. A bar from the MAR2 channel plug spilled over in the MAR1 channel, partially covering the MAR1 plug (Fig. 4.4b). The plug length measured between 125 and 240 m and had maximum thickness of about 2 m. The downstream part of the plug was formed by the coalescence of several longitudinal bars (Facies F-III). Each of them showed a steep lee face that prograded on top of the channel lag deposits (Table 4.3 MAR3). The younger bars that partially covered the previously deposited ones were thus slightly more elevated (0.3-0.5 m) but also slightly shorter (20-30 m) (Fig. 4.4b). The MAR 2 channel then joined the still active downstream part of the MAR 1 channel (Fig. 4.4b). The bed of the downstream parts of both channels formed by very coarse channel lag deposits (Facies F-I), similar to those observed in the active channel (Fig. 4.5e). The slope ratio between the active and abandoned channel was 0.41.

b) Upstream and downstream plugs: MOL site

The MOL channel disconnected from the active channel through upstream and downstream plugging (Fig. 4.4a), which developed between February 2003 and 2005. A pool formed at the bend apex. On the left bank of the abandoned channel, flow from a small creek contributed to create a pool of stagnant water that was still connected to the disconnected channel pool in 2018 (Fig. 4.4a). The upstream part of the channel was plugged by an amalgamation of vegetalized gravel bars (Facies F-III), in the lows of which a thalweg was preserved (Fig. 4.4a). The plug had a length of 1050-1250 m. Its elevation progressively decreased downstream by around 2 m. The upstream part of the channel plug was topped with high stage flood deposits (Facies F-IV) (Fig. 4.4a & 4.5e). The thalweg was composed of channel lag deposits (Facies F-I) (Table 4.3 MOL 2), which were locally covered by sand and clay (Facies F-V) (Fig. 4.5f). Around the channel bends, the channel narrowed by the formation of lateral accretion deposits (Facies F-II) without lateral migration of the channel itself during disconnection (Fig. 4.4a). The lateral accretion bar at the channel apex was slightly higher (around 0.5-1 m) than the other fill deposits at this point of the channel, but also 0.5-1 m lower than the channel plug maximal elevation. Although they were lower, the downstream migrating bars rested on top of the lowest parts of the lateral accretion deposits when they were in contact with them (Fig. 4.4a), indicating that they were formed at a later stage. The bottom of the pool situated at the channel apex was formed by channel lag deposits (Facies F-I) (Table 4.3, MOL 7) covered by a thin layer of fine-grained sediments (Facies F-V). The downstream part of the channel was plugged by a 0.5-0.8 m thick gravel bars that progressively thinned upstream over 350-400 m until it plunged into the pool (Fig. 4.4a). Part of a thalweg composed of channel lag deposits was locally still visible among these gravel bars (Table 4.3, MOL 9). The slope ratio between the active and abandoned channel was 0.84.

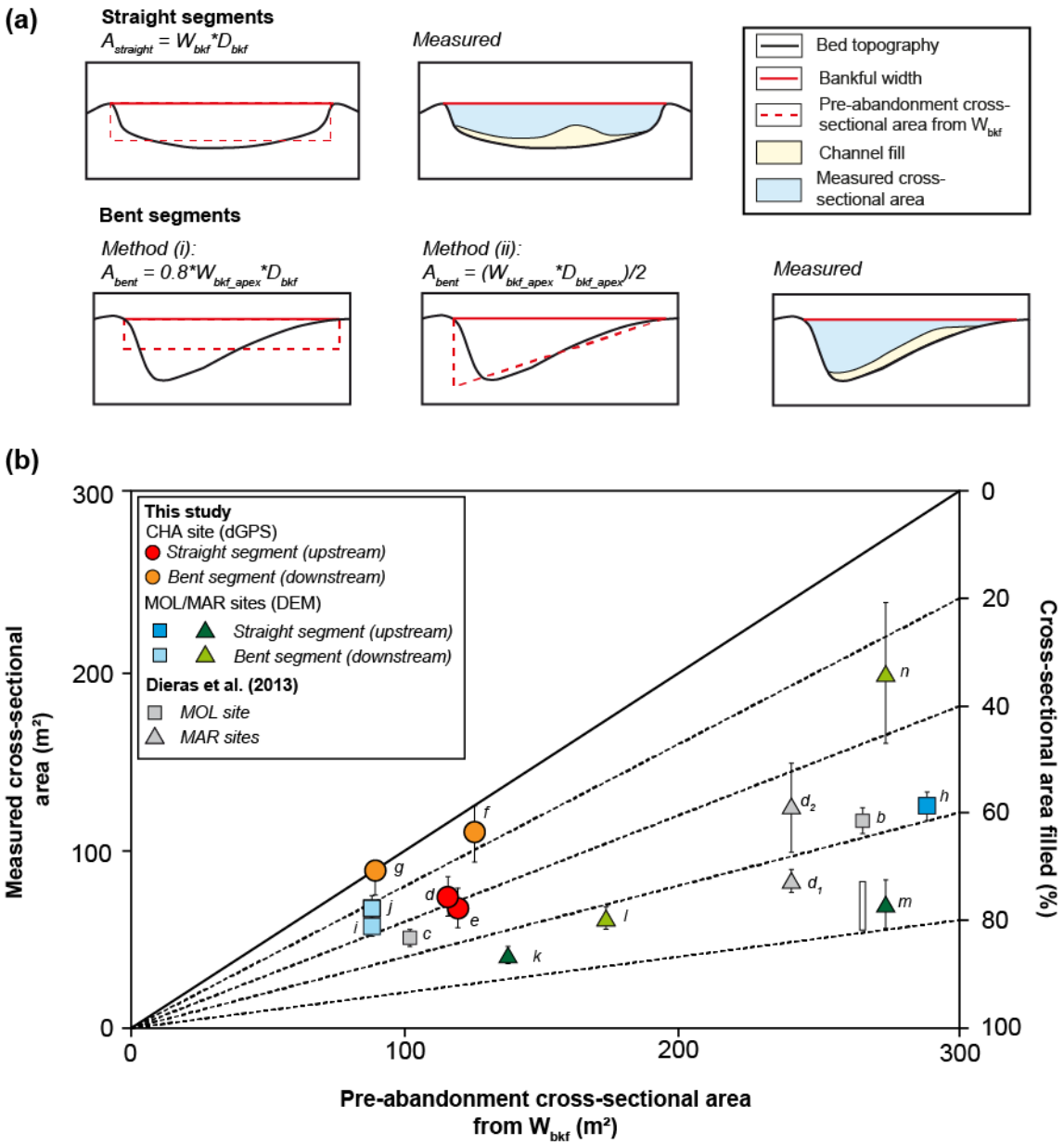

Figure 4.9: Bedload fill volume estimation for CHA, MOL and MAR sites. Scheme illustrating the methods to evaluate the pre-abandonment cross-sectional area **(a)** and plot of the pre-abandonment cross-sectional area of the channel plotted against the cross-sectional area **(b)**. Dieras et al.'s (2013) d transect was subdivided in two smaller ones based on geomorphic assumptions for comparison with new transects.

4.5.3. Geometrical controls on planar geometry and volume of channel fills

The dimensionless channel plug length is mostly independent from both the diversion angle and the water-surface slope ratios, with a dimensionless length varying for most cases between 5 to 7 times the channel width (Fig. 4.10a-a'). Similarly the dimensionless area of the channel plug oscillates roughly between 50 and 70% of the abandoned channel area, with no visible control of the water-surface slope ratio (Fig. 4.10b). More uncertainties are associated to the channel plug dimensionless volume, which could be estimated only for the MAR, MOL and CHA cutoffs. However, it also appears unrelated to the length ratio, with values ranging from 0.15 to 0.40 (Fig. 4.10c).

In the more mature MOL and MAR channels, results from the cross-sections made by Dieras et al. (2013) and those using the 2008 DEM (Fig. 4.4) show that the cross-section fill decreases downstream, diminishing from a maximum around 70% in the most upstream parts of the plugs to a minimum around 35% at its downstream extremity (Fig. 4.9b). The dGPS cross-sections made in the CHA site show the same trend, with around 40% of the upstream part of the channel occupied by bedload deposits while in the bent reach at the channel apex bedload deposits occupied only 5 to 15% of the cross sections areas (Fig. 4.9b). As channel plug construction is still underway at the CHA site, the cross-sections fill and thus its dimensionless fill volume are expected to increase in time. It is worth noting that although the CHA site channel plug was still in construction in 2019, its dimensionless channel plug length and channel fill area were already consistent with those of the other channels and their relation to the diversion angle (Fig. 4.10a-b).

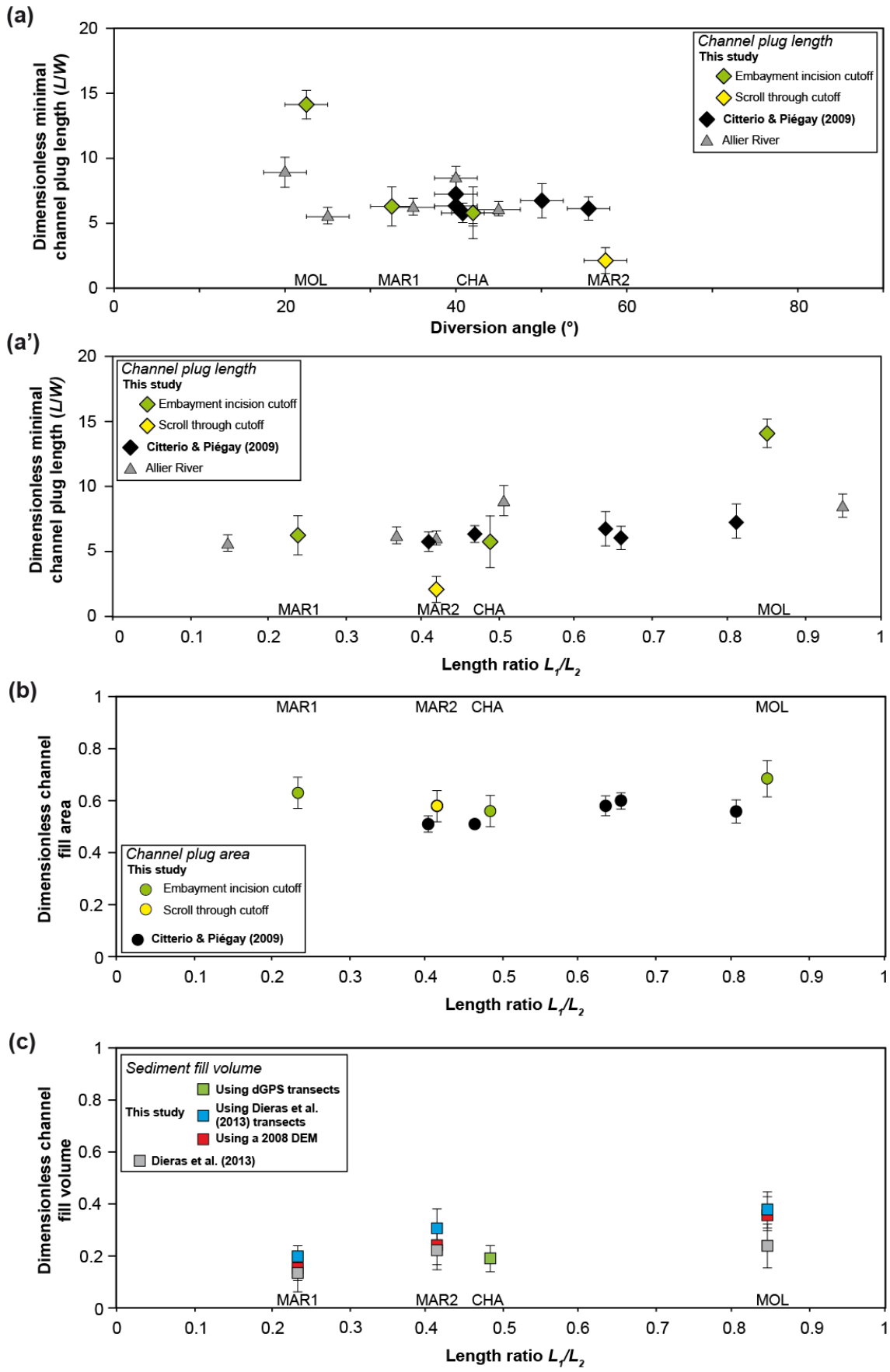

Figure 4.10: Dimensionless channel plug length function of the channel diversion angle **(a)** and length ratio **(a')**, and dimensionless channel area **(b)** and volume **(c)** function of the channels length ratio. Data comes from this study (4 sites) and from Citterio & Piégay (2009) (5 sites). Data for the volume of bedload deposits in the MOL and MAR cutoffs are measured or extracted from Dieras et al. (2013).

4.6. Discussion

4.6.1. Depositional processes of the bedload fill

Combined observations of channels at different stages of disconnection allow us to propose a generic model for the formation of bedload deposits in chute cutoff channels (Fig. 4.11), which result from the combined processes of channel narrowing and plugging (Tooneen et al., 2012). As disconnection is initiated, a first bar starts forming in the flow separation zone, whose width is controlled by the diversion angle value (Fig. 4.11b; Constantine et al., 2010a). This initial bar deposition is a quick process (Chapter 2) and its construction limits the discharge and sediment input in the channel. The channel starts narrowing in response of the decrease in energy induces by both the plug bar construction initiation and the capture of part of the discharge in a newly-opened chute channel (Fig. 4.11c; Sorrells & Royall, 2014; Reynolds & Royall, 2019). Associated with the decreasing discharge, lateral accretion deposits form benches around the bends of the channel (Facies F-II) (Fig. 4.11c, c') but at a lower elevation than the point-bar (Fig. 4.8f, g). They grow on top of the channel lag (Facies F-I), creating a grain size contrast at the contact of the two features (Figs. 4.7b CHA 2018-4 & 4.11c'). The position, elevation and grain size of the benches are directly linked to the decreased discharge to which the channel must adapt its width. This process is well described on avulsion channels (Erskine & Livingstone, 1999; Kleinhans et al., 2011; Sorrells & Royall 2014; Reynolds & Royall 2019) and the cross sections profiles made by Sorrells & Royall (2014) are very similar to the f and g cross sections of Figure 4.8. As long as the channel is in an open-stage, these deposits grow laterally. In bedload dominated rivers, the presence and extent of these benches can be a relative indication of the channel bifurcation stability duration.

When the bifurcation becomes unstable, i.e., an increased part of the discharge flows into the new channel, disconnection accelerates. A channel plug (Facies F-III) forms at the upstream mouth of the channel. Its formation starts at the inner part of the bend just downstream of the bifurcation (Figs. 4.3, 4.4 & 4.11d) in the flow separation zone (Constantine et al., 2010a). Growth along the outer part of the bend is usually enhanced by the presence of a point bar and curved channel upstream of the bifurcation (e.g., Kleinhans et al., 2013) (Figs. 4.3 & 4.4). The bar grows downstream and laterally, occupying a portion of the channel width proportional to the diversion angle. Other bars (Facies F-III) grow anchored to the initial channel plug bar (Figs. 4.3, 4.4 & 4.11c-d) and form a single, amalgamated body, as they are connected to each

other laterally, longitudinally or vertically (Fig. 4.11d-e'). The observed amalgamation process is close to the one described experimentally by Szewczyk et al. (2020). This amalgamated body grows and thins downstream, with a tapered extremity leaning towards the concave part of the bend (Fig. 4.4). Its extremity forms a topographic step over the initial channel bed (Figs. 4.3b, 4.6a, 4.11c'-e').

In the CHA site in the open-stage of disconnection, the channel plug occupies a length and area comparable to those of the other sites although it is still in construction (Fig. 4.10). This suggests that channel plug formation occurs in two stages: a first phase of progradation (Fig. 11dc-d') and a second phase of aggradation above the first deposits (Fig. 11e-e'). During the second phase, the bars forming in the channel are finer-grained. Some reworking also occurs during the plug formation stage but a balance appears to be found between erosion and deposition of new bars (Fig. 4.3), although strong floods that could reactivate the channel. As such channel disconnection and plug construction timings are partially controlled by flood frequency and intensity, as well as sediment availability.

Throughout the plug growth, a thalweg remains in the disconnected channel (Fig. 4.11c), until aggradation fills it and the channel is permanently disconnected from bedload supply (Figs. 4.4b & 4.11e). Following the initial stage of channel narrowing by lateral accreting bars, the growth of the downstream longitudinal bars contribute to the aggradation at an elevation higher than that of the lateral accreting bars (Table 4.3; Fig. 4.9b). Finally, the fact that grain-size in the downstream riffle of the CHA channel is much finer than in the pool may be interpreted as the initiation of a plug above the riffle, sediment being brought from the confluence during floods.

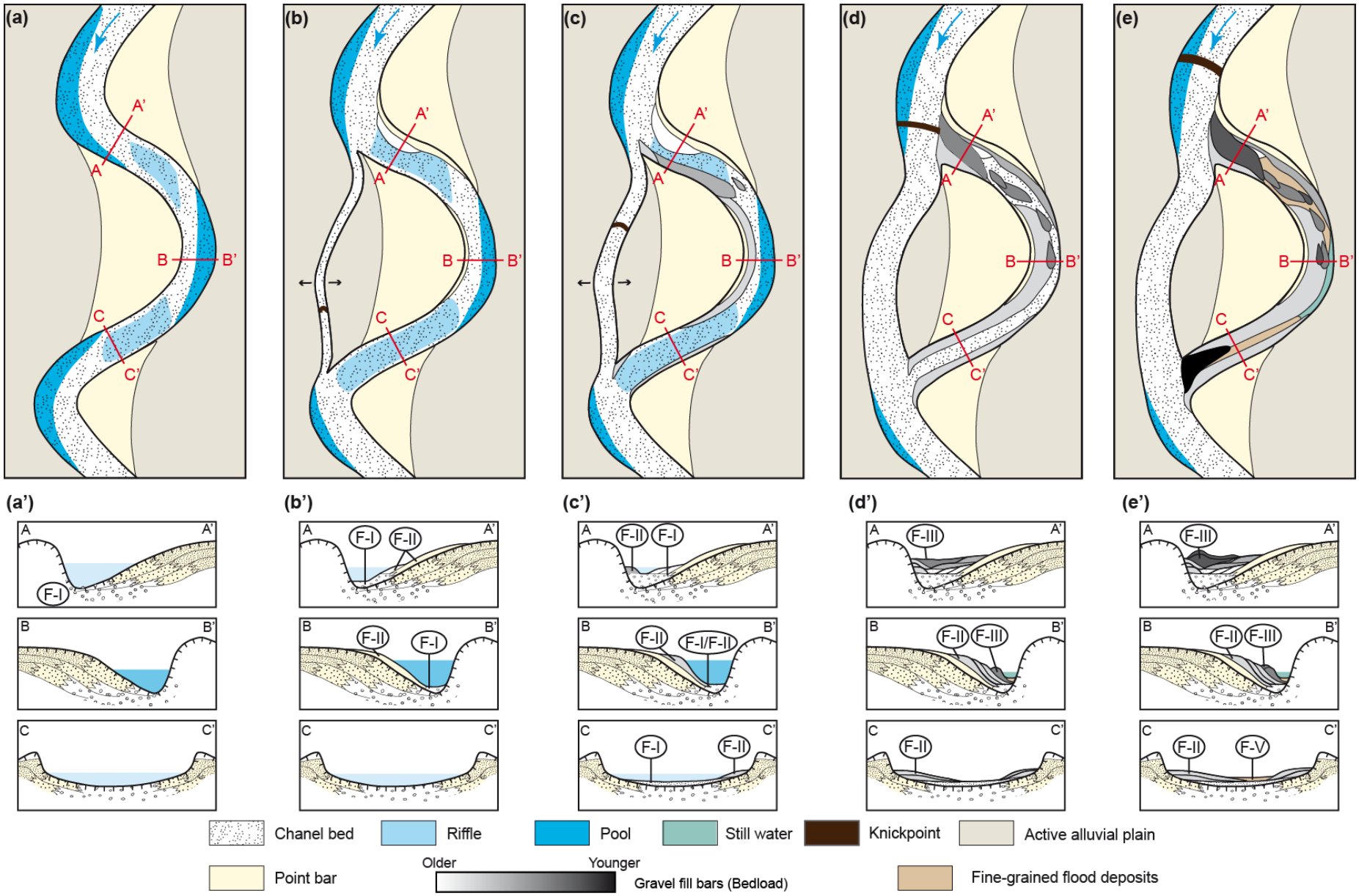

Figure 4.11: Scheme of a channel fill planform **(a-e)** and cross-sectional architecture during a cutoff process **(a'-e')** in a bed load dominated river. Roman numerals refer to the facies of Table 4.2 and Fig. 4.7.

4.6.2. Grain-size changes associated with plug formation

Due to the progressive decrease in energy in the disconnecting channels, the mean bedload grain-size and its range decreases (Figs. 4.7a, b & 4.11a'-d'). The lateral accretion deposits (Facies F-II) are finer than the channel lag deposits (Facies I) due to the reduced energy in the disconnecting channel (Table 4.3; MOL 8, CHA 2018 1, CHA 2019 1), and become even finer as the plug is formed (Facies F-III) and energy decreases further in the channel (Table 4.3; CHA 2018 1, CHA 2019 1). As the plug is built and thickens, stronger floods are needed to supply bedload to the channel, making the sediment supply scarcer. Moreover, only the shallower, finer portion of the bedload can pass over the topographic threshold of the plug and be diverted into the channel (Slingerland & Smith, 2004). Consequently, as the channel plug aggrades, the grain-size of the new bars that thicken (Fig. 4.6c) and extend (Fig. 4.6b) the channel plug decreases (Table 4.3; Fig. 4.11). Although we lack some of the data from intermediary and older deposits, this study logically shows a consistent vertical decrease in grain-size for the bedload sediments forming the channel plug through time (Fig. 4.7a) (Leddy et al., 1993). The Wolman counts performed along the channels show that this vertical evolution of the bedload channel fill grain-size is observed along the whole channel length (Table 4.3). Furthermore, the bedload fill deposits grain-size of a same generation of bars is independent from both the channel diversion angle and the distance at which they are found from the bifurcation point (Fig. 4.7a). It is instead controlled by the grain size of the river reach. However, the grain-size of the finer sediment deposited in the channel once the plug is fully built (sands, silts and clays, Facies F-IV & V) appear controlled by the distance from the active channel (bifurcation point) (Fig. 4.3). Overall, the D_{50} measured in the abandoned channels fill is comparable to or coarser than the D_{50} measured by Rollet (2007) on top of the shallowest bars of the active channel (Fig. 4.7a). This suggests that the active channel bars surface D_{50} can be used to approximate the grain size of the finer bedload fill deposits in abandoned channels. Monitoring the disconnection process from the beginning would allow refining the knowledge on grain-size evolution inside the bedload fill deposits, notably whether the grain-size in the channel plug fines only vertically during the aggrading phase of the plug construction, or also downstream during its progradation phase as the new bars are formed while the flow energy decreases.

The channel plug architecture of amalgamated fining upward bars, as well as the fact that its grain-size appears to be similar to that of the active channel point bars (Table 4.3) makes the channel plug a good connectivity bridge between point bars (Larue & Hovadik, 2006;

Donselaar & Overeem, 2008). This is an important point considering the channel plugs position at the contact of point bars or other coarse-grained sedimentary bodies, especially in the case of abandonment by cutoff processes. The fact that the fill deposits, and particularly the channel plugs, are favorable to fluid circulation or storage is of interest for flow circulation modeling in the floodplain when used in conjunction with the architectural model presented above (Miall, 1996; Hornung & Aigner, 1999; Fleckenstein et al., 2006; Flipo et al., 2014). Similar studies need to be conducted in mixed load systems in order to compare the deposition processes and resulting architectures to our model.

4.6.3. Geometry, extent and volumes of channel plugs

In this study, we proposed a method that uses the classic hydraulic equations for reconstructing the channel cross-sectional area when no survey of the initial channel is available. Volumetric estimate of the sediment deposited in the abandoned channel since abandonment is classically based on several methods. When available, difference in DEM collected at the time of diversion and stability of the channel provides the most accurate calculation (Dieras et al. 2013). Otherwise, the topographic difference between the same cross-sections surveyed at different times and multiplied by the reach length provides a good estimate (Goff & Ashmore, 1994; Martin & Church, 1995; Lane, 1997; Ham & Church, 2000; Fuller et al., 2002; Martin, 2003; Surian & Cisotto, 2007). Our estimation of the pre-abandonment cross-sectional area has several advantages. First, it allows doing an estimation of the bedload fill sediments volume without having previously mapped the abandoned channel bed topography during its active phase, which is difficult and time consuming. Additionally, by using a set of equations determined experimentally and empirically on active rivers that rely on the measurement of a single parameter that is easily obtained (W_{bkf}, Fig. 4.9a), this method is easy to implement both on the field and on remotely acquired 3D data. However, this method underestimates the possible channel bed erosion due to the early stages of plug construction and averages the cross-sectional area on long stretches of the channels, which is notably problematic in the curved segments along which the channel cross-sectional geometry varies quickly.

The systematic overestimation of the volumes by our method compared to Dieras' (Fig. 4.10c) can be explained by two factors. The first one is that the channel width was taken from slope breaks along the channel sides in our method and as the length of the surveyed section in Dieras et al. (2013), resulting in larger sections in our study. The second one that is channel depth was taken as the channel mean bankfull depth our study, i.e., at equilibrium, and along

surveyed sections in Dieras et al. (2013) where some fill deposits may have been already deposited.

Dimensionless channel plug length, surface and volume are roughly constant in all channels and seemingly independent of any geometrical control, except in the case of the MOL (larger dimensionless length; area and volume) and MAR 2 (lower dimensionless length) sites (Fig. 4.10). These results are discussed based on the observations from our previous experiments that showed that although channel plug length, surface and volume depend on the bifurcation angle (and bed slope) in free flow systems (Section 2.1), their construction, extent and volume are affected by the presence of backwater effects (Section 2.2) that results in channel plug lengths hovering around 5 to 6 times the channel width (Fig. 2.16). Chapter 3 further demonstrated that the water-surface slope ratio at equilibrium controls both channel plug length and volume (Fig. 3.12).

Considering the channels geometries and slope ratios, of the 4 channels studied on the field only the MOL channel plug was expected to have formed fully outside of the influence of a downstream hydraulic effects. Indeed, the MOL channel had a low diversion angle and the cutoff channel was only slightly shorter than the abandoned channel. Consequently its slope ratio was high at 0.84 (Table 4.1). Following Chapters 2 & 3 results, its dimensionless length should be around 10 times the channel width at the bifurcation (Fig. 3.12) and this high slope ratio indicates that water-surface slope modification likely did not reach the bifurcation point and thus did not affect the channel plug construction and length. The still water area observed in the current state of the channel was due to the downstream channel plug that formed once the upstream plug construction sufficiently reduced the discharge in the disconnecting channel (Chapter 3). The downstream plug prevents the small tributary from flowing freely (Fig. 4.4a). The MAR1 and MAR2 channels had water-surface slope ratios of 0.26 and 0.41, respectively (Table 4.1) and, their plugs formed at least partly under the influence of downstream hydraulic effects induced by the two tributaries that flow into the channels at their apexes (Fig. 4.4b). Thus development of their channel plug was expected to be affected by the presence of downstream hydraulic effects, reducing their length compared to plugs formed in free flow conditions (Chapter 2). Similarly, the CHA site length ratio of 0.47 (Table 4.1) and possible interactions occurring at the confluence with yet another small tributary (Fig. 4.3) indicate that its channel plug growth is also probably affected by water-surface slope modifications.

Overall, no clear relationship between either the diversion angle or the channels slope (or length) ratio and the channel plug length is visible (Fig. 4.10 a-a'). It is interesting to note that most channels, even some with slope or length ratios > 0.5, have plug lengths around 5 to 7 times the channel width, similarly to what was observed in Chapter 2 when plugs formed in the backwater zone (Fig. 2.16). The presence of small tributaries at many of the abandoned channels apexes could play a role in this, further lowering the water-surface slope in the disconnecting channel and fixing the channel plug length.

The overall consistency in surface and volume values is surprising, especially when considering the differences in geometries and controls on the channel plug deposition. The channel plugs occupy around 50-70% of the channel surface (Fig. 4.10b) regardless of the channel plug length. Indeed, although the MAR2 channel plug is the shortest, both its area and the volume are equivalent to those of the other channel plugs (Fig. 4.10). The MAR2 channel plug formed in the wide upstream part of the channel, whose downstream part is narrower (Fig. 4.4b), explaining its high dimensionless area and volume. However, the plug width is constant (Fig. 4.4b). It is possible that the channel narrowing discouraged further plug growth. Indeed the channels length, width, curvature and depth as well as the possible presence of riffles and pools, slope breaks or erosional processes reworking the channel bed affect the area and volume available for sediment storage and can encourage deposition. A steep curvature in a channel that loses energy due to the capture of part of the discharge by a chute channel would encourage important deposition on the internal bend. Likewise the transition from riffle to pool may encourage deposition due to the flow slowing as the depth increases.

Although volume data are sparser and more uncertain than length and area data, channel plug volumes are also unaffected by the water-surface slope ratio (Fig. 4.10c). However, the MAR1 and CHA channel plug dimensionless volume are lower than the MOL and MAR2 ones, despite occupying the same area of the channel. Considering that the CHA channel is still open its fill volume is likely to increase in time. Figure 4.9b suggests (based on data from the closed-stage channel) that the upstream part of the channel plug could evolve from occupying 35-45% of the channel cross-section as measured in 2019 to occupying around 60-65% of the channel cross section once the channel will be fully abandoned. However, the MAR1 channel was completely disconnected before its plug was fully formed. As the channel plug appears to take more time to thicken than to grow, it is very likely that the MAR2 channel cutoff started its disconnection before the MAR1 plug reached its maximal thickness,

thus cutting of the sediment supply to the MAR1 plug and explaining its low volume. Indeed the sedimentary body mapping and aerial photographs even suggest that some of the gravels deposited on the MAR1 plug where it separates from the MAR2 channel originated from the MAR2 plug and spilled over in the MAR1 channel as its channel plug was not high enough to fully constrain the flow (Fig. 4.4b). Thus channel plug area and volume appear controlled by both the sediment supply and the inherited geometry of the channel.

4.6.4. Cutoffs initiation and bifurcations stability

In the lower valley of the Ain River, cutoffs form mostly by reoccupation of previously abandoned channel reaches that form topographic lows in a narrow entrenched alluvial plain (Fig. 4.1; Table 4.1). The abandoned channels are rarely fully filled, leaving depressions in the alluvial plains. Furthermore, very little fine-grained deposits are present in the abandoned channels and their fills appear mostly composed of gravels and pebbles easily eroded once incision is initiated. Both these factors make the abandoned channels prone to reoccupation (Howard 1992; Smith et al. 1998; Berendsen & Stouthamer, 2000; Schwendel et al. 2015).

However a trigger is generally needed to initiate the formation of a cutoff channel. Disconnection of the CHA and MAR1 cutoffs started soon after the initiation of the bifurcation during a period of high water stage (2yr and 5yr floods) over a period of a month (Fig. 4.2). MAR2 disconnection was similar but associated to a lower water stage (1yr flood). Conversely, the MOL bifurcation had been stable for 7 years and no notable flood occurred at the time of its disconnection between February and May 2003. However, it should be noted that it occurred after a period of high flows (2 years floods) that may have modified the river bed morphology (Fig. 4.2).

Schwenk & Foufoula-Georgiou (2016) showed that cutoff formation creates perturbations that accelerate river migration and favor channel widening both upstream and downstream of the cutoff, provoking an “avalanche” of cutoffs as the active channel tries to adjust to the new conditions. In the study area, the disconnection of the MAR1 channel could have been the trigger for the destabilization of the MOL channel bifurcation (e.g., through knickpoint retreat), forcing its disconnection in early 2003 despite the fact that no strong flood was recorded (Fig. 4.2). Widening and incision of the MOL cutoff channel supplied an important volume of sediment to the MAR area situated just downstream. Constantine et al. (2014) and Ahmed et al. (2019) found that the evolution of meandering rivers is tied to the upstream supply of sediments, and that an important supply will induce channel migration and cutoff

formation. Consequently, the combined effects of the MAR1 and MOL cutoff formation on the reach stability and of the release in the system of a high amount of sediment during the MOL chute channel incision could have encouraged the formation of the MAR2 cutoff in turn in early 2005, leading to the MAR1 channel abandonment before its plug reached its maximum thickness (Fig. 4.10c). Dieras et al. (2013) calculated the sedimentary budget of the MOL/MAR area and determined that a significant proportion of the sediment eroded from the Mollon area in the 2003-2010 interval could have been trapped in both MAR channels, which can also explain the important MAR2 fill deposits volume relatively to the channel plug length.

4.7. Conclusion

Field surveys in three abandoned channels and one channel in the process of being disconnected in the Ain River, France, provided the opportunity to study the bedload fill deposits formation processes, architecture and temporal evolution as well as the controls on their extension and volume in the abandoned channels.

1) A model for bedload architecture is proposed. Bedload fill sediments consist of an initial plug at the mouth of the channel being abandoned, downstream laterally accreted bars contributing to channel narrowing and downstream prograding longitudinal bars from the initial plug that finally aggrade until disconnection is effective.

2) Grain-size of the bedload fill deposits in the abandoned channel fine upwards and downstream in response to the decreasing flow during the abandonment process and are comparable to that of the highest bars formed in the active channel.

3) A method for measuring the volume of the channel fills based on the hydraulic section is proposed when there is no survey before disconnection. Most of the volume of the bedload fill deposits is made by downstream migrating bars forming the channel plug, with some benches formed during channel narrowing downstream of the plug.

4) On these field examples, most channel plugs have a length of 5-7 times the channel width at the bifurcation while the upstream plug systematically spreads over 50-60% of the disconnected channels surface. Hence, no clear control of channel planform geometry on channel plug length was determined, although the influence of water-surface slope modification, inherited geometry or sediment supply may be suggested locally.

Chapter 5: Long-term preservation of coarse-grained fill deposits: tests on field observations

Ce chapitre étudie les processus qui peuvent affecter la préservation et l'architecture des dépôts sédimentaires de remplissage grossiers lors des décennies à millénaires suivant la déconnexion du chenal. Des données tirées d'études de terrain et de la littérature sont utilisées pour vérifier les relations déterminées dans le Chapitre 3 sur les portions du remplissage de chenal préservées après la déconnexion.

Une portion des études de terrain présentées dans ce chapitre (Vimpelles, Vieille Seine) ont été présentées à un colloque sur les relations entre société et environnement du Mésolithique à la fin du Moyen-Âge qui a eu lieu à Troyes (France) les 17 Septembre 2019.

This chapter investigates the processes that may affect the coarse-grained sedimentary fill preservation and its architecture during the decades to millennia long periods of time following channel disconnection. Additionally, data from the field and literature are used to test the relationships determined in Chapter 3 on the parts of the channel fill preserved after disconnection.

Parts of the field study (Vimpelles, Old Seine) has been presented during a colloquium on the relationships between society and environment from the Mesolithic to the end of the Middle-Ages that was held at Troyes (France) the 17th of September 2019, and published in the conference acts:

PETIT, C., CHARRONDIÈRE-LEWIS, P., COJAN, I., CRUZ, F., DEBORDE, G., DELEPLANCQUE, B., DUROST, R., FECHNER, K., FONTANA, L., FROUIN, M., GOUGE, P., GRANAI, S., GRIMAUD, J.-L, PELTIER, V., RIQUIER, V., SZEWCZYK, L., TEGEL, W., VANMORKERKE, J., *in press*. Relations sociétés – milieux en Petite-Seine du Mésolithique à la fin du Moyen Âge : nouvelles problématiques et résultats récents d'archéologie environnementale. *In:* V. Riquier (eds.), *L'Aube, un espace clé sur le cours de la Seine*.

5.1. Introduction

The previous chapters have been dedicated to the observation of coarse-grained sediment deposition in abandoned channels during the disconnection phase, and the resulting bedload deposits architecture, with a strong focus on the channel plug. Based on these results, a synthetic model describing the different sedimentation phases and their controls was proposed. In this model, two geometrical controls influence the deposits architecture: the abandoned channel diversion angle, and the water-surface slope ratio between the abandoned and active channels (Fig. 5.1).

However, this model only covers the disconnection phase, from the beginning of the initial plug bar deposition to the end of the channel plug construction by bedload sediments. In natural cases, this phase is relatively short, spanning in most case a few years to a decade in cutoff cases (Petersen, 1963; Gagliano & Howard, 1984; Hooke, 1995). This brings the question of (i) the coarse-grained deposits preservation through long periods of time after the disconnection (centuries to millennia) and (ii) the possibility to predict their extent or volume based on the channel geometry for integration in channel fill modeling.

In this chapter, the long term preservation of coarse deposits is tested through the study of the temporal evolution of coarse-grained fill architecture in abandoned channels during or after their infilling phase. In a first section, a well constrained channel avulsion channel from a southern segment of the Old Seine, near Vimpelles (France), is studied using boreholes and field mapping. In the second section, the coarse-grained deposits preservation of this channel is compared with data from the literature. In the third section, the pertinence of maps and aerial pictures analysis of channel fill is discussed using examples from the Ain, Allier and Mississipi rivers.

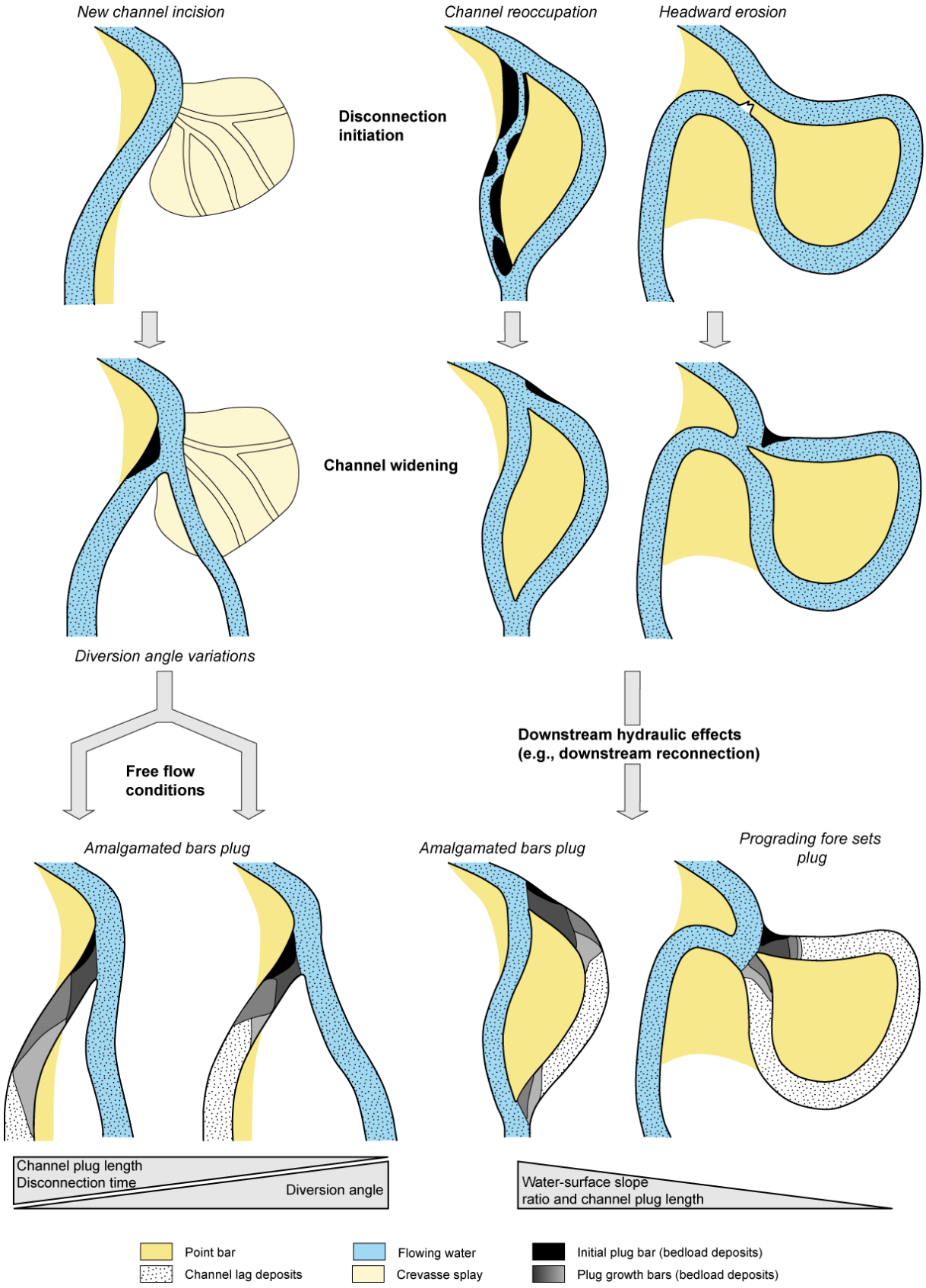

Figure 5.1: Schematic representation of the channel plug length and growth pattern based on bifurcation and channels geometry and downstream hydraulic effects.

5.2. Reconstruction of a pluri-centenal abandoned channel fill architecture: the Vimpelles avulsion channel (Seine, France).

The Vimpelles abandoned channel was formed several millennia ago, during a period of anabranching of the Seine River. The Vimpelles channel still forms a topographic depression in the Bassée alluvial plain (France), allowing an easy identification and study of its coarse deposits architecture.

5.2.1. Geographical and geological contexts

The Seine River flows 770 km from the Langres Plateau (France) to the English Channel and drains the major part of the Paris basin (Fig. 5.2a). The Seine is a meandering, mixed-load river that initially flows through Jurassic and Cretaceous deposits composed of limestones, sands, clay-rich shales and chalk (Fig. 5.2a). In its upstream part, to the southeast of Paris, the Seine created a 365 km² (60 by 6 km) alluvial plain, between the confluences with the Aube and Yonne rivers, called the "plaine de la Bassée" (Fig. 5.2b) (Viennot et al., 2009).

In the Bassée alluvial plain, the Seine has a mean discharge comprised between 77.4 m^3s^{-1} and 79.8 m^3s^{-1} (Deleplancque et al., 2018) and its course was heavily modified for navigational purposes (Fig. 5.2b-c). There the Seine formed several alluvial terraces that are grouped in two units (Mégnien et al., 1965; Lautridou et al., 1999): the upper terraces and the modern alluvial deposits. All terraces have a similar structure: they are on average 6 m thick and composed of fining-upwards alluvial deposits, ranging in size from gravel conglomerates to silts (Deleplancque et al., 2018). The upper terraces are found on the hillsides at the periphery of the alluvial plain (Terraces T_{IV} to T_I) while the modern deposits fill the valley (Terraces T_1 & T_2) (Fig. 5.2c-d). Two nested fluvial sequences (Fz_a &Fz_b) incised and reworked the T_1 and T_2 terraces fluvial deposits (Fig. 5.2d) (Deleplancque et al., 2018).

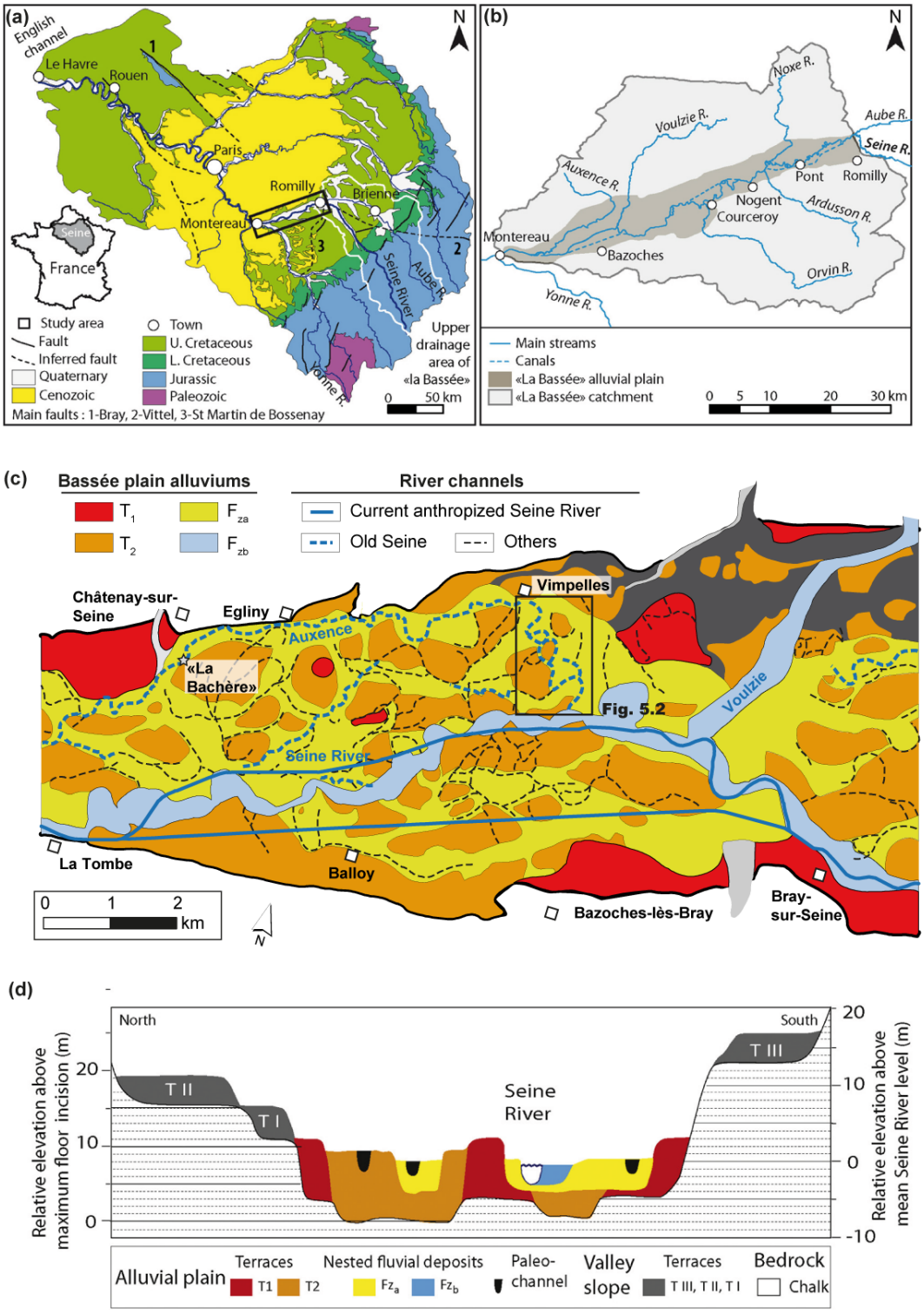

Figure 5.2: The Bassée alluvial plain context. Simplified geological map of the Seine River basin **(a)**. Catchment area of the Bassée alluvial plain and current Seine course **(b)**. Geomorphologic map of the downstream part of the Bassée alluvial plain showing the Old Seine paleo channels reconstruction and the studied channel position **(c)**. Schematic cross-section of the Bassée alluvial plain **(d)**. Deleplancque et al. (2018) and Petit et al. (*in press*), adapted from Mégnien et al. (1965).

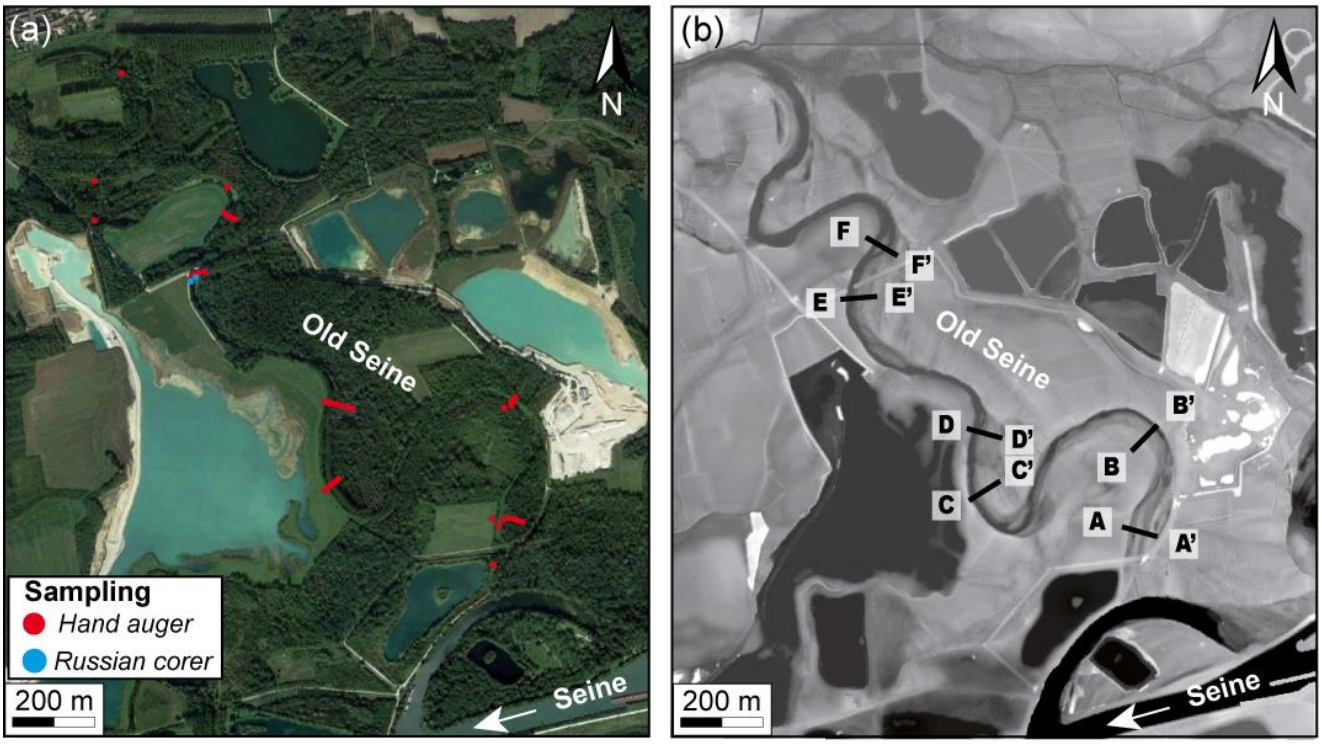

Figure 5.3: Current channel morphology. Aerial picture and boreholes position **(a)**. Lidar DEM and cross-sections positions **(b)**.

The studied channel was part of the "Old Seine" system that was probably formed 6000 ago by a transition from a single thread meandering channel to an anabranch system (Deleplancque, 2016), as was observed in numerous deltas due to a slower eustatic rise and the installation of a cool and dry climate (Törnqvist, 1993; Jerolmack, 2009). The Vimpelles channel was formed by an avulsion with partial reoccupation through old channels incised in the T_2 terrace (Deleplancque, 2016).The channel discharge decreased progressively, and was possibly artificially maintained for a time, until its abandonment during the XIVth century (Songeux, 1888). The channel could be surveyed along 5 meander loops with a total length of 3 km (Fig. 5.3). Paleohydraulic reconstructions made using the bends curvature radiuses and bankfull width determined that the mean discharge was about 55 m^3s^{-1} and that the channel bankfull depth was comprised between 1.8 m in straight segments and 2.7 m at the bends apexes (Deleplancque, 2016). Today, the channel is completely disconnected of the current Seine River active channel, even during floods. However, it is inundated during winter high water table stage.

5.2.2. Methods

The studied channel forms a partly vegetalized topographic depression in the alluvial plain (Fig. 5.3). As the channel is not fully filled, topographic features such as bars are still discernible on the field and on Lidar data (Fig. 5.3b). Field surveys were conducted to ascertain the coarsely-grained channel fill deposits architecture in surface and subsurface. The bar contours were mapped on the field and with the help of Lidar data corrected for the vegetation with a lateral accuracy of 1 m (courtesy of VNF). 38 boreholes were made in the channel at key locations (i.e., at channel apexes, through bars, in riffles and pools) (Fig. 5.3a) in order to determine the channel fill architecture and grain-size. The sampling was made using either hand auger or Russian corer and the sediment texture, grain size and organic matter content was field logged for each borehole at a 5 to 10 cm interval (Appendix D). It was considered that the channel lag was reached when the auger could no longer penetrate the ground, was turning with a grinding sound and could only sample a few gravels.

Six cross-sections were interpreted using boreholes and surface topography data (Fig. 5.3b & 5.4) as well as the depth of the channel lag and the paleohydrological reconstructions of Deleplancque (2016). 4 of the boreholes yielded organic matter fragments suitable for radiocarbon dating, resulting in the determination of 6 absolute ages on 3 cross-sections (Fig. 5.4). The surface data, interpreted cross-sections and isolated boreholes were used to reconstruct the variations of the channel activity through time (Fig. 5.7) and draw an interpreted map of the current coarse channel fill deposits position (Fig. 5.5).

The proportion of coarse-grained fill deposits along the channel length could be determined using the interpreted cross-sections. The cross-sectional area was defined as the area between the channel banks and channel lag deposits and the virtual limit representing the bankfull width, as defined in Chapter 4: the bankfull width was taken as the maximum width between the levees, measured perpendicularly to the channel and the bankfull depth as the height between the top of the channel lag deposits and the levee height. The coarse-grained deposits area was defined as the area inside the cross-sectional area (thus excluding channel lag) occupied by sands or coarser deposits.

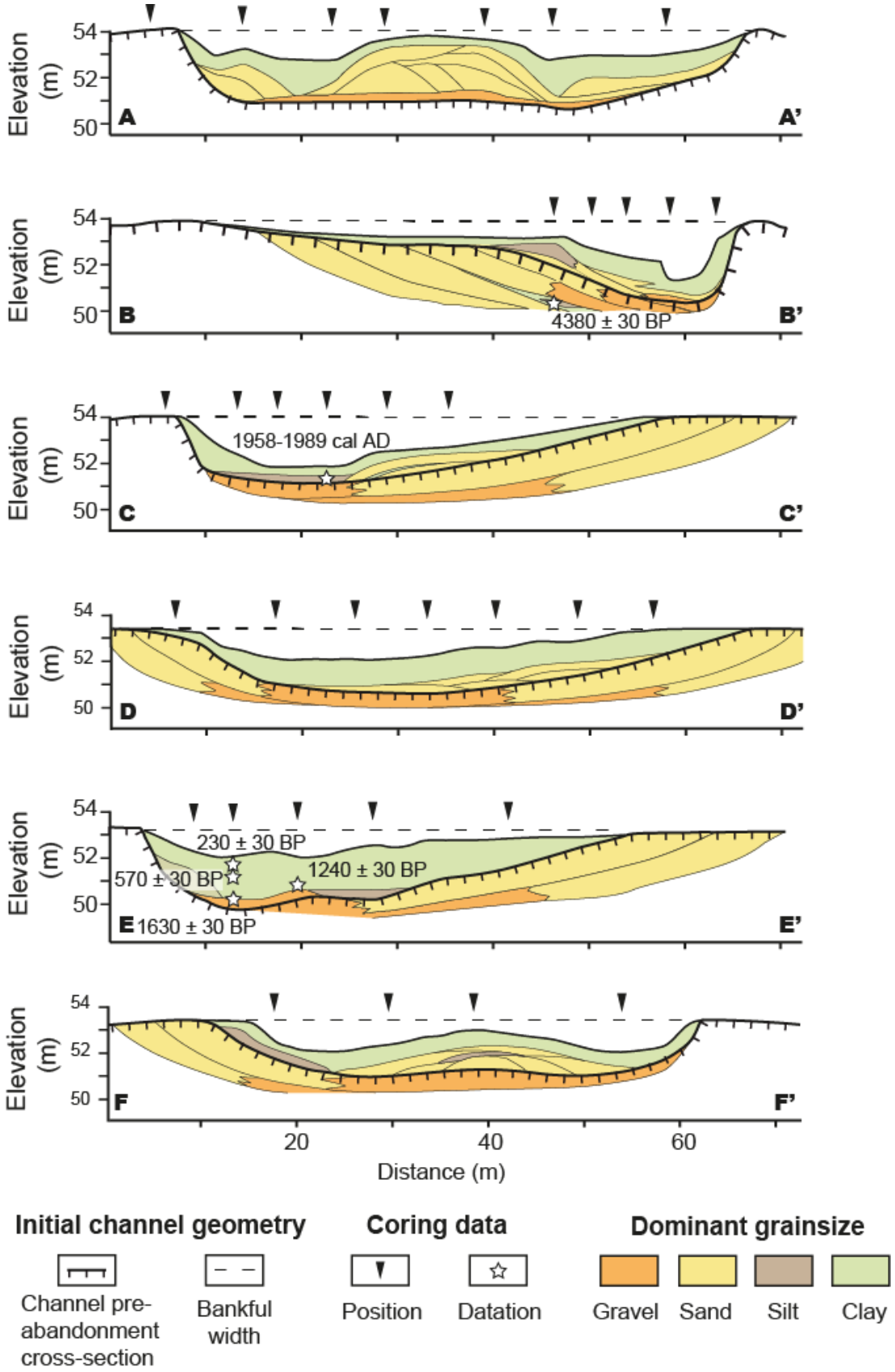

Figure 5.4: Interpreted cross-sections. A, B and E from Petit et al. (*in press*).

5.2.3. Channel fill present architecture

Two types of deposits were found in the channel. First, several amalgamated and composite bars formed at the upstream extremity of the channel (Figs. 5.4a & 5.5). Their thickness decreased downstream and a topographic step was formed between these deposits and the rest of the channel (Fig. 5.6). In light of Chapters 2 through 4 results, these bars were identified as the downstream part of a channel plug. Although human activity affected the upstream part of the channel plug surface topography (road and conveyor belt construction), the borehole just south of the visible channel limit (Fig. 5.3a) showed thick amalgamated coarse sand deposits (Appendix D) identified as channel plug deposits.

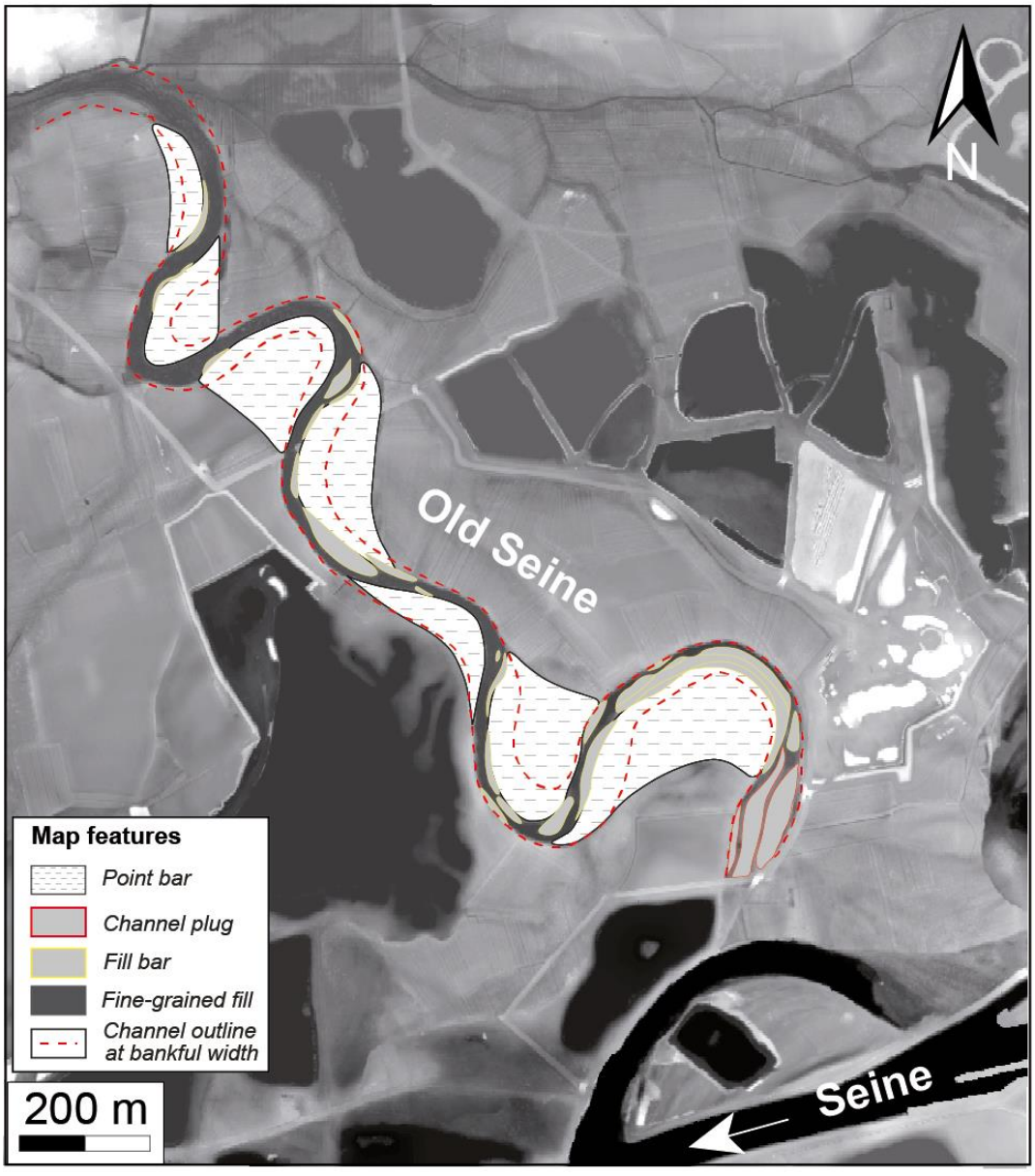

Figure 5.5: Interpreted coarse-grained deposits map.

Second, downstream of the channel plug, the channel had a riffle and pool morphology that was accentuated by the deposition of several extensive coarsely-grained fill bars. Most of these bars were deposited at the inner bank of the channel bends (Fig. 5.5). These position in the channel, their geometry, and elevation relative to the channel banks (Figs. 5.4b-d & 5.5) are reminiscent of the lateral accretion deposits described in the Ain River (Chapter 4) and other mixed load rivers such as the Arkansas River (Sorells & Royall, 2014; Reynolds & Royall, 2019). More bars were sometimes deposited where the channel widens (Fig. 5.5), often close to counter point bars (Smith et al., 2011). These composite mid-channel bars (Fig. 5.4f) were likely deposited due to the flow loss in energy induced by the channel widening (Leopold & Wolman, 1957; Miall, 1996). The coarse-grained fill architecture resulting from this disconnection phase is comparable to the architectural model built in Chapters 2 & 4, with the formation of a channel plug and the occurrence of narrowing and shallowing processes.

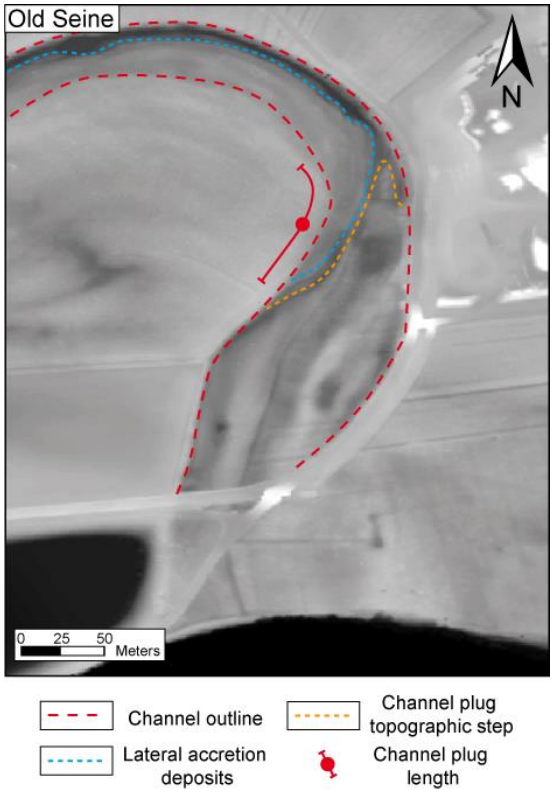

Figure 5.6: Close-up on the Vimpelles channel plug deposits showing its topographic step and the downstream variations in coarse deposits fill volume.

The apparent occurrence and dimensions of the coarse-grained bars decreased with the distance to the bifurcation point (Fig. 5.5). Toonen et al. (2012) observed the same trend in avulsion channels, due to the coarse sediments preferential deposition in the upstream part of the channel. Conversely, the thickness of the fine-grained fill sediments deposited after channel disconnection increased downstream with the distance to the bifurcation point (Toonen et al., 2012) and in the channel pools due to the greater depth of the disconnected channel (Citterio & Piégay, 2009). The fine-grained fill deposits were formed by successive drapes overlaying the channel lag and coarse-grained channel fill deposits. The coarse-grained fill deposits topography was progressively erased by finely-grained sedimentation (Fig. 5.4), and it is thus possible that in the downstream reach of the channel coarse-grained deposits were formed but not observed during the surveys, as the increased thickness of fine-grained deposits downstream hid the bars and fewer boreholes were made in the downstream reach.

5.2.4. Coarse-grained fill deposits long-term preservation

Thus in the Vimpelles channel some of the main notable features of the coarse-grained channel fill, i.e., the channel plug and the downstream narrowing and shallowing bars, were preserved after the channel disconnection. However, some parts of the channel fill are missing and the sedimentary fill recorded reworking events. Indeed, radiocarbon ages and topographic evidences demonstrate that the evolution of the Vimpelles channel fill is more complex than it appears at first glance.

5.2.4.1. Evidences of several phases of activity

The point bar of the first meander bend of the Vimpelles channel (cross-section BB') showed two phases of growth separated by a phase of quiescence (Petit et al., *in press*). The first phase built most of the point bar, while the second phase resulted in roughly 10 m of lateral growth. Thin (~15-20 cm) shreds of silts and clays dated at 4380 (±30) BP were found between these two active phase deposits (Fig. 5.4b). The first active phase probably corresponds to the transition of the Old Seine to an anabranch system as proposed by Deleplancque (2016), while the fine-grained deposits correspond to either the establishment of a counter point bar, a period of lower-energy floods or to a first phase of channel fill following a disconnection that occurred around 4600 years ago (Fig. 5.7). The first hypothesis can be discounted due to the cross-section position at the bend apex. Both the second and third explanation seems reasonable considering the scarcity of available data. Considering the position of the dated sample, the second point bar deposits would have grown roughly a third of the size of the first point bar in at most twice the time of activity. This means that either at

equivalent channel dimensions (and thus probably equivalent hydraulic conditions) the channel migration rate slowed drastically due to less energetic or less frequent floods without disconnection, or that a first disconnection with finely-grained sediment deposition occurred between both phases of point bar growth.

Regardless of the process that resulted in fine-grained sedimentation inside the point bar, the subsequent growth of younger point bar deposits indicates that the energy in the channel increased at some point between 4380 and 1240 (±30) BP (Fig. 5.4),causing the channel to migrate slightly (Fig. 5.7). As it induced channel migration and point bar formation at the same dimensions than the previous phase deposits, this increase in energy was likely a total reactivation of the channel. Thus it is probable that if the channel was partially or totally filled during the quiescence phase a large part of the fill deposits that had formed were then reworked by a high-energy reactivation process (Stouthamer, 2001). The channel was disconnected around 1630-1240 (±30) BP, inducing its infilling. The resulting fill deposits are the ones currently observed in the Vimpelles abandoned channel.

5.2.4.2. Recent moderate-energy reworking events

Thus, in the channel 6000 years long life it is likely that a first channel fill was significantly reworked by a reactivation of the migration dynamic. The current channel fill started its deposition approximately 1500 years ago. Indeed, the radiocarbon ages show that following the system reactivation between 4380 and 1630 (±30) BP with point bar construction (Fig. 5.4b), a second decrease in energy between 1630 and 1240 (±30) BP occurred. During this time interval coarse- to medium-grained sedimentation took place (Fig. 5.4e). This sedimentation was likely indicative of a slow avulsion process that led to channel disconnection, after which a long period of fine-grained sedimentation occurred (Fig. 5.7). Radiocarbon ages in the downstream cross-section EE' (Fig. 5.4e) indeed show a sedimentation rate of approximately 0.87 mm/year since 1240 (±30) BP. However, despite evidences of continuous sedimentation in the downstream parts of the channel, and the fact that the current channel fill exhibits extensive bedload architectures comparable to what is expected following the model developed in Chapters 2 through 4, parts of the fill have been reworked since their deposition.

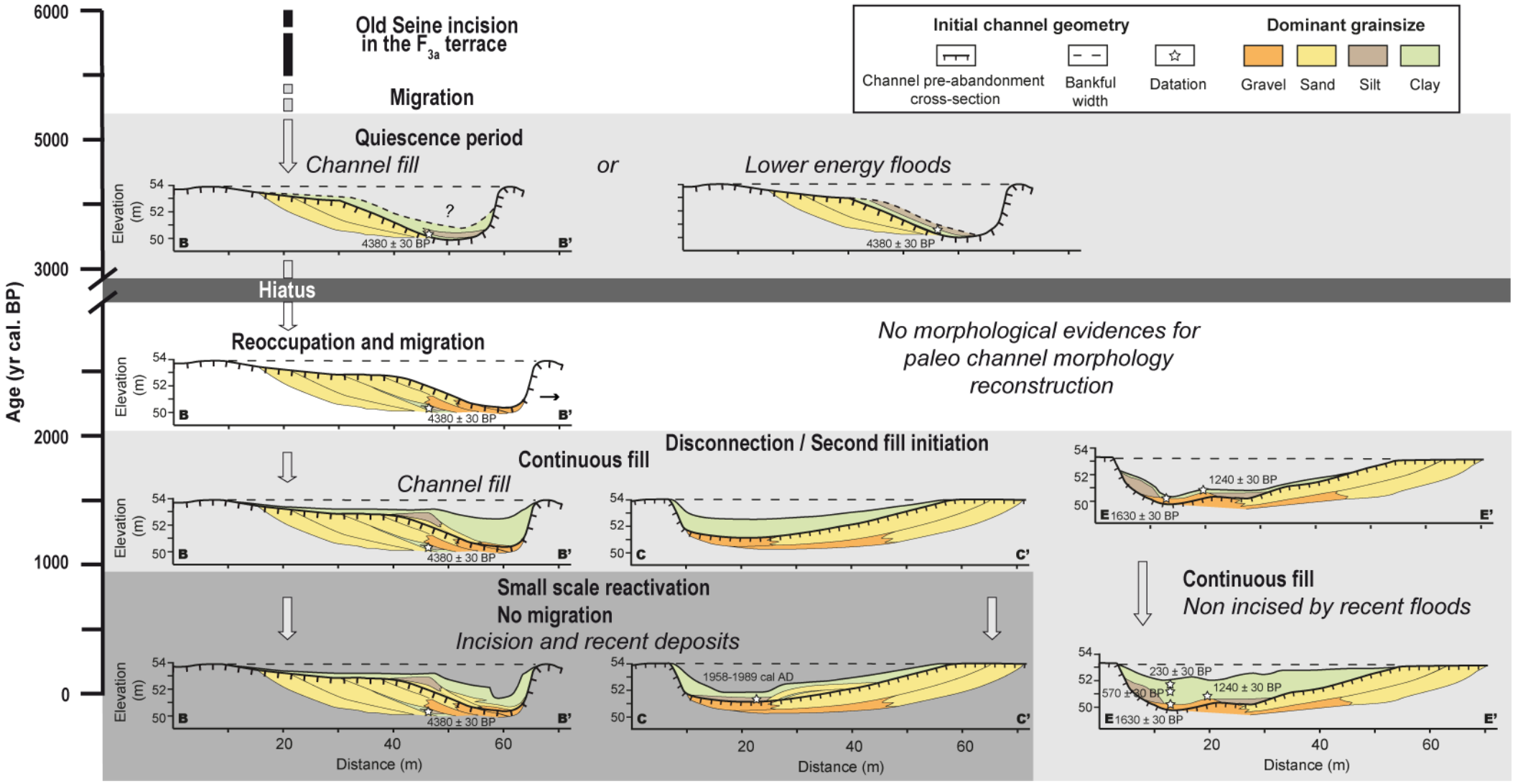

Figure 5.7: Reconstruction of the temporal and morphologic evolution of the Vimpelles channel.

Although subsurface deposits attributed to the channel plug were found in the reworked area south of the channel, the channel bifurcation point position is unknown and the upstream portion of the channel plug missing. Both human interventions, numerous in the area (Fig. 5.2b-c), and the Seine River migrations are responsible for this. Active channel migration is known to sometimes heavily rework the bifurcation area (Stouthamer, 2001), potentially eroding the upstream portion of the channel plug. This can happen at any time after the disconnection, depending on the active channel migration rate. If a sufficient portion of the channel plug is eroded, it can lead to channel reactivation. This process is a potential explanation for the Vimpelles channel reactivation after its quiescence phase (Fig. 5.7). In case of partial reactivation of the channel, punctual or in the long-term, some coarse-grained deposits can be eroded from the channel plug and deposited further downstream in the channel, forming new coarse-grained bars.

The current channel fill shows a small transversal topographic step in the channel at cross-sections BB', CC', and potentially DD' (Fig. 5.4). Furthermore these cross-sections showed finer-grained, low elevation, sand and silt lateral accretion deposits indicative of lower-energy channel activity. This could be caused by either a progressive decrease in discharge during the disconnection, or by an ulterior lower-energy reactivation of the channel. The radiocarbon ages found in the fine-grained channel fill at cross-section EE' indicate that the fill was initiated 1200 years ago and that the sedimentary fill rate was more or less constant. However, the radiocarbon age measured in cross-section CC' at 1958-1989 cal AD (Fig. 5.4c) validates the second hypothesis. Indeed the organic matter used for the datation was sampled in the silt layers deposited at the base of the channel fill, just above the channel lag. It indicates not only that at least one recent deposition event took place in the upstream part of the channel, but also due to its position that the previous fill was eroded.

Thus topographic, architectural and radiocarbon evidences point towards two episodes of channel fill following the channel second phase of migration (Fig. 5.7). The high lateral accretion deposits (Fig. 5.4b) and the progressive fine-grained channel fill (Fig. 5.4e) indicate that the channel was disconnected 1200 years ago and that it started filling normally. Topographic evidences of incision (Fig. 5.4 b-c) with the formation of low elevation lateral accretion deposits (Fig. 5.4 b-d) and recent channel fill deposits close to the channel lag (Fig. 5.4c) demonstrate that the upstream part of the channel was reactivated at some point with at least one recent (30-60 years old) deposition event. The downstream part of the channel was unaffected by the incision (Fig. 5.4e-f), indicating that the channel reactivation had a limited

scale and was likely caused by moderate energy floods. Considering this relative low energy and the fact that the low-elevation lateral accretion deposits were formed by silts and fine- to medium sands the recent fill deposits were probably provided by suspended sediments and not by a reworking of the coarse-grained channel plug.

These findings demonstrate that the coarse-grained deposits architecture as determined in the model developed in the previous chapters is resilient to moderate energy reactivation events. The evidences in the Vimpelles channel show that the partial reactivations can also probably be held responsible for further coarse-grained sediments deposition. However, high-energy events such as active channel migration in the bifurcation zone significantly rework the fill deposits, whereas total channel reoccupation almost resets the system.

5.3. Coarse-grained fill deposits preservation in several systems

Architectural and temporal data in the Vimpelles channel showed that a significant part the coarse-grained fill deposits were preserved on a ~ 1500 year-long period. The study of the coarsely-grained channel fill topography is generally difficult due to the following fine-grained sedimentation. Thus this section focuses on channel-scale depositional patterns and uses cross-sections made in abandoned channels described in the literature to attempt to determine whether the coarse-grained fill architecture described earlier is common in natural systems, and then compare this large-scale architecture in different abandoned channels.

5.3.1. Studied abandoned channels

The interpreted cross-sections of 5 channels studied in 4 different systems were used to compare the channel-scale deposition patterns of coarse-grained sediments. The Vimpelles mixed load channel, disconnected around 780 AD and the Mollon and Martinaz 1 channels of the bedload dominated Ain River (France), disconnected in 2002-2003 AD, were described and measured in Section 5.2 and Chapter 4, respectively. Similar data acquisition was performed in the Boire Torse channel (Loire River, France) and the Rijnstrangen channel (Rhine River, Netherlands) in order to compare the coarse-grained fill proportion along the channel length. These two channels, and the context surrounding them, are described in the following.

5.3.1.1. The Boire Torse channel

The Loire River is a gravel-bed braided system that occupies, in the study area (roughly 7 km upstream of Nantes) a 1 to 2.5 km wide alluvial plain delimited by Würmian terraces (Miéjac & Athuis, 2007). The Loire channel occupies alternatively the left or right edge of the alluvial plain, with large islands delimited by the channel braids (Fig. 5.8) and in the study area the substratum is composed of normal graded gravels fining upwards to sands and clays (Arthuis et al., 2005). The Boire Torse is a narrow, 15 km long channel that used to follow the right bank of the Loire River (France), diverging from it near Ingrandes and flowing back into the Loire at Ancenis (Fig. 5.8).

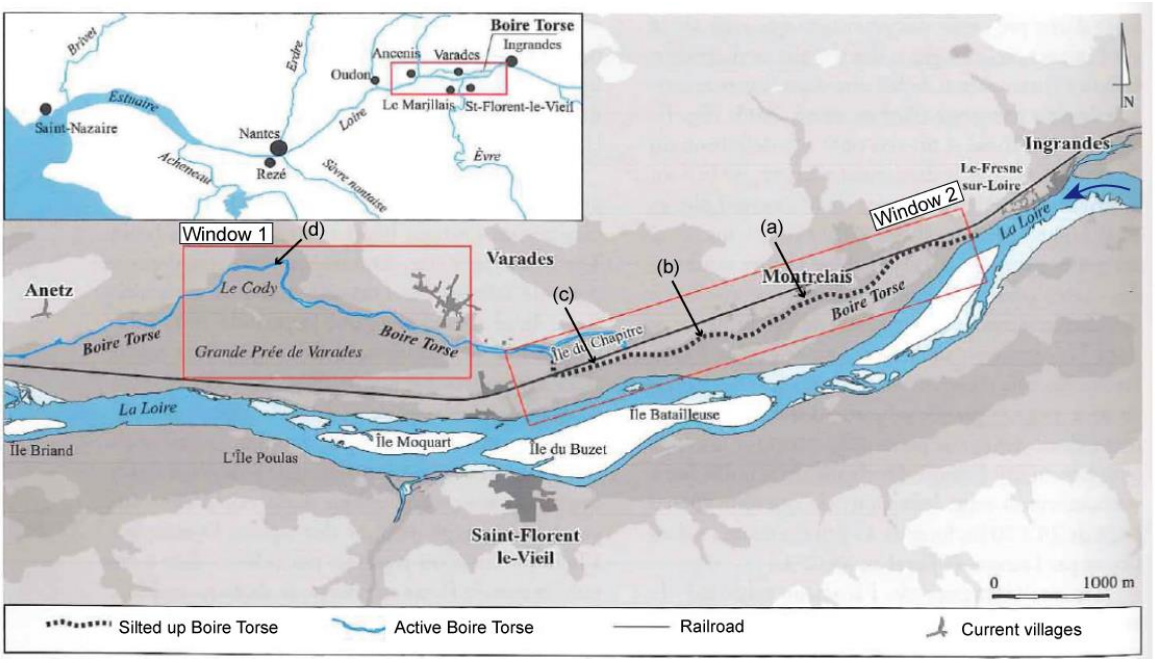

Figure 5.8: The Boire Torse channel localisation and the cross-sections position, after Arthuis et al. (2015) and Miéjac & Arthuis (2007).

Geomorphic analysis and palynologic and radiocarbon dating show that the now filled upstream part of the Boire Torse channel was artificially formed (Fenêtre 2, Fig. 5.8) while the downstream part naturally occupies an abandoned arm of the Loire River (Fenêtre 1, Fig. 5.8) (Arthuis et al., 2015). The upstream channel was dug between the XIIth and the XIIIth centuries, likely to facilitate navigation between the inland villages and the Loire, thus avoiding the swamps (Arthuis et al., 2015). The upstream reach of the Boire Torse was apparently fully disconnected in 1849 due to the construction of a railroad dike that prevented both floods and sediments to enter the upstream artificial channel. This upstream part of the channel is totally silted up (Fig. 5.9a), save from a second sanitation channel that was dug in

1858 to prevent the spread of diseases due to water stagnation after the disconnection (Arthuis et al., 2015). The natural downstream part of the channel still hosts water and flows into the Loire at Ancenis (Fig. 5.8). The channel has a gravely to sandy bed and is filled by coarse- to medium-grained sands with some silty to clayey bioturbated layers (Arthuis et al., 2015), indicating a filling by successive flooding events with a consequent time interval between floods. Thus aggradation occurred in the abandoned channel, while a further entrenchment of the Loire River following human intervention and dredging, resulting in the total disconnection of the upstream reach of the channel.

More than 200 trenches were dug in and along the channel banks to study its abandonment during the archaeological works of Miéjac & Arthuis (2007). Four synthetic cross-sections were interpreted (Fig. 5.9) along the Boire Torse channel (Fig. 5.8). These for cross-sections were used to estimate the sand fraction of the channel fill along the channel length.

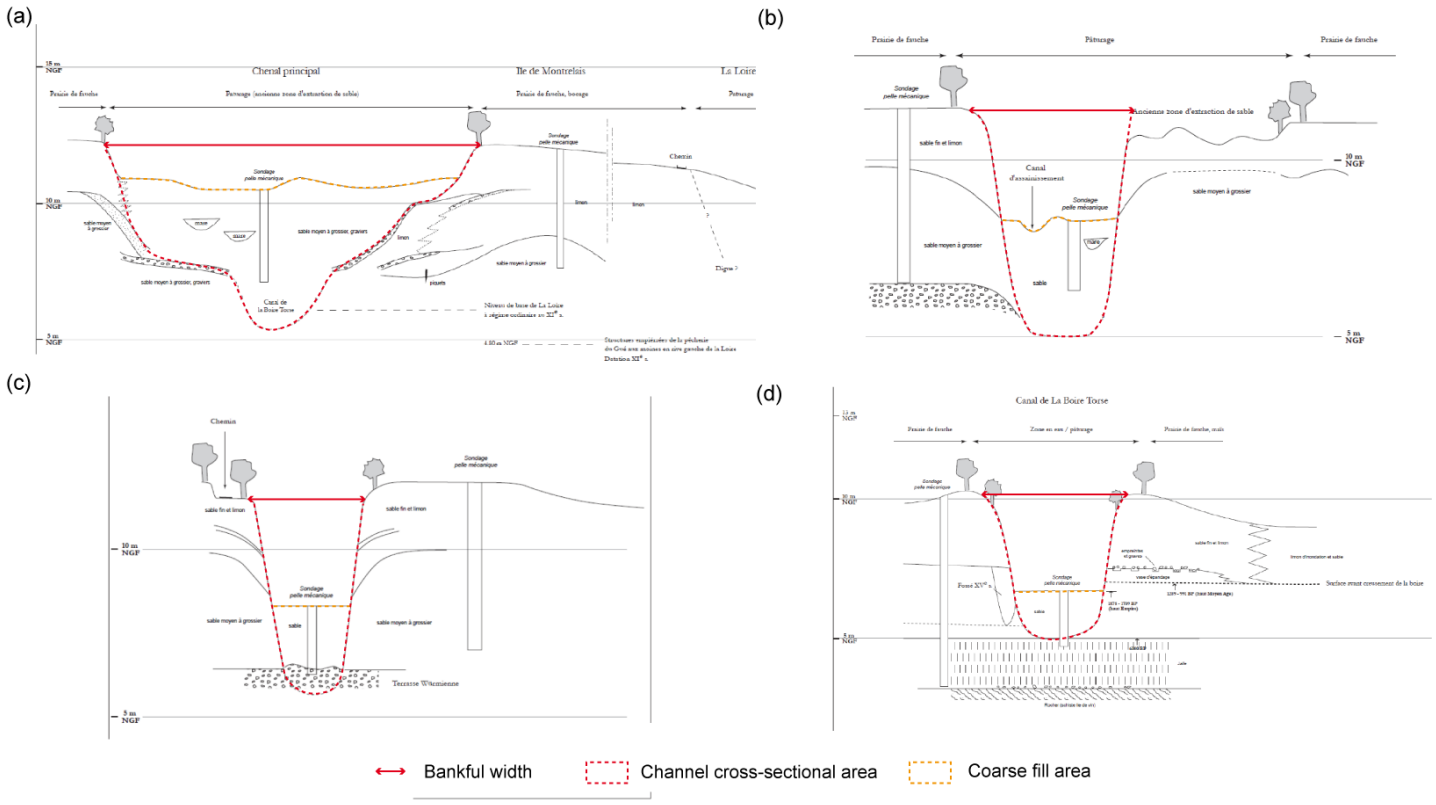

Figure 5.9: Channel cross-sections in the Boire Torse and measurement method. Cross-sections from Miéjac & Arthuis (2007).

5.3.1.2. The Rijnstrangen channel

The Rijnstrangen channel was part of the Rhine mixed load system (Netherlands), and was abandoned by an avulsion resulting in its disconnection in 1707 AD (Toonen et al., 2012). The channel is located at the apex of the Rhine delta, where the delta plain borders Saalian ridges. It forms the right part of the ”Nederrijn” bifurcation of the Rhine River (Fig. 5.10), located near to the border between Germany and the Netherlands along the Rhine River, and was abandoned after a ~2000 years long avulsion that started ~2500 years ago (Paas & Teunisseen, 1975). In the last 3000 years numerous avulsions occurred due to prehistoric deforestation and the subsequent aggradation (Erkens & Cohen, 2009; Stouthamer et al., 2011). The Rijnstrangen channel is currently completely disconnected from the Rhine in its upstream part, except for groundwater exchange, and is used to carry local drainage downstream (Toonen et al., 2012).

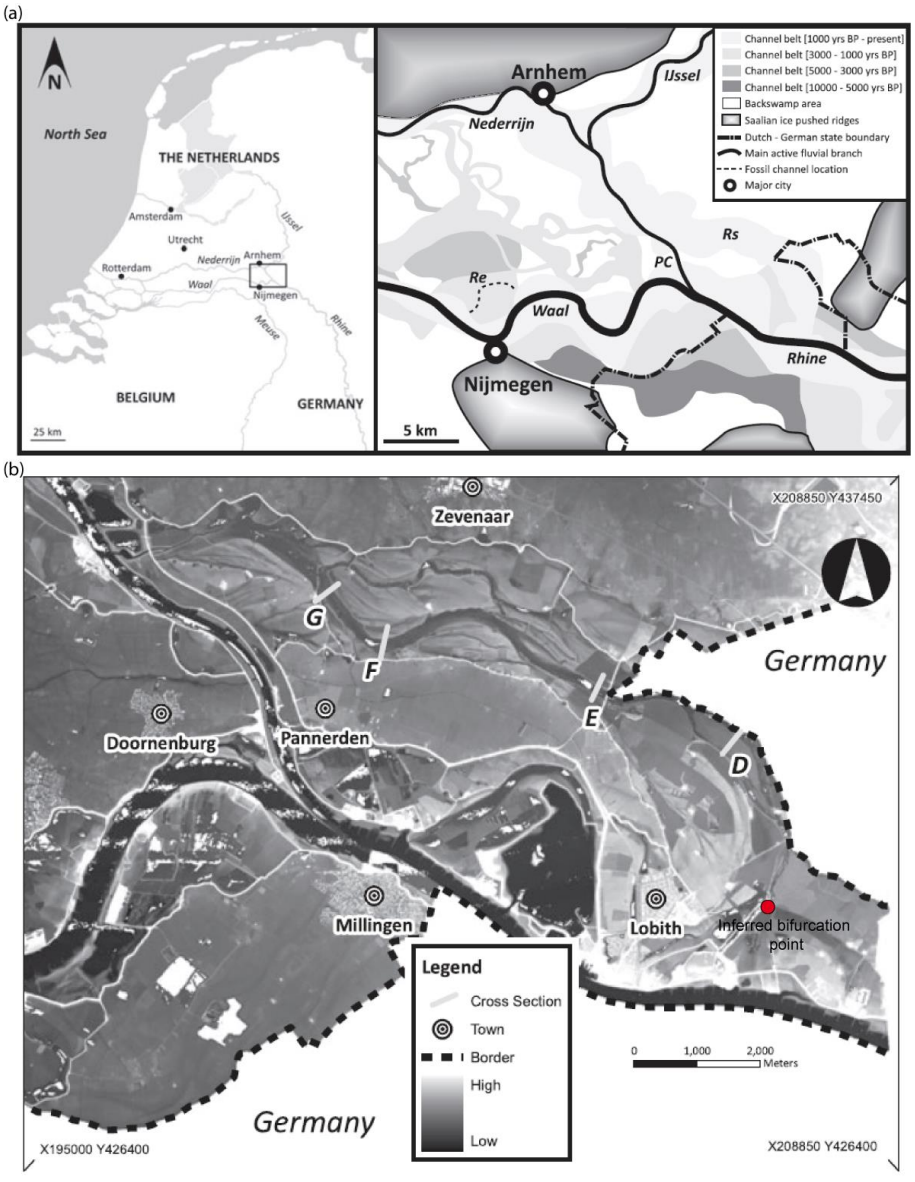

Figure 5.10: Location and geology of the studied area showing the Rijnstrangen disconnected channel **(a)** and laser altimetry view of the Rijnstrangen channel with the cross-sections positions **(b)**. From Toonen et al. (2012).

Toonen et al. (2012) realized 4 cross-sections in the Rijnstrangen channel, two of them located in straight sections of the channel and the other two in more curved segments (Fig. 5.10). The cross-sections were interpreted using laser altimetry for the channel topography, borehole and core descriptions (Berendsen et al., 2007) and 25 additional hand-cored boreholes (Fig. 5.11). The boreholes were logged in 10 cm intervals describing sediment texture, organic matter content, colour, plant remains, carbonate content, interbedding, and flood layers thickness and frequency. The boreholes had a depth of 4 to 5 meters. The cross-sections were realized every few kilometres, and thus allow the estimation of the fill deposits geometry along most of the abandoned channel length (Fig. 5.10).

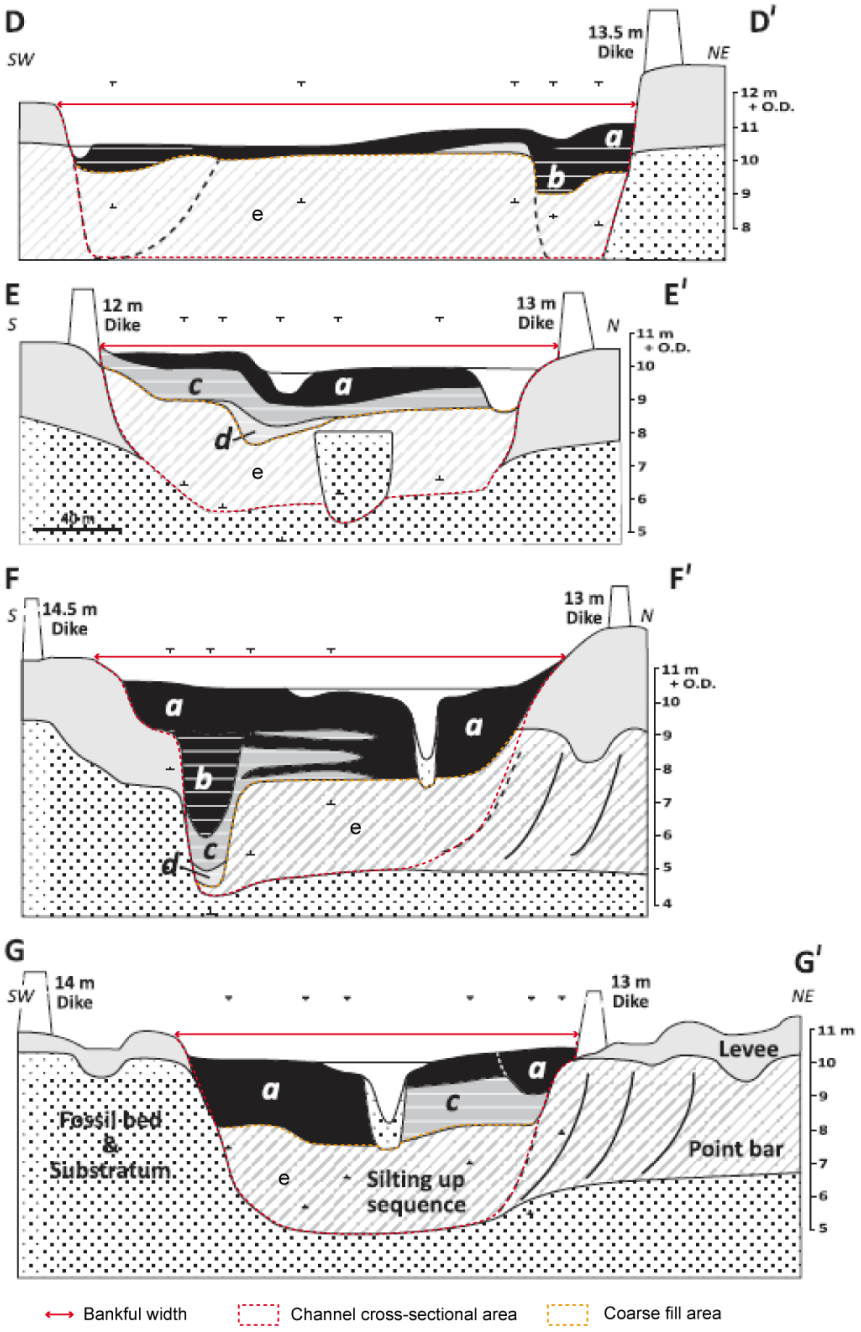

Figure 5.11: Interpreted cross-sections of the channel fill geometry in the Rijnstrangen channel. a: Bioturbated non-laminated clays. b: Calcareous, humic finely laminated (<1 cm) clayey silts showing flood pulses. c: Calcareous, humic laminated (1-3 cm) silts showing flood pulses. d: Calcareous, coarsely laminated (>3 cm) silty sands showing flood pulses and plant debris. e: Gravels and sands. From Toonen et al. (2012).

The channel fill consists in finer-grained deposits than the gravely channel lag, although the transition between the two is gradual, from the channel lag gravels to fining-upwards sands that were interpreted as shallowing deposits, and whose thickness decreases downstream. The overlying finer-grained (silts, clays and peat) fill increases in thickness downstream, and its base is laminated (Fig. 5.11) (Toonen et al., 2012).

5.3.2. Results and discussion

In order to enable comparison between different channels, the distance between the inferred bifurcation point and the cross-section was rendered dimensionless by dividing it by the channel width at the bifurcation or, when the bifurcation is lost, at the closest point to the bifurcation in the channel where the width is measurable (Fig. 5.12). Uncertainties on the bifurcation point exact position exist for the Vimpelles and Rijnstrangen channels, whereas the other channels bifurcation points were either found on maps or observed on aerial pictures.

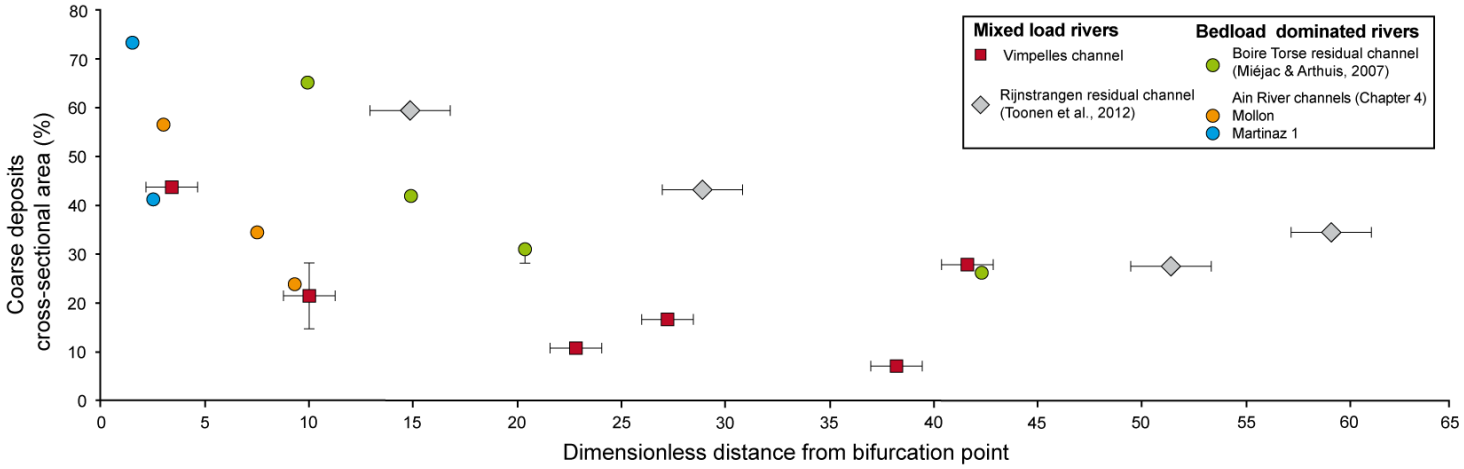

Figure 5.12: Percentage of coarse-grained fill deposits in cross-sections in function of the distance to the channel bifurcation point for 5 different river channels.

In all systems the percentage of coarse-grained channel fill in the cross-sections was high (45-70 %) close to the bifurcation point and decreased gradually when the distance increases. In the downstream part of the channel, the coarse-grained fill quantity appears to reach a plateau downstream, around 25 % in bedload dominated systems (all Martinaz 1 measurements were made on the plug), whereas in mixed load systems the coarse-grained fill percentage fluctuates between 5 and 35 %.

This shared deposition pattern was interpreted as the amalgamated body of the channel plug thinning downstream and, in mixed load systems, higher presence of lateral accretion deposits

or mid-channel bars. Indeed, the local increases in coarse-grained fill downstream of the channel plug in mixed load systems were linked to the channel morphology, i.e., the presence of bends or channel widening (Figs. 5.3b & 5.5; Toonen et al., 2012). In mixed load system the bedload fraction of the sedimentary charge is likewise deposited in the upstream reach of the channel but the suspended load fraction can be transported further downstream, and deposited when the flow locally slows due to channel morphology. Conversely, the strict decrease in coarse-grained fill deposits along the channel length in bedload dominated systems can be attributed to the inability of the flow to transport bedload once it enters the disconnecting channel due to the loss in energy. However, it is also possible that there is a bias in the sampling and that the cross-sections realized in bedload dominated system did not intersect coarse-grained fill sediments and that coarse-grained fill proportion was underestimated.

Thus the channel plug, or at least parts of it, appears to be always preserved in the abandoned channels. This demonstrates both the resilience of the architectural model, as its most notable feature is preserved in the long-term, and a preservation bias. Indeed, in case of reactivation the energy in the channel is likely sufficient to rework the fill deposits. However, if the channel is only partially reoccupied, the energy lower energy does not allow the reworking of the coarse-grained deposits. It is thus unlikely that an abandoned channel fill is preserved without the associated channel plug. Whether the remnant of the plug can be found after hydraulic works or, in the fossil record, exhumation and possible erosion, is another matter.

Despite the possible sampling bias, comparison of the Vimpelles data with other abandoned channels showed that when a channel fill was preserved the coarse-grained fraction of the channel fill likely retains a channel plug morphology through time. Thus, when a channel fill is preserved, the architectural model for coarse-grained channel fill remains valid in its broad lines even centuries after the initial disconnection.

5.4. Cutoff channel plug length prediction using aerial pictures

In this section the relationships between channel plug length and the channels length ratio determined in Chapter 3 are tested. Due to the amount of data that has become available these last decades, many fluvial geomorphic studies were conducted using aerial or Landsat imagery, especially in areas difficult to reach such as the Amazonian region (e.g., Gautier et al., 2007; Schwenk & Foufoula-Georgiou, 2016). This section aims to determine in which cases, if any, can aerial imagery be used at the channel scale instead of field surveys to determine the coarse-grained fill deposits extent. To do so, the aerial pictures of abandoned channels in the Ain and Allier rivers used in Chapter 4 (Appendixes B & C) are used conjointly to maps of the Lower Mississippi Valley (LMV) drawn using aerial pictures (Krinitzsky et al., 1965; Saucier, 1994) and compared to Chapter 3 experimental relationship.

5.4.1. Study area

The Lower Mississippi Valley (USA) is the part of the Mississippi River system that lies between the confluence of the Mississippi and Ohio rivers, in the town of Cairo, and the Gulf of Mexico, which represent a distance of around 965 km (Saucier, 1994) (Fig. 5.13). The valley width varies between 50 and 145 km and a deltaic plain that formed at the coastline extends roughly 240 km both in the north-south and east-west directions. The Lower Mississippi valley slope is in average 0.0111 % (Saucier 1994). Numerous alluvial terraces can be found in the valley, the older being pre-Pleistocene in age and unrelated to the Mississippi River (Autin et al. 1991). In the Lower Mississippi Valley, the mixed load Mississippi River is unconfined and prone to migration and thus channels abandonment. Most of these channels, and their filling, were mapped and dated relatively by Fisk (1944), and mapped again by the Mississippi River Commission (Krinitzsky et al., 1965; Saucier, 1967, 1969; Fleetwood, 1969; Smith & Russ, 1974) and the data compiled by Saucier (1994).

5.4.2. Channel selection and measurement method

5.4.2.1. Data source

A combination of the work of Fisk (1944), which provides dates for the channel fills, and the maps from Saucier's (1994) synthesis, were used to gather the data. Saucier's synthesis was supplemented with some of the more detailed maps, made at a smaller scale, focusing on the Yazoo (Krinitzsky et al., 1965) and Boeuf-Tensas (Saucier, 1967) basins (Fig. 5.13), as they were the only basins in which channel plug morphologies were mapped. The Yazoo Basin maps were drawn in 1965 using data gathered between 1958 and 1965 via aerial photography,

field surveys and boreholes data study. The Boeuf-Tensas detailed maps were drawn in 1967 using aerial pictures of the area taken during campaign spanning 1933-1935 to 1962-1965 and data from boreholes.

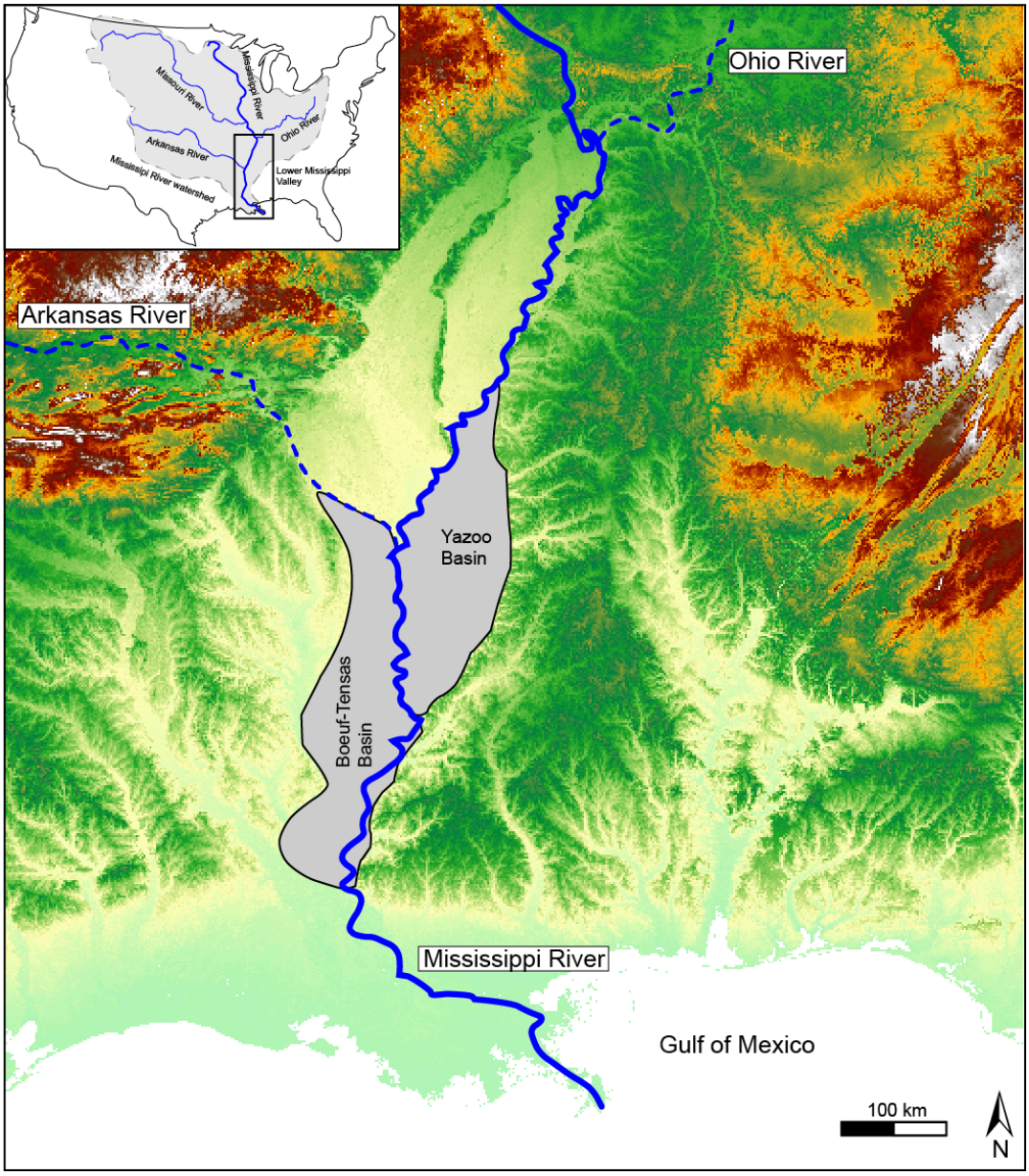

Figure 5.13: Lower Mississippi Valley position along the Mississippi River reach and situation of the Yazoo and Boeuf-Tensas basins in the Lower Mississippi Valley.

5.4.2.2. Channel selection

Although several hundreds of abandoned channels – and in some cases, their migration – were mapped in the aforementioned works, most of them were fully filled by sediments at the time of the surveys. Data acquisition includes some channels abandoned by the Arkansas River in the Boeuf-Tensas Basin (Fig. 5.13). Furthermore, in order to be compared with the studies conducted in the previous chapters, the selected channels needed to correspond to several criterions (Fig. 5.14):

- A plug discernible from the lateral accretion deposits (Fig. 5.14a-b).
- Measurable bifurcation and confluence angles (Fig. 5.14a-b).
- Simple geometry, i.e., no channel reoccupation or amalgamation (Fig. 5.14c).

Hence most selected channels were close – or sometimes still connected at one extremity – to the active channel. Channels connected to other abandoned channels were discarded, as it was impossible to determine whether the river migration eroded the channel fill or not (Fig. 5.14a). Similarly, although some apparently non-eroded oxbow lakes still exist several kilometres away from the active channel, it was impossible to estimate their bifurcation and confluence angles, and as such they were discarded. Finally, channels that were at the fringe of two maps which showed discrepancies in scale or interpretation, incompletely mapped channels or channels that showed signs of multiple stages of abandonment and reoccupation were discarded (Fig. 5.14c-d).

Twenty-six channels met the requirements, 12 of which were abandoned by chute cutoff processes while the other 14 were abandoned by neck cutoff processes. Three of the channels abandoned by chute cutoff displayed only an upstream channel plug while all 23 other channels had both upstream and downstream channel plugs.

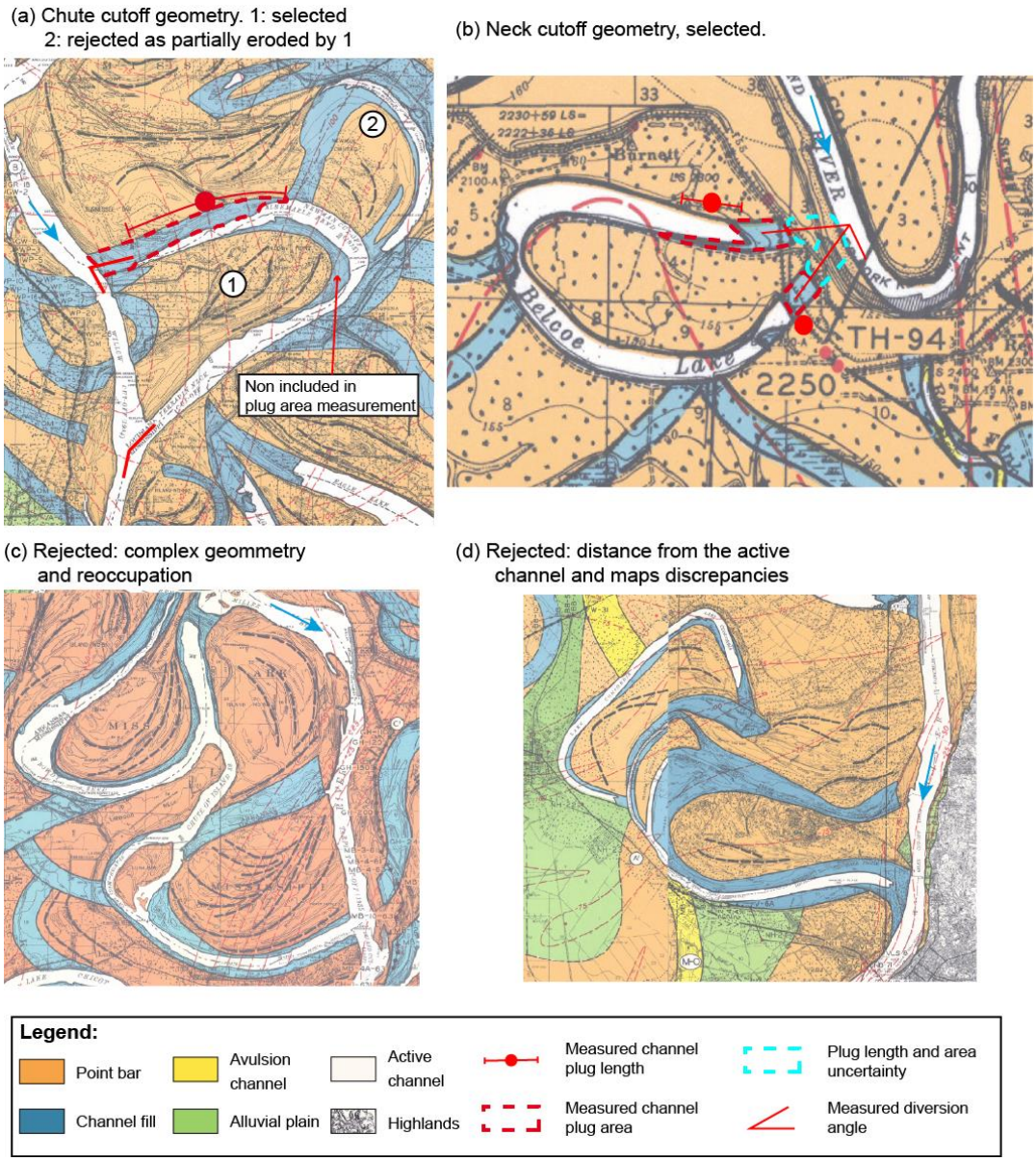

Fig. 5.14: Examples of the typical geometries mapped in the Lower Mississippi Valley and illustrations of the criterions used for channel selection. Maps from Krinitzsky et al., 1965 Saucier, 1967.

5.4.2.3. Measurement method and uncertainties

Data on channel plug length and area was collected from the historical maps of the Lower Mississippi Valley projected in ArcMap 10.6 on a Digital Terrain Model (DTM) obtained from the Shuttle Radar Topography Mission 1 (SRTM1) missions (horizontal resolution = 31 m at equator, Farr et al. 2007). This allowed making direct measurements of the geomorphic features displayed on the maps while making sure that the maps were at the right scale in order to get accurate measurements, by using lasting topographic features (i.e., cliff edges, hills…) as landmarks.

Middle Mississippi Valley	Sources :	US Army Corps of Engineers	Saucier 1994	Fisk 1947														
Channel	Saucier 1	Saucier 2	Saucier 3	Saucier 4	Saucier 5	Saucier 6	Saucier 7	Saucier 8	Saucier 9	BT1	BT2	BT3	BT4	BT5	BT6	BT7	BT8	BT9
Geometry	Neck	Neck	Neck	Neck	Neck	Neck	Neck	Chute	Chute	Chute	Chute	Chute	Neck	Neck	Neck	Chute	Chute	Neck
Disconnection age	> 1765	1820-1880	1765-1820	1880-1944	> 1765	1880-1944	1880-1944	1880-1944	1880-1944	<1944	> 1765	<1944	> 1765	1820-1944	1820-1880	> 1765	1820-1944	1820-1880
Upstream plug																		
Diversion angle (°)	61	58	128	112	117	78	77	40	42	64	94	105	148	98	65	60	84	120
Dimensionless sand plug length	9.13	7.43	10.05	2.38	11.46	4.35	9.83	4.55	4.7	5.97	3.53	4.7	1.66	6.2	0.74	3.86	2.44	4.07
Dimensionless sand plug area (%)	20.9	30.7	58.6	17.9	26.9	11.3	46.6	40.5	21.8	40.8	22.5	42.7	3.3	41.6	11	22.5	16.6	11.5
Downstream plug																		
Confluence angle (°)	63	104	34	71	50	81	128	30	46	46	78	59	71	79	33	35	111	105
Dimensionless sand plug length	14.63	1.57	0.94	2.65	2.15	1.23	3.35	2.41	0	0.54	1.59	3.55	6.6	1.9	4.1	0	0	5.2
Dimensionless sand plug area (%)	29	8.2	10.3	14.7	12.9	2.4	10.9	13.9	0	3.4	5.6	24.5	17.9	11.1	31.5	0	0	18.1
Length ratio L_1/L_2	0.13	0.1	0.12	0.14	0.07	0.07	0.12	0.34	1.4	0.27	0.43	0.26	0.05	0.23	0.13	0.33	0.31	0.04
Estimated length ratio error (%)	10	10	14	16	6	7	11	8	0	7	0	0	20	13	14	0	0	11

Channel	ARK1	ARK2	ARK3	ARK4	ARK5	ARK6	ARK7	ARK8
Geometry	Neck	Chute	Chute	Neck	Chute	Chute	Neck	Neck
Disconnection age	-	-	-	-	-	-	-	-
Upstream plug								
Diversion angle (°)	112	105	86	117	130	106	120	141
Dimensionless sand plug length	1.77	5.77	9.15	8.14	4.04	5.99	2.58	10.44
Dimensionless sand plug area (%)	7.5	40.6	27.6	42.4	22.8	35.2	38.3	35.5
Downstream plug								
Confluence angle (°)	84	143	103	88	99	131	102	113
Dimensionless sand plug length	1.4	2.89	5.66	2.83	1.64	3.15	2.77	5.15
Dimensionless sand plug area (%)	4.8	23.2	8.4	16.1	8.7	13.6	30.8	27.9
Length ratio L_1/L_2	0.04	0.79	0.06	0.13	0.24	0.56	0.14	0.13
Estimated length ratio error (%)	21	20	2	25	12.5	5	20	8

Table 5.1: Mississippi and Arkansas River channel plugs measurements.

The lengths of the channel plugs were measured following the same method as in the previous chapters, i.e., the mean of the length where they occupy the whole channel width and of their maximum length. The bifurcation and confluence angles were measured as the value by which the flow was diverted from its initial direction (Fig. 5.14), and the length ratio L_1/L_2 used to estimate the water-surface slope ratio between the channels. The channel plugs measurements (length and area) as well as the angles and length ratios are given in Table 5.1., and were rendered dimensionless by dividing the channel plug length by the channel width at the bifurcation, and its area by the total channel area.

Other than the 60 m error estimated by Saucier (1967) in the maps realisation, the largest error in the plugs measurements stems from the fill deposits covering or erosion by the active channel migration. While in some cases of recent disconnection the abandoned channel was still connected to the active channel and the measurements can be assumed to be accurate (Fig. 5.14a), in some cases the bifurcation point position must be inferred and its position taken into account in the length ratio measurement (Fig. 5.14b). Thus in many cases the measured plug length is a minimal length and the length ratio measured is the maximal one, with a 0 to 20 % lower uncertainty (Table 5.1).

5.4.3. Results and discussion

The data extracted from aerial pictures of the Ain and Allier rivers abandoned channels (and confirmed on the field for 4 of the Ain channels in Chapter 4), and from maps of the Lower Mississippi Valley are plotted in Figure 5.15 together with the experimental relationship tying channel plug length and channels length ratio determined in Chapter 3 (Eq. 3.2). This relationship was chosen over the water-surface slope ratio as the field and maps data did not allow water-surface slope measurement. Currently, the so called relationship is delicate to use as it is because of the limited amount of data available. One should keep in mind that further experimental investigations are necessary to define properly this relationship.

As described in Chapter 4, the channel plugs measured in the bedload dominated Ain and Allier rivers had a roughly constant length, around 5 to 7 times the channel width. The difference between their measured length and the one predicted by the experimental relationships was at most the double of the predicted length. The field measurements of the Ain and Allier rivers and the experimental relationship intersect at length ratios ≥ 0.6 (Fig. 5.15). The Lower Mississippi Valley channel plugs were separated into two groups with a different behavior. The first group corresponded to the channel plugs formed in chute cutoff

channels (*sens*u Fisk (1947), i.e., not formed by a neck cutoff). Their length ratios were comprised in the most cases between 0.25 and 0.8 and most of these channel plug lengths for the experimental relationship (Fig. 5.15). The second group was composed of the channels formed by neck cutoff events. Their length ratios were inferior to 0.25, and their length could be 12 times superior to the length predicted by the channel plug. It is worth noting that the experimental relationship rarely overestimated the measured channel plug length, and then only slightly, excepted in the one case of a cutoff failure and subsequent fill (Fig. 5.11).

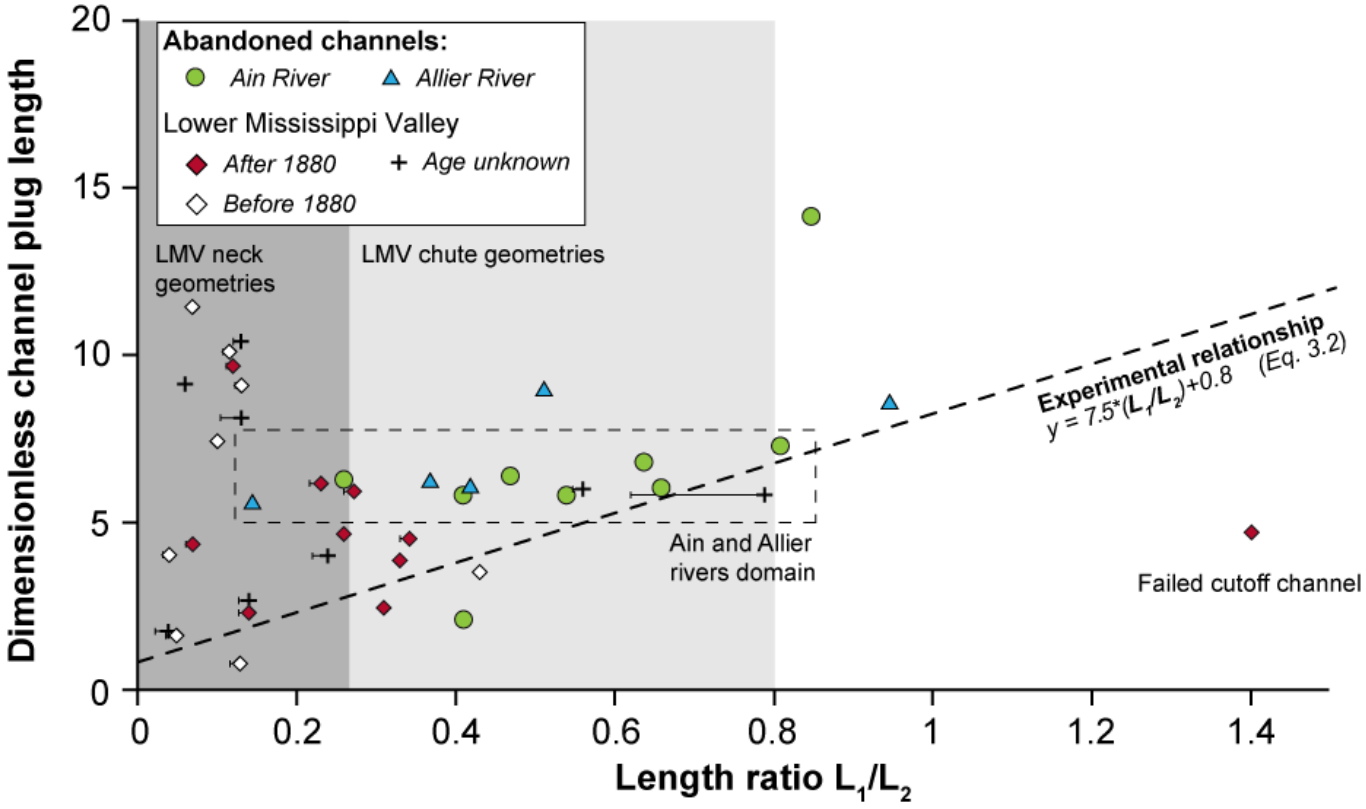

Figure 5.15: Ain and Allier rivers and Lower Mississippi Valley (LMV) apparent channel plug length function of the channel length ratio.

As the Ain and Allier rivers are bedload dominated and the channel plugs were measured a few months to a few years after their disconnection, it can be considered that in these cases the actual channel plugs, as defined in Chapters 2 & 3 (i.e., the coarse-grained deposits formed during the disconnection phase whose growth started in the flow separation zone) were measured. Their apparent fixed length was attributed in Chapter 4 to downstream hydraulic effects, and the comparatively short or long length of the two that do have this fixed length were attributed to the channel geometry and disconnection duration.

On the other hand, considering that the Lower Mississippi Valley channels were disconnected decades to centuries ago (Table 5.1), and that the Mississippi and Arkansas rivers are mixed load rivers (Fisk, 1944; Saucier, 1994), the plugs morphology was likely modified by heterolithic sediments deposition during the open-stage and fine-grained sedimentation afterwards. Thus their apparent length was increased while the submerged or covered bedload fill deposits were not mapped (Fig. 5.16a-b).

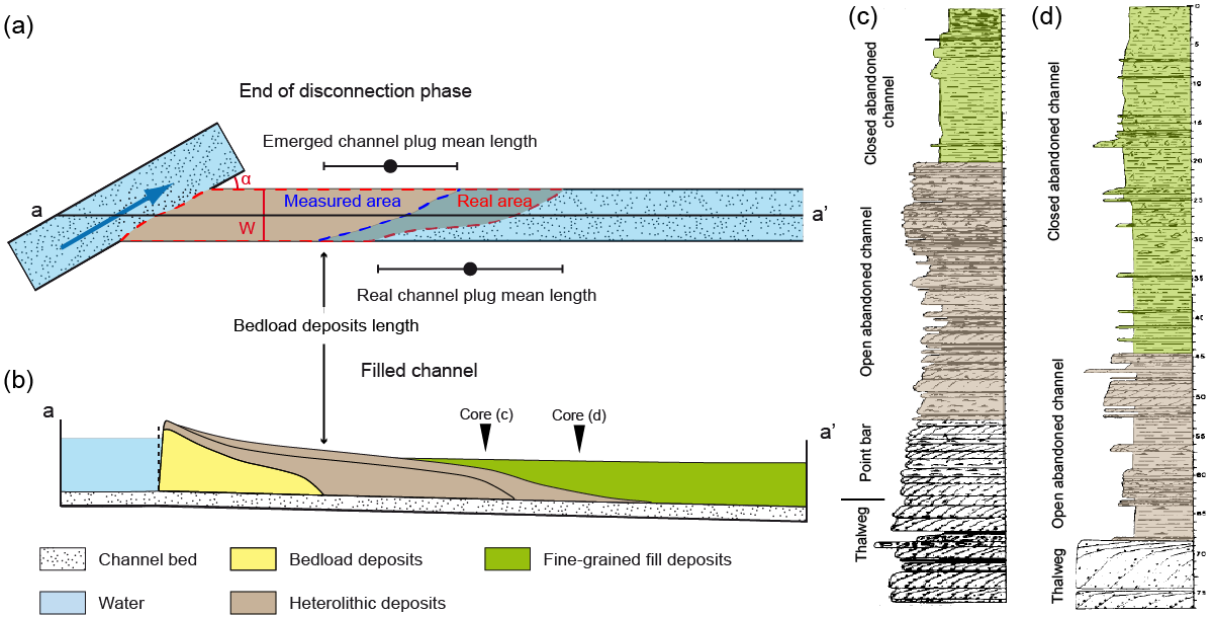

Figure 5.16: Conceptual sketch representing channel fill deposits appearance at the end of the disconnection **(a)** and the sediments architecture at the end of the channel fill **(b)**. Differentiation and accurate mapping of the open-stage deposits can then only be made using coring **(c-d)**. Cores are from Jordan & Pryor (1992).

This is especially visible in the case of neck cutoffs (Fig. 5.15), and all the more surprising as the plugs formed in channels abandoned by neck cutoffs are generally considered to be shorter (Fisk, 1947; Allen, 1965), which was confirmed by the flume experiments of Chapter 3 and tied to the water-surface slope modifications linked to the channel geometry. Although the thickness of heterolitic deposits was demonstrated to increase with the channel disconnection time (Piégay et al., 2008; Citterio & Piégay 2009), the apparent channel plug morphology extension in the Lower Mississippi Valley abandoned channels appears independent or non-linearly correlated to the abandoned channel age (Fig. 5.15). Other processes, such as tie channel formation which formed in 65 % of the Mississippi River abandoned channels before river modification (Rowland et al., 2005) must have helped to fill these channels. Regardless of these finer-grained sediments deposition process, as heterolithic deposits sedimentation rates vary over time due to their control by different factors such as

flood frequency, sediment supply and active channel migration (Makaske et al. 2002; Rowland et al., 2005; Wren et al. 2008; Citterio & Piégay 2009; Gray et al. 2016) it appears impossible to use the channel disconnection age to estimate the length of coarse-grained deposits from which the heterolithic deposits have grown. Furthermore, the study of boreholes in two channels abandoned by neck cutoff (Alexandrowicz, 2015) of the Lower Mississippi River show that the heterolithic deposits formed during the open stage of channel disconnection (Jordan & Pryor, 1992) do not necessarily drape the bedload deposits but can create a plug-like topography between bedload deposits bars (Fig. 5.17), and can thus significantly extend the apparent channel plug length even before the end of the disconnection phase.

Thus aerial pictures appear unlikely to provide a suitable replacement for field surveys to study the bedload fill of abandoned channels unless they are taken in the short window of time between the initial disconnection process and the formation of heterolithic or fine deposits. This issue is less marked in bedload dominated rivers (Chapter 4). However, the comparison of these apparent channel plug lengths with the experimental relationships determined in Chapter 3 showed that even though the channel plug apparent morphology is often longer than predicted, the relationships are accurate to predict the minimal channel plug length, especially considering that the measured part of the plug was shorter than its real length due to the use of maps and pictures (Fig. 5.16 a-b). Indeed, the few channel plugs below the predicted value for a given length ratio are only slightly shorter than expected, and their increase of length with the length ratio closely follows the experimental relationship slope (Fig. 5.15).

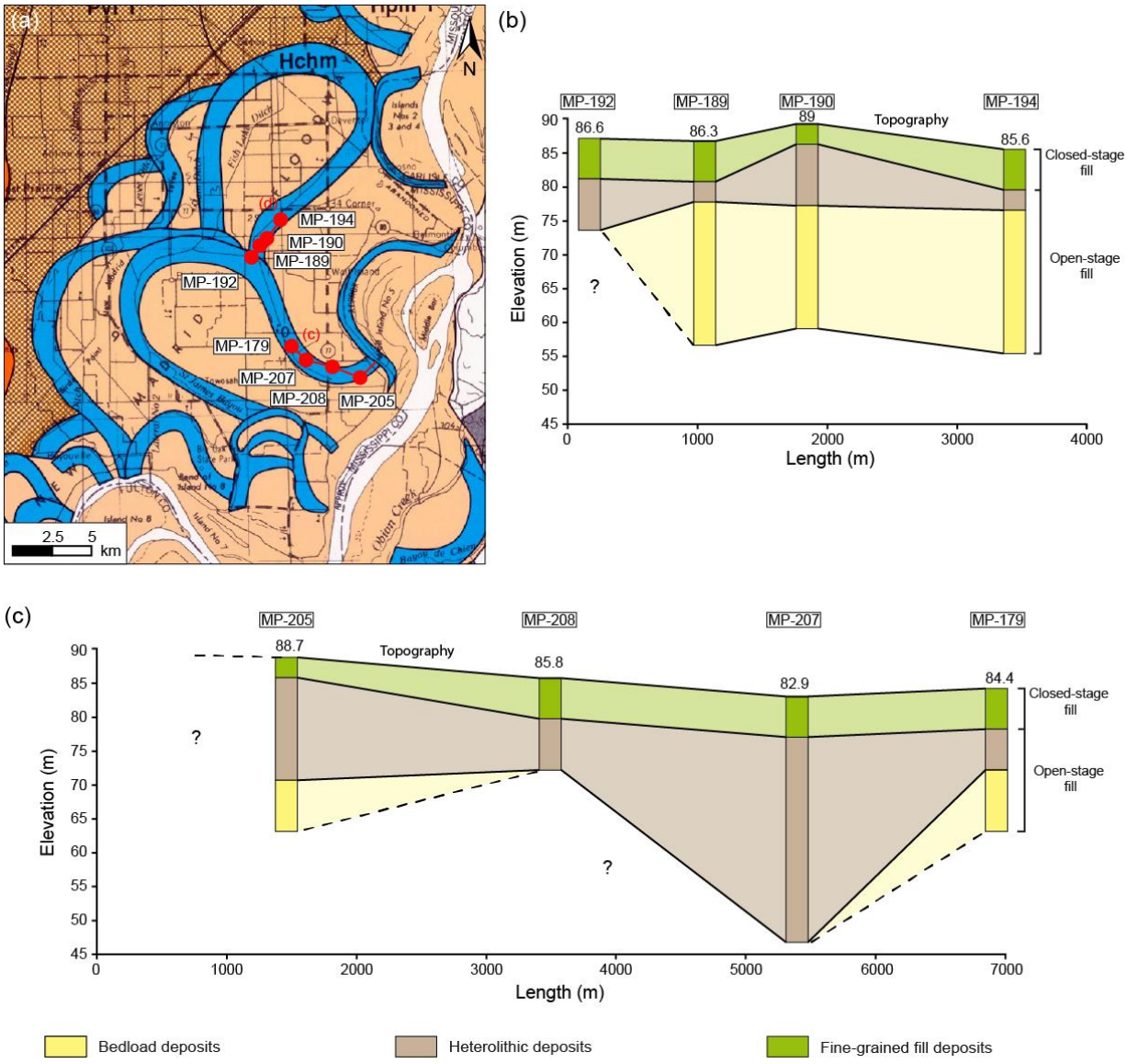

Figure 5.17: Mississippi River abandoned channel fill in Hickman County (Kentucky). Boreholes position in the channels **(a)**. Borehole data taking into account the surface topography and longitudinal distance in the channel and interpreted facies longitudinal evolution **(b-c)**. Data from Alexandrowicz (2015).

Although it appear difficult to replace field surveys with aerial pictures analysis, the length-based experimental relationship already shows promises as it appear to reliably estimate the minimal channel plug length. Thus it would be interesting to conduct extensive coring campaigns (e.g., Berendsen & Stouthamer, 2000) focused on mapping the coarse-grained part of channel plugs in mixed load systems in order to quantify the discrepancy between the channel plug predicted and real length, estimate the extension of the downstream part of the channel plug and thus refine the relationship to propose a minimal and maximal length of the coarse-grained part of the channel plug. This relationship could then be used to predict channel plug length and possibly, with Eq. 3.4, volume, using aerial pictures and this relationship.

5.5. Conclusion

Field surveys in a channel abandoned 1500 years ago provided the opportunity to assess the long-term preservation of the architectural model developed during Chapters 2 through 4. Although high energy events can significantly rework the coarse-grained deposits, the main features of the bedload fill could still be identified. The bedload deposits architectural pattern was also identified at channel-scale in other abandoned channels, both in bedload dominated and mixed load rivers. The architectural model proposed in this dissertation thus appears preserved through time as long as the abandoned channel itself is preserved. The channel plug coarse-grained deposits form the part of the bedload fill that is the most sensible to erosion due to its proximity to the active channel. Its geometry remains difficult to identify in abandoned channels without studying the subsurface as heterolithic deposits can form on it and extend its apparent morphology. However, the experimental relationship developed in Chapter 3 to predict channel plug length appears suitable to predict its minimal length based on the abandoned and active channels length ratios. This relationship thus provides a less accurate but faster and remotely applicable solution to estimate the minimal channel plug length in cutoff cases, as long as its planform geometry is known.

Chapter 6: Conclusion and perspectives

6.1. Main contributions of the PhD

Channel disconnection occurs through different stages, each associated with different deposits in the abandoned channel. This PhD focused on the open-channel stage, which occurs in the first decade of abandonment through bedload sedimentation by combining field and experimental investigations. The goal was to link hydrology, geomorphic evolution and resulting sedimentary facies. A depositional and architectural model for bedload fill sediments was proposed and tested against historically abandoned channels.

6.1.1. Experimental results

Regardless of the bifurcation or channels planar geometry, bed- or water-surface slope or the presence of a downstream reconnection of the channels, the bedload fill deposition processes observed is very similar in all experiments. Two phases may be distinguished:

- **Sedimentation is initiated in the flow separation zone** located against the internal bank of the channel just downstream of the bifurcation. An initial plug bar forms following the width and length of the flow separation zone (Fig. 2.4).
- The channel plug then widens until it occupies the whole channel width at the bifurcation and downstream from this initial bar, **forming a composite and amalgamated sedimentary body** (Fig. 2.6). The channel plug progressively thickens until hydraulic disconnection.

The disconnection time and initial plug bar width are controlled by the width of the flow separation zone, which was shown to be controlled by the channel diversion angle. High diversion angle is associated with large flow separation zone and thus faster thickening of the channel plug. The controls on final channel plug length, volume and geometry vary with the channel geometry and flow conditions at the bifurcation:

- In **free flow conditions** – i.e., the water-surface slope roughly parallel to the channel bed – **the diversion angle controls the channel plug length and volume**. An increase of the diversion angle results in a linear decrease of both channel plug length and volume (Fig. 2.7). In these conditions the plug grows by the amalgamation of downstream elongating bars (Fig. 2.4).

- When water-surface slope modifications reach the bifurcation or plug construction zone, the plug becomes shorter and its length and volume are no longer controlled by the diversion angle (Fig. 3.10) but by the **water-surface slope ratio between the disconnecting and active channels** (Fig. 3.11). In this case, the channel plug grows by the downstream progradation of fore sets (Fig. 2.13b) and the channel plug length and volume increase with the water-surface slope ratio (Fig. 3.11).

Results of the flume experiments were used to determine relationships between the water-surface slope ratio and:

- The channel plug length (Fig. 3.11).
- The channel plug volume (Figs. 3.12 & 3.13).

6.1.2. Comparison with field examples

Field surveys conducted in channels in both open- and closed-stages allowed comparisons with the experimental results.

Fieldwork in the Ain River provided high resolution mappings of the channels bedload fill deposits showed that:

- The morphologies of the **channel plug deposits are similar to the one observed in flume experiments** supporting comparable deposition processes (Figs. 4.3 & 4.4), as suggested by the evolution observed on satellite images.
- In addition, **lateral accretion deposits formed in the channel downstream of the channel plug** (Figs. 4.5c & 4.8) due to the decrease in energy induced by the channel plug construction were observed. They contribute to the channel infilling through channel narrowing.
- The **bedload fill** sediments **fine upwards and downstream** (Figs. 4.6 & 4.7), probably due to the decrease in flow energy accompanying the plug construction (Fig. 2.3f-g).
- These observations allowed the update of the architectural model for bedload channel fill along the whole length of the channel (Fig. 4.11).

Surface mapping combined with borehole data in a well preserved channel that disconnected 1500 years ago (Old Seine of Vimpelles) showed that:

- **Bedload fill deposits architecture is comparable to experimental results** (Figs. 5.4 & 5.5), and sand fraction follows a similar trend in other field examples from the literature (Fig. 5.12).
- **Coarse-grained fill deposits are resilient** to moderate energy reactivation or flooding events (Fig. 5.7), but not to reactivation of channels.

The channel plug lengths of cutoff channels measured in the Ain, Allier and Lower Mississippi Valley were compared to the experimental relationship linking channel plug length and channel length ratio:

- The length of the channel plugs formed in the bedload dominated Ain and Allier rivers is close to the experimental relationship (Fig. 5.15).
- However, the channel plugs measured in the Lower Mississippi Valley are up to 12 times longer than predicted using the experimental relationship (Fig. 5.15). This is attributed to the channel plug extension by heterolithic sediments deposition at the end of the disconnection phase. Hence detailed sedimentary cross-sections are required to strictly decipher between channel plugs and the subsequent deposits.
- Despite this, **the experimental relationship appears reliable to estimate the minimal length of the channel plug** (Fig. 5.15).

6.2. Future work and perspectives

6.2.1. Experimental setup improvement

The experimental setup used throughout this PhD proved appropriate to observe the bedload fill deposition processes and their architecture, and to link them to hydraulic effects. However, the accuracy of the measurement of hydraulic parameters, that proved crucial in the disconnection and channel plug formation processes, could be improved.

The discharge in the distributaries was measured in bifurcation configurations using the weight of the water collected in a pierced cylinder at the downstream extremity of the system, similarly to the system of Salter et al. (2019). This system was not usable in the flume configurations with downstream reconnection and no measurements of the discharge in the disconnecting channel could be made. An attempt was made to use hot-wire anemometry (King, 1914; Davis, 1922) to measure the mean flow velocity and, from it, compute the discharge. However, the range of variations caused by the flow in the experimental setting

was too narrow to use with the tested probe. Considering that the experimental setup already uses an overhead camera, Particle Image Velocimetry (PIV), tracking of particles patterns moving with the flow in a pair of successive images can be envisaged (see Lemay, 2019).

Additionally, the water-surface slope, which has proven to be a major control on channel disconnection and channel plug extent and architecture, was manually measured at preset locations. This process was time consuming and gave low resolution results. A better acquisition system should be adopted to obtain a higher resolution on the water-surface elevation and slope along the whole flume. Several methods could be tested:

- Pulses of a mixture of water and titanium in the flume immediately before the experiment interruption to scan the deposits topography (Salter et al., 2019). As this mixture is opaque, its surface can be scanned using photogrammetry or laser technique. Flow depth can then be obtained by subtracting the scan of the bed topography made immediately after the water-surface scan.
- The measure of the flow depth using color-intensity variations of the dyed water (Winterbottom & Gilvear, 1997; Tal et al., 2012). The water-surface elevation can then be measured for the whole duration of the flume experiment based on overhead pictures. This potentially allows real-time monitoring of bedload deposits thickness as a negative of the flow depth.

6.2.2. Complexification of the flume experiments

The flume experiments focused on channel-scale planar geometry and its effects on hydraulic parameters. Although it yielded results that were used to formulate the bedload fill model and tentatively predict the minimal extent of the channel plug, the experimental setup was obviously less complex than natural rivers. Several adjustments are proposed that -combined with the setup modifications proposed above- should help refining the experimental relationships and testing the effects of other forcings on bedload fill architecture:

- *Testing more curved channel geometries*, in order to refine relationships based on slope and length ratios.
- *Testing the effects of unsteady input flow discharge* on channel disconnection and channel fill deposition or erosion.
- *The installation of a curved channel upstream of the bifurcation*. Numerical modeling has shown that the presence of an upstream curve affects discharge partitioning, water-

surface slope and flow separation zone dimension in the downstream channels (Kleinhans et al., 2008; Hardy et al., 2011). Such features are often present in natural settings and as such it is important to quantify their effects on bedload fill deposits architecture for a given downstream architecture.

- *Using a fully erodible substrate (bed + banks)*. Channel curvature and width variations through time affect the bifurcation stability by modifying discharge and sediment partitioning at the bifurcation (Wang et al., 1995; Zolezzi et al., 2006). Furthermore, an erodible bed opens the possibility of scour formation, which can reduce bedload supply to disconnecting channels and thus affect disconnection duration and plug construction (Richards & Konsoer, 2020). *Using a mixed sedimentary load* would help enabling meandering in the flume (Smith, 1998).

6.2.3. Transitional phase and heterolithic deposits study

This PhD focused on the bedload deposits formed in abandoned channels during the disconnection phase. However, heterolithic deposits can form during the open-stage of channel abandonment in close association to the bedload sediments and fill important volumes the abandoned channel with coarse- to fine-grained sediments (Bridge et al., 1986; Jordan & Pryor, 1992). Due to their potential volume, grain size and close geometrical relationship with the bedload fill the heterolithic deposits are interesting for reservoir modeling as they potentially increase the overall connectivity and volume of porous deposits in the channel fill. Thus their deposition processes and geometry should be further investigated to try to include them into architectural models, such as the one developed in this dissertation. To do so several options are available:

- The realization of flume experiments focusing on their formation processes, for instance in fixed-bank and mixed load settings with an artificial plug, to simulate the transition phase with overbank deposition in the abandoned channel and/or tie channel establishment and the subsequent fill evolution.
- The surveying of recently disconnected channels in mixed load settings to study the heterolithic sediments deposition processes and architecture as well as their sedimentation rate (e.g., Rowland et al., 2005).
- The use of borehole data or realization of new coring campaigns combined with geophysical surveys to study heterolithic (and coarse-grained) deposits in transects of

abandoned channels, such as those conducted in the Old Seine (Chapter 5) or the Rhine delta (Berendsen & Stouthamer, 2000).

6.2.4. Channel fill under tidal influence

This PhD focused on fluvial meandering rivers. However, channel abandonment is common in deltas. While similar to those happening in meandering systems, bifurcations in deltas are more likely to be affected by backwater effects, and are often under tidal influence. This likely affects the abandoned channel fill architecture. Delta networks are also prone to avulsions (Jerolmack, 2009) and can form extensive reservoirs that currently host an important part of the global oil and gas reserves (Tyler & Finley, 1991). Thus understanding how the channel fill architecture and properties are affected by their proximity to the shore line has high economical implications. Compared to fluvial meandering systems, two major additional effects need to be investigated:

- In the reach of tidal effects, the bedload fill deposition is slowed by tidally-induced scours, and the coarse-grained bedload fill is interspaced with heterolithic to fine-grained tidal deposits that reduce the fill overall permeability (Makaske & Weerts, 2005; van Veen et al., 2005; Kleinhans et al., 2010; Gray et al., 2016). Close to the shore line, abandoned channels can be almost completely filled by fine-grained tidal deposits (Li et al., 2020; Wu et al., 2020).
- On a longer time scale, climate change greatly can affects deltas by causing sea level increase that result in the adoption of an anastomosing channel pattern with rapid aggradation, promoting channel abandonment and fill deposits formation (Jerolmack, 2009).

References

AALTO, R., LAUER, J. W., DIETRICH, W. E., 2008. Spatial and temporal dynamics of sediment accumulation and exchange along Strickland River floodplains (Papua New Guinea) over decadal-to-centennial timescales. J. Geophys. Res., 113, 1-22.

AHMED, J., CONSTANTINE, J.A., DUNNE, T., 2019. The role of sediment supply in the adjustment of channel sinuosity across the Amazon Basin. Geology 47, 807–810.

ALLEN, J. R. L., 1963, Henry Clifton Sorby and the sedimentary structures of sands and sandstones in relation to flow conditions: Geologie en Mijnbouw, 42, 223–228.

ALLEN, J.R.L., 1965. A review of the origin and characteristics of recent alluvial sediments. Sedimentology 5, 89–191. https://doi.org/10.1111/j.1365-3091.1965.tb01561.x

ALLEN, J. R. L., 1970a. Physical Processes of Sedimentation. xv + 248 pp., figs. George Allen and Unwin Ltd., London. (Earth Science Series 1. Edited by J. Sutton & J. V. Watson). Geol. Mag. 108, 188-190. https://doi.org/10.1017/S0016756800051281

ALLEN, J. R. L., 1970b. Studies in Fluviatile Sedimentation: A Comparison of Fining-Upwards Cyclothems, with Special Reference to Coarse-member Composition and Interpretation. SEPM J. Sediment. Res. 40, 298-323. https://doi.org/10.1306/74D71F32-2B21-11D7-8648000102C1865D

ALEXANDROWICZ, N., 2015. Predicting variability of basal scour and quantifying vertical connectivity for channel-belt reservoirs using observations from the Holocene Mississippi River and channel-belt. PhD dissertation, University of Texas, Arlington.

AMOROS, C., 2001. The Concept of Habitat Diversity Between and Within Ecosystems Applied to River Side-Arm Restoration. Environ. Manage. 28, 805–817. https://doi.org/10.1007/s002670010263

ARNAUD, F., PIÉGAY, H., SPITONI M., WAWRZYNIAK, V., COLLERY, P., 2015. Characterization of aquatic habitats and sedimentary dynamic on a regulated gravel bed river. 2nd International Conference I.S. Rivers, Jun 2015, Lyon, France. I.S. Rivers 2015 Conference Proceedings.

ARTHUIS, R., CYPRIEN, A.-L., BATARDY, C., 2005. Les alluvions fossiles de la Loire et de ses affluents entre Ancenis et Champtocé-sur-Loire : chronologie et stratigraphie des alluvions, structuration de l'espace ligérien, Estuaria.

ARTHUIS, R., MIEJAC, E., NAULEAU, J.-F., 2015. La navigation fluviales : une affaire de canal ? La « Boire Torse », exemple d'un canal creusé au Moyen-Âge entre Ingrandes et Anetz.

ASHMORE, P.E., 1987. Bed load transfer and channel morphology in braided streams, in Beschta, R.L., Blinn, T., Grant, G.E., Swanson, F.J. and Ice, G.G. (eds), Erosion and Sedimentation in the Pacific Rim. International Association of Hydrologic Sciences Publication 165, Wallingford, 333-342.

ASHMORE, P.E., 1988. Bed load transport in braided gravel-bed stream models. Earth Surface Processes and Landform 13, 677-695.

ASHMORE, P.E., 1991. How do gravel-bed rivers braid? Canadian journal of earth Sciences 28, 326-341.

ASLAN, A. AND BLUM, M.D., 1999. Constrasting Styles of Holocene Avulsion, Texas Gulf Coastal Plain, USA, in: Smith, N.D., Rogers, J. (eds), Fluvial Sedimentology VI. Blackwell Publishing Ltd., Oxford, UK, pp. 193–209. https://doi.org/10.1002/9781444304213.ch15

ASLAN, A., AUTIN, W.J., BLUM, M.D., 2005. Causes of River Avulsion: Insights from the Late Holocene Avulsion History of the Mississippi River, U.S.A. J. Sediment. Res. 75, 650–664. https://doi.org/10.2110/jsr.2005.053

AUTIN, W., J., BURNS, S., F., MILLER, B., J., SAUCIER, R., T., SNEAD, J., I., 1991. Quaternary geology of the Lower Mississippi Valley *In* Quaternary nonglacial geology, Conterminous U.S.. R. B. Morrison, eds., Geological Society of America, Boulder, Colorado, 547-582.

BARTON M.D., 1994. Outcrop characterization of architecture and permeability structure in fluvial-deltaic sandstones, Cretaceous Ferron sandstone, Utah, *PhD Dissertation*, University of Texas, Austin, Texas, 260 p.

BERENDSEN H.J.A., COHEN KM, STOUTHAMER E., 2007. The use of GIS in reconstructing the Holocene palaeogeography of the Rhine-Meuse delta, the Netherlands. International Journal of Geographical Information Science 21, 589–602.

BERENDSEN, H.J.A. AND STOUTHAMER, E., 2000. Late Weichselian and Holocene palaeogeography of the Rhine–Meuse delta, The Netherlands. Palaeogeogr. Palaeoclimatol. Palaeoecol. 161, 311–335. https://doi.org/10.1016/S0031-0182(00)00073-0

BERNAL, C., CHRISTOPHOUL, F., DARROZES, J., LARAQUE, A., BOURREL, L., SOULA, J.-C., GUYOT, J.-L., BABY, P., 2012. Crevassing and capture by floodplain drains as a cause of partial avulsion and anastomosis (lower Rio Pastaza, Peru). Journal of South American Earth Sciences 44, 63–74. https://doi.org/10.1016/j.jsames.2012.11.009

BERTOLDI, W., 2012. Life of a bifurcation in a gravel-bed braided river: Life of a bifurcation in a gravel bed braided river. Earth Surf. Process. Landf. 37, 1327–1336. https://doi.org/10.1002/esp.3279

BERTOLDI, W. AND TUBINO, M., 2007. River bifurcations: Experimental observations on equilibrium configurations: River bifurcations.Water Resour. Res., 43, 1–10.

BERTOLDI, W., ZANONI, L., MIORI, S., REPETTO, R., TUBINO, M., 2009. Interaction between migrating bars and bifurcations in gravel bed rivers: Interaction between migrating bars and bifurcations in gravel bed rivers. Water Resources Research 45. https://doi.org/10.1029/2008WR007086

BLAKE D.H. AND OLLIER C.D., 1971. Alluvial plains of the Fly River, Papua. Zeitschrift fur Geomorphologie Suppl. 12, 1–17.

BLUM, M.D., GUCCIONE, M.J., WYSOCKI, D.A., ROBNETT, P.C., RUTLEDGE, E.M., 2000. Late Pleistocene evolution of the lower Mississippi River valley, southern Missouri to Arkansas. Geol. Soc. Am. Bull. 112, 221–235. https://doi.org/10.1130/0016-7606(2000)112<221:LPEOTL>2.0.CO;2

BOLLA PITTALUGA, M., COCO, G., KLEINHANS, M.G., 2015. A unified framework for stability of channel bifurcations in gravel and sand fluvial systems: Gravel bed and sand bed river bifurcations. Geophys. Res. Lett. 42, 7521–7536. doi: 10.1002/2015GL065175

BOLLA PITTALUGA M, NOBILE G, SEMINARA G. 2009. A nonlinear model for river meandering. Water Resources Research 45: W04432 doi: 10.1029/2008WR007298.

BOLLA PITTALUGA, M., REPETTO, R., TUBINO, M., 2003. Channel bifurcation in braided rivers: Equilibrium configurations and stability: Water Resour. Res. 39. https://doi.org/10.1029/2001WR001112

BRIDGE, J.S., 2003. Rivers and floodplains: forms, processes, and sedimentary record. Blackwell Pub, Oxford, UK ; Malden, MA, USA, 504 pp.

BRIDGE, J.S., ALEXANDER, J., COLLIER, R.E.L., GAWTHORPE, R.L., JARVIS, J., 1995. Ground-penetrating radar and coring used to study the large-scale structure of point-bar deposits in three dimensions. Sedimentology 42, 839–852. https://doi.org/10.1111/j.1365-3091.1995.tb00413.x

BRIDGE, J.S. AND GLABEL, S.L., 1992. Flow and sediment dynamics in a low sinuosity, braided river: Calamus River, Nebraska Sandhills. Sedimentology 39, 125-142.

BRIDGE, J.S. AND LEEDER, M.R., 1979. A simulation model of alluvial stratigraphy. Sedimentology 26, 617–644. https://doi.org/10.1111/j.1365-3091.1979.tb00935.x

BRIDGE, J. S., SMITH, N. D., TRENT, F., GABEL, S. L., BERNSTEIN, P., 1986. Sedimentology and morphology of a low-sinuosity river: Calamus River, Nebraska Sand Hills. Sedimentology, 33, 851–870

BRIDGE, J.S. AND TYE, R.S., 2000. Interpreting the dimensions of ancient fluvial channel bars, and channel belts from wireline-logs and cores. AAPG Bulletin 84, 1205-1226.

BRYANT, M., FALK, P., PAOLA, C., 1995. Experimental study of avulsion frequency and rate of deposition. Geology 23, 365-368. https://doi.org/10.1130/0091-7613(1995)023<0365:ESOAFA>2.3.CO;2

BULLE, H., 1926. Untersuchungen über die Geschiebeableitungbei der Spaltung von Wasserläufen. VDI Verlag, Berlin (in German), 42 pp.

CABELLO, P., DOMÍNGUEZ, D., MURILLO-LÓPEZ, M.H., LÓPEZ-BLANCO, M., GARCÍA-SELLÉS, D., CUEVAS, J.L., MARZO, M., ARBUÉS, P., 2018. From conventional outcrop datasets and digital outcrop models to flow simulation in the Pont de Montanyana point-bar deposits (Ypresian, Southern Pyrenees). Mar. Pet. Geol. 94, 19-42 https://doi.org/10.1016/j.marpetgeo.2018.03.040

CANT, D. AND WALKER, R.G., 1978. Fluvial processes and facies sequences in the sandy braided South Saskatchewan River, Canada. Sedimentology, 25, 625-648.

CASTANET, C., 2008. La Loire en val d'Orléans. Dynamiques fluviales et socio-environnementales durant les derniers 30 000 ans : de l'hydrosystème à l'anthroposystème. PhD Thesis, Université Paris I Panthéon Sorbonne.

CHATANANTAVET, P., LAMB, M.P., NITTROUER, J.A., 2012. Backwater controls of avulsion location on deltas: Backwater controls on delta avulsions. Geophys. Res. Lett. 39, L01402. https://doi.org/10.1029/2011GL050197

CHATANANTAVET, P. AND LAMB, M.P., 2014. Sediment transport and topographic evolution of a coupled river and river plume system: An experimental and numerical study. Journal of Geophysical Research: Earth Surface, 119, 1263-1282.

CHOW, V. T., 1959. Open-Channel Hydraulics: New York, McGraw-Hill, 680 p.

CHURCH, M., 2006. Bed material transport and the morphology of alluvial river channels. Annual Review of Earth and Planetary Sciences 34, 325–354. https://doi.org/10.1146/annurev.earth.33.092203.122721

CITTERIO, A. AND PIÉGAY, H., 2009. Overbank sedimentation rates in former channel lakes: characterization and control factors. Sedimentology 56, 461–482. https://doi.org/10.1111/j.1365-3091.2008.00979.x

COFFEY, T.S. AND SHAW, J.B., 2017. Congruent Bifurcation Angles in River Delta and Tributary Channel Networks: Geophys. Res. Lett. 44, 11427-11436. https://doi.org/10.1002/2017GL074873

COLOMBERA, L., MOUNTNEY, N.P., RUSSELL, C.E., SHIERS, M.N., MCCAFFREY, W.D., 2017. Geometry and compartmentalization of fluvial meander-belt reservoirs at the bar-form scale: Quantitative insight

from outcrop, modern and subsurface analogues. Mar. Pet. Geol. 82, 35–55. https://doi.org/10.1016/j.marpetgeo.2017.01.024

CONSTANTINE, J.A., DUNNE, T., AHMED, J., LEGLEITER, C., LAZARUS, E.D., 2014. Sediment supply as a driver of river meandering and floodplain evolution in the Amazon Basin. Nature Geoscience 7, 899–903.

CONSTANTINE, J. A., DUNNE, T., PIEGAY, H. AND KONDOLF, G. M., 2010a. Controls on the alluviation of oxbow lakes by bed-material load along the Sacramento River, California. Sedimentology 57, 389-407.

CONSTANTINE, J. A., MC LEAN, S. R. AND DUNNE, T., 2010b. A mechanism of chute cutoff along large meandering rivers with uniform floodplain topography. Geological Society of America Bulletin 122, 855-869.

COSTIGAN, K.H. AND GERKEN, J.E., 2016. Channel morphology and flow structure of an abandoned channel under varying stages: Varying flow-structure and morpology of an abandonned channel. Water Resour. Res. 52, 5458–5472. https://doi.org/10.1002/2015WR017601

CROWLEY, K.D., 1983. large-scale bed configurations (macroforms), Platte River basin, Colorado and Nebraska: primary structures and formative processes. Geol. Soc. Am. Bull. 94, 117-133.

DAVIS, A.H., 1922. The cooling power of a stream of viscous fluid. Philos. Mag 6, 940-944.

DE HEER, A. AND MOSSELMAN, E., 2004. Flow structure and bedload distribution at alluvial diversions. Delft University of Technology & Wl/Delft Hydraulics 801-806. 10.1201/b16998-103.

DELEPLANCQUE, B., 2016. Caractérisation des heterogeneities sédimentaires d'une plaine alluviale : Exemple de l'évolution de la Seine supérieure depuis le dernier maximum glaciaire. PhD dissertation.

DELEPLANCQUE, B., COJAN, I., BEUCHER, H., MEHL, C., STAB, O., 2018. Spatial and temporal patterns of the upper Pleistocene alluvial fill deposits of the upstream Seine River alluvial plain, la Bassée, France. Geomorphology 318, 148–161. https://doi.org/10.1016/j.geomorph.2018.06.005

DELORME, P., VOLLER, V., PAOLA, C., DEVAUCHELLE, O., LAJEUNESSE, É., BARRIER, L., METIVIER, F., 2017. Self-similar growth of a bimodal laboratory fan. Earth Surf. Dynam., 5, 239–252, https://doi.org/10.5194/esurf-5-239-2017.

DEPRET, T., RIQUIER, J., PIEGAY, H., 2017. Evolution of abandoned channels: Insights on controlling factors in a multi-pressure river system. Geomorphology 294, 99–118 https://doi.org/10.1016/j.geomorph.2017.01.036.

DESCHAMPS, R., GUY, N., PREUX, C., LERAT, O., 2012. Analysis of Heavy Oil Recovery by Thermal EOR in a Meander Belt: From Geological to Reservoir Modeling. Oil Gas Sci. Technol. – Rev. D'IFP Energ. Nouv. 67, 999–1018. https://doi.org/10.2516/ogst/2012015f

DIERAS, P.L., 2013. The persistence of oxbow lakes as aquatic habitats: an assessment of rates of change and patterns of alluviation. PhD Thesis, Cardiff University.

DIERAS, P.L., CONSTANTINE, J.A., HALES, T.C., PIÉGAY, H., RIQUIER, J., 2013. The role of oxbow lakes in the off-channel storage of bed material along the Ain River, France. Geomorphology 188, 110–119. https://doi.org/10.1016/j.geomorph.2012.12.024

DONSELAAR, M.E. AND OVEREEM, I., 2008. Connectivity of fluvial point-bar deposits: An example from the Miocene Huesca fluvial fan, Ebro Basin, Spain. AAPG Bull. 92, 1109–1129. https://doi.org/10.1306/04180807079

DURKIN, P.R., BOYD, R.L., HUBBARD, S.M., SHULTZ, A.W., BLUM, M.D., 2017. Three-Dimensional Reconstruction of Meander-Belt Evolution, Cretaceous Mcmurray Formation, Alberta Foreland Basin, Canada. J. Sediment. Res. 87, 1075–1099. https://doi.org/10.2110/jsr.2017.59

DURKIN, P.R., HUBBARD, S.M., BOYD, R.L., LECKIE, D.A., 2015. Stratigraphic Expression of Intra-Point-Bar Erosion and Rotation. J. Sediment. Res. 85, 1238–1257. https://doi.org/10.2110/jsr.2015.78

DUTU, L.T., PROVANSAL, M., LE COZ, J., DUTU, F., 2014. Contrasted sediment processes and morphological adjustments in three successive cutoff meanders of the Danube Delta. Geomorphology, Elsevier, ,204, 154–164.

EDMONDS, D.A., HOYAL, D.C.J.D., SHEETS, B.A., SLINGERLAND, R.L., 2009. Predicting delta avulsions: Implications for coastal wetland restoration. Geology 37, 759–762. https://doi.org/10.1130/G25743A.1

EDMONDS, D.A. AND SLINGERLAND, R.L., 2008. Stability of delta distributary networks and their bifurcations: Stability of deltaic bifurcations. Water Resour. Res. 44. https://doi.org/10.1029/2008WR006992

ERKENS G. AND COHEN K.,M., 2009. Quantification of intra-Holocene sedimentation in the Rhine-Meuse delta: A record of variable sediment delivery. Netherlands Geographical Studies 388, 117–171.

ERKENS, G., HOFFMANN, T., GERLACH, R., KLOSTERMANN, J., 2011. Complex fluvial response to Lateglacial and Holocene allogenic forcing in the Lower Rhine Valley (Germany). Quat. Sci. Rev. 30, 611–627. https://doi.org/10.1016/j.quascirev.2010.11.019

ERSKINE, W. D. AND LIVINGSTONE, E.A., 1999. In-channel benches: the role of floods in their formation and destruction on bedrock confined rivers. In: Miller, A.J., Gupta, A. (eds.), Varieties of Fluvial Form, Wiley, New York, NY, 445–475.

ERSKINE, W., MCFADDEN, C., BISHOP, P., 1992. Alluvial cutoffs as indicators of former channel conditions. Earth Surf. Process. Landf. 17, 23–37. https://doi.org/10.1002/esp.3290170103

ETHRIDGE, F.G. AND SCHUMM, S.A., 1977. Reconstructing paleochannel morphologic and flow characteristics: methodology, limitations, and assessment. Fluvial Sedimentology 5, 703-721.

ETHRIDGE, F.G., SKELLY, R.L., BRISTOW, C.S., 1999. Avulsion and Crevassing in the Sandy, Braided Niobrara River: Complex Response to Base-Level Rise and Aggradation. *In* Smith, N.D., Rogers, J. (eds.), Fluvial Sedimentology VI. Blackwell Publishing Ltd., Oxford, UK, pp. 179–191. https://doi.org/10.1002/9781444304213.ch14

FARR, T.G., ROSEN, P.A., CARO, E., CRIPPEN, R., DUREN, R., HENSLEY, S., KOBRICK, M., PALLER, M., RODRIGUEZ, E., ROTH, L., SEAL, D., SHAFFER, S., SHIMADA, J., UMLAND, J., WERNER, M., OSKIN, M., BURBANK, D., ALSDORF, D., 2007. The Shuttle Radar Topography Mission. Rev. Geophys. 45, RG2004 https://doi.org/10.1029/2005RG000183

FEDERICI, B. AND PAOLA, C., 2003. Dynamics of channel bifurcations in noncohesive sediments: Dynamics of bifurcations. Water Resour. Res. 39. https://doi.org/10.1029/2002WR001434

FERNANDES, A.M., TÖRNQVIST, T.E., STRAUB, K.M., MOHRIG, D., 2016. Connecting the backwater hydraulics of coastal rivers to fluvio-deltaic sedimentology and stratigraphy. Geology 44, 979–982. https://doi.org/10.1130/G37965.1

FISK, H. N., 1944. Geological Investigation of tes Alluvial Valley of the Lower Mississippi River. Mississippi River Commission, Vicksburg, Miss., 78 pp.

FISK, H. N., 1947. Fine Grained Alluvial Deposits and their Effects on Mississippi River Activity. Mississippi River Commission, Vicksburg, Miss., 82 pp.

FITZPATRICK, F.A., WAITE, I.R., D'ARCONTE, P.J., MEADOR, M.R., MAUPIN, M.A., GURTZ, M.E. 1998. Revised Methods for Characterizing Stream Habitat in the National Water-Quality Assessment Program. Report 98-4052, U.S. Geological Survey, Raleigh.

FLECKENSTEIN, J., NISWONGER., R., FOGG, G., 2006. River-Aquifer Interactions, Geologic Heterogeneity, and Low-Flow Management,Ground Water, 44, 837–852.

FLEETWOOD, A., R., 1969. Geological investigation of the Ouachita River area, Lower Mississippi Valley. Technical report No. S-69-2, U.S. Army Engineer Waterways Experiment Station, Vicksburg, MS.

FLIPO, N., MOUHRI, A., LABARTHE, B., BIANCAMARIA, S., RIVIÈRE, A., WEILL, P., 2014. Continental hydrosystem modelling: the concept of nested stream-aquifer interfaces. Hydrol. Earth Syst. Sc. 18, 3121–3149.

FULLER, I.C., PASSMORE, D.G., HERITAGE, G.L., LARGE, A.R.G., MILAN, D.J., BREWER, P.A., 2002. Annual sediment budgets in an unstable gravel-bed river: the River Coquet, northern England. In: Jones, S.J., Frostick, L.E. (Eds.), Sediment Flux to Basins: Causes, Control and Consequences. Geological Society Special Publication. Geological Soc Publishing House, Bath, pp. 115–131.

FULLER, I.C., LARGE, A.R.G., CHARLTON, M.E., HERITAGE, G.L., MILAN, D.J., 2003. Reach-scale sediment transfers: an evaluation of two morphological budgeting approaches. Earth Surface Processes and Landforms 28, 889–903.

FUSTIC, M., HUBBARD, S.M., SPENCER, R., SMITH, D.G., LECKIE, D.A., BENNETT, B., LARTER, S., 2012. Recognition of down-valley translation in tidally influenced meandering fluvial deposits, Athabasca Oil Sands (Cretaceous), Alberta, Canada. Mar. Pet. Geol. 29, 219–232. https://doi.org/10.1016/j.marpetgeo.2011.08.004

GAGLIANO, S.M. AND HOWARD, P.C., 1984. The neck cutoff oxbow lake cycle along the Lower Mississippi River C. Elliott (Ed.), River Meandering, ASCE, New York (1984), 147-158.

GANTI, V., CHADWICK, A.J., HASSENRUCK-GUDIPATI, H.J., FULLER, B.M., LAMB, M.P., 2016a. Experimental river delta size set by multiple floods and backwater hydrodynamics. Sci. Adv. 2, e1501768–e1501768. https://doi.org/10.1126/sciadv.1501768

GANTI, VAMSI, CHADWICK, A.J., HASSENRUCK-GUDIPATI, H.J., LAMB, M.P., 2016b. Avulsion cycles and their stratigraphic signature on an experimental backwater-controlled delta: Backwater-Controlled Avulsion Cycles. J. Geophys. Res. Earth Surf. 121, 1651–1675. https://doi.org/10.1002/2016JF003915

GAUTIER, E., BRUNSTEIN, D., VAUCHEL, P., ROULER, M., FUERTES, O., GUYOT, J.L., DAROZZES, J., BOURREL, L., 2007. Temporal relations between meander deformation, water discharge and sediment fluxes in the floodplain of the Rio Beni (Bolivian Amazonia). Earth Surface Processes and Landforms 32, 230-248.

GAY, G.R., GAY, H.H., GAY, W.H., MARTINSON, H.A., MEADE, R.H., MOODY, J.A., 1998. Evolution of cutoffs across meander necks in Powder River, Montana, USA. Earth Surf. Process. Landf. 23, 651–662. https://doi.org/10.1002/(SICI)1096-9837(199807)23:7<651::AID-ESP891>3.0.CO;2-V

GHINASSI, M., 2011. Chute channels in the Holocene high-sinuosity river deposits of the Firenze plain, Tuscany, Italy: Chute channels in high sinuous channels. Sedimentology 58, 618–642. https://doi.org/10.1111/j.1365-3091.2010.01176.x

GIBLING, M.R., 2006. Width and Thickness of Fluvial Channel Bodies and Valley Fills in the Geological Record: A Literature Compilation and Classification. J. Sediment. Res. 76, 731–770. https://doi.org/10.2110/jsr.2006.060

GIOSAN, L. AND BHATTACHARYA, J.P., 2005. River Deltas-Concepts, Models, and Examples. SEPM (Society for Sedimentary Geology). https://doi.org/10.2110/pec.05.83

GOFF, J.R. AND ASHMORE, P., 1994. Gravel transport and morphological change in braided Sunwapta River, Alberta, Canada. Earth Surface Processes and Landforms 19, 195–212.

GOUW, M., 2007. Alluvial architecture of fluvio-deltaic successions: A review with special reference to Holocene settings. Netherlands Journal of Geosciences. 86.

GOMEZ, B., EDEN, D.N., PEACOCK, D.H., PINKNEY, E.J., 1998. Floodplain construction by recent, rapid vertical accretion: Waipaoa River, New Zealand. Earth Surf. Process. Landf. 23, 405–413. https://doi.org/10.1002/(SICI)1096-9837(199805)23:5<405::AID-ESP854>3.0.CO;2-X

GRAY, A.B., PASTERNACK, G.B., WATSON, E.B., GOÑI, M.A., 2016. Abandoned channel fill sequences in the tidal estuary of a small mountainous, dry-summer river. Sedimentology 63, 176–206. https://doi.org/10.1111/sed.12223

GRECO, S.E. AND ALFORD, C.A., 2003. Historical Channel Mapping of the Sacramento River from Historical Maps, Colusato Red Bluff, California: 1870–1920. Davis, Landscape Analysis and Systems Research Laboratory, University of California-Davis, Davis, CA, 117 pp.

GRENFELL, M., 2012. Dynamics and morphodynamics implications of chute channels in large, sand-bed meandering rivers. PhD Thesis, University of Exeter.

GRENFELL, M., AALTO, R., NICHOLAS, A., 2012. Chute channel dynamics in large, sand-bed meandering rivers: Chute channel dynamics. Earth Surf. Process. Landf. 37, 315–331. https://doi.org/10.1002/esp.2257

HAM, D.G. AND CHURCH, M., 2000. Bed-material transport estimated from channel morphodynamics: Chilliwack River, British Columbia. Earth Surface Processes and Landforms 25, 1123–1142.

HAN, B. AND ENDRENY, T.A., 2014. Detailed river stage mapping and head gradient analysis during meander cutoff in a laboratory river. Water Resources Research 50, 1689–1703. https://doi.org/10.1002/2013WR013580

HARDY, R.J., LANE, S.N., YU, D., 2011. Flow structures at an idealized bifurcation: a numerical experiment: Flow structures and mixing at an idealized bifurcation. Earth Surface Processes and Landforms 36, 2083–2096. https://doi.org/10.1002/esp.2235

HARRISON, L.R., DUNNE, T., FISHER, G.B., 2015. Hydraulic and geomorphic processes in an overbank flood along a meandering, gravel-bed river: implications for chute formation: Meandering River-Floodplain Interactions. Earth Surf. Process. Landf. 40, 1239–1253. https://doi.org/10.1002/esp.3717

HAUER, C. AND HABERSACK, H., 2009. Morphodynamics of a 1000-year flood in the Kamp River, Austria, and imapcts on floodplain morphology. Earth Surface Processes and Landforms, 34, 654-682.

HAUSMANN, J., STEINEL, H., KRECK, M., WERBAN, U., VIENKEN, T., DIETRICH, P., 2013. Two-dimensional geomorphological characterization of a filled abandoned meander using geophysical methods and soil sampling. Geomorphology 201, 335–343. https://doi.org/10.1016/j.geomorph.2013.07.009

HELLER, P.L. AND PAOLA, C., 1996. Downstream Changes In Alluvial Architecture: An Exploration of Controls on Channel-stacking Patterns. SEPM J. Sediment. Res. Vol. 66, 297-306. https://doi.org/10.1306/D4268333-2B26-11D7-8648000102C1865D

HORNUNG, J. AND AIGNER, T., 1999. Reservoir and aquifer characterization of fluvial architectural elements: Stubensandstein, Upper Triassic, southwest Germany, Sediment. Geol., 129, 215–280.

HOOKE, J.M., 1995. River channel adjustment to meander cutoffs on the River Bollin and River Dane, northwest England. Geomorphology 14, 235–253. https://doi.org/10.1016/0169-555X(95)00110-Q

HOWARD, A.D., 1992. Modeling Channel Migration and Floodplain Sedimentation in Meandering Streams. *In*: Carling, P. and Petts, G.E., Eds., Lowland Floodplain Rivers: Geomorphological Perspectives, John Wiley, Hoboken, USA, 1-41.

HOWARD, A. D., 1996. Modeling channel evolution and floodplain morphology. *In* Anderson, M. G., Walling, D. E., Bates, P. D., Eds., Floodplain Processes, John Wiley & Sons, Hoboken, USA, 15-62.

HOYAL, D.C.J.D. AND SHEETS, B.A., 2009. Morphodynamic evolution of experimental cohesive deltas. J. Geophys. Res. 114, F02009 https://doi.org/10.1029/2007JF000882

ISHII, Y. AND HORI, K., 2016. Formation and infilling of oxbow lakes in the Ishikari lowland, northern Japan. Quaternary International 397, 136–146.
IWANTORO, A. P., VAN DER VEGT, M., KLEINHANS, M. G., 2019. Morphological evolution of bifurcations in tide-influenced deltas. Earth Surf. Dynam. Discuss., https://doi.org/10.5194/esurf-2019-63 2019.
JACOBSON, R.B. AND COLEMAN, D.J., 1986. Stratigraphy and Recent evolution of Maryland Piedmont flood plains. Am. J. Sci. 286, 617–637. https://doi.org/10.2475/ajs.286.8.617
JEROLMACK, D.J., 2009. Conceptual framework for assessing the response of delta channel networks to Holocene sea level rise. Quaternary Science Reviews 28, 1786–1800. https://doi.org/10.1016/j.quascirev.2009.02.015
JEROLMACK, D.J. AND MOHRIG, D., 2007. Conditions for branching in depositional rivers. Geology 35, 463-466. https://doi.org/10.1130/G23308A.1
JOHN, S. AND KLEIN, A., 2004. Hydrogeomorphic effects of beaver dams on floodplain morphology: avulsion processes and sediment fluxes in upland valley floors (Spessart, Germany). Quaternaire 15, 219–231. https://doi.org/10.3406/quate.2004.1769
JOHNSON, R.H. AND PAYNTER, J., 1967. Development of a cutoff on the River Irk at Chadderton, Lancashire. Geography 52, 41-49.
JONES, L.S. AND BLAKEY, R.C., 1997. Eolian-fluvial interaction in the Page Sandstone (Middle Jurassic) in south-central Utah, USA — a case study of erg-margin processes. Sediment. Geol. 109, 181–198. https://doi.org/10.1016/S0037-0738(96)00044-9
JONES, H.L. AND HAJEK, E.A., 2007. Characterizing avulsion stratigraphy in ancient alluvial deposits. Sediment. Geol. 202, 124–137. https://doi.org/10.1016/j.sedgeo.2007.02.003
JONES, L.S. AND SCHUMM, S.A., 1999. Causes of Avulsion: An Overview, *In*: Smith, N.D., Rogers, J. (eds.), Fluvial Sedimentology VI. Blackwell Publishing Ltd., Oxford, UK, pp. 169–178. https://doi.org/10.1002/9781444304213.ch13
JORDAN D., W. AND PRYOR W., A., 1992. Hierarchical Levels of Heterogeneity in a Mississippi River Meander Belt and Application to Reservoir Systems: Geologic Note 76, 1601-1624. https://doi.org/10.1306/BDFF8A6A-1718-11D7-8645000102C1865D
JOSHI, S. AND XU, Y.J., 2017. Bedload and Suspended Load Transport in the 140-km Reach Downstream of the Mississippi River Avulsion to the Atchafalaya River. Water , 9, 716.
KELLER, E. A. AND SWANSON, F. J., 1979. Effects of large organic material on channel form and fluvial processes. Earth Surface Processes and Landforms 4(4), 361-380.
KERRIEN, Y., MONJUVENT, G., CORNA, M., GIREL, J., MANDIER, P., COMBIER, J., 1987. Carte Géologique d'Ambérieu-en-Bugey, Bureau des Recherches Géologiques et minières, Orléans.
KESHAVARZI, A. AND HABIBI, L., 2005. Optimizing water intake angle by flow separation analysis. Irrigation and Drainage 54, 543–552. https://doi.org/10.1002/ird.207
KHAN, H.R., 1971. Laboratory studies of alluvial river morphology. PhD dissertation, Civil Engineering Deppartment, Colorado State University, Ft. Collins, CO.
KLEINHANS, M.G., COHEN, K.M., HOEKSTRA, J., IJMKER, J.M., 2011. Evolution of a bifurcation in a meandering river with adjustable channel widths, Rhine delta apex, The Netherlands: Bifurcation model for meandering rivers with adjusting channel widths. Earth Surf. Process. Landf. 36, 2011–2027. https://doi.org/10.1002/esp.2222
KLEINHANS, M.G., FERGUSON, R.I., LANE, S.N., HARDY, R.J., 2013. Splitting rivers at their seams: bifurcations and avulsion: Bifurcations and avulsion. Earth Surf. Process. Landf. 38, 47–61. https://doi.org/10.1002/esp.3268
KLEINHANS, M.G., JAGERS, H.R.A., MOSSELMAN, E., SLOFF, C.J., 2008. Bifurcation dynamics and avulsion duration in meandering rivers by one-dimensional and three-dimensional models: Bifurcation in meandering rivers. Water Resour. Res. 44, W08454 https://doi.org/10.1029/2007WR005912
KLEINHANS, M.G. AND VAN DEN BERG, J.H., 2011. River channel and bar patterns explained and predicted by an empirical and physics-based method. Earth Surface Processes and Landforms 36, 721–738. doi:10.1002/esp.2090.
KLEINHANS, M.G., WEERTS, H.J.T., COHEN, K..M., 2010. Avulsion in action: reconstruction and modeling sedimentation pace and upstream flood water levels following a medieval tidal-river diversion catastrophe (Biesbosch, The Netherlands, 1421-1750 AD). Geomorphology, 118, 65–79.
KING, L.V., 1914. On the convection of heat from small cylinders in a stream of fluid: determination of the convection constants of small platinum wires with applications to hot-wire anemometry. Philosophical Transactions of the Royal Society of London, 214, 373-432.
KNIGHTON, D., 1998. Fluvial forms and processes. Edward Arnold, London, 377 p
KRINITZSKY, E., L., FERGUSON, J., S., SMITH, F., L., 1965. Geological investigation of the Yazoo Basin. US Army Corps of Engineers, Technical Report 3-480.

LABRECQUE, P.A., JENSEN, J.L., HUBBARD, S.M., NIELSEN, H., 2011a. Sedimentology and stratigraphic architecture of a point bar deposit, Lower Cretaceous McMurray Formation, Alberta, Canada. Bulletin of Canadian Petroleum Geology 59, 147–171. https://doi.org/10.2113/gscpgbull.59.2.147

LABRECQUE, P.A., JENSEN, J.L., HUBBARD, S.M., 2011b. Cyclicity in Lower Cretaceous point bar deposits with implications for reservoir characterization, Athabasca Oil Sands, Alberta, Canada. Sedimentary Geology, 242, 18-33. 10.1016/j.sedgeo.2011.06.011

LACEY, G., 1930. Stable channels in alluvium. Minutes of the Proceedings of the Institution of Civil Engineers, 229, 259–292.

LAMB, M., P., NITTROUER, J., A., MOHRIG, D., SHAW, J., 2012. Backwater and river plume controls on scour upstream of river mouths: Implications for fluvio-deltaic morphodynamics. J. Geophys. Res. 117, 1-15. https://doi.org/10.1029/2011JF002079

LANE, S.N., 1997. The reconstruction of bed material yield and supply histories in gravel-bed streams. Catena 30, 183–196.

LANE, S.N., RICHARDS, K.S., CHANDLER, J.H., 1995. Morphological estimation of the time integrated bed-load transport rate. Water Resoures Research 31, 761–772.

LARUE, D.K. AND HOVADIK, J., 2006. Connectivity of channelized reservoirs: a modelling approach. Petroleum Geoscience 12, 291–308. https://doi.org/10.1144/1354-079306-699

LASSETTRE, N.S., PIEGAY, H., DUFOUR, S., ROLLET, A.J., 2008. Decadal changes in distribution and frequency of wood in a free meandering river, the Ain River, France. Earth Surface Processes and Landforms 33, 1098–1112.

LATTERELL, J.J., SCOTT BECHTOLD, J., O'KEEFE, T.C., PELT, R., NAIMAN, R.J., 2006. Dynamic patch mosaics and channel movement in an unconfined river valley of the Olympic Mountains. Freshw. Biol. 51, 523–544. https://doi.org/10.1111/j.1365-2427.2006.01513.x

LAUER, J. W. AND PARKER, G. 2008. Net local removal of floodplain sediment by river meander migration. Geomorphology 96(1-2), 123-149.

LAUTRIDOU, J.P., AUFFRET, J.-P., BALTZER, A., CLET, M., LECOLLE, F., LEFEBVRE, D., LERICOLIAS, G., ROBLIN-JOUVE, A., LALESCU, S., CARPENTIER, G., DESCOMBES, J.-C., OCCHIETTI, S., ROUSSEAU, D., DESCOMBES, J.-C., 1999. Le fleuve Seine, le fleuve Manche. Bull. Soc. Géol. Fr. 170 (4), 545–558.

LECCE, S.A., 1997. Spatial patterns of historical overbank sedimentation and floodplain evolution, Blue river, Wisconsin. Geomorphology 18, 265–277. https://doi.org/10.1016/S0169-555X(96)00030-X

LE COZ, J., MICHALKOVÁ, M., HAUET, A., COMAJN M., DRAMAIS, G., HOLUBOVÁ, K., PIÉGAY, H., PAQUIER, A., 2010. Morphodynamics of the exit of a cutoff meander: experimental findings from field and laboratory studies. Earth Surface Processes and Landforms 35, 249-261.

LEDDY, J.O., ASHWORTH, P.J., BEST, J.L., 1993. Mechanisms of anabranch avulsion within gravel-bed braided rivers: observations from a scaled physical model. Geol. Soc. Lond. Spec. Publ. 75, 119–127. https://doi.org/10.1144/GSL.SP.1993.075.01.07

LEEDER, M.R., 1978. A quantitative stratigraphic model for alluvium with special reference to channel deposit density and interconnectedness. *In*: Fluvial Sedimentology, (eds) A.D. Miall, 5:587–96. Calgary: Can. Soc. Petrol. Geol.

LEMAY, M., 2019. Transposition à l'environnement turbiditique chenalisé d'un modèle de systèmes fluviatiles méandriformes pour la modélisation de réservoirs. (Doctoral dissertation, MINES ParisTech). Retrieved from theses.fr (http://theses.fr/2018PSLEM033).

LEOPOLD, L.B. AND MADDOCK, T. 1953. Hydraulic geometry of stream channels and some physiographic implications. U.S. Geol. Surv. Prof. Pap., 252.

LEOPOLD, L.B. AND WOLMAN, M.G., 1957. River Channel Patterns: Braided, Meandering and Straight. Physiographic and Hydraulic Studies of Rivers, Geological Survey Professional Paper 282, 35-85.

LEOPOLD, L.B. AND WOLMAN, M.G., 1960. River meanders. Geol. Soc. Am. Bull. 71, 769-793. https://doi.org/10.1130/0016-7606(1960)71[769:RM]2.0.CO;2

LEWIS, G. W. AND LEWIN, J., 1983. Alluvial Cutoffs in Wales and the Borderlands. Modern and Ancient Fluvial Systems: International Association of Sedimentologists Special Publication 6, 145-154.

LI, Z., WANG, H., NITTROUER, J.A., BI, N., WU, X., CARLSON, B., 2020. Modeling the infilling process of an abandoned fluvial-deltaic distributary channel: An example from the Yellow River delta, China. Geomorphology 361, 107204. https://doi.org/10.1016/j.geomorph.2020.107204

LIÉBAULT, F. AND PIÉGAY, H., 2002. Causes of 20th century channel narrowing in mountain and piedmont rivers of southeastern France: Causes of channel narrowing in SE France. Earth Surf. Process. Landf. 27, 425–444. https://doi.org/10.1002/esp.328

LINDNER, C. P., 1953. Diversion from alluvial streams: Am. Soc. Civil Engineers Proc., 118, 245-288.

LOPEZ, S., COJAN, I., RIVOIRARD, J., GALLI, A., 2008. Process-based stochastic modelling: meandering channelized reservoirs. Special Publication of the International Association of Sedimentologists, 40, 139-144.

MAKASKE, B., 2001. Anastomosing rivers: a review of their classification, origin and sedimentary products. Earth-Sci. Rev. 53, 149–196. https://doi.org/10.1016/S0012-8252(00)00038-6

MAKASKE, B., SMITH, D.G., BERENDSEN, H.J.A., 2002. Avulsions, channel evolution and floodplain sedimentation rates of the anastomosing upper Columbia River, British Columbia, Canada. Sedimentology 49, 1049–1071. https://doi.org/10.1046/j.1365-3091.2002.00489.x

MARRA, W.A., PARSONS, D.R., KLEINHANS, M.G., KEEVIL, G.M., THOMAS, R.E., 2014. Near-bed and surface flow division patterns in experimental river bifurcations. Water Resources Research 50, 1506–1530. https://doi.org/10.1002/2013WR014215

MAKASKE, B. AND WEERTS, H.J.T., 2005. Muddy lateral accretion and low stream power in a sub-recent confined channel belt, Rhine-Meuse delta, central Netherlands. Sedimentology 52, 651–668. https://doi.org/10.1111/j.1365-3091.2005.00713.x

MARTIN, Y., 2003. Evaluation of bed load transport formulae using field evidence from the Vedder River, British Columbia. Geomorphology 53, 75–95.

MARTIN, Y. AND CHURCH, M., 1995. Bed-material transport estimated from channel surveys: Vedder River, British Columbia. Earth Surface Processes and Landforms 20, 347–361.

MCCARTHY, T.S., ELLERY, W.N., STANISTREET, I.G., 1992. Avulsion mechanisms on the Okavango fan, Botswana: the control of a fluvial system by vegetation. Sedimentology 39, 779–795. https://doi.org/10.1111/j.1365-3091.1992.tb02153.x

MEGNIEN, CL., BERTON, Y., DASSIBAT, C., DIFFRE, PH., DUERMAEL, G., JONQUET, P., RAMPON, G., STANUDIN, B., RAMON, S., BEAUFOND, S., BERGER, G., CARDONA, A., MARQUET, G., MERCIER, F., PINELLI, M., RENAULT, PH., TURLAND, M., MARREC, C., MULLER, J.-P., OLTRA, M., STRAT, P., MAZOIT, M., VILLEMAINE, H., 1965. Possibilités aquifères des alluvions du val de Seine entre Nogent-s-Seine et Montereau. Ministère de l'industrie, BRGM, Paris (DSGR.65. A76), 1065 pp.

METIVIER, F., LAJEUNESSE, E., DEVAUCHELLE, O., 2017. Laboratory rivers: Lacey's law, threshold theory, and channel stability. Earth Surf. Dynam., 5, 187–198, https://doi.org/10.5194/esurf-5-187-2017.

MIALL, A.D., 1977. A review of the braided river depositional environment. Earth Sci. Rev. 13, 1-62.

MIALL, A.D., 1979. Mesozoic and Tertiary geology of Banks Island, Arctic Canada. Geological Survey of Canada paper 79-9, 1-25.

MIALL, A.D., 1996. The Geology of Fluvial Deposits. Springer Berlin Heidelberg, Berlin, Heidelberg. https://doi.org/10.1007/978-3-662-03237-4

MICHELI, E.R. AND LARSEN, E.W., 2011. River channel cutoff dynamics, Sacramento River, California, USA. River Res. Appl. 27, 328–344. https://doi.org/10.1002/rra.1360

MIÉJAC, E. AND ARTHUIS, R., 2007. La Boire Torse, la Loire entre Ingrandes et Ancenis, étude historique et géomorphologique, rapport d'étude, 2005.

MIORI, S., HARDY, R.J., LANE, S.N., 2012. Topographic forcing of flow partition and flow structures at river bifurcations: Topographic flow forcing at bifurcations. Earth Surf. Process. Landf. 37, 666–679. https://doi.org/10.1002/esp.3204

MIORI, S., REPETTO, R., TUBINO, M., 2006. A one-dimensional model of bifurcations in gravel bed channels with erodible banks. Water Resour. Res. 42. https://doi.org/10.1029/2006WR004863

MOHRIG, D., HELLER, P.L., PAOLA, C. , LYONS, W.J., 2000, Interpreting avulsion process from ancient alluvial sequences: Guadalope-Matarranya system (Northern Spain) and Wasatch formation (Western Colorado). Bulletin of the Geological Society of America, 112-12, 1787-1803. DOI: 10.1130/0016-7606(2000)112<1787:IAPFAA>2.0.CO;

MONTGOMERY, D.R. AND PIÉGAY, H., 2003. Wood in rivers: interactions with channel morphology and processes. Geomorphology 51, 1–5. https://doi.org/10.1016/S0169-555X(02)00322-7

MOROZOVA, G.S. AND SMITH, N.D., 2000. Holocene avulsion styles and sedimentation patterns of the Saskatchewan River, Cumberland Marshes, Canada. Sediment. Geol. 130, 81–105. https://doi.org/10.1016/S0037-0738(99)00106-2

MUNIR, S., 2011. Role of Sediment Transport in Operation and Maintenance of Supply and Demand Based Irrigation Canals: Application to Machai Maira Branch Canals. UNESCO-IHE PhD Thesis, Delft, the Netherlands.

NANSON, G.C., 1980. Point bar and floodplain formation of the meandering Beatton River, northeastern British Columbia, Canada. Sedimentology 27, 3–29. https://doi.org/10.1111/j.1365-3091.1980.tb01155.x

NANSON, G.C. AND KNIGHTON, A.D., 1996. Anabranching rivers: their cause, character and classification. Earth Surface Processes and Landforms 21, 217–239.

NEARY, V. S., SOTIROPOULOS, F., ODGAARD, A. J., 1999. Three-Dimensional Numerical Model of Lateral-Intake Inflows. J. Hydraul. Eng. 125, 126–140, https://doi.org/10.1061/(ASCE)0733-9429(1999)125:2(126).

NICHOLAS, A.P. AND WALLING, D.E., 1997. Modelling flood hydraulics and overbank deposition on river floodplains. Earth Surf. Process. Landf. 22, 59–77. https://doi.org/10.1002/(SICI)1096-9837(199701)22:1<59::AID-ESP652>3.0.CO;2-R

NITTROUER, J.A., SHAW, J., LAMB, M.P., MOHRIG, D., 2012. Spatial and temporal trends for water-flow velocity and bed-material sediment transport in the lower Mississippi River. Geol. Soc. Am. Bull. 124, 400–414. https://doi.org/10.1130/B30497.1

NOVAK, P., MOFFAT, A., NALLURI, C., NARAYANAN, R., 1990. Hydraulic Structures, Pitman, London, UK, 546 pp.

NOVITZKY, R .P., SMITH, R. D., FRETWELL J.D., 1996. Wetland functions, values, and assessment. US Geological Survey Water Supply Paper 2425, 79-86.

PAAS W. AND TEUNISSEN, D., 1975. Die geologische Geschichte der Duffel, eine linksniederrheinische Flussaue zwischen Kleve und Nimwegen. Mededelingen van de Afdeling Biogeologie van de Sectie Biologie van de K.U.Nijmegen 7.

PAOLA, C. AND MOHRIG, D., 1996. Paleohydraulics revisited: Paleoslope estimation in coarse-grained braided rivers. Basin Research 8, 243-254.

PARKER, G., SHIMIZU, Y., WILKERSON, G.V., EKE, E.C., ABAD, J.D., LAUER, J.W., PAOLA, C., DIETRICH, W.E., VOLLER, V.R., 2011. A new framework for modeling the migration of meandering rivers. Earth. Surf. Proc. Land. 36, 70–86. 10.1046/j .1365 -2117 .1996 .00253 .x.

PEAKALL, J., ASHWORTH, P.J., BEST, J.L., 2007. Meander-Bend Evolution, Alluvial Architecture, and the Role of Cohesion in Sinuous River Channels: A Flume Study. Journal of Sedimentary Research 77, 197–212. https://doi.org/10.2110/jsr.2007.017

PÉREZ-ARLUCEA, M. AND SMITH, N.D., 1999. Depositional patterns following the 1870s avulsion of the Saskatchewan River (Cumberland Marshes, Saskatchewan, Canada). J. Sediment. Res. 69, 62–73. https://doi.org/10.2110/jsr.69.62

PETERSEN, M.S., 1963. Hydraulic aspects of Arkansas River stabilization. Journal of the Waterways and Harbors Division 89(4), 29–65.

PETIT, C., CHARRONDIÈRE-LEWIS, P., COJAN, I., CRUZ, F., DEBORDE, G., DELEPLANCQUE, B., DUROST, R., FECHNER, K., FONTANA, L., FROUIN, M., GOUGE, P., GRANAI, S., GRIMAUD, J.-L, PELTIER, V., RIQUIER, V., SZEWCZYK, L., TEGEL, W., VANMORKERKE, J., *in press.* Relations sociétés – milieux en Petite-Seine du Mésolithique à la fin du Moyen Âge : nouvelles problématiques et résultats récents d'archéologie environnementale. *In:* V. Riquier (eds.), L'Aube, un espace clé sur le cours de la Seine.

PIÉGAY, H., BORNETTE, G., CITTERIO, A., HÉROUIN, E., MOULIN, B., STATIOTIS, C., 2000. Channel instability as a control on silting dynamics and vegetation patterns within perifluvial aquatic zones. Hydrological Processes 14, 3011–3029. https://doi.org/10.1002/1099-1085(200011/12)14:16/17<3011::AID-HYP132>3.0.CO;2-B

PIÉGAY, H., BORNETTE, G., GRANTE, P., 2002. Assessment of silting-up dynamics of eleven cut-off channel plugs on a free-meandering river (Ain River, France). *In*: Allison, R.J. (Ed.), Applied Geomorphology. Wiley, New York, 227–247.

PIÉGAY, H., HUPP, C.R., CITTERIO, A., DUFOUR, S., MOULIN, B., WALLING, D.E., 2008. Spatial and temporal variability in sedimentation rates associated with cutoff channel infill deposits: Ain River, France: Water Resour. Res. 44. W05420 https://doi.org/10.1029/2006WR005260

PIÉGAY, H., WALLING, D.E., LANDON, N., HE, Q., LIÉBAULT, F., PETIOT, R., 2004. Contemporary changes in sediment yield in an alpine mountain basin due to afforestation (the upper Drôme in France). CATENA 55, 183–212. https://doi.org/10.1016/S0341-8162(03)00118-8

PLINT, A. G., 1995. Sedimentary facies analysis: a tribute to the research and teaching of Harold G. Reading. Special publication of the International Association of Sedimentologists. Blackwell Science, Oxford, England ; Cambridge, Mass, 400 pp.

PRANTER, M.J., ELLISON, A.I., COLE, R.D., PATTERSON, P.E., 2007. Analysis and modeling of intermediate-scale reservoir heterogeneity based on a fluvial point-bar outcrop analog, Williams Fork Formation, Piceance Basin, Colorado. AAPG Bull. 91, 1025–1051. https://doi.org/10.1306/02010706102

QIAN, N., 1990. Fluvial processes in the lower Yellow River after levee breaching at Tongwaxiangin 1855. Int. J. Sediment Res. 5, 1–13

REITZ, M.D., JEROLMACK, D.J., SWENSON, J.B., 2010. Flooding and flow path selection on alluvial fans and deltas. Geophys. Res. Lett. 37, L06401. https://doi.org/10.1029/2009GL041985

REITZ, M.D., PICKERING, J.L., GOODBRED, S.L., PAOLA, C., STECKLER, M.S., SEEBER, L., AKHTER, S.H., 2015. Effects of tectonic deformation and sea level on river path selection: Theory and application to the Ganges-Brahmaputra-Meghna River Delta: Tectonics and river path selection. J. Geophys. Res. Earth Surf. 120, 671–689. https://doi.org/10.1002/2014JF003202

REYNOLDS, J. AND ROYALL, D., 2020. Morphological Response to Discharge Reduction in a Partially Abandoned Channel of the Catawba River, North Carolina, USA. Geomorphology 351, 106959.
RICHARDS, D. AND KONSOER, K., 2020. Morphologic adjustments of actively evolving highly curved neck cutoffs. Earth Surface Processes and Landforms 45, 1067–1081. https://doi.org/10.1002/esp.4763
ROBERT, A., 2003. River processes: an introduction to fluvial dynamics. Arnold, London : New York : Distributed in the United States by Oxford University Press.
RODRIGUES, S., BREHERET, J.-G., MACAIRE, J.-J., MOATAR, F., NISTORAN, D., JUGE, P., 2006. Flow and sediment dynamics in the vegetated secondary channels of an anabranching river: The Loire River (France). Sediment. Geol. 186, 89–109. https://doi.org/10.1016/j.sedgeo.2005.11.011
ROLLET, A.J., 2007. Etude et gestion de la dynamique sedimentaire d'un troncon alluvial a l'aval d'un barrage: le cas de la basse vallee de l'Ain. PhD University Jean Moulin Lyon 3, Lyon, 305 pp.
ROLLET, A.J., DUFOUR, S., PIEGAY, H., 2005. Programme LIFE Nature. Conservation des habitats créés par la dynamique de la rivière d'Ain. CNRS–UMR 5600, Lyon.
ROLLET, A.J., PIÉGAY, H., DUFOUR, S., BORNETTE, G., PERSAT, H., 2013. Assessment of consequences of sediment deficit on a gravel river bed downstream of dams in restoration perspectives: application of a multicriteria, hierarchical and spatially explicit diagnosis. River Research and Applications 30, 939-953.
ROWLAND, J.C., LEPPER, K., DIETRICH, W.E., WILSON, C.J., SHELDON, R., 2005. Tie channel sedimentation rates, oxbow formation age and channel migration rate from optically stimulated luminescence (OSL) analysis of floodplain deposits. Earth Surf. Process. Landf. 30, 1161–1179. https://doi.org/10.1002/esp.1268
RUST, B.R., 1978. A classification of alluvial channel systems. In: Fluvial Sedimentology (Ed. A. D. Miall, Mem. Can. Soc. Petrol. Geol. 5, 187-198.
RUST, B.R., 1981. Sedimentation in an arid-zone anastomosing fluvial system: Cooper's Creek, Central Australia. Journal of Sedimentary Petrology 51, 745–755.
SAHOO, H., GANI, M.R., GANI, N.D., HAMPSON, G.J., HOWELL, J.A., STORMS, J.E.A., MARTINIUS, A.W., BUCKLEY, S.J., 2020. Predictable patterns in stacking and distribution of channelized fluvial sand bodies linked to channel mobility and avulsion processes. Geology 48, 903-907. https://doi.org/10.1130/G47236.1
SALTER, G., PAOLA, C., VOLLER, V. R., 2018. Control of Delta Avulsion by Downstream Sediment Sinks. J. Geophys. Res.-Earth, 123, 142– 166.
SALTER, G., VOLLER, V. R., PAOLA, C., 2019. How does the downstream boundary affect avulsion dynamics in a laboratory bifurcation? Earth Surf. Dynam., 7, 911–927, https://doi.org/10.5194/esurf-7-911-2019.
SAUCIER, R.T., 1967. Geological inverstigation of the Boeuf-Tensas Basin, Lower Mississippi Valley. Technical report 3-757. U.S. Army Corps of Engineers, Mississippi River Commission, Vicksburg, MS.
SAUCIER, R., T., 1969. Geological investigation of the Mississippi River area, Artonish to Donaldsonville, La. Technical report No. S-69-4, U.S. Army Engineer Waterways Experiment Station, Vicksburg, MS.
SAUCIER, R.T., 1994. Geomorphology and Quaternary geologic history of the Lower Mississippi Valley. U.S. Army Corps of Engineers, Mississippi River Commission, Vicksburg, MS.
SCHIELEN, R.M.J. AND BLOM, A., 2018. A reduced complexity model of a gravel-sand river bifurcation: Equilibrium states and their stability. Advances in Water Resources 121, 9–21. https://doi.org/10.1016/j.advwatres.2018.07.010
SCHUMANN, R.R., 1989. Morphology of Red Creek, Wyoming, an arid-region anastomosing channel system. Earth Surf. Process. Landf. 14, 277–288. https://doi.org/10.1002/esp.3290140404
SCHUMM, S,. A., 1960. The effect of sediment type on the shape and stratification of some modern fluvial deposits. American Journal of Sciences, 258, 177-184.
SCHUMM, S.A., 1985. Patterns of alluvial rivers. Annual Review of Earth and Planetary Sciences 13, 5–27.
SCHUMM, S.A. AND KHAN H.R., 1972. Experimental Study of Channel Patterns.Geological Society of America Bulletin, 83, 55–70.
SCHWENDEL, A.C., NICHOLAS, A.P., AALTO, R.E., SAMBROOK SMITH, G.H., BUCKLEY, S., 2015. Interaction between meander dynamics and floodplain heterogeneity in a large tropical sand-bed river: the Rio Beni, Bolivian Amazon. Earth Surface Processes and. Landforms 40, 2026–2040. https://doi.org/10.1002/esp.3777
SCHWENK, J. AND FOUFOULA-GEORGIOU, E., 2016. Meander cutoffs nonlocally accelerate upstream and downstream migration and channel widening: Nonlocal Influence of Cutoffs. Geophys. Res. Lett. 43, 12,437-12,445. https://doi.org/10.1002/2016GL071670

SEAR, D.A., MILLINGTON, C.E., KITTS, D.R., JEFFRIES, R., 2010. Logjam controls on channel:floodplain interactions in wooded catchments and their role in the formation of multi-channel patterns. Geomorphology 116, 305–319. https://doi.org/10.1016/j.geomorph.2009.11.022

SEIZILLES, G., LAJEUNESSE, E., DEVAUCHELLE, O., BAK, M., 2013. Crossstream diffusion in bedload transport. Phys. Fluids, 26, 1–13.

SEMINARA, G., 2006. Meanders. Journal of Fluid Mechanics 554: 271-297.

SHI, C., ZHANG, L., XU, J., GUO, L., 2010. Sediment load and storage in the Lower Yellow River during the Late Holocene. Geogr. Ann. Ser. Phys. Geogr. 92, 297–309. https://doi.org/10.1111/j.1468-0459.2010.00396.x

SHIELDS, F.D. AND ABT, S.R., 1989. Sediment deposition in cutoff meander bends and implications for effective management. Regul. River 4, 381–396.

SHIELDS, F. D., NUNNALLY, N. R., ASCE, A. M., 1984. Environmental aspects of clearing and snagging. J. Environ. Eng., 110, 152–165.

SIDORCHUK, A., 2001. Fluvial response to the Late Valdai/Holocene environmental change on the East European Plain. Glob. Planet. Change 28, 303–318. https://doi.org/10.1016/S0921-8181(00)00081-3

SIDORCHUK, A.Y., PANIN, A.V., BORISOVA, O.K., 2009. Morphology of river channels and surface runoff in the Volga River basin (East European Plain) during the Late Glacial period. Geomorphology 113, 137–157. https://doi.org/10.1016/j.geomorph.2009.03.007

SLINGERLAND, R. AND SMITH, N.D., 1998. Necessary conditions for a meandering-river avulsion. Geology 26, 435-438. https://doi.org/10.1130/0091-7613(1998)026<0435:NCFAMR>2.3.CO;2

SLINGERLAND, R. AND SMITH, N.D., 2004. River avulsions and their deposits. Annu. Rev. Earth and Planetary Sciences 32, 257–285. https://doi.org/10.1146/annurev.earth. 32.101802.120201

SMITH, C.E., 1998. Modeling high sinuosity meanders in a small flume. Geomorphology 25, 19–30. https://doi.org/10.1016/S0169-555X(98)00029-4

SMITH, N.D., CROSS, T.A., DUFFICY, J.P., CLOUGH, S.R., 1989. Anatomy of an avulsion. Sedimentology 36, 1–23. https://doi.org/10.1111/j.1365-3091.1989.tb00817.x

SMITH, D.G., HUBBARD, S.M., LAVIGNE, J.R., LECKIE, D.A., FUSTIC, M., 2011. Stratigraphy of Counter-Point-Bar and Eddy-Accretion Deposits in Low-Energy Meander Belts of the Peace-Athabasca Delta, Northeast Alberta, Canada, *In*: From River to Rock Record: The Preservation of Fluvial Sediments and Their Subsequent Interpretation. SEPM Society for Sedimentary Geology. https://doi.org/10.2110/sepmsp.097.143

SMITH, N.D., MCCARTHY, T.S., ELLERY, W.N., MERRY, C.L., RÜTHER, H., 1997. Avulsion and anastomosis in the panhandle region of the Okavango Fan, Botswana. Geomorphology 20, 49–65. https://doi.org/10.1016/S0169-555X(96)00051-7

SMITH, N., D. AND PÉREZ-ARLUCEA, M., 1994. Fine-grained splay deposition in the avulsion belt of the Lower Saskatchewan River, Canada. Journal of Sedimentary Research, 64(2), 159-168.

SMITH, F., L. AND RUSS, D., P., 1974. Geological investigation of the Lower Red River – Atchafayla Basin area. Technical report No. S-74-5, U.S. Army Engineer Waterways Experiment Station, Vicksburg, MS.

SMITH, N.D., SLINGERLAND, R.L., PÉREZ-ARLUCEA, M., MOROZOVA, G.S., 1998. The 1870s avulsion of the Saskatchewan River. Can. J. Earth Sci. 35, 453–466. https://doi.org/10.1139/e97-113

SMITH, D.G. AND SMITH, N.D., 1980. Sedimentation in anastomosed river systems: examples from alluvial valleys near Banff,Alberta. Journal of Sedimentary Petrology 50, 157–164.

SONGEUX, G., 1888. Archives départementales de Seine-et-Marne, manuscrit inédit, 30Z155.

SORRELLS, R.M. AND ROYALL, D., 2014. Channel bifurcation and adjustment on the upper Yadkin River, North Carolina (USA). Geomorphology 223, 33–44.

STOUTHAMER, E., 2001. Sedimentary products of avulsions in the Holocene Rhine–Meuse Delta, The Netherlands. Sediment. Geol. 145, 73–92. https://doi.org/10.1016/S0037-0738(01)00117-8

STOUTHAMER, E., 2005. Reoccupation of Channel Belts and its Influence on Alluvial Architecture in the Holocene Rhine-Meuse Delta, the Netherlands. *In*: Giosan, L., Bhattacharya, J.P. (eds.), River Deltas–Concepts, Models, and Examples. SEPM Society for Sedimentary Geology. https://doi.org/10.2110/pec.05.83.0319

STOUTHAMER, E. AND BERENDSEN, H.J.A., 2000. Factors Controlling the Holocene Avulsion History of the Rhine-Meuse Delta (The Netherlands). J. Sediment. Res. 70, 1051–1064. https://doi.org/10.1306/033000701051

STOUTHAMER, E. AND BERENDSEN, H.J.A., 2001. Avulsion Frequency, Avulsion Duration, and Interavulsion Period of Holocene Channel Belts in the Rhine-Meuse Delta, The Netherlands. J. Sediment. Res. 71, 589–598. https://doi.org/10.1306/112100710589

STOUTHAMER E., COHEN K.M., GOUW M.J.P. 2011. Avulsion and its Implications for Fluvial-deltaic Architecture: Insights from the Holocene Rhine- Meuse delta, SEPM Special Publication 97. SEPM (Society for Sedimentary Geology): Tulsa, OK; 215–231.

SZEWCZYK, L., 2020. Relevant data for the Esurf paper "Experimental evidence for bifurcation angles control on abandoned channel fill geometry". OSF data repository, https://doi.org/10.17605/OSF.IO/MTR69.

SZEWCZYK, L., GRIMAUD, J.-L., COJAN, I., 2020. Experimental evidence for bifurcation angles control on abandoned channel fill geometry. Earth Surface Dynamics, 8, 275-288. https://doi.org/10.5194/esurf-8-275-2020.

SURIAN, N. AND CISOTTO, A., 2007. Channel adjustments, bedload transport and sediment sources in a gravel-bed river, Brenta River, Italy. Earth Surface Processes and Landforms 32, 1641–1656.

SUTTON, R.I., NICHOLAS, A.P., WALLING, D.E., 2004. Monitoring and modelling flow and suspended sediment transport processes in alluvial cutoffs. IAHS-AISH Publication. 410-416.

TAL, M., FREY, P., KIM, W., LAJEUNESSE, E., LIMARE, A., METIVIER, F., 2012. The Use of Imagery in Laboratory Experiments, in: Carbonneau, P.E., Piégay, H. (eds.), Fluvial Remote Sensing for Science and Management. John Wiley & Sons, Ltd, Chichester, UK, pp. 299–321. https://doi.org/10.1002/9781119940791.ch13

THOMPSON, D. M., 2003. A geomorphic explanation for a meander cutoff following channel relocation of a coarse-bedded river. Environmental Management 31, 385-400.

TOONEN, W.H.J., KLEINHANS, M.G., COHEN, K.M., 2012. Sedimentary architecture of abandoned channel fills: Earth Surf. Process. Landf. 37, 459–472. https://doi.org/10.1002/esp.3189

TÖRNQVIST, T.E., 1993. Fluvial sedimentary geology and chronology of the Holocene Rhine–Meuse delta, The Netherlands. Ph.D. thesis, Utrecht University, KNAG/Faculteit Ruimtelijke Wetenschappen Universiteit Utrecht, Netherlands Geographical Studies 166, 176 pp.

TÖRNQVIST, T.E., 1994. Middle and late Holocene avulsion history of the River Rhine (Rhine-Meuse delta, Netherlands). Geology 22, 711-714. https://doi.org/10.1130/0091-7613(1994)022<0711:MALHAH>2.3.CO;2

TYLER, N., AND R. J. FINLEY, 1991. Architectural controls on the recovery of hydrocarbons from sandstone reservoirs, in: A. D. Miall and N. Tyler (eds.), The three-dimensional facies architecture of terrigenous clastic sediments, and its implications for hydrocarbon discovery and recovery. SEPM Concepts and Models in Sedimentology and Paleontology 3, 1–5.

VAN DENDEREN, R.P., SCHIELEN, R.M.J., BLOM, A., HULSCHER, S.J.M.H., KLEINHANS, M.G., 2018. Morphodynamic assessment of side channel systems using a simple one-dimensional bifurcation model and a comparison with aerial images: Morphodynamic assessment of side channel systems. Earth Surface Processes and Landforms 43, 1169–1182. https://doi.org/10.1002/esp.4267

VAN DER MARK, C.F. AND MOSSELMAN, E., 2012. Effects of helical flow in one-dimensional modelling of sediment distribution at river bifurcations. Earth Surf. Process. Landf. 38, 502–511. https://doi.org/10.1002/esp.3335

VAN DIJK, W.M., SCHUURMAN, F., VAN DE LAGEWEG, W.I., KLEINHANS, M.G., 2014. Bifurcation instability and chute cutoff development in meandering gravel-bed rivers. Geomorphology 213, 277–291. https://doi.org/10.1016/j.geomorph.2014.01.018

VAN DINTER, M., COHEN, K.M., HOEK, W.Z., STOUTHAMER, E., JANSMA, E., MIDDELKOOP, H., 2017. Late Holocene lowland fluvial archives and geoarchaeology: Utrecht's case study of Rhine river abandonment under Roman and Medieval settlement. Quaternary Science Reviews 166, 227–265. https://doi.org/10.1016/j.quascirev.2016.12.003

VAN VEEN, J., VAN DER SPEK, A.J.F., STIVE, M.J.F., ZITMAN, T., 2005. Ebb and flood channel systems in the Netherlands tidal waters. J. Coastal Res., 21, 1107–1120.

VELLA, C., FLEURY, T.-J., RACCASI, G., PROVANSAL, M., SABATIER, F., BOURCIER, M., 2005. Evolution of the Rhône delta plain in the Holocene. Mar. Geol. 222–223, 235–265. https://doi.org/10.1016/j.margeo.2005.06.028

VIENNOT, P., DUCHARNE, A., HABETS, F., LAMY, F., LEDOUX, E., 2009. Hydrogéologie du bassin de la Seine, comprendre et anticiper le fonctionnement hydrodynamique du bassin pour une gestion durable de la ressource. Agence de l'eau Seine-Normandie, Fascicule PIREN. v. 2, 55 p.

WALKER, R.G., 1984. Facies models, 2nd ed. Eds Geoscience Canada reprint series. Geological Association of Canada Publications, Business and Economic Service, Toronto, Ontario, 317 pp.

WALLING, D.E., OWENS, P.N., FOSTER, I.D.L., LEES, J.A., 2003. Changes in the fine sediment dynamics of the Ouse and Tweed basins in the UK over the last 100-150 years. Hydrol. Process. 17, 3245–3269. https://doi.org/10.1002/hyp.1385

WANG, Z.B., DE VRIES, M., FOKKINK, R.J., LANGERAK, A., 1995. Stability of river bifurcations in ID morphodynamic models. J. Hydraul. Res. 33, 739–750. https://doi.org/10.1080/00221689509498549

WARD, J. V., TOCKNER, K, SCHIEMER, F., 1999. Biodiversity of floodplain river ecosystems: ecotones and connectivity. Regulated Rivers, Research and Management 15, 125-139.
WILLIAMS, G.P. 1978. Bankfull discharge of rivers. Water Resources Research, 14: 1141-1154.
WILLIAMS, G.P. 1986. River Meanders and Channel Size. Journal of Hydrology, 88: 147-164.
WILLIS, B.J., 1989. Palaeochannel reconstructions from point bar deposits: a three-dimensional perspective. Sedimentology 36, 757–766. https://doi.org/10.1111/j.1365-3091.1989.tb01744.x
WILLIS, B.J., BEHRENSMEYER, A.,K., 1994. Architecture of Miocene overbank deposits in northern Pakistan. J. Sediment. Res. 64, 60-67.
WILLIS, B.J. AND TANG, H., 2010. Three-Dimensional Connectivity of Point-Bar Deposits. J. Sediment. Res. 80, 440–454. https://doi.org/10.2110/jsr.2010.046
WILSON, C.A. AND GOODBRED, S.L., 2015. Construction and Maintenance of the Ganges-Brahmaputra-Meghna Delta: Linking Process, Morphology, and Stratigraphy. Annu. Rev. Mar. Sci. 7, 67–88. https://doi.org/10.1146/annurev-marine-010213-135032
WINTERBOTTOM, S.J AND GILVEAR, D.J. 1997. Quantification of channel bed morphology in gravel-bed rivers using airborne multispectral imagery and aerial photography, Regulated Rivers: Research & Management 13: 489–499.
WOLMAN, M.G., 1954. A method of sampling coarse river-bed material. Transactions American Geophysical Union 35-6, 951-956.
WOLMAN, G. AND LEOPOLD, L.B., 1957. River flood plains: Some observations on their formation. Geological Survey Professional Paper 282, 87-104.
WREN, D.G., DAVIDSON, G.R., WALKER, W.G., GALICKI, S.J., 2008. The evolution of an oxbow lake in the Mississippi alluvial floodplain. J. Soil Water Conserv. 63, 129–135. https://doi.org/10.2489/jswc.63.3.129
WU, X., WANG, H., BI, N., NITTROUER, J.A., XU, J., CONG, S., CARLSON, B., LU, T., LI, Z., 2020. Evolution of a tide-dominated abandoned channel: A case of the abandoned Qingshuigou course, Yellow River. Marine Geology 422, 106116. https://doi.org/10.1016/j.margeo.2020.106116
ZINGER, J.A., RHOADS, B.L., BEST, J.L., 2011. Extreme sediment pulses generated by bend cutoffs along a large meandering river. Geograhy and Geophysics Information Science, Geology, Natural Resources and Environmental Sciences, 10, 675-678. 10.1038/ngeol260
ZOLEZZI, G., BERTOLDI, W., TUBINO, M., 2006. Morphological Analysis and Prediction of River Bifurcations, in: Sambrook Smith, G.H., Best, J.L., Bristow, C.S., Petts, G.E. (eds.), Braided Rivers. Blackwell Publishing Ltd., Oxford, UK, 233–256. https://doi.org/10.1002/9781444304374.ch11

Appendix A: Supplementary material for Section 2.2

Also available online at: https://doi.org/10.5194/esurf-8-275-2020-supplement.

Movies of the experiments and topography data (point clouds) of the final state of the experiments are available in the OSF data repository

(https://doi.org/10.17605/OSF.IO/MTR69; Szewczyk, 2020).

Experiment	Bifurcation angle α (°)	Distributary 1						Distributary 2						Sandplug			
		β1 (°)	Bed Slope S1 (%)	Equilibrium water discharge ($L.h^{-1}$)	Shields parameter θ	Froude number	Reynolds number	β2 (°)	Bed Slope S2 (%)	Equilibrium water discharge ($L.h^{-1}$)	Shields parameter θ	Froude number	Reynolds number	Length / channel width	Sandplug volume (cL)	Total sand volume (cL)	Sandplug slope (%)
1	30	10	1.468	-	0.213	-	-	20	1.418	-	0.123	-	-	-	-	-	-
2				-	0.213	-	-			-	0.082	-	-	-	-	-	-
3		15	1.443	153.4	0.209	0.94	833	15	1.443	146.6	0.209	0.94	833	-	-	-	-
4				150.6	0.209	0.999	874			149.4	0.084	3.74	952	-	-	-	-
5		0	1.48	250	0.172	1.31	864	30	1.312	50	0.114	2.03	910	10.5	13.09	-	2.5/1
6				262	0.214	1.24	1098			38	0.076	2.54	646	6.625	8.84	13.25	3.9/2.5
7	45	22.5	1.405	150.6	0.204	1.85	829	22.5	1.405	149.4	0.204	2.19	982	-	-	-	-
8				161.4	0.204	0.987	874			138.6	0.244	0.894	792	-	-	-	-
9		0	1.48	299	0.172	2.08	1377	45	1.193	1	0.138	0.54	359	9.625	12.38	-	2.7/1
10				274.2	0.214	6.296	1604			25.8	0.069	1.14	290	5.25	9.12	18.86	4/1.1
11	60	30	1.312	181.5	0.190	1.75	1157	30	1.312	118.5	0.114	1.35	604	-	-	-	-
12		0	1.48	270.1	0.214	0.63	561	60	0.98	29.9	0.085	2.685	1202	8	9.45	-	4.3/0.6
13				294.3	0.214	1.39	1232			5.7	0.085	1.06	472	3.4	6.16	17.51	5/3.4
14	90	45	1.193	193.6	0.138	1.69	1120	45	1.193	106.4	0.207	0.51	568	-	-	-	-
15		0	1.48	294.3	0.172	1.45	957	90	0	5.7	0.116	1.18	779	4.375	6.31	-	7.8/3.4
16				258	0.214	1.593	1411			42	0.058	1.14	290	1.845	2.76	12.61	4/3.4
17				299	0.214	1.64	1456		1	1	0.087	0.51	229	7.375	7.32	-	10.6/2.2
18				294.3	0.214	1.47	1299		1.282	5.7	0.149	0.58	383	10	7.87	-	3.4
19				291.6	0.214	1.83	1620		2.56	8.4	0.074	0.581	55	11.125	4.8	-	1.45

Table A1: List of experiments and detail of all associated parameters.

Figure A1: Final deposits of the 8 asymmetrical experiments, without and with levee breach. **(a-b)** β2 = 30°. **(c-d)** β2 = 45°. **(e-f)** β2 = 60°. **(g-h)** β2 = 90°.

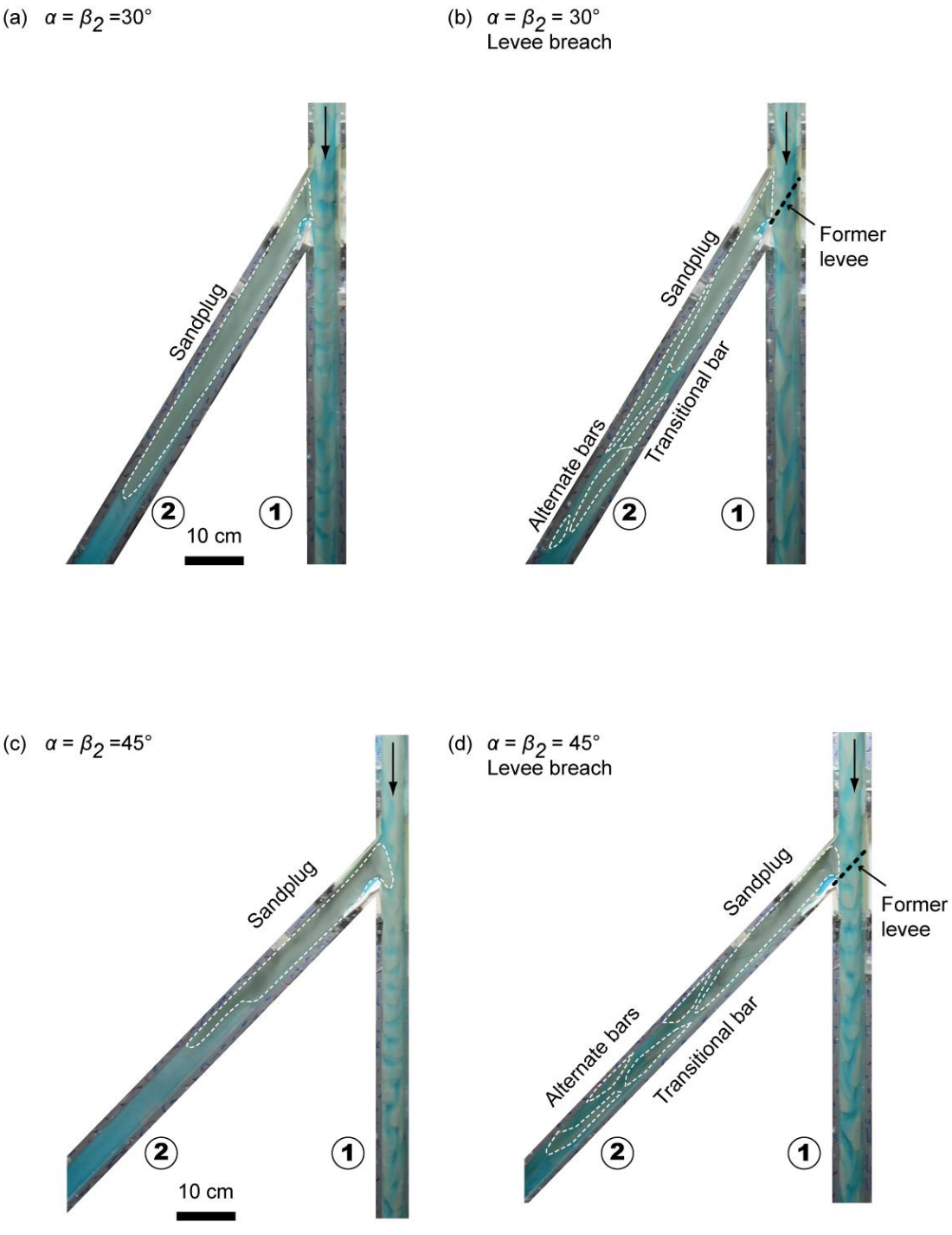

Figure A1 (continued):

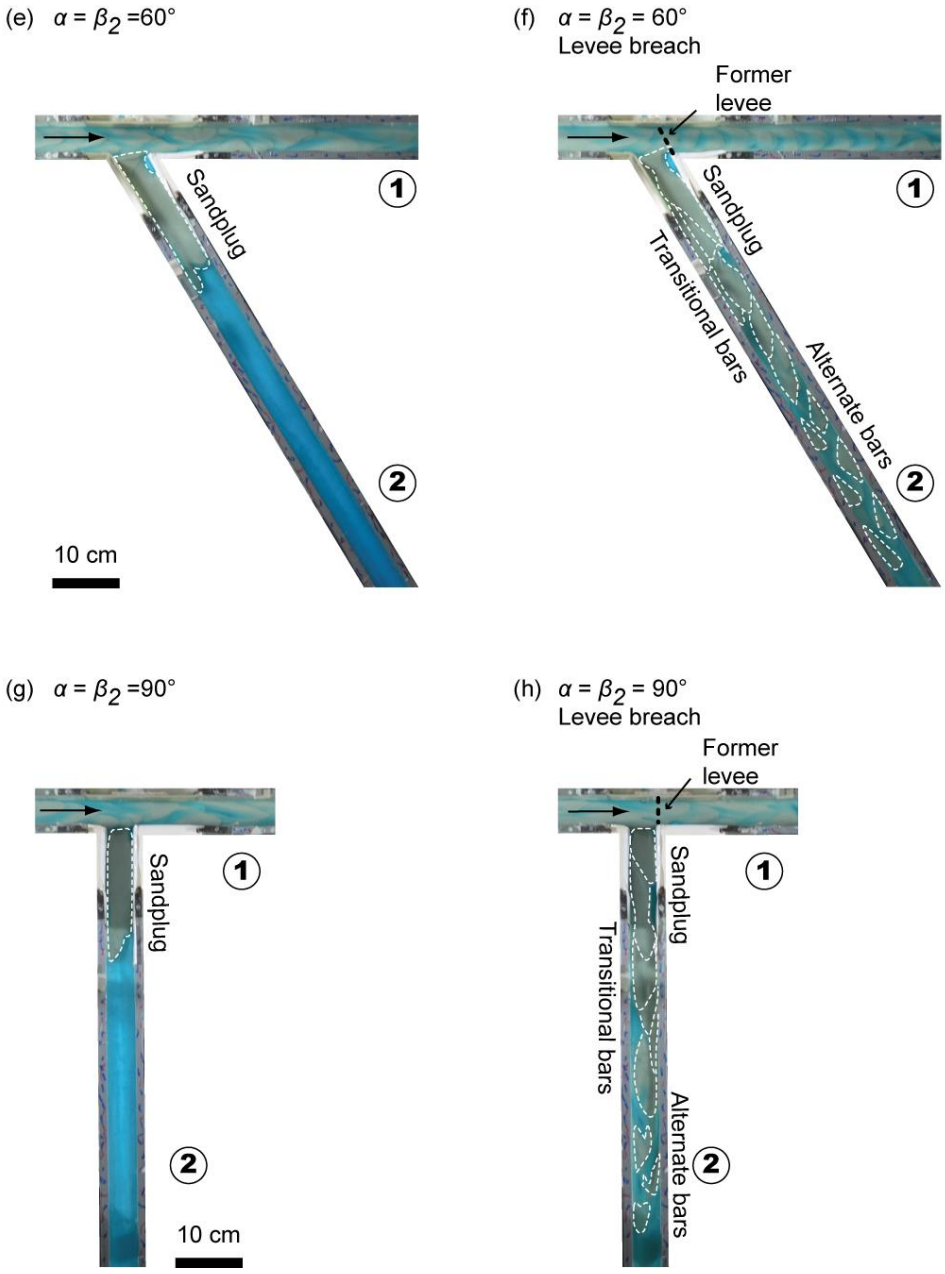

Appendix B: Supplementary material for Chapter 4 – Ain River channels aerial pictures

This Appendix first displays a series of pictures showing the temporal evolution of the sites studied along the Ain River in Chapter 4, and then the historical aerial pictures used to make measurements on 5 other channels.

Finally, a table regrouping the different cross-sections fill percentage used to build Figures 4.9 & 4.10c is displayed.

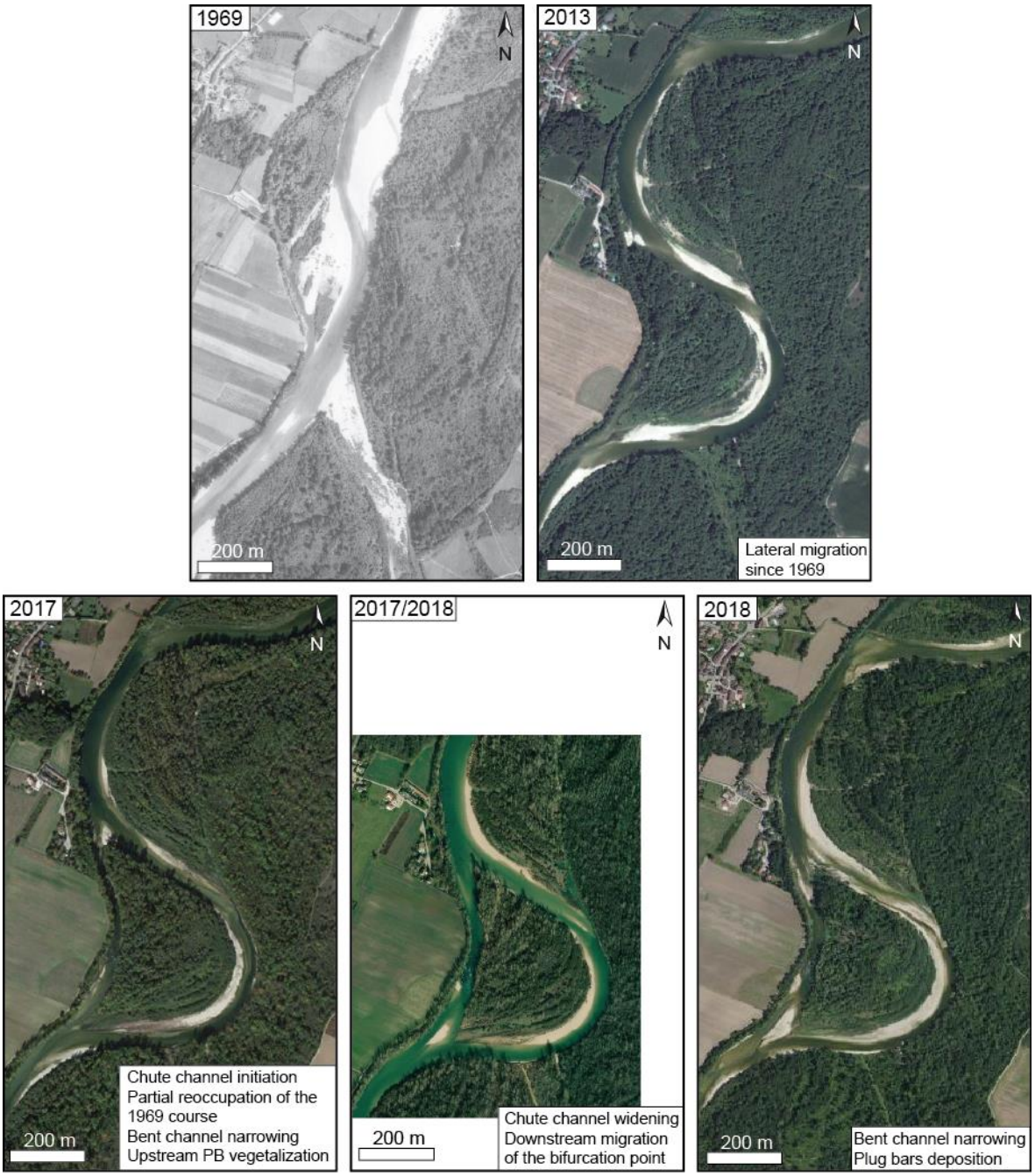

Figure B1: Temporal evolution of the CHA site.

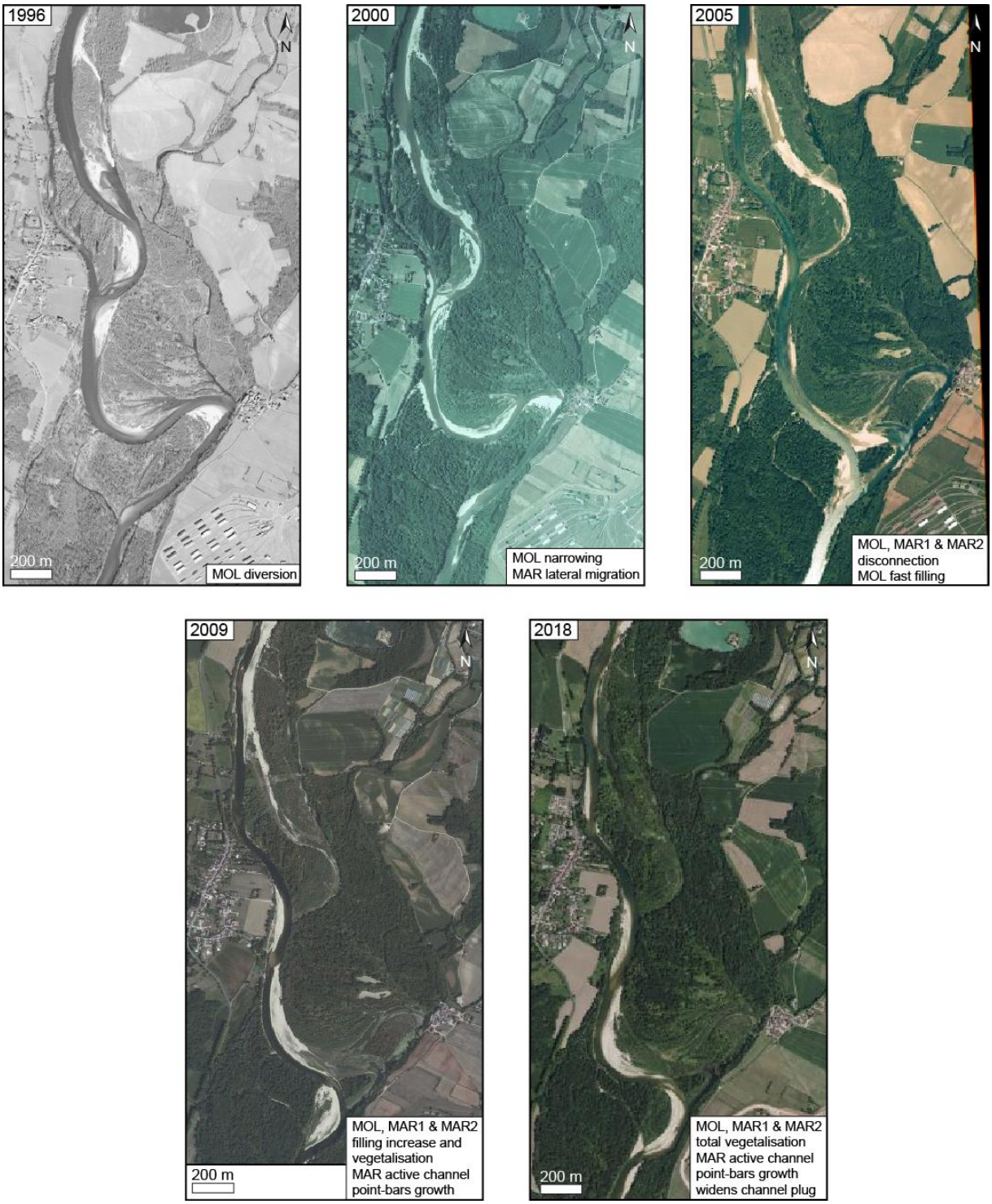

Figure B2: Temporal evolution of the MOL/MAR sites.

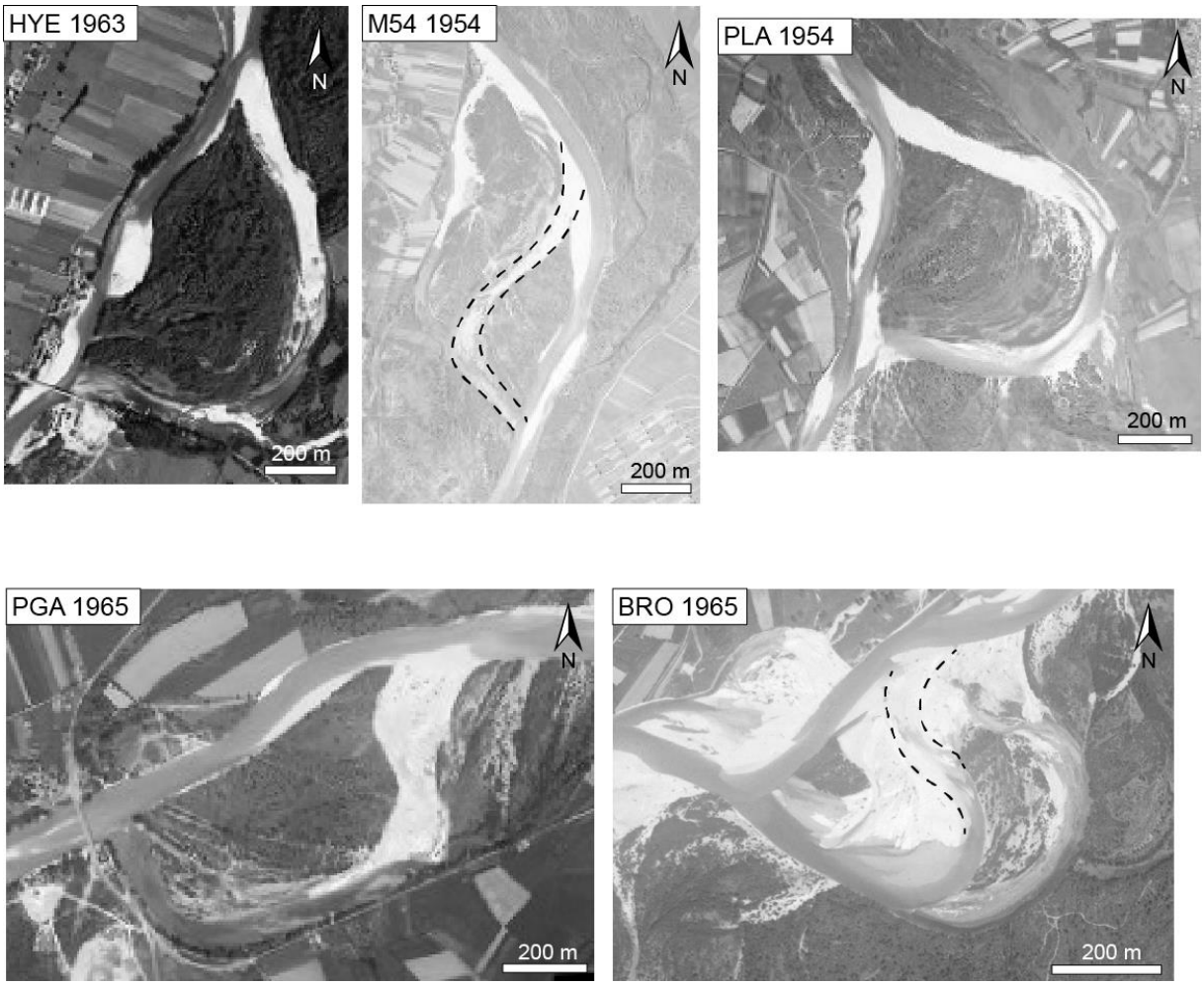

Figure B3: Aerial views of the closed stage of the five historical cutoffs (1954-1965) described in Table 4.1.

Site	Cross section	Bankfull width W (m)	Hydraulic mean bankfull depth D (m)	Estimated bankfull cross section A (m²)			Area filled (m²)		Area filled (%)		Distance from bifurcation point (m)
				Straight segment	Curved segment method (i)	Curved segment method (ii)					
CHA	a	75	4.03	-	141.6	151.3	0 (active)		-		-100
	b	90	4.58	-	192.7	205.9	0 (active)		-		-30
	c	95	2.78	-	-	-	-		-		70
	d	58	1.98	114.7	-	-	40.6		35.4		150
	e	59	2.00	118.0	-	-	50		42.4		450
	f	68	3.77	-	120.0	128.2	18.2	10	8.3	14.2	630
	g	56	3.30	-	86.4	92.3	4.3	0	0	4.7	780
MOL	Dieras et al. (2013) b	72	3.92	282.4	-	-	154		54.5		350
	Dieras et al. (2013) c	40	2.61	104.6	-	-	55		52.6		770
	h	100	2.88	287.9	-	-	136.4		56.7		300
	i	55	3.26	-	83.8	89.6	27.1	32.9	32.4	36.7	750
	j	55	3.26	-	83.8	89.6	17.8	23.6	21.3	26.3	930
MAR1	Dieras et al. (2013) d1	90	2.68	240.9	-	-	153		63.5		110
	k	72	3.92	165.2	-	-	121.7		73.7		120
	l	77	4.11	-	148.1	158.2	59.3	69.4	40.0	43.9	200
MAR2	Dieras et al. (2013) d2	90	2.68	240.9	-	-	117		48.6		10
	m	110	3.07	338.2	-	-	280.3		82.9		80
	n	110	5.26	-	270.5	289.0	57.2	75.7	21.2	26.2	150

Table B1: Hydraulic parameters, cross-sectional area and filled area of the cross sections displayed in Figures 4.3, 4.4 & 4.8.

Appendix C: Supplementary material for Chapter 4 – Allier River channels aerial pictures

This Appendix quickly presents the Allier River and the aerial pictures used to measure the channel plugs of 5 of its abandoned channels are displayed.

The 420.7 km long Allier River flows northwards in central France from the Massif Central into the Loire River. It has a pluvial hydraulic regime, with a mean annual discharge of 150 $m^3 s^{-1}$ and a mean annual flood discharge of 500 $m^3 s^{-1}$ and drains a 14310 km² catchment. The Allier is a very dynamic gravel-bed meandering river (Kleinhans & Van Den Berg, 2011) which flows in a valley with a gradient of 3.3 m km^{-1} and migration rates going up to 60 m yr^{-1} (Van Dijk et al., 2014). Consequently it is prone to channel abandonment.

Historical aerial photographs (IGN, remonterletemps.ign.fr) going back to 1948 were used to study the channel plug of 5 abandoned channels that were disconnected prior 1960 (Fig. C1). The channels exact disconnection dates are unknown and the gap between two aerial pictures surveying was often several years. Consequently the historical photographs were selected as the first available showing the disconnected channels, before the channel plug was colonized by vegetation. Measurements of the channel plug length were aided by comparing the differences between aerial pictures taken before and after the disconnection. Furthermore the gravels forming the plug are more lightly colored, however the contrast in color between the fill and bed deposits is less marked than in the Ain River (Appendix B). The length ratios between the channels were used to estimate the slope ratios (Table C1). Length of channel plug deposits was measured from the bifurcation point to the point where: (1) the gravel bars occupied the whole channel width, (minimum plug length), and (2) only one or several sediment tongues extended downstream from the main body of the channel plug (maximum plug length), as previously done in this dissertation. The mean channel plug length corresponds to the average between these measurements rendered dimensionless by dividing it by the channel width at the bifurcation.

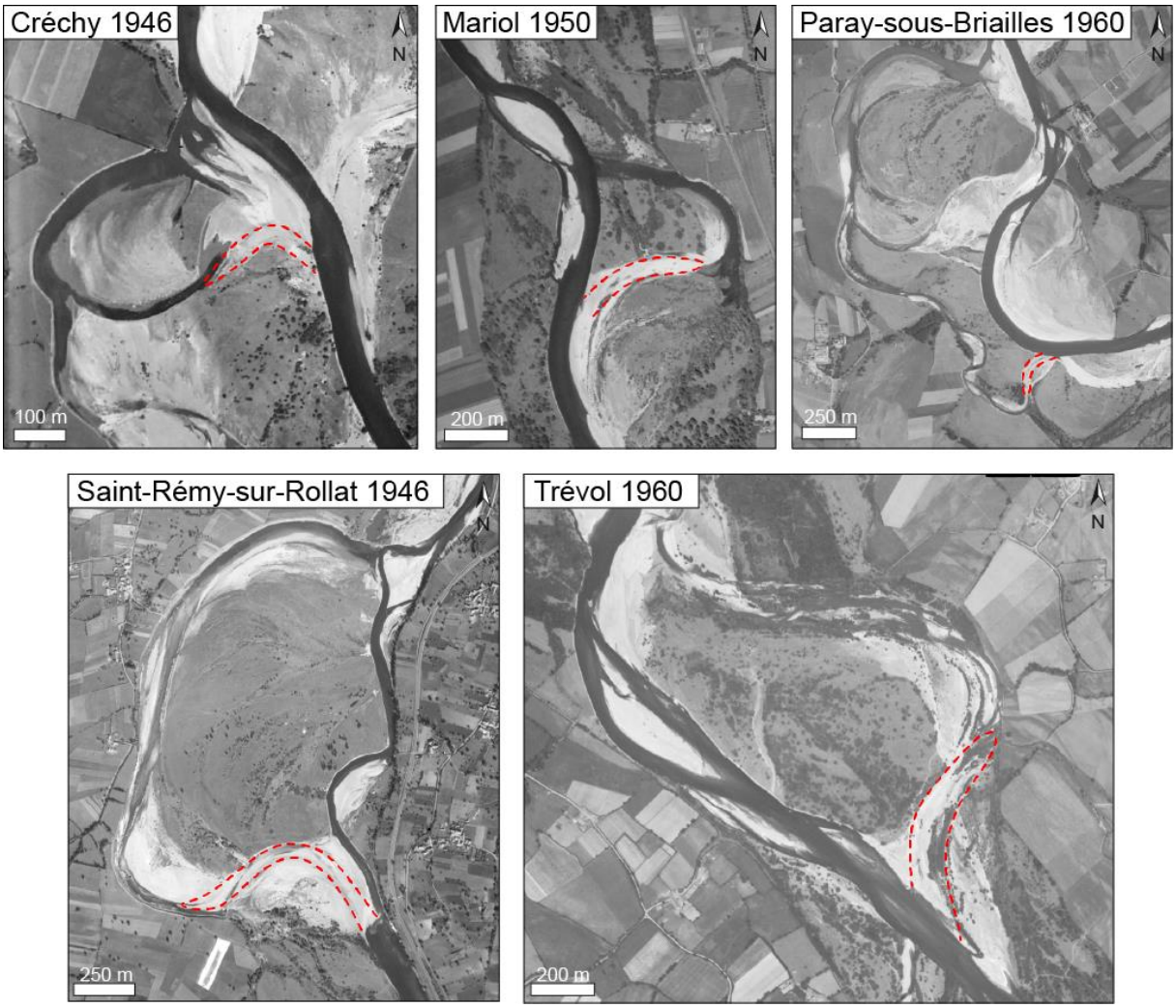

Figure C1: Aerial views of the closed stage of the five historical cutoffs (1946-1960) described in Table E2.

Allier River (France)	Sources :	IGN			
Channel	Créchy	Mariol	Paray-sous-Briailles	Sait-Rémy-en-Rollat	Trévol
Disconnection age	<1946	1946-1950	1954-1960	1880-1944	> 1765
Diversion angle (°)	35 ± 2.5	45 ± 2.5	25 ± 2.5	20 ± 2.5	40 ± 2.5
Length ratio L_1/L_2	0.37	0.42	0.15	0.51	0.95
Dimensionless sand plug length	6.2	6.0	5.6	8.9	8.5

Table C1: Allier River channel plugs measurements.

Appendix D: Location and log of the auger and corer holes made in tne Vimpelles channel

This Appendix locates each auger and russian corer holes made in the Vimpelles channel during the different field surveys, and logs each of these boreholes for the purpose of reconstructing the channel fill architecture in Chapter 5.

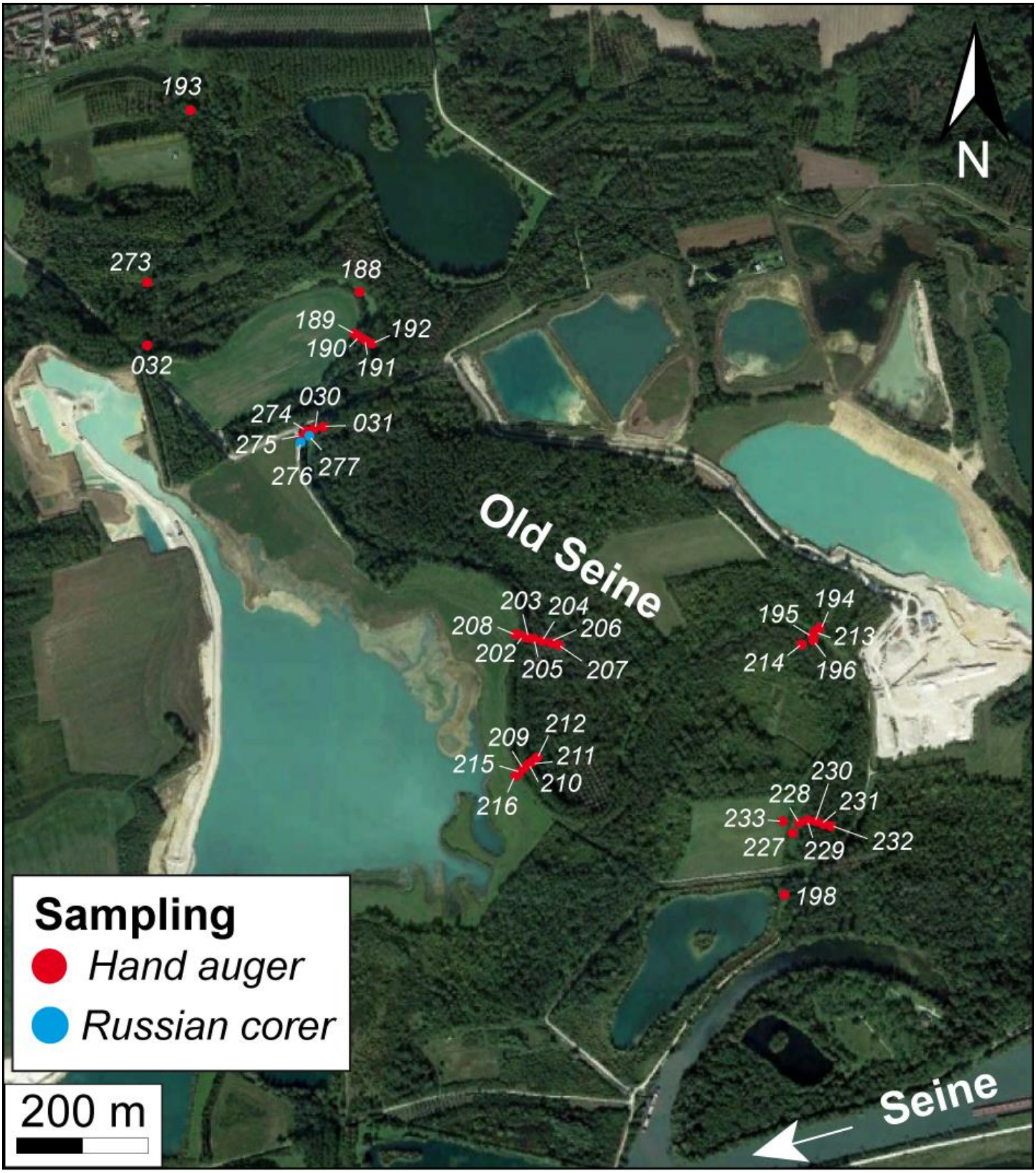

Figure D1: Location of each borehole in the Vimpelles channel.

Figure D2: Borehole sampling method. Coring using a hand auger **(a)**. Samples retrieved using a hand auger **(b)** and a Russian corer **(c)**. Hand auger sampling is less continuous but allow sampling of sands and thin layers of fine gravels while the Russian corer can only sample peat, clays and silts.

Figure D3: Log of each of the 38 boreholes. Designation corresponds to the number of the GPS waypoint made to locate the borehole.

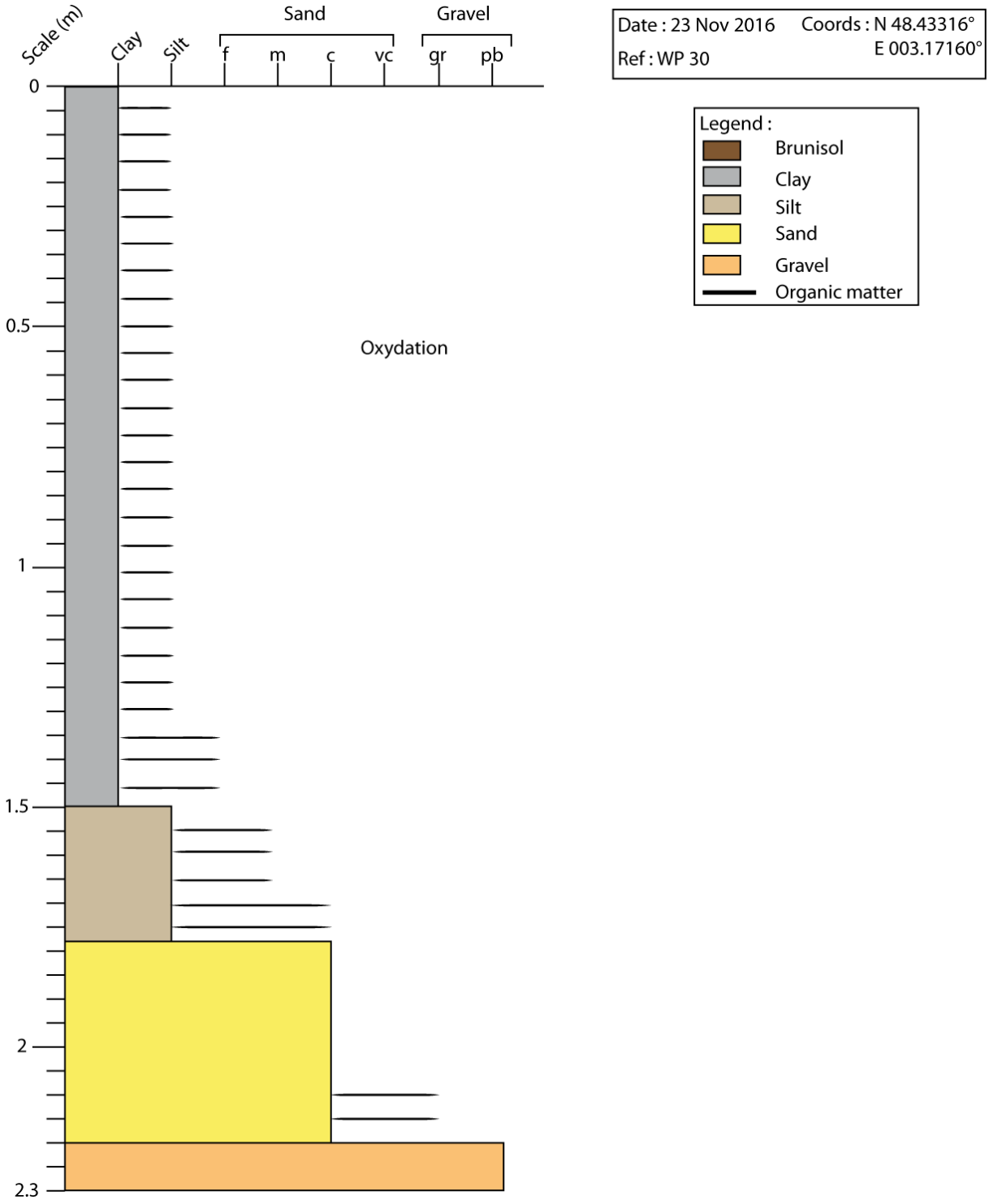

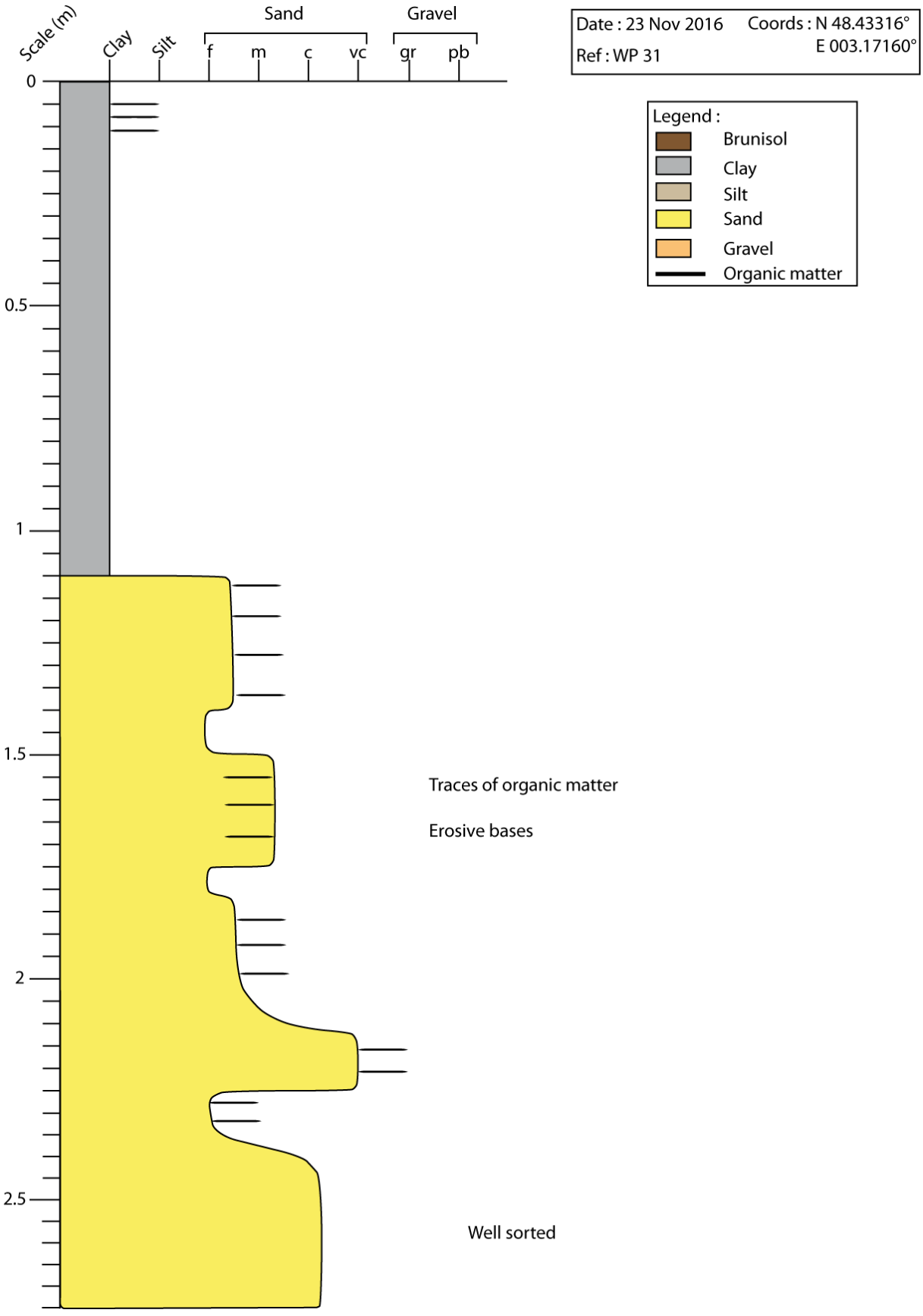
Scale (m)
Clay
Silt
Sand
f
m
c
vc
Gravel
gr
pb
0
0.5
1
1.5
2
2.5
Date : 23 Nov 2016
Coords : N 48.43316°
E 003.17160°
Ref : WP 31
Legend :
Brunisol
Clay
Silt
Sand
Gravel
Organic matter
Traces of organic matter
Erosive bases
Well sorted

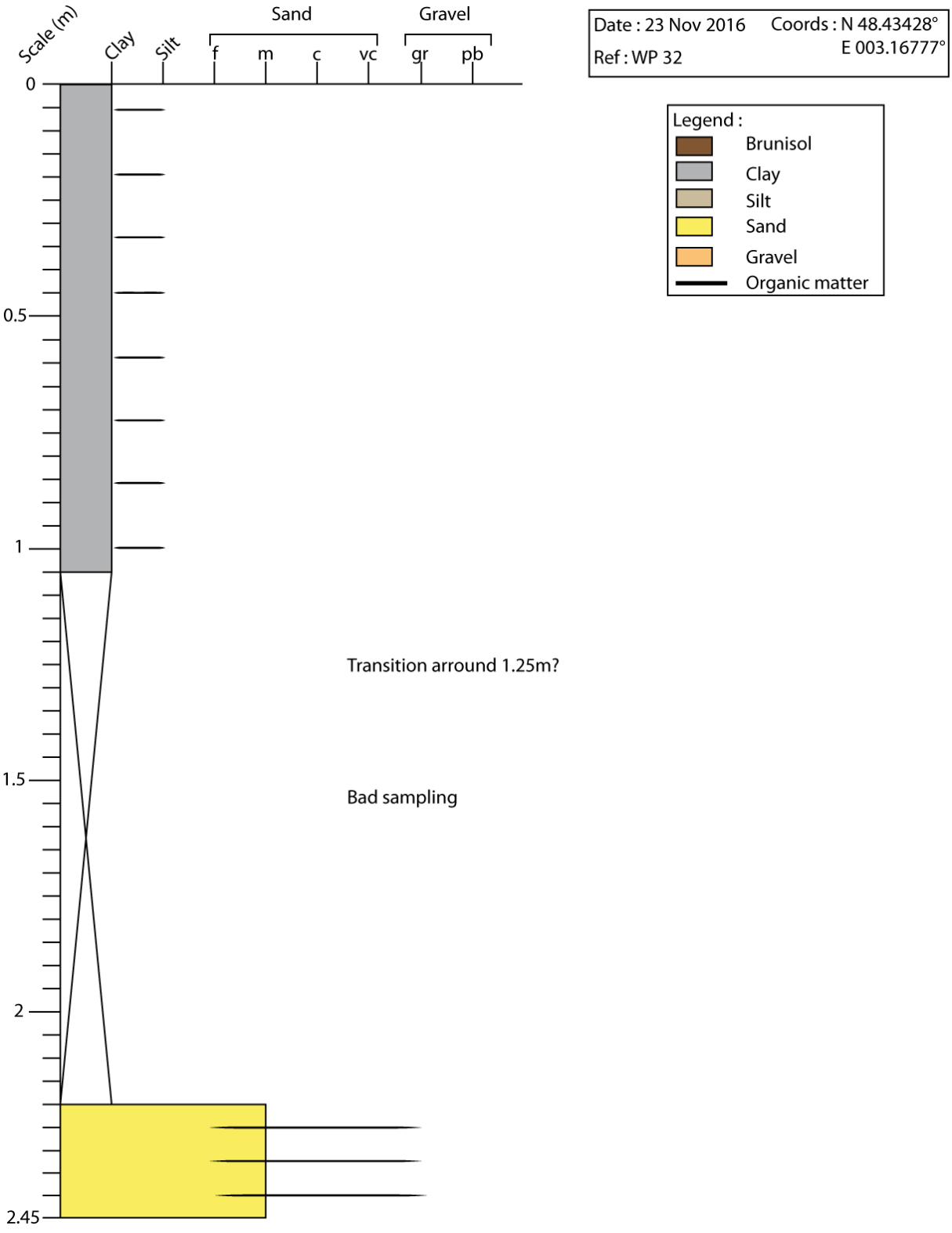
Scale (m)
Clay
Silt
Sand
f
m
c
vc
Gravel
gr
pb
0
0.5
1
1.5
2
2.45
Date : 23 Nov 2016
Coords : N 48.43428°
E 003.16777°
Ref : WP 32
Legend :
Brunisol
Clay
Silt
Sand
Gravel
Organic matter
Transition arround 1.25m?
Bad sampling

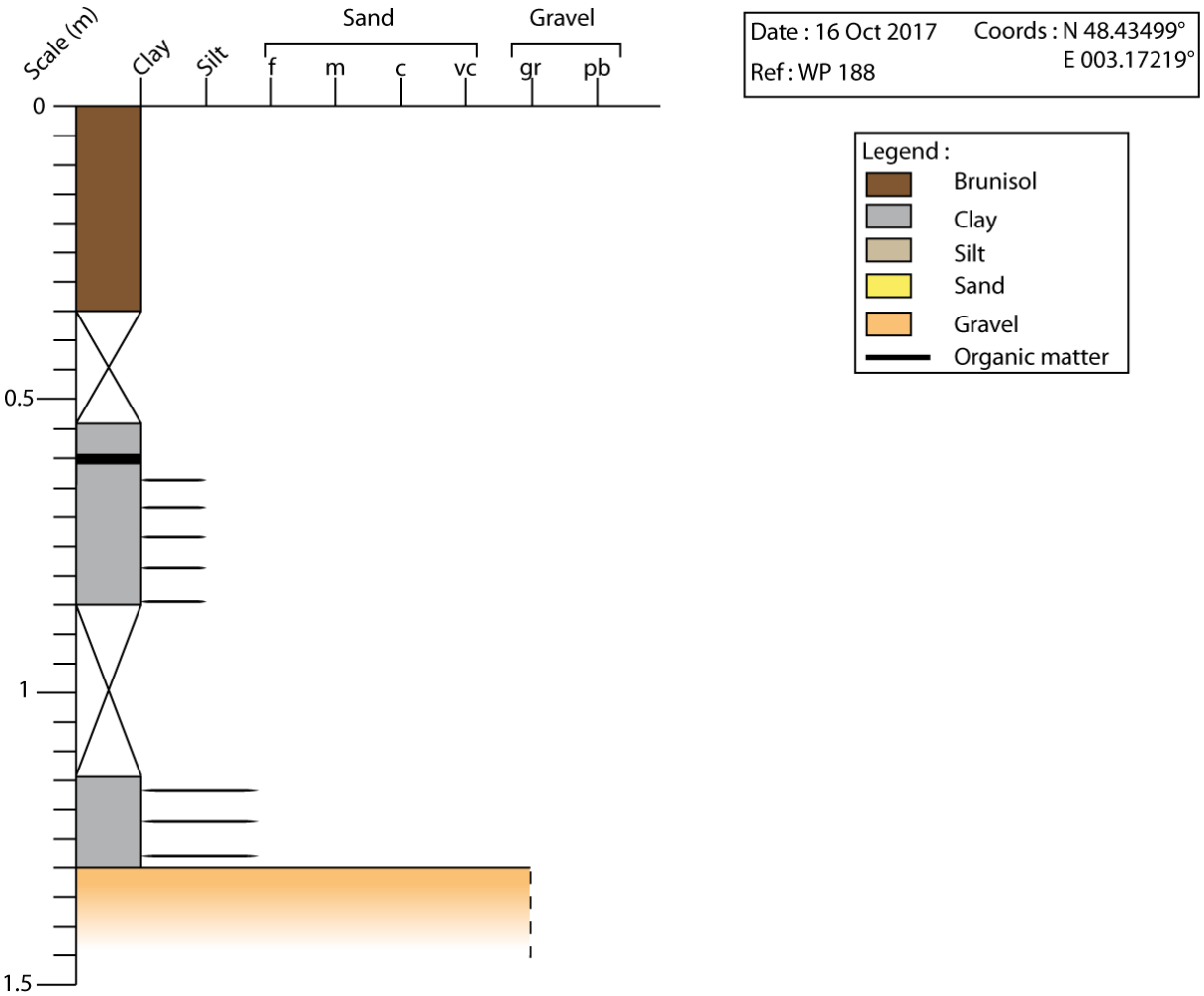
Scale (m)
Clay
Silt
Sand
f
m
c
vc
Gravel
gr
pb
0
0.5
1
1.5
Date : 16 Oct 2017
Coords : N 48.43499°
E 003.17219°
Ref : WP 188
Legend :
Brunisol
Clay
Silt
Sand
Gravel
Organic matter

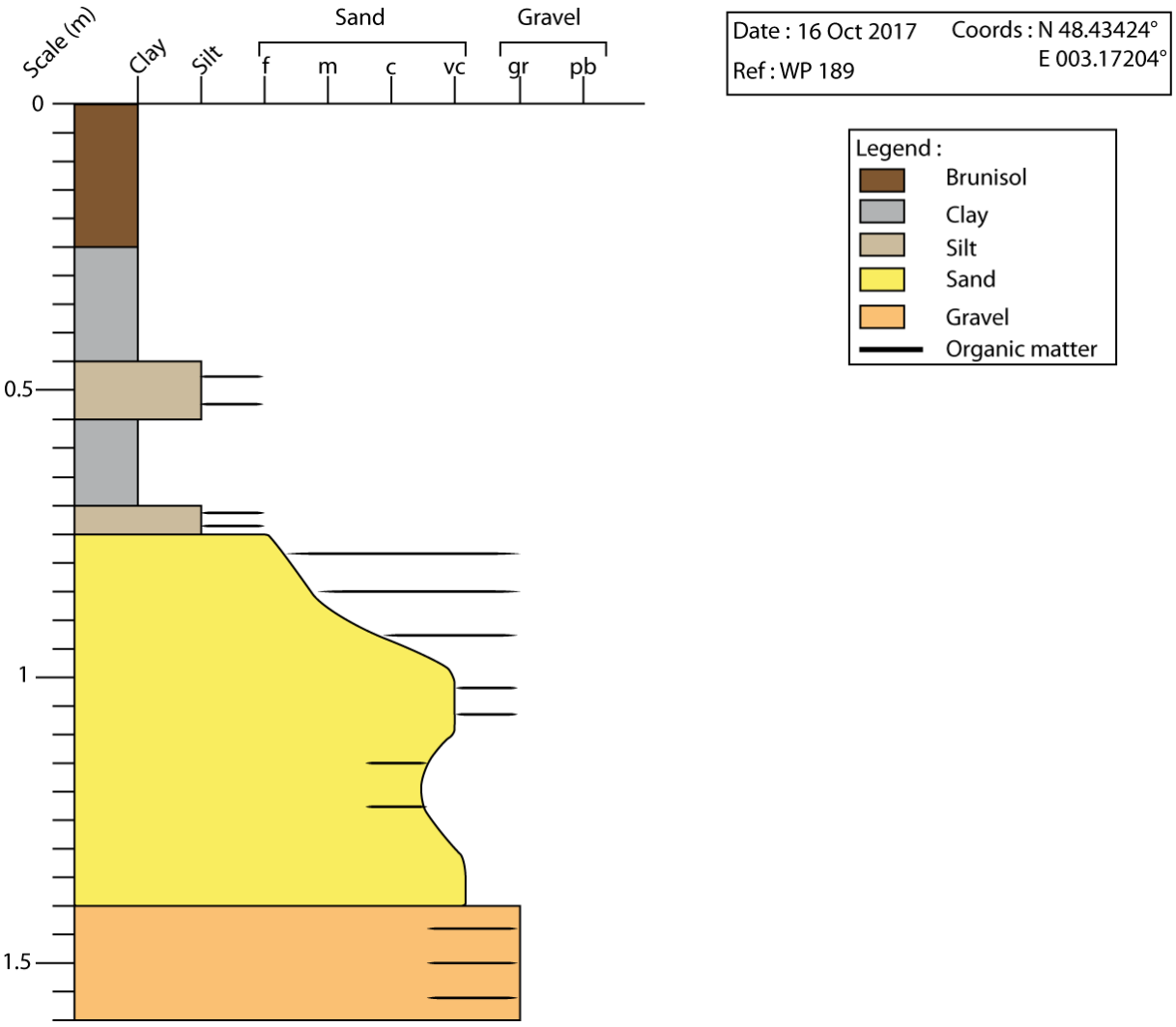
Scale (m)
Clay
Silt
Sand
f
m
c
vc
Gravel
gr
pb
0
0.5
1
1.5
Date : 16 Oct 2017
Ref : WP 189
Coords : N 48.43424°
E 003.17204°
Legend :
Brunisol
Clay
Silt
Sand
Gravel
Organic matter

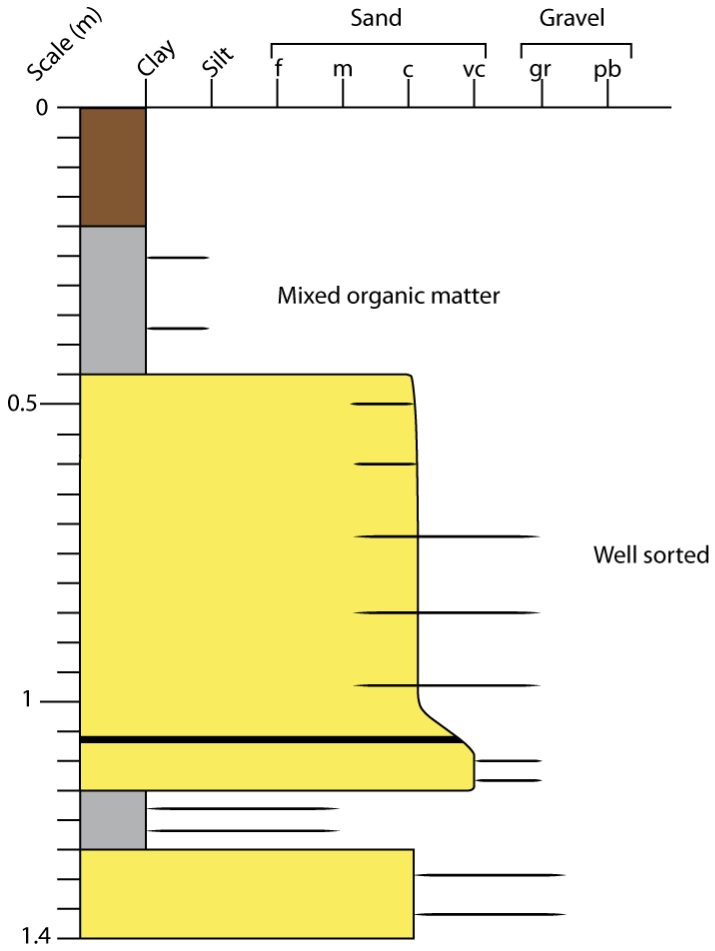

Date : 16 Oct 2017 Coords : N 48.43414° E 003.17195°
Ref : WP 190

Legend :
- Brunisol
- Clay
- Silt
- Sand
- Gravel
- Organic matter

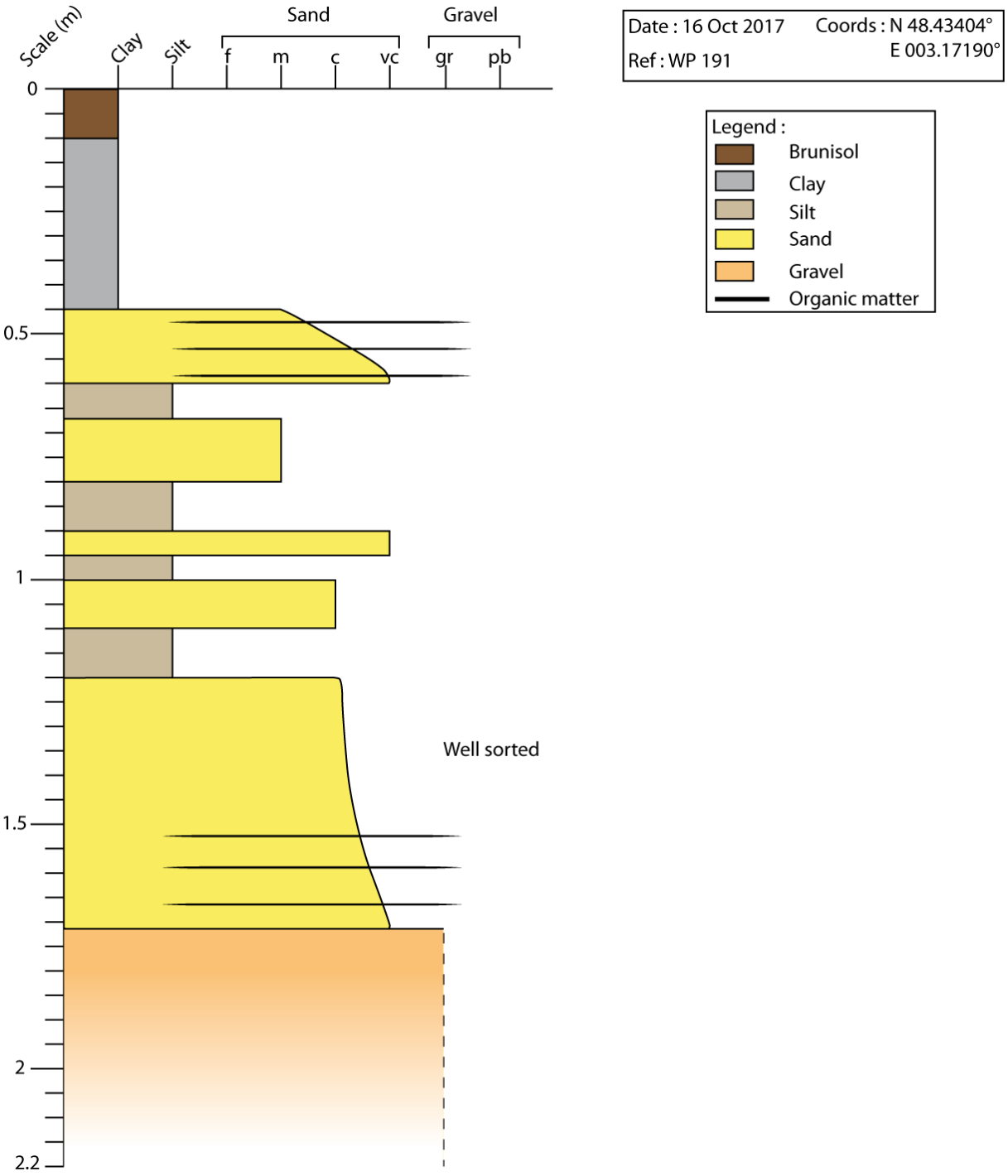
Scale (m)
Clay
Silt
Sand
f
m
c
vc
Gravel
gr
pb
0
0.5
1
1.5
2
2.2
Well sorted
Date : 16 Oct 2017
Coords : N 48.43404°
E 003.17190°
Ref : WP 191
Legend :
Brunisol
Clay
Silt
Sand
Gravel
Organic matter

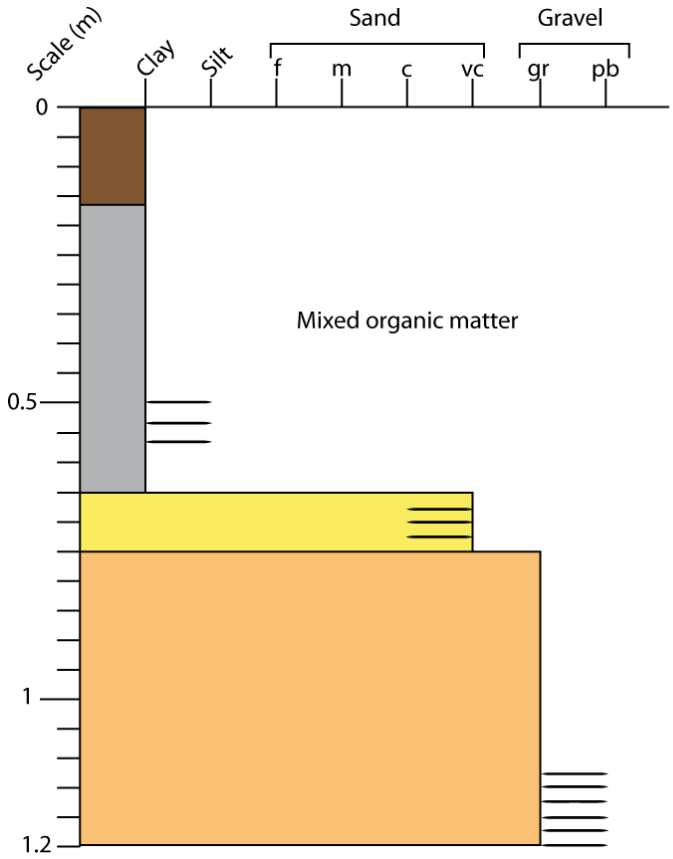

Date : 16 Oct 2017 Coords : N 48.43396° E 003.17234°
Ref : WP 192

Legend :
- Brunisol
- Clay
- Silt
- Sand
- Gravel
- Organic matter

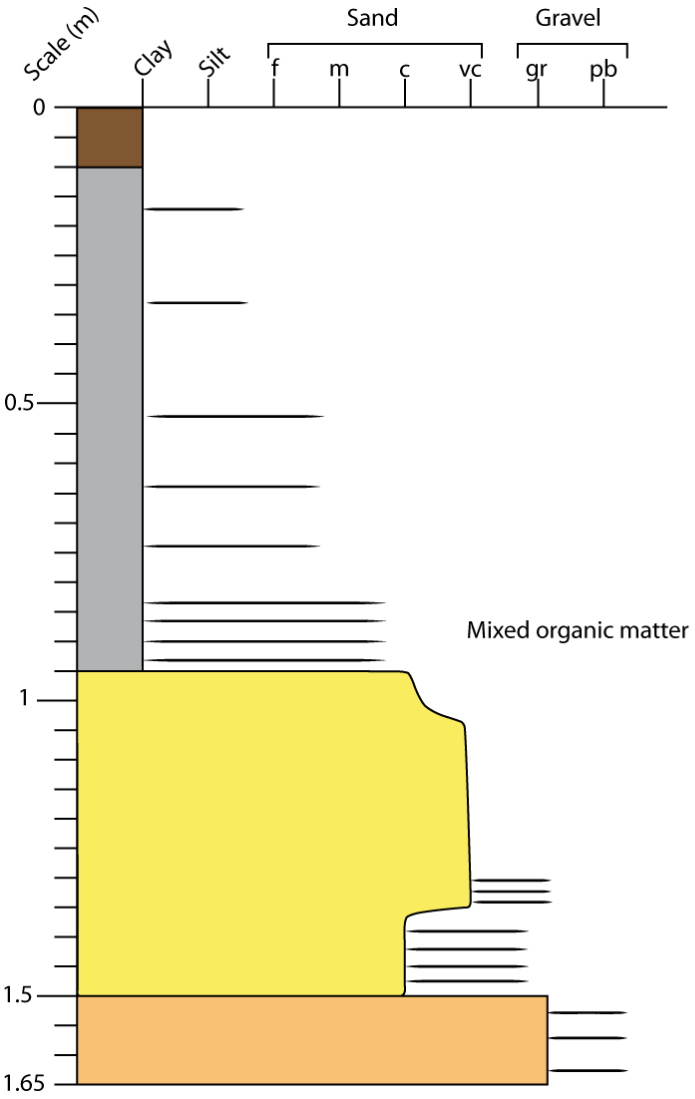

Date : 16 Oct 2017 Coords : N 48.43799° E 003.16885°
Ref : WP193

Legend :
- Brunisol
- Clay
- Silt
- Sand
- Gravel
- Organic matter

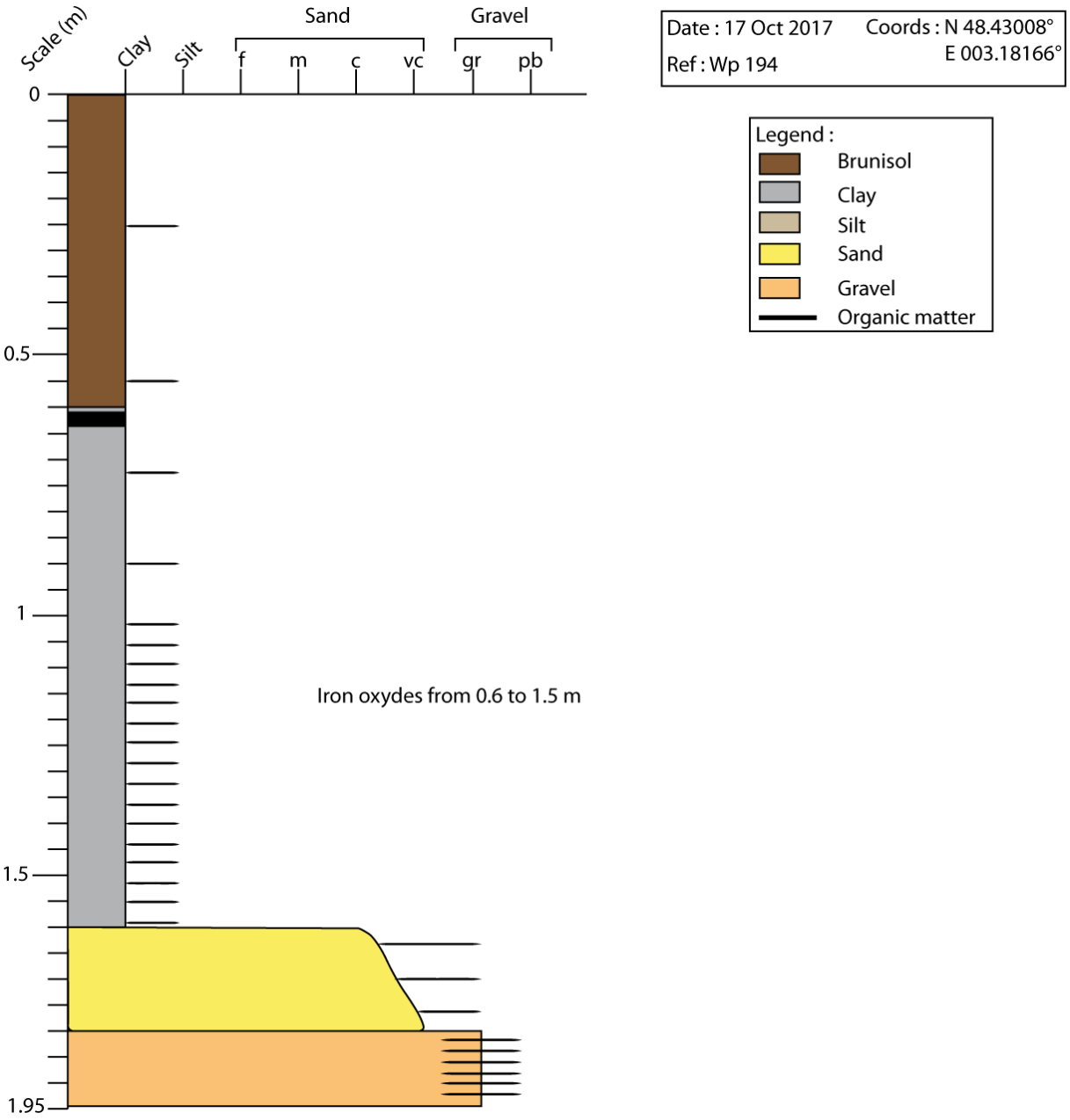
Scale (m)
Clay
Silt
Sand
f
m
c
vc
Gravel
gr
pb
0
0.5
1
1.5
1.95
Iron oxydes from 0.6 to 1.5 m
Date : 17 Oct 2017
Coords : N 48.43008°
E 003.18166°
Ref : Wp 194
Legend :
Brunisol
Clay
Silt
Sand
Gravel
Organic matter

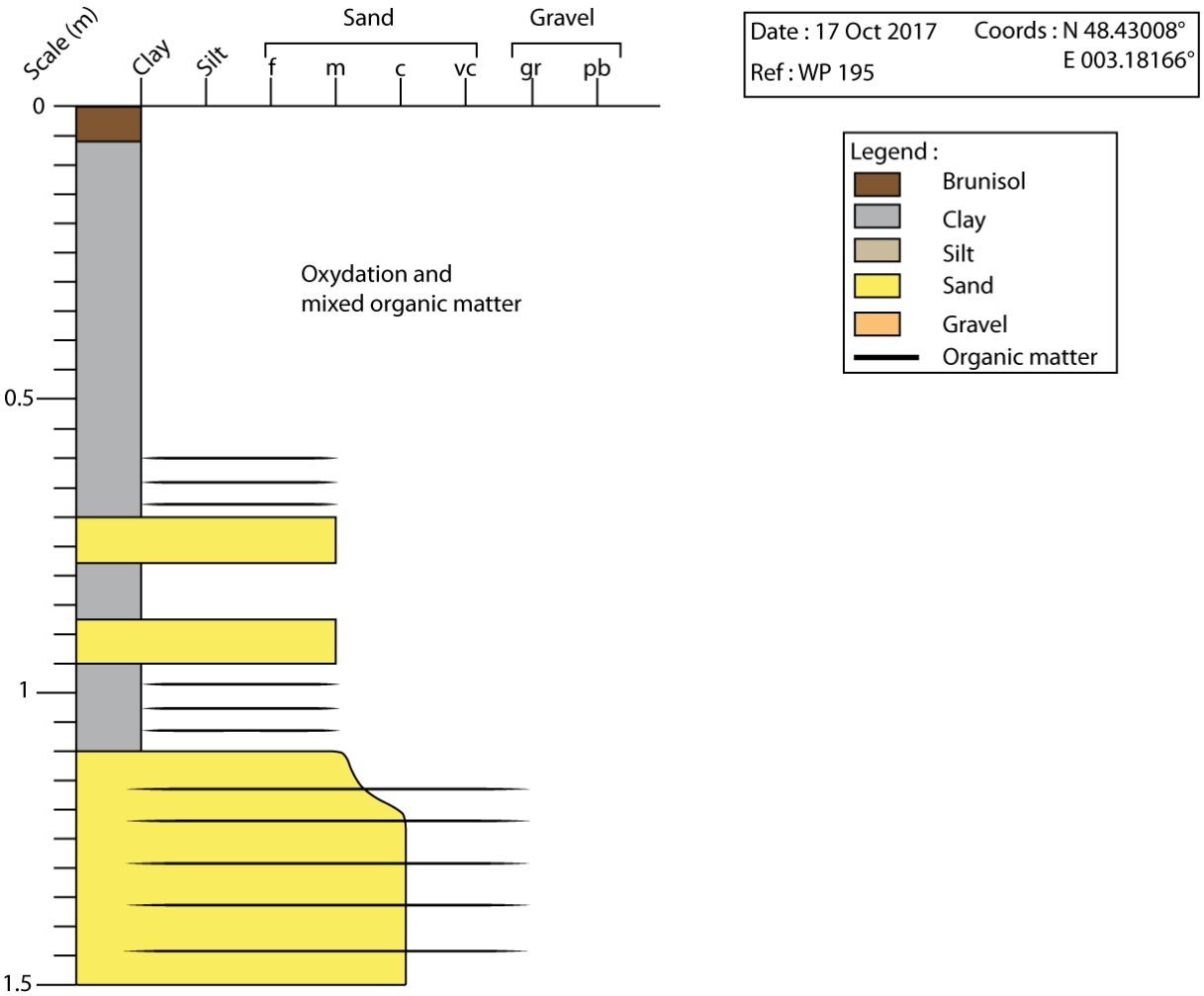
Scale (m)
Clay
Silt
Sand
Gravel
f
m
c
vc
gr
pb
0
0.5
1
1.5
Oxydation and
mixed organic matter
Date : 17 Oct 2017
Coords : N 48.43008°
E 003.18166°
Ref : WP 195
Legend :
Brunisol
Clay
Silt
Sand
Gravel
Organic matter

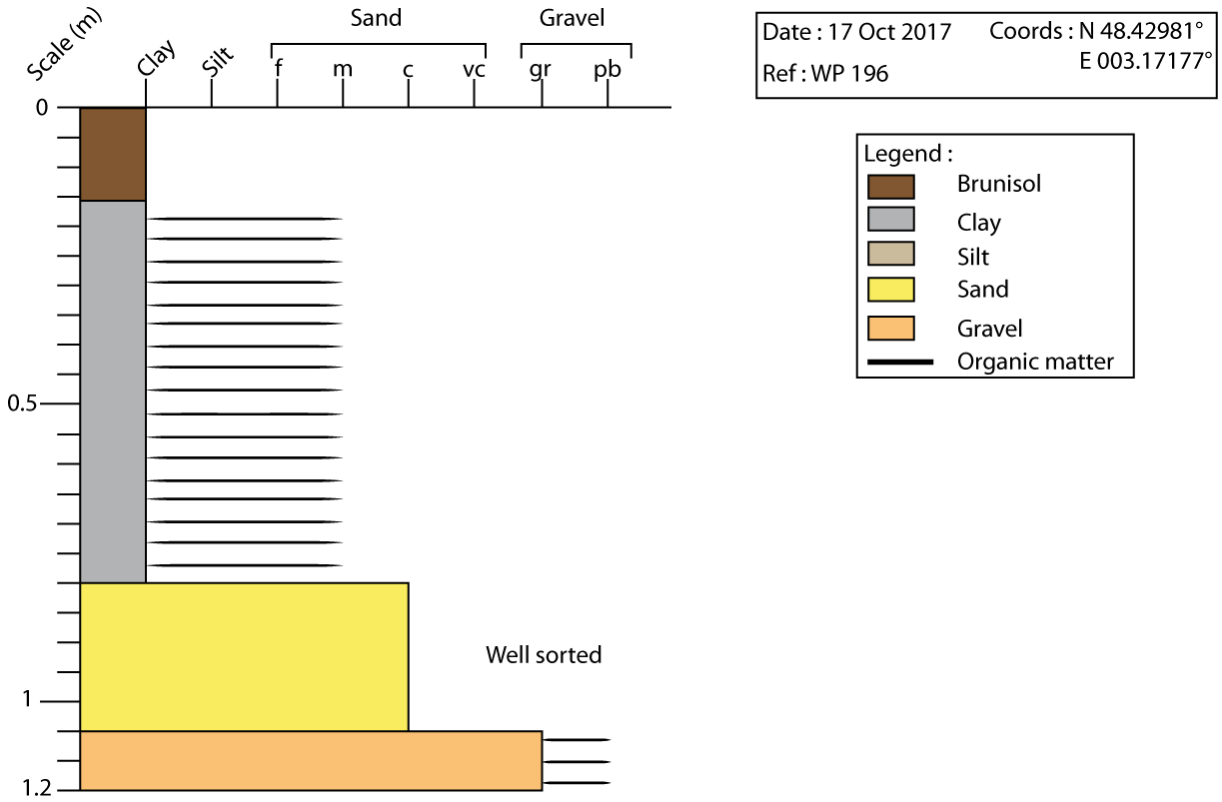
Scale (m)
Clay
Silt
Sand
f
m
c
vc
Gravel
gr
pb
0
0.5
1
1.2
Well sorted
Date : 17 Oct 2017
Coords : N 48.42981°
E 003.17177°
Ref : WP 196
Legend :
Brunisol
Clay
Silt
Sand
Gravel
Organic matter

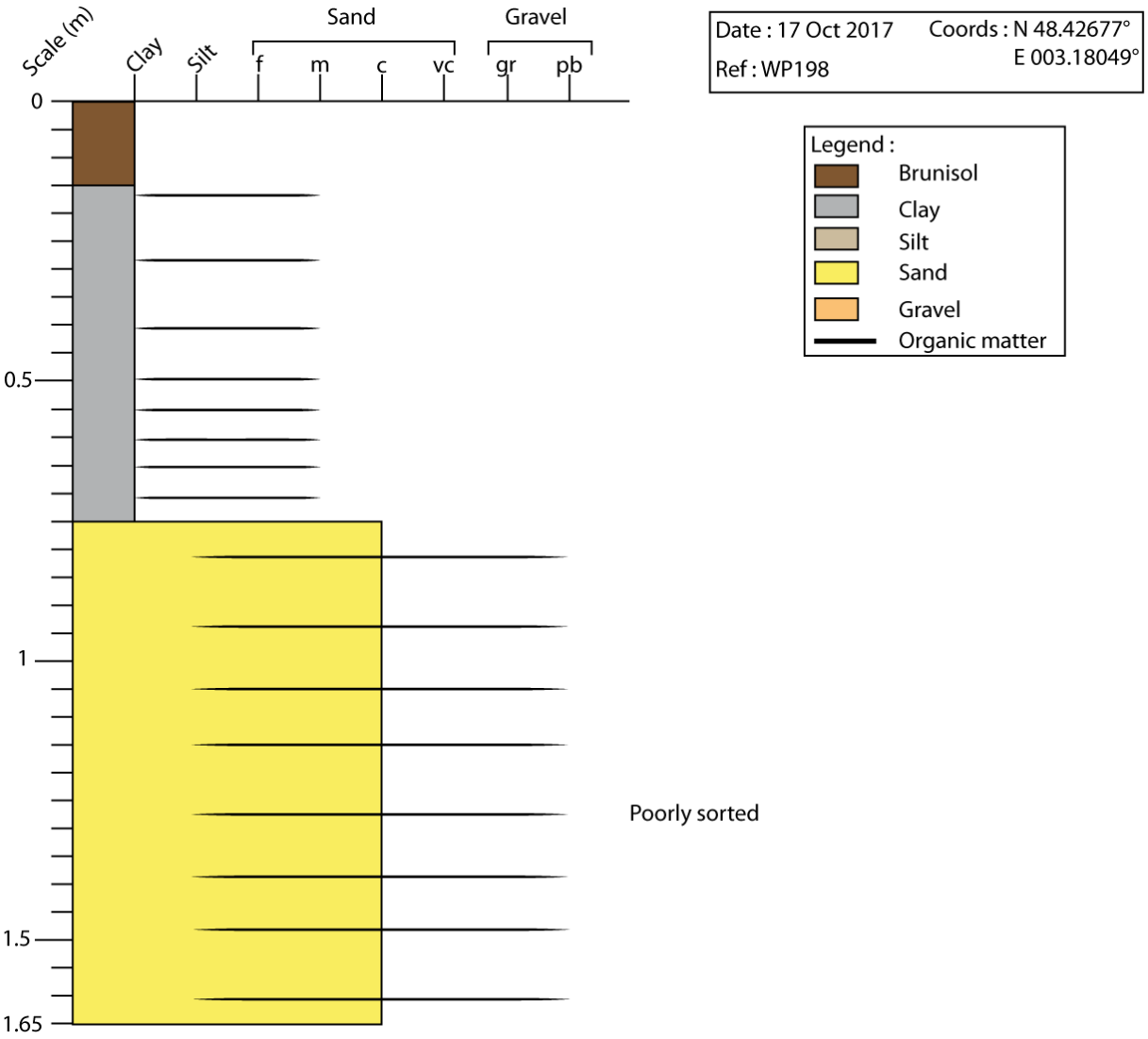
Scale (m)
Clay
Silt
Sand
f
m
c
vc
Gravel
gr
pb
0
0.5
1
1.5
1.65
Date : 17 Oct 2017
Ref : WP198
Coords : N 48.42677°
E 003.18049°
Legend :
Brunisol
Clay
Silt
Sand
Gravel
Organic matter
Poorly sorted

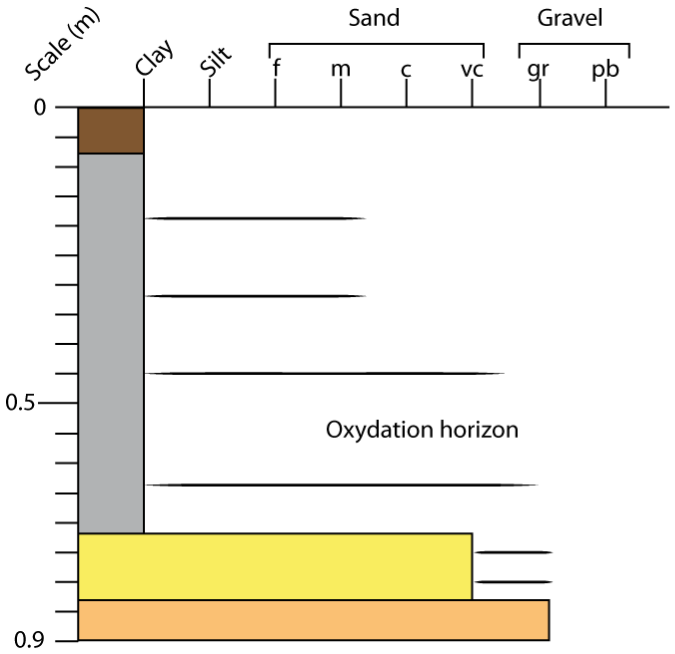

Date : 17 Oct 2017 Coords : N 48.42998° E 003.17545°
Ref : WP 202 (201)

Legend :
- Brunisol
- Clay
- Silt
- Sand
- Gravel
- Organic matter

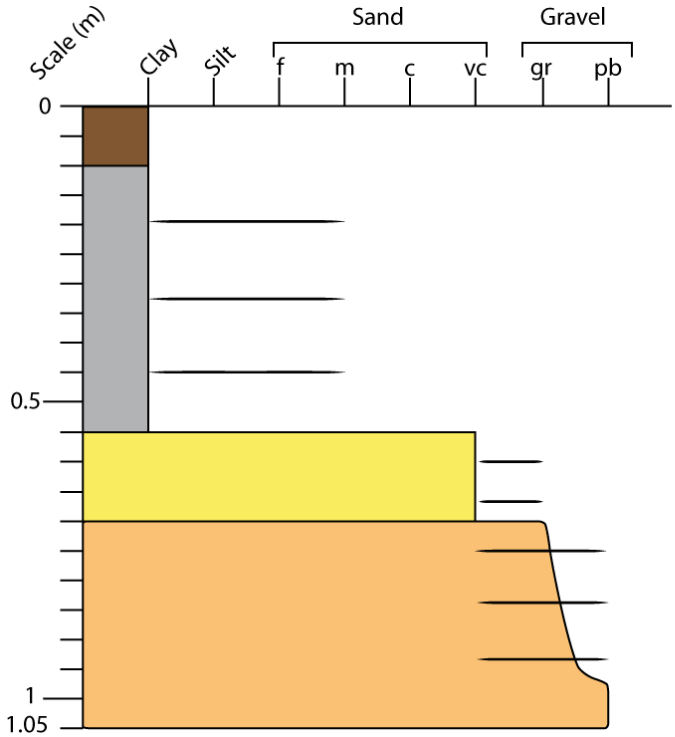

Date : 17 Oct 2017 Coords : N 48.42996° E 003.17548°
Ref : WP 203 (200)

Legend :
- Brunisol
- Clay
- Silt
- Sand
- Gravel
- Organic matter

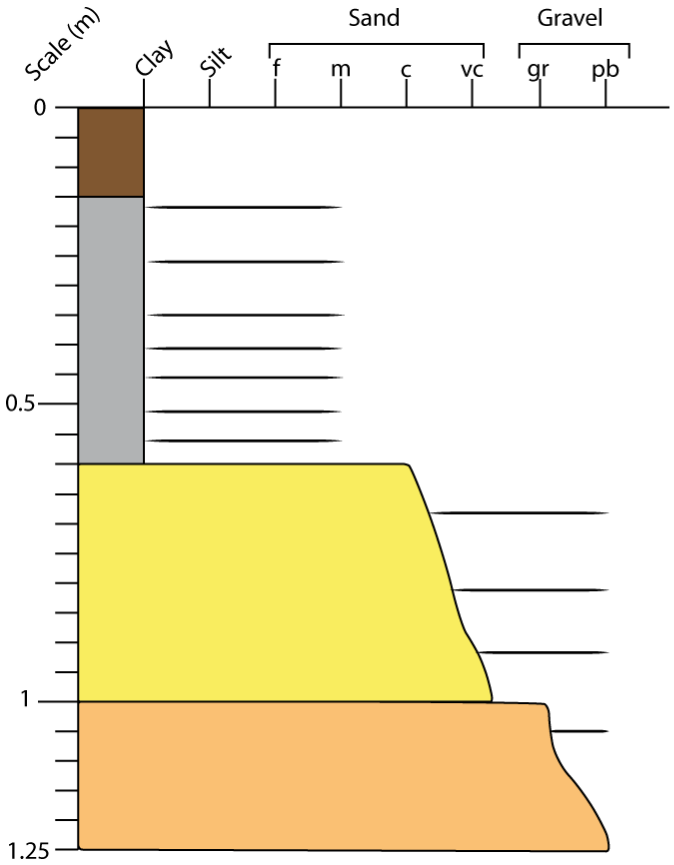

Date : 17 Oct 2017 Coords : N 48.42993°
Ref : WP 204 (199) E 003.17570°

Legend :
- Brunisol
- Clay
- Silt
- Sand
- Gravel
- Organic matter

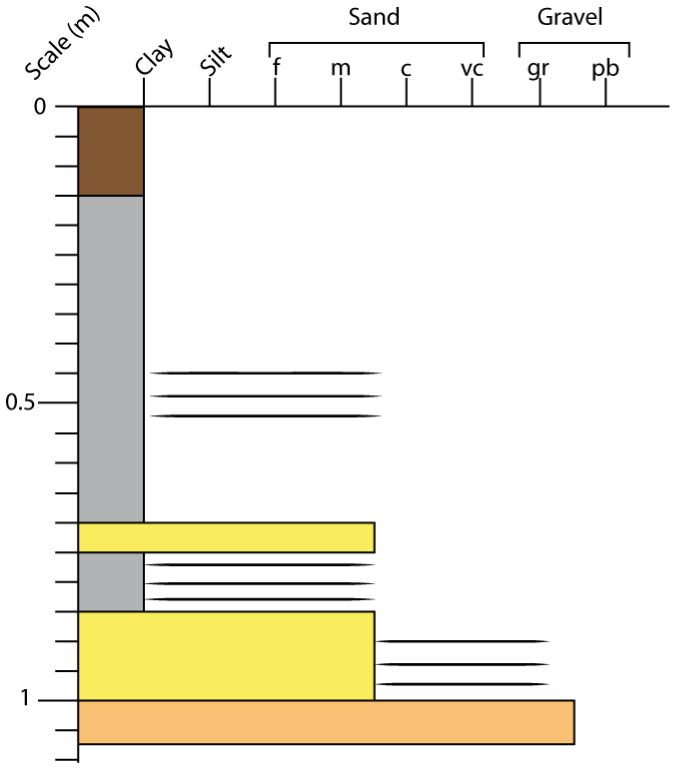

Date : 21/11/17 Coords : N 48.42996°
Ref : WP205 E 003.17558°

Legend :
- Brunisol
- Clay
- Silt
- Sand
- Gravel
- Organic matter

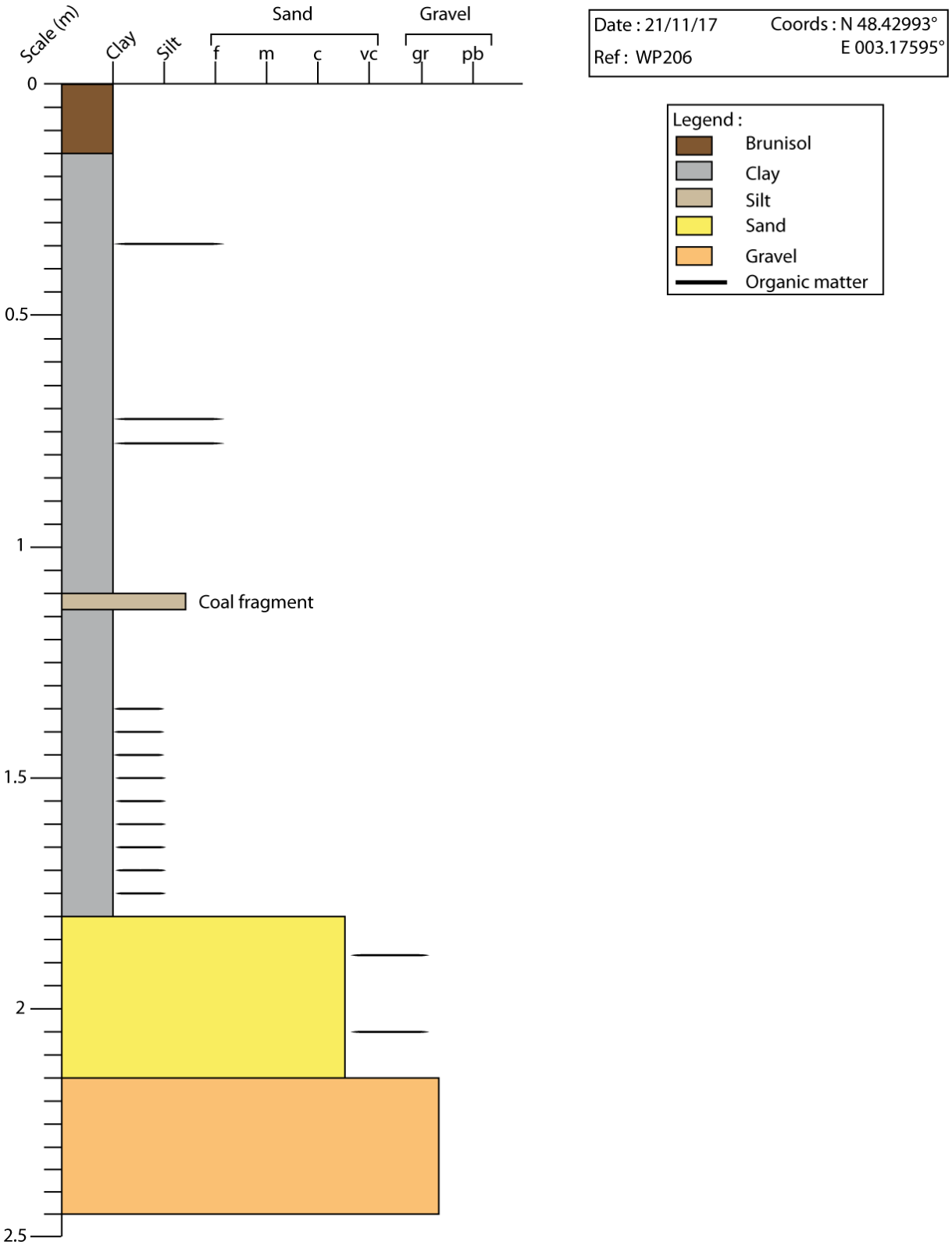
Scale (m)
Clay
Silt
Sand
f
m
c
vc
Gravel
gr
pb
0
0.5
1
1.5
2
2.5
Coal fragment
Date : 21/11/17
Ref : WP206
Coords : N 48.42993°
E 003.17595°
Legend :
Brunisol
Clay
Silt
Sand
Gravel
Organic matter

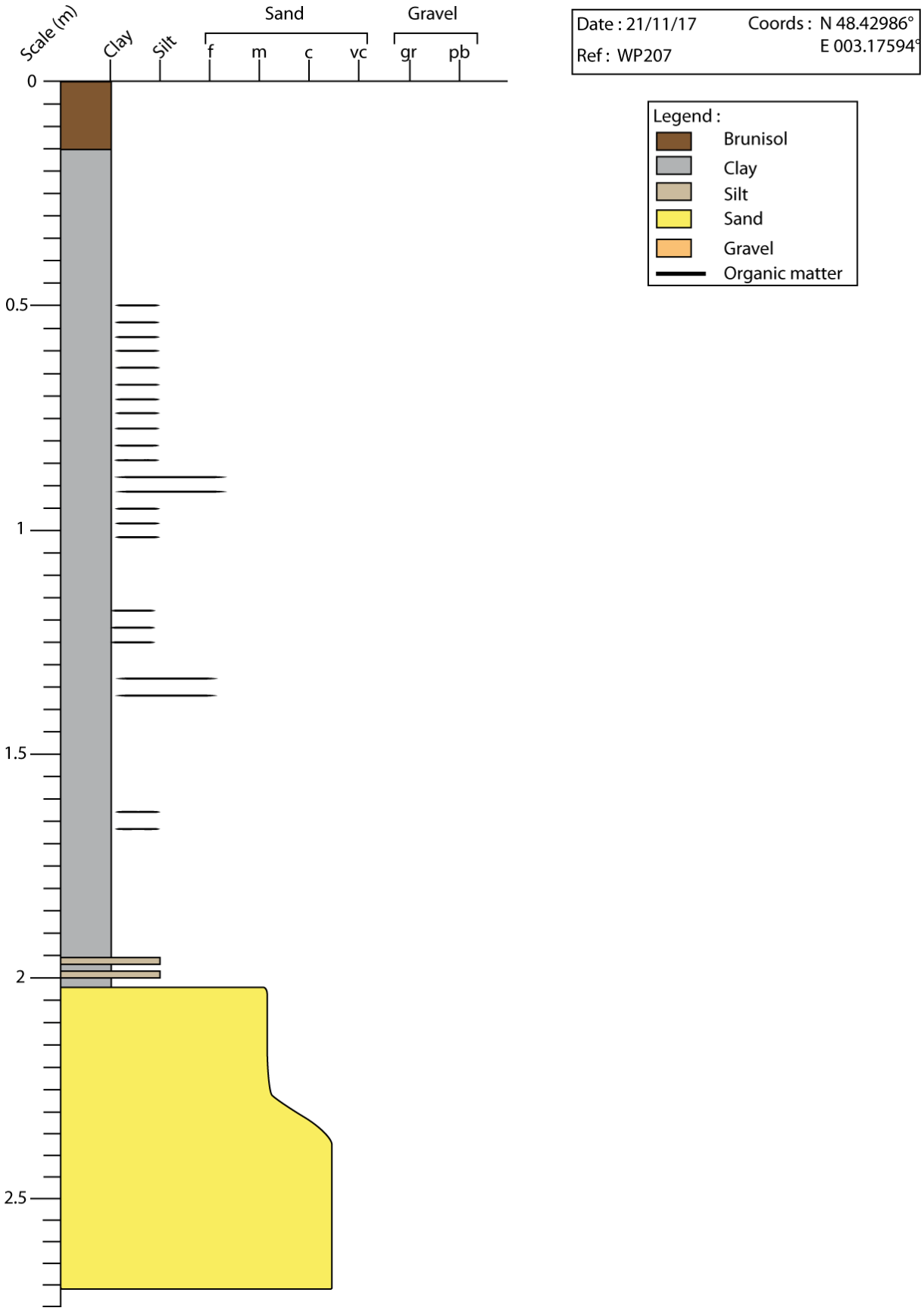
Scale (m)
Clay
Silt
Sand
f
m
c
vc
Gravel
gr
pb
0
0.5
1
1.5
2
2.5
Date : 21/11/17
Ref : WP207
Coords : N 48.42986°
E 003.17594°
Legend :
Brunisol
Clay
Silt
Sand
Gravel
Organic matter

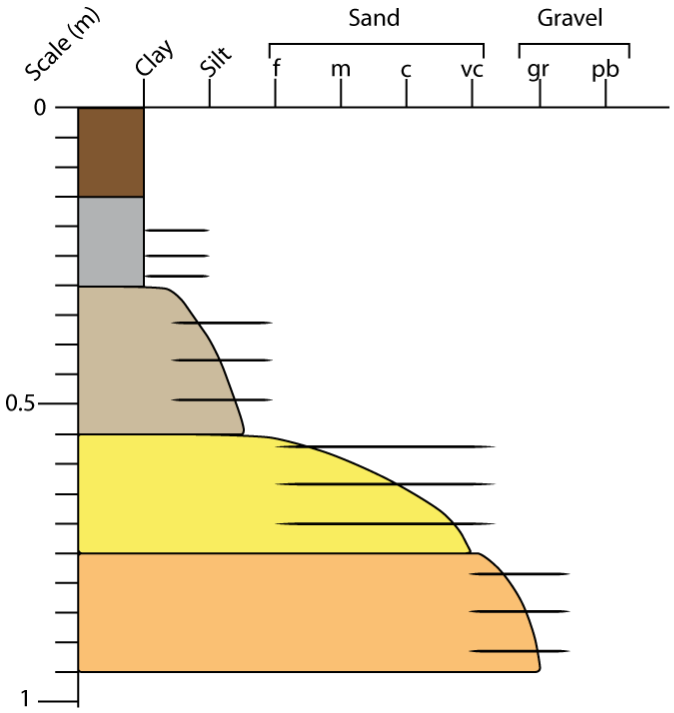

Date : 21/11/17 Coords : N 48.43002° E 003.17533°
Ref : WP208

Legend :
- Brunisol
- Clay
- Silt
- Sand
- Gravel
- Organic matter

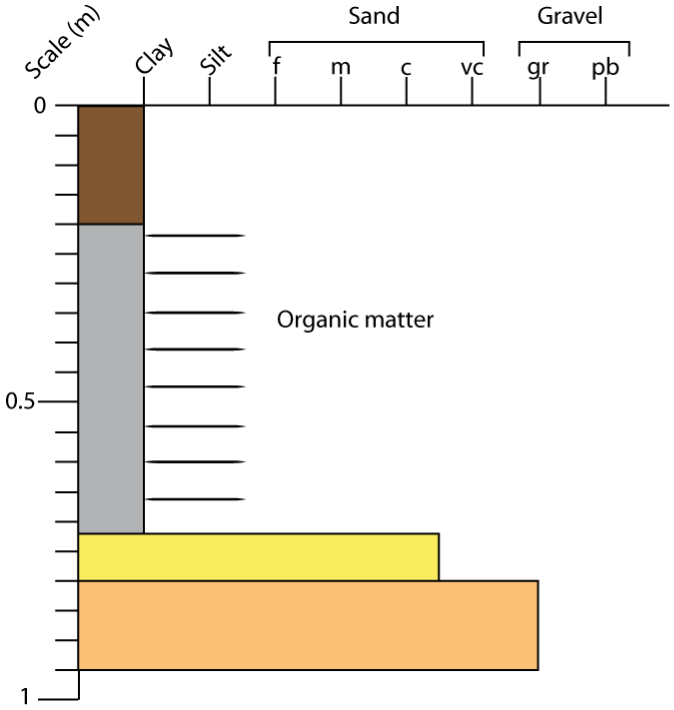

Date : 21/11/17 Coords : N 48.42833° E 003.17550°
Ref : WP209

Legend :
- Brunisol
- Clay
- Silt
- Sand
- Gravel
- Organic matter

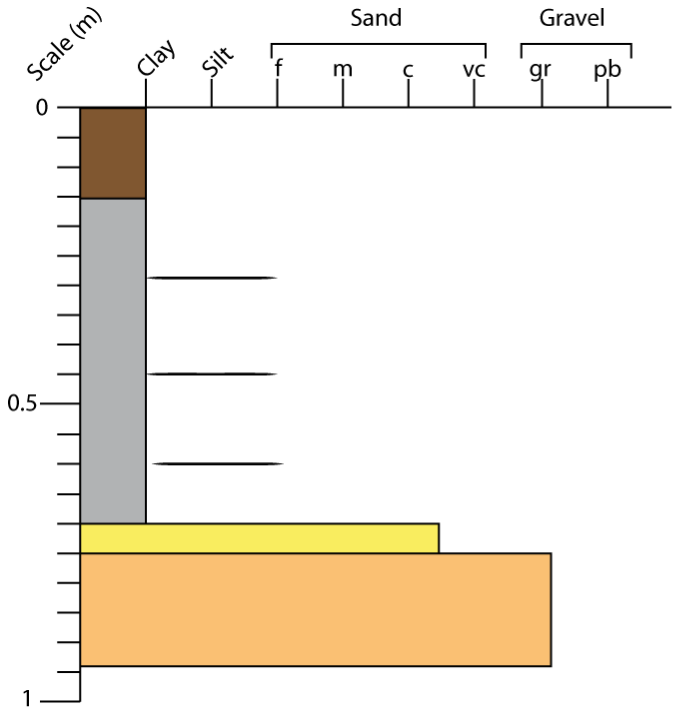

Date : 21/11/17
Ref : WP210
Coords : N 48.42841°
E 003.17549°

Legend :
- Brunisol
- Clay
- Silt
- Sand
- Gravel
- Organic matter

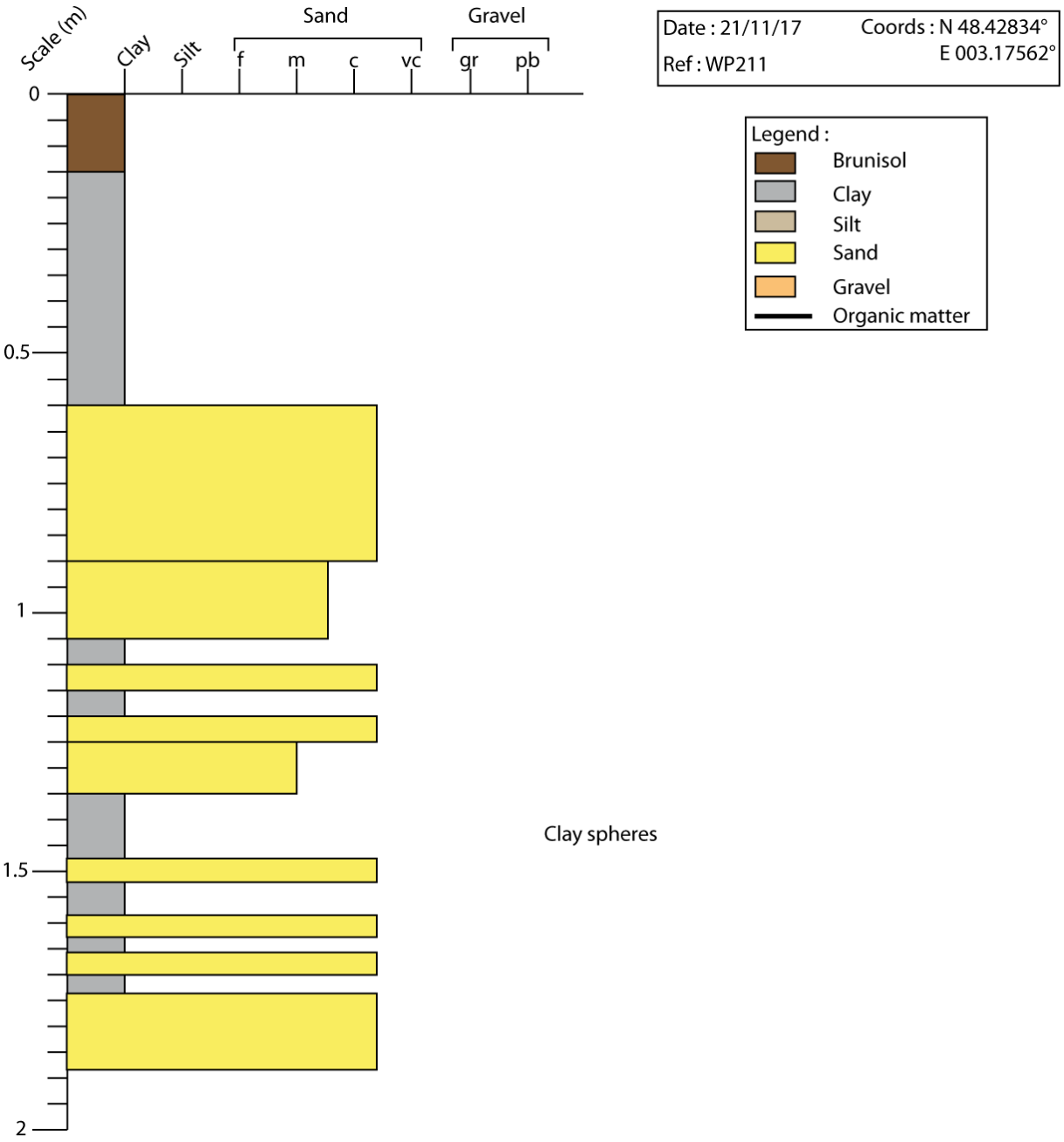
Scale (m)
Clay
Silt
Sand
Gravel
f
m
c
vc
gr
pb
0
0.5
1
1.5
2
Date : 21/11/17
Ref : WP211
Coords : N 48.42834°
E 003.17562°
Legend :
Brunisol
Clay
Silt
Sand
Gravel
Organic matter
Clay spheres

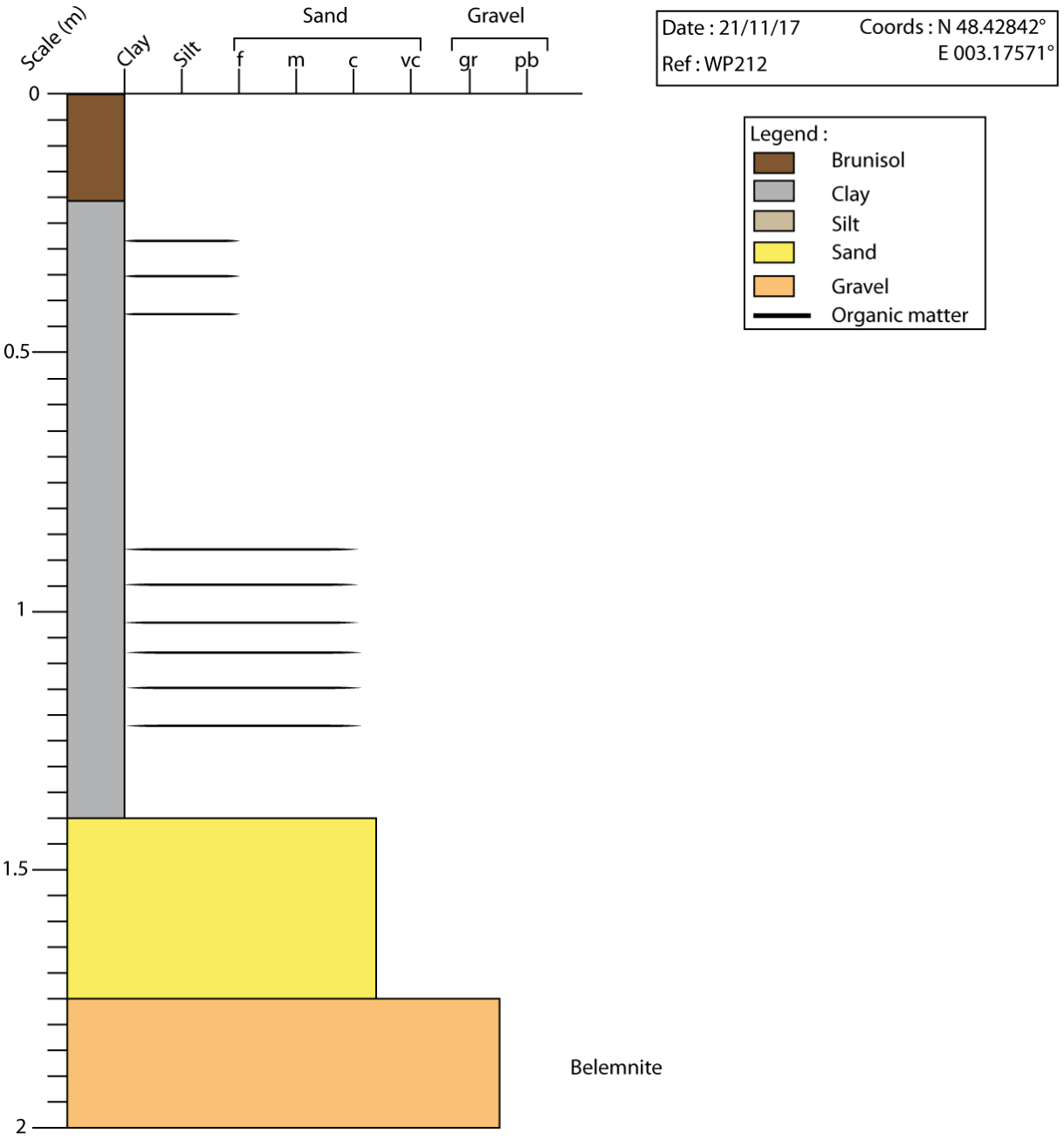
Scale (m)
Clay
Silt
Sand
f
m
c
vc
Gravel
gr
pb
0
0.5
1
1.5
2
Belemnite
Date : 21/11/17
Ref : WP212
Coords : N 48.42842°
E 003.17571°
Legend :
Brunisol
Clay
Silt
Sand
Gravel
Organic matter

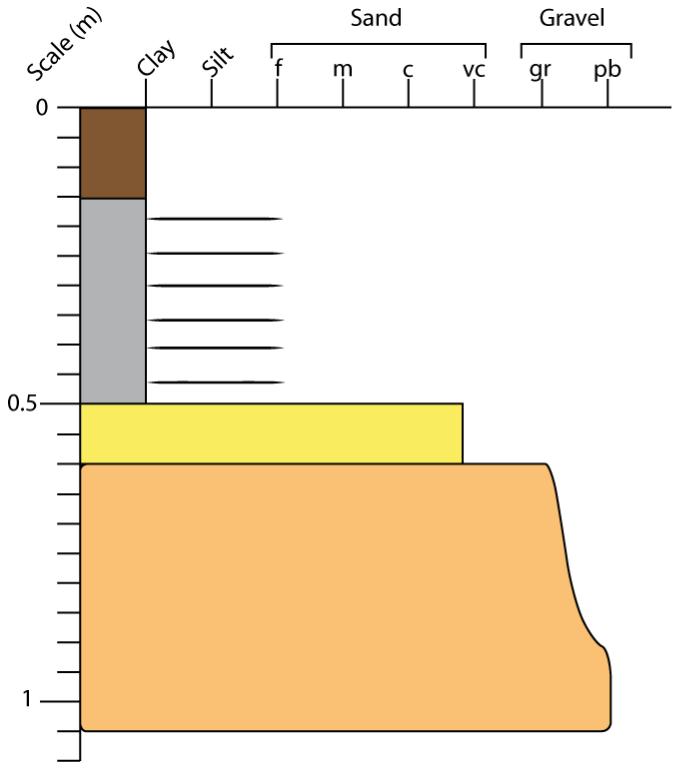

Date : 22/11/17
Ref : WP213

Coords : N 48.42994°
E 003.18146°

Legend :
- Brunisol
- Clay
- Silt
- Sand
- Gravel
- Organic matter

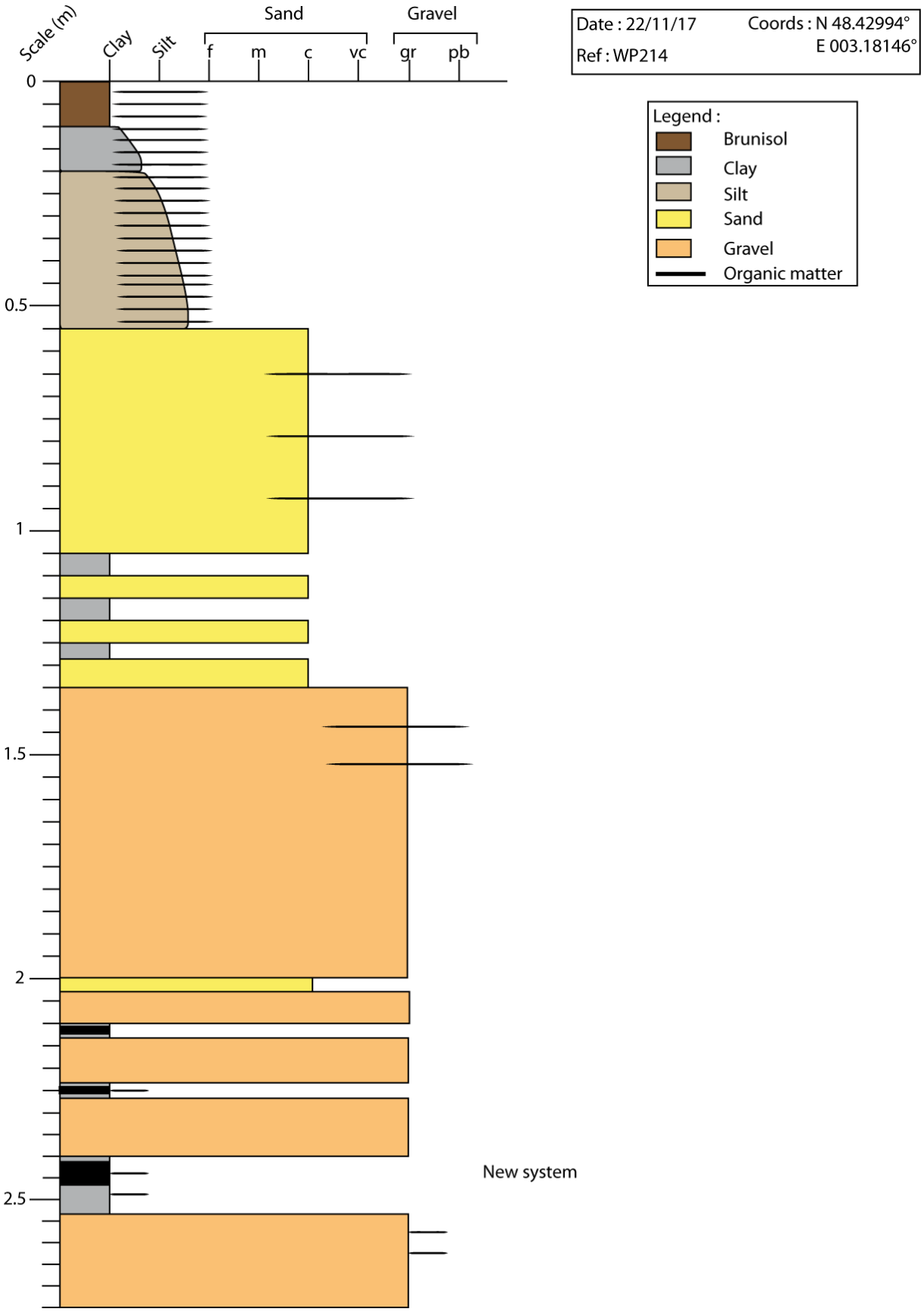
Scale (m)
Clay
Silt
Sand
f
m
c
vc
Gravel
gr
pb
0
0.5
1
1.5
2
2.5
Date : 22/11/17
Ref : WP214
Coords : N 48.42994°
E 003.18146°
Legend :
Brunisol
Clay
Silt
Sand
Gravel
Organic matter
New system

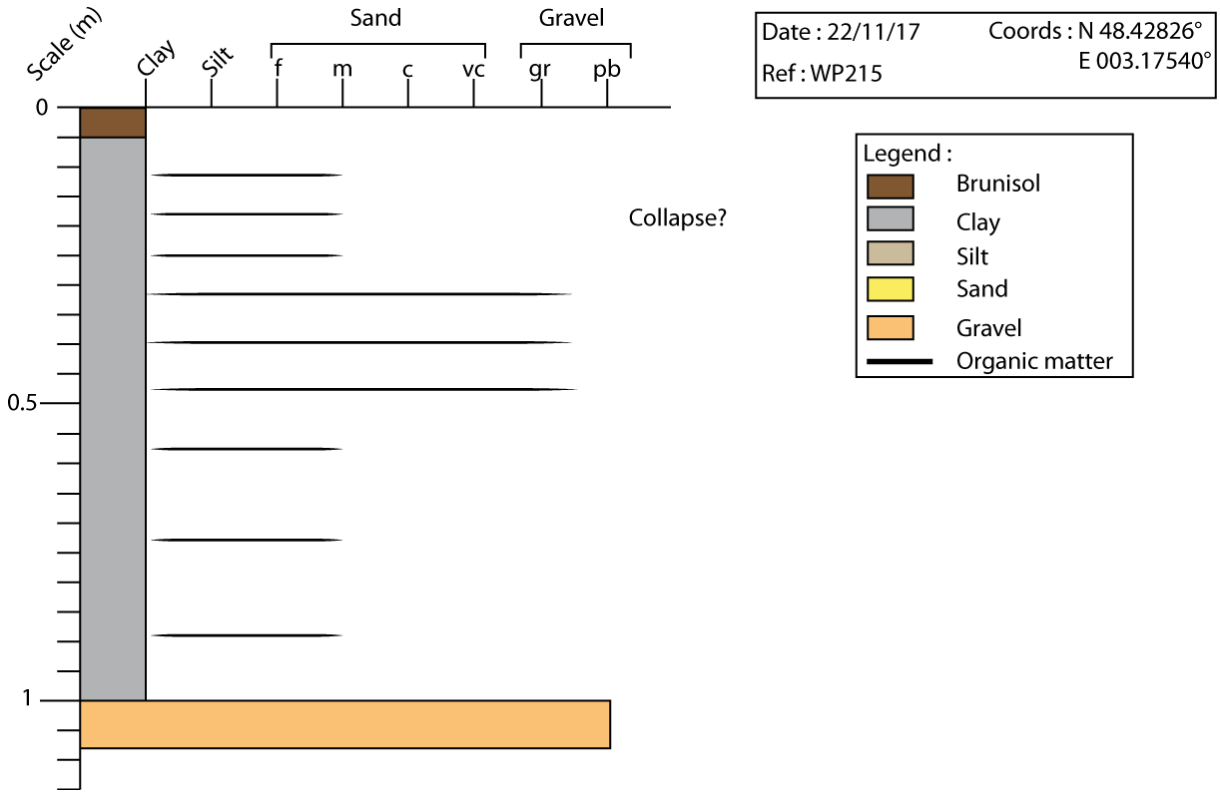
Scale (m)
Clay
Silt
Sand
Gravel
f
m
c
vc
gr
pb
0
0.5
1
Collapse?
Date : 22/11/17
Ref : WP215
Coords : N 48.42826°
E 003.17540°
Legend :
Brunisol
Clay
Silt
Sand
Gravel
Organic matter

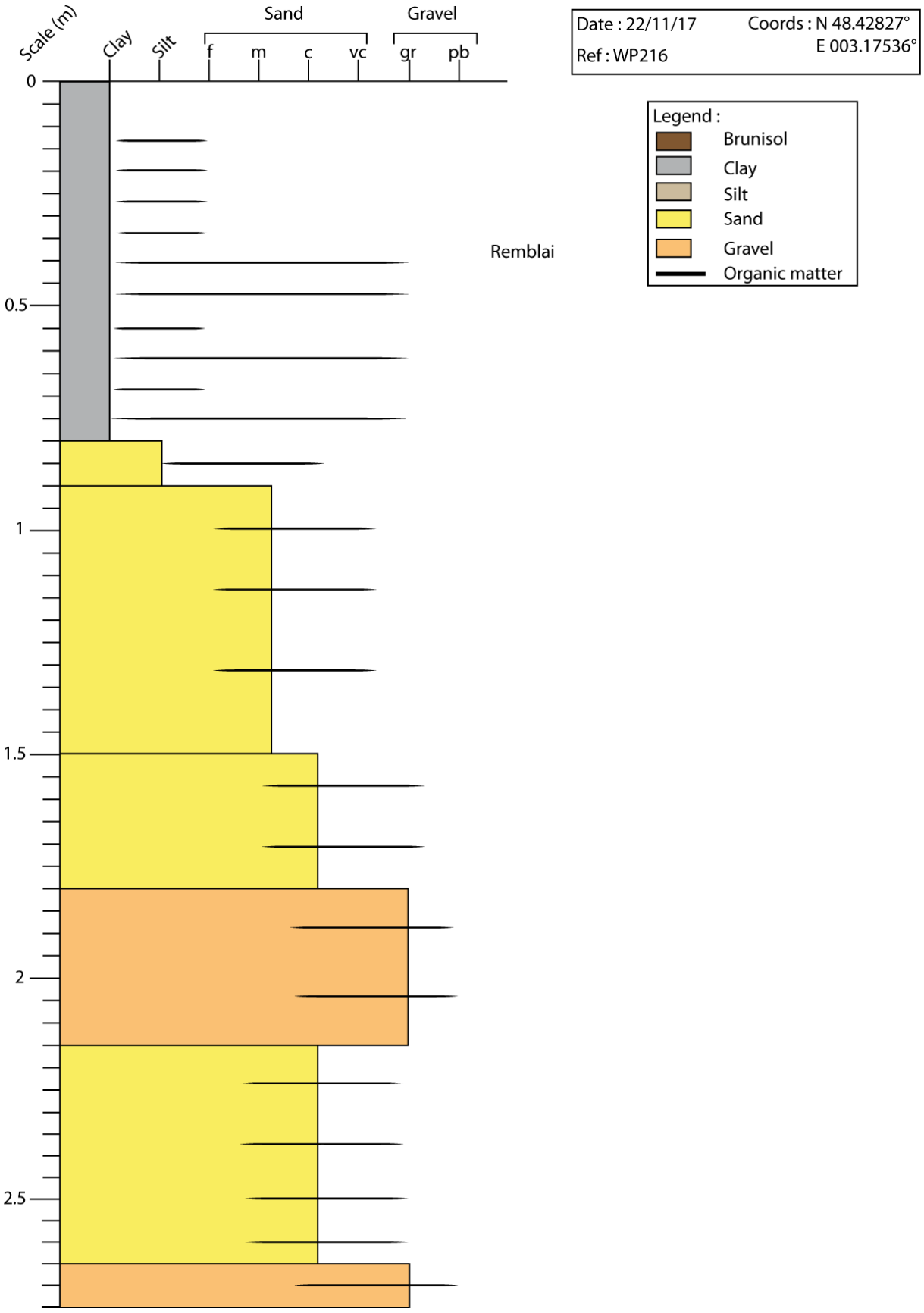
Scale (m)
Clay
Silt
Sand
f
m
c
vc
Gravel
gr
pb
0
0.5
1
1.5
2
2.5
Remblai
Date : 22/11/17
Ref : WP216
Coords : N 48.42827°
E 003.17536°
Legend :
Brunisol
Clay
Silt
Sand
Gravel
Organic matter

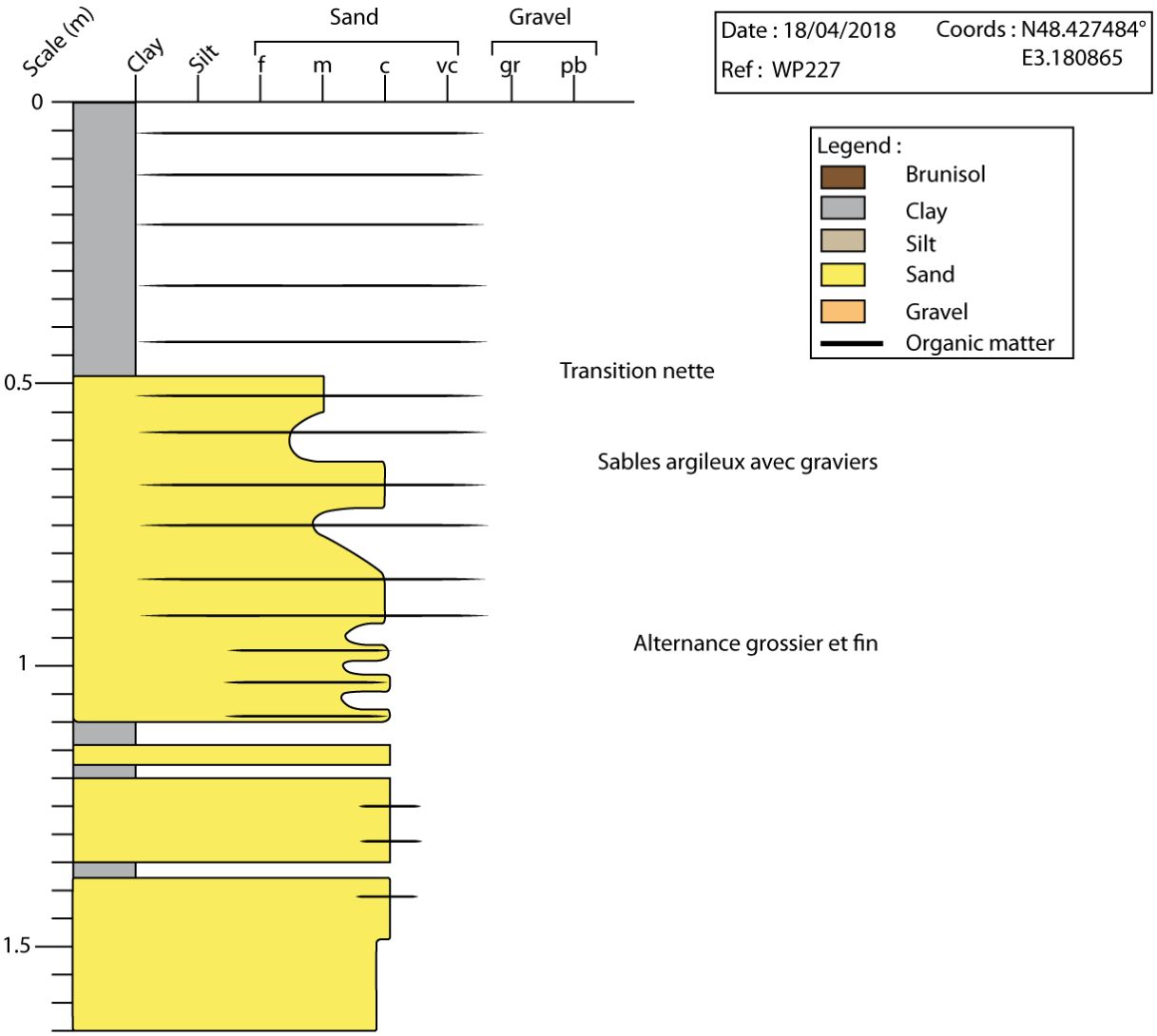
Scale (m)
Clay
Silt
Sand
f
m
c
vc
Gravel
gr
pb
0
0.5
1
1.5
Date : 18/04/2018
Coords : N48.427484° E3.180865
Ref : WP227
Legend :
Brunisol
Clay
Silt
Sand
Gravel
Organic matter
Transition nette
Sables argileux avec graviers
Alternance grossier et fin

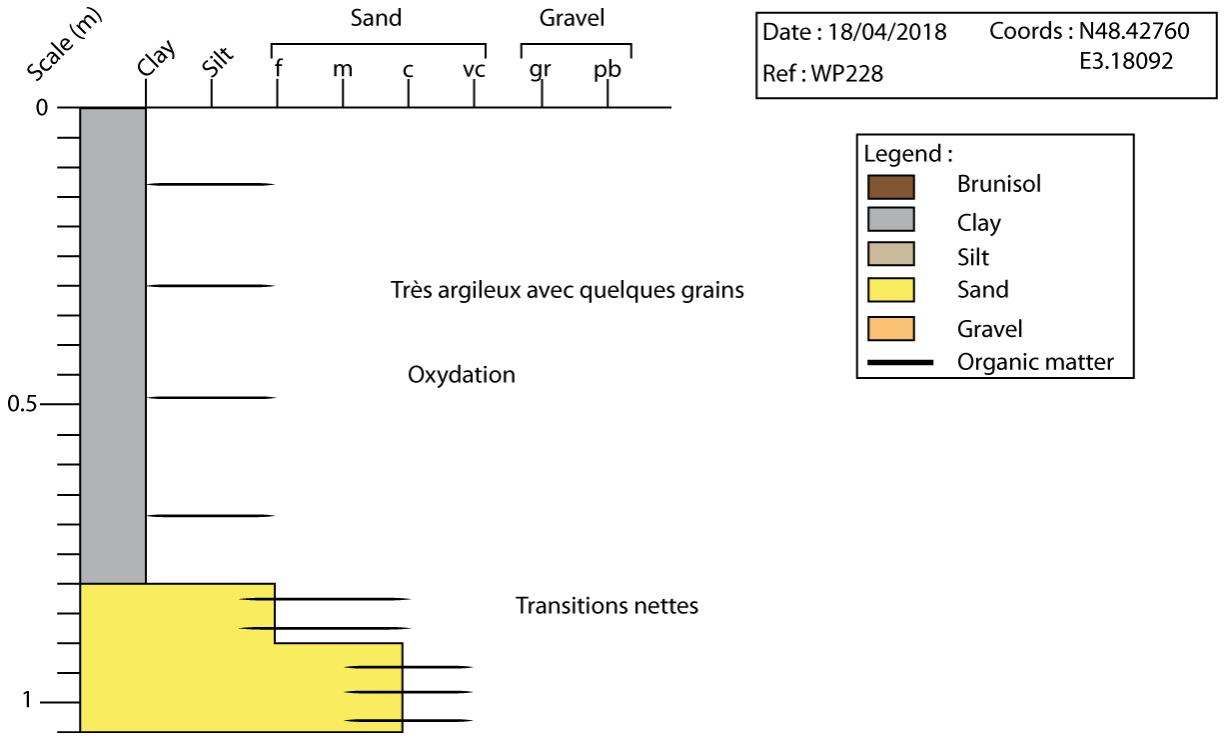
Scale (m)
Clay
Silt
Sand
f
m
c
vc
Gravel
gr
pb
0
0.5
1
Très argileux avec quelques grains
Oxydation
Transitions nettes
Date : 18/04/2018
Coords : N48.42760
E3.18092
Ref : WP228
Legend :
Brunisol
Clay
Silt
Sand
Gravel
Organic matter

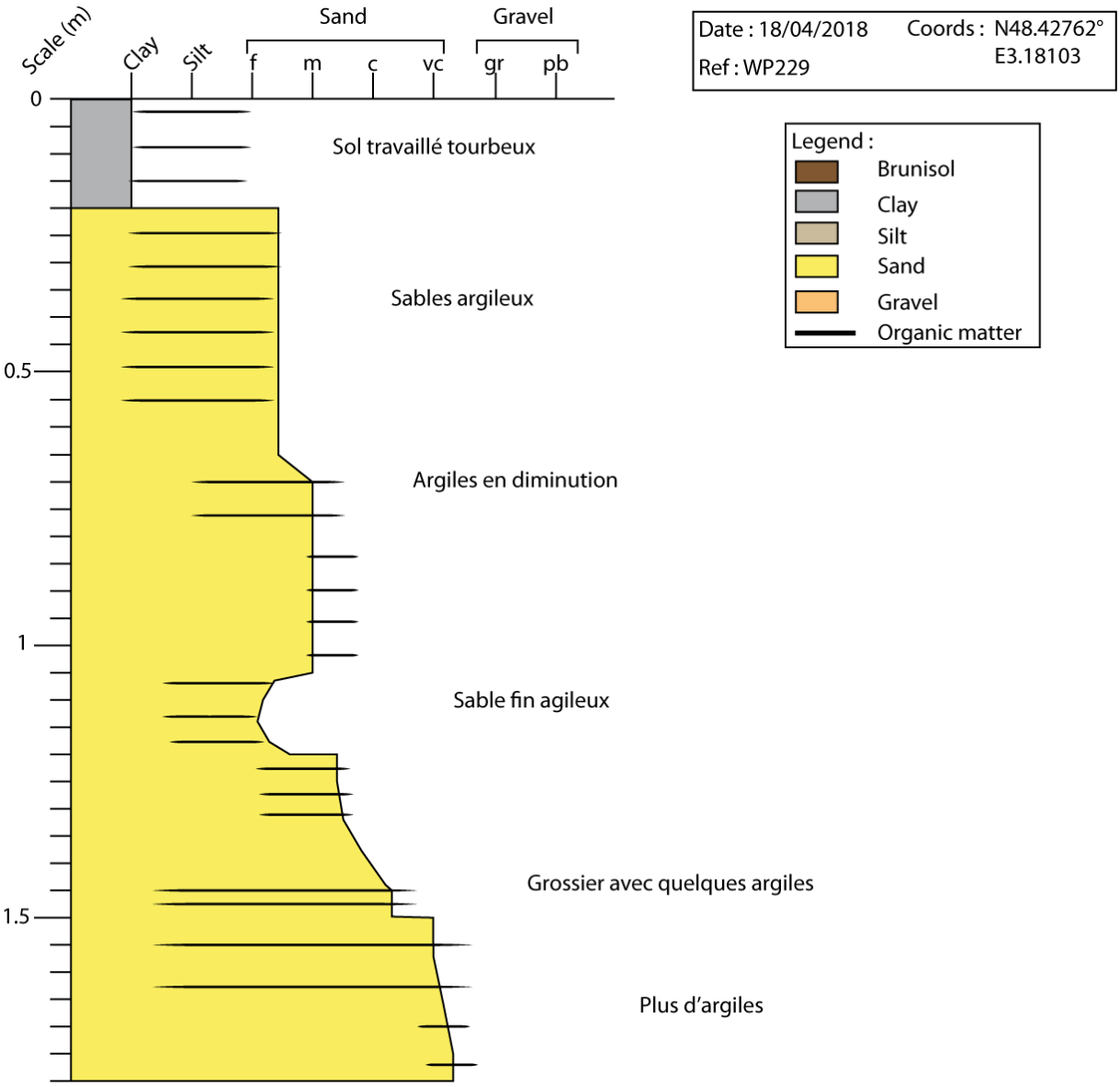
Scale (m)
Clay
Silt
Sand
f
m
c
vc
Gravel
gr
pb
0
0.5
1
1.5
Date : 18/04/2018
Coords : N48.42762° E3.18103
Ref : WP229
Legend :
Brunisol
Clay
Silt
Sand
Gravel
Organic matter
Sol travaillé tourbeux
Sables argileux
Argiles en diminution
Sable fin agileux
Grossier avec quelques argiles
Plus d'argiles

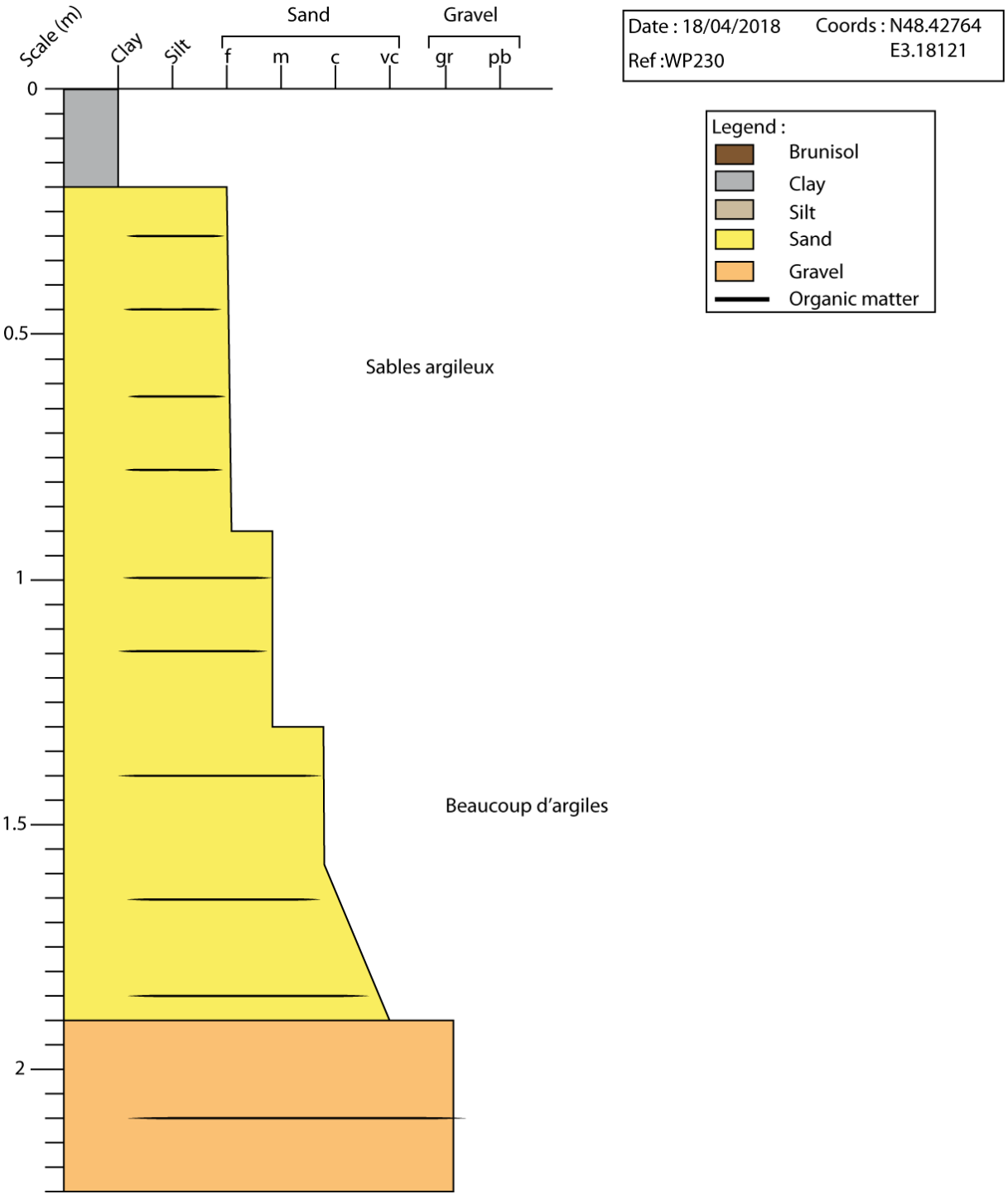
Scale (m)
Clay
Silt
Sand
f
m
c
vc
Gravel
gr
pb
0
0.5
1
1.5
2
Sables argileux
Beaucoup d'argiles
Date : 18/04/2018
Coords : N48.42764
E3.18121
Ref :WP230
Legend :
Brunisol
Clay
Silt
Sand
Gravel
Organic matter

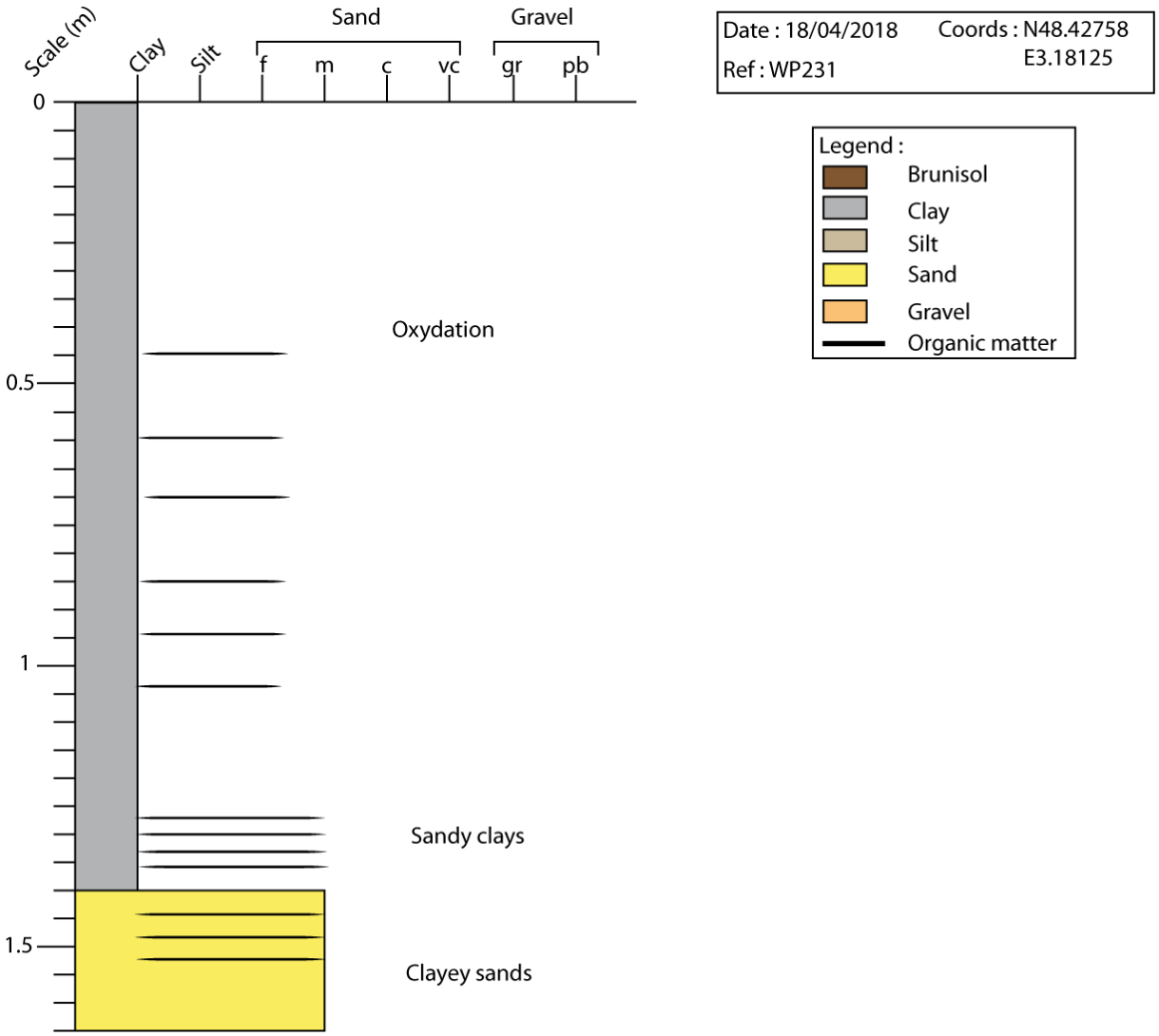
Scale (m)
Clay
Silt
Sand
f
m
c
vc
Gravel
gr
pb
0
0.5
1
1.5
Oxydation
Sandy clays
Clayey sands
Date : 18/04/2018
Coords : N48.42758
E3.18125
Ref : WP231
Legend :
Brunisol
Clay
Silt
Sand
Gravel
Organic matter

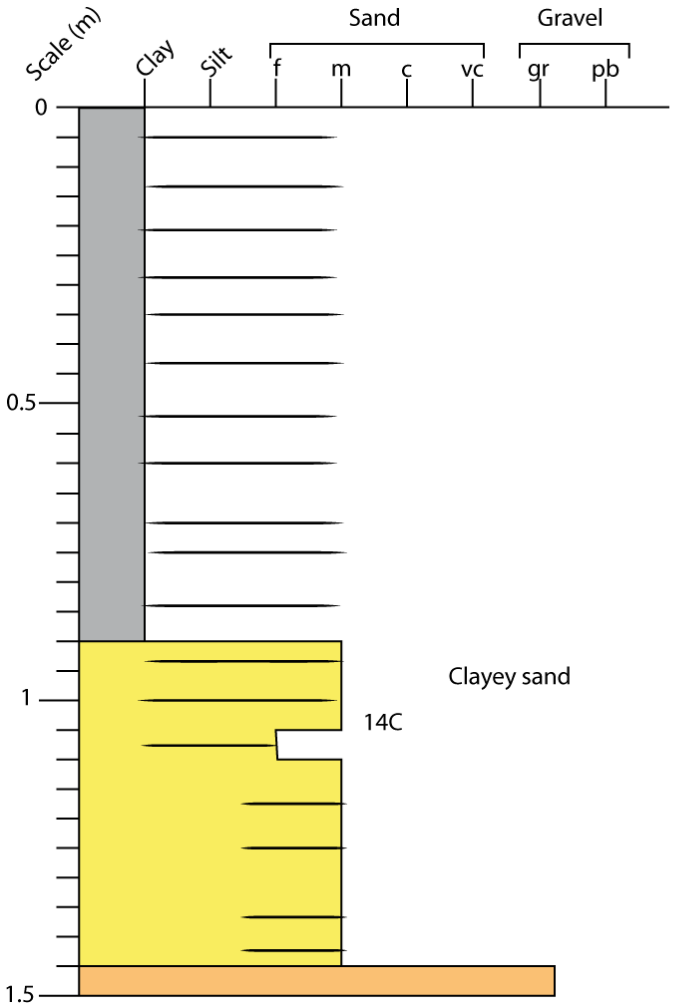

Date : 18/04/2018 Coords : N48.42754
E3.18140
Ref : WP232

Legend :
- Brunisol
- Clay
- Silt
- Sand
- Gravel
- Organic matter

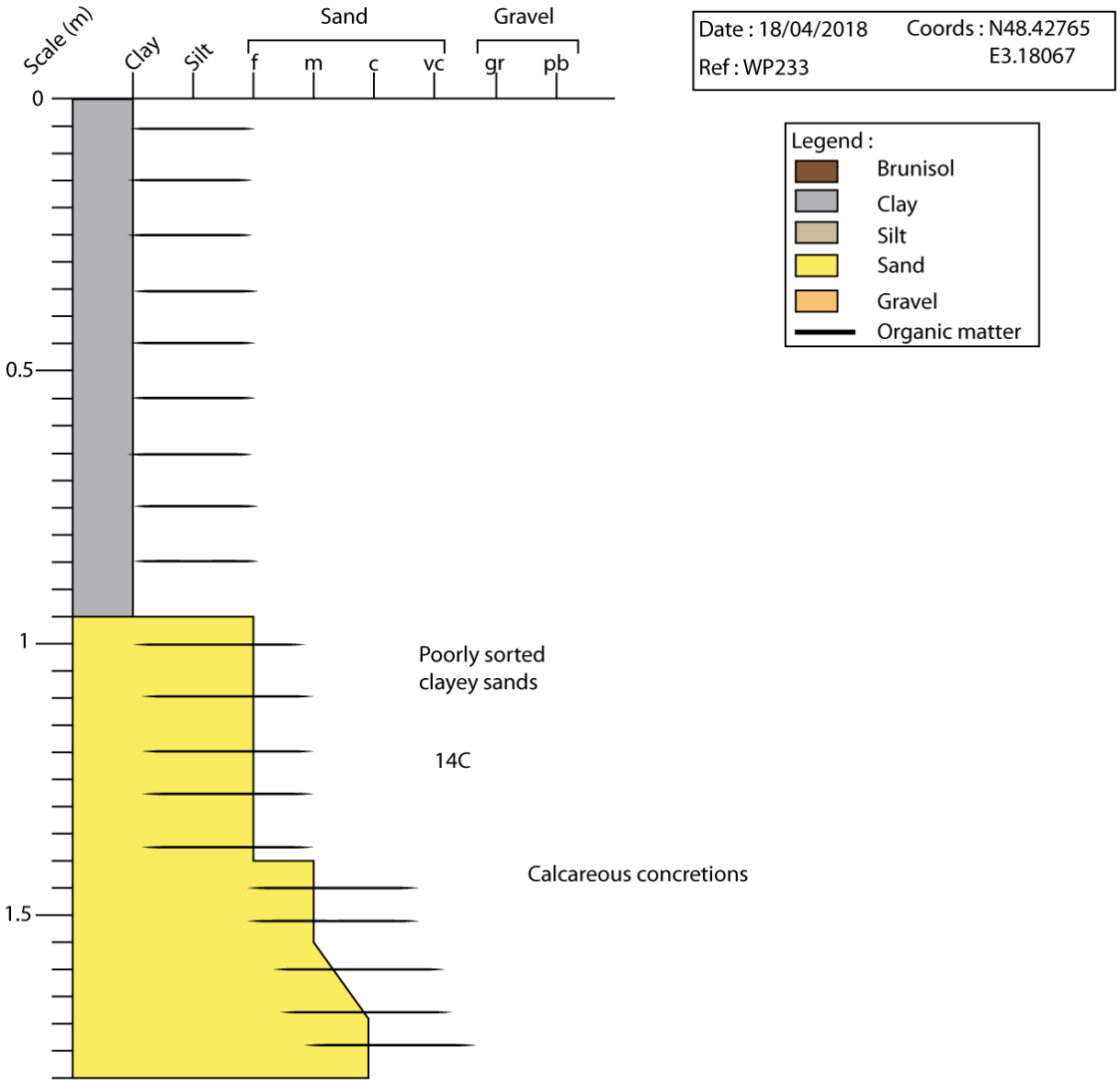
Scale (m)
Clay
Silt
Sand
f
m
c
vc
Gravel
gr
pb
0
0.5
1
1.5
Date : 18/04/2018
Coords : N48.42765
E3.18067
Ref : WP233
Legend :
Brunisol
Clay
Silt
Sand
Gravel
Organic matter
Poorly sorted
clayey sands
14C
Calcareous concretions

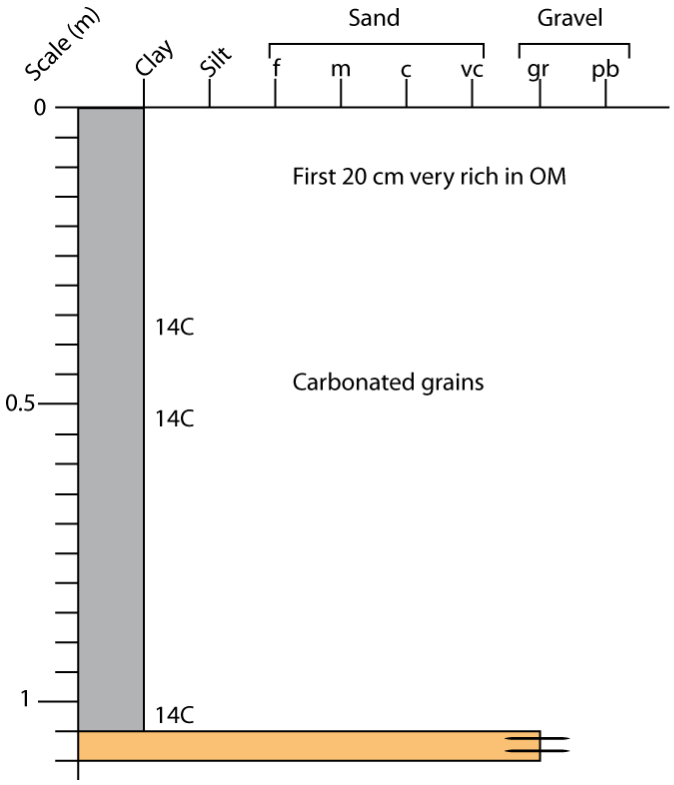

Date : 17/10/2018 Coords : N48.43315° E3.17123°
Ref : WP274

Legend :
- Brunisol
- Clay
- Silt
- Sand
- Gravel
- Organic matter

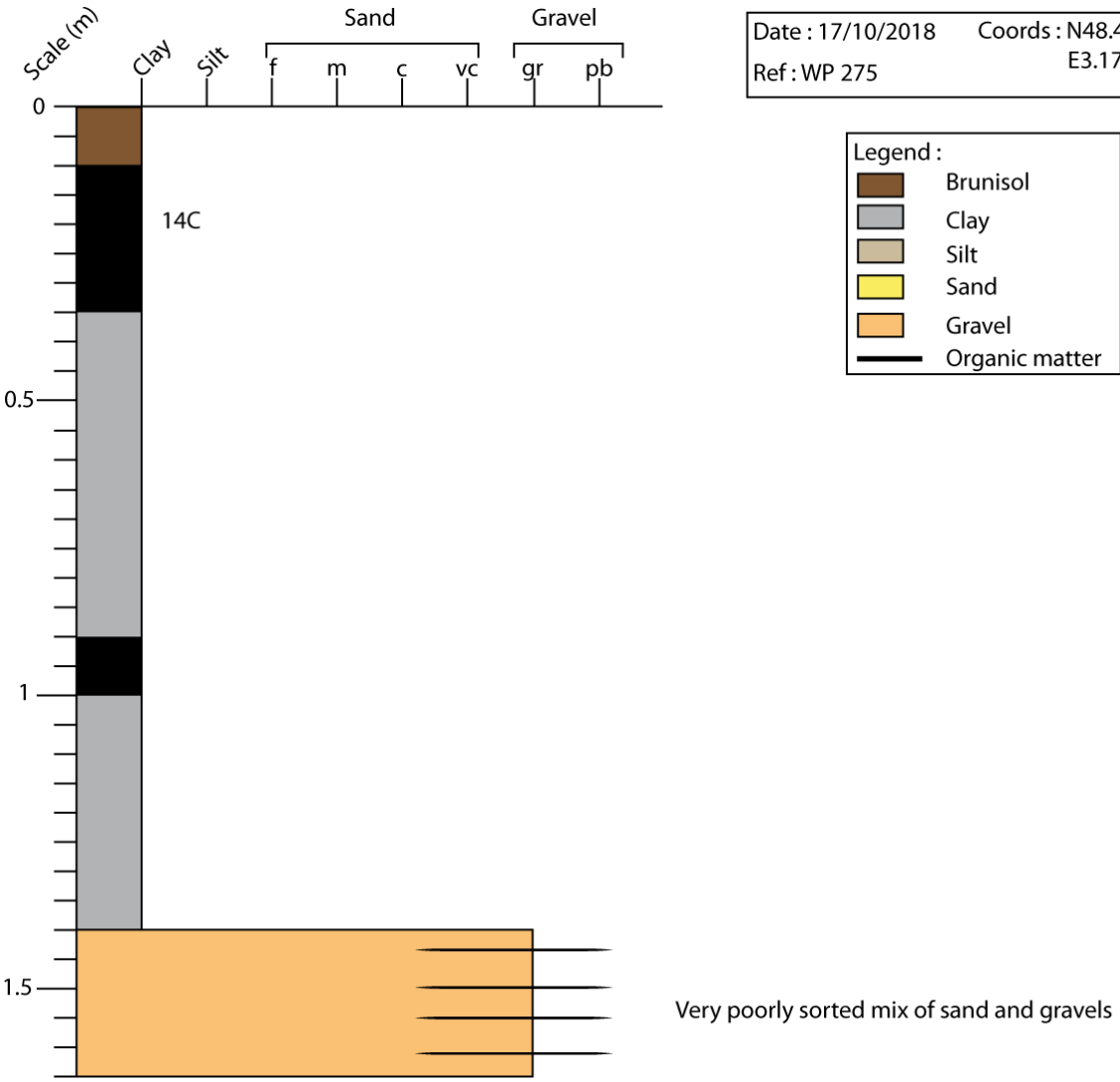
Scale (m)
Clay
Silt
Sand
f
m
c
vc
Gravel
gr
pb
0
0.5
1
1.5
14C
Date : 17/10/2018
Coords : N48.43303°
E3.17113°
Ref : WP 275
Legend :
Brunisol
Clay
Silt
Sand
Gravel
Organic matter
Very poorly sorted mix of sand and gravels

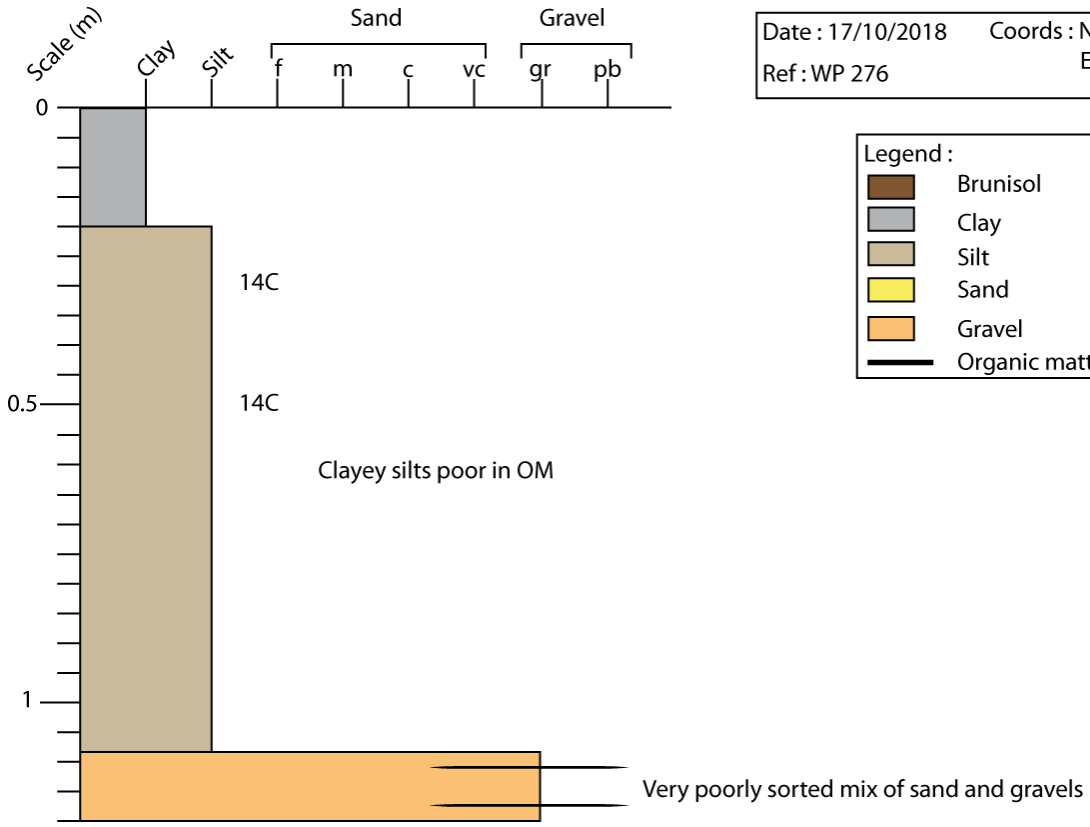
Scale (m)
Clay
Silt
Sand
Gravel
f
m
c
vc
gr
pb
0
0.5
1
14C
14C
Clayey silts poor in OM
Very poorly sorted mix of sand and gravels
Date : 17/10/2018
Coords : N48.43302°
E3.17121°
Ref : WP 276
Legend :
Brunisol
Clay
Silt
Sand
Gravel
Organic matter

RÉSUMÉ

Les dépôts grossiers de remplissage de chenal abandonné sont étudiés à partir de modèles analogiques et d'exemples de terrain. Un modèle détaillé de leur architecture est proposé et les facteurs contrôlant leur formation sont identifiés dans les expériences. Des effets hydrauliques liés à l'asymétrie et à l'angle de diversion de la bifurcation contrôlent le dépôt des sédiments grossiers ainsi que leur extension. Ces relations sont quantifiées pour la première fois. L'influence du niveau de base, de la longueur ou pente du chenal abandonné sont discutés. Les études de terrain montrent que l'architecture des dépôts grossiers peut être préservée sur le long terme et que la relation expérimentale prédit la longueur minimale des dépôts grossiers formant le bouchon de chenal.

MOTS CLÉS

Chenal abandonné ; Remplissage grossier ; Bouchon de chenal ; Géométrie de la bifurcation

ABSTRACT

Abandoned channels coarse-grained fill deposits are studied using flume experiments and field surveys. A detailed model of the channel plug architecture is proposed, and controls on its formation identified from flume experiments. Hydraulic effects, controlled by the asymmetry and diversion angle of the bifurcation, determine the sedimentation pattern and extent of the bedload deposits in abandoned channels. These relationships are quantified for the first time. Influence of base level, abandoned channel length or slope is discussed. Field surveys of abandoned channels demonstrate that the bedload channel fill architecture can be preserved in time and that the experimental relationship is reliable to predict the channel plug coarse deposits minimal extent.

KEYWORDS

Abandoned channel; Coarse-grained fill; Channel plug; Bifurcation geometry